UC Santa Cruz

Title

Hydrologic and Biogeochemical Dynamics of Infiltration for Managed Aquifer Recharge and Implications for Groundwater Management

Permalink

Author

Pensky, Jennifer

Publication Date

2023

Peer reviewed|Thesis/dissertation

UNIVERSITY OF CALIFORNIA
SANTA CRUZ

**HYDROLOGIC AND BIOGEOCHEMICAL DYNAMICS OF
INFILTRATION FOR MANAGED AQUIFER RECHARGE AND
IMPLICATIONS FOR GROUNDWATER MANAGEMENT**

A dissertation submitted in partial
satisfaction of the requirements for
the degree of

DOCTOR OF PHILOSOPHY

in

EARTH SCIENCES

by

Jennifer Pensky

June 2023

The dissertation of Jennifer Pensky
is approved:

_____

Distinguished Professor Andrew T. Fisher, Chair

_____

Assistant Professor Margaret Zimmer

_____

Professor Helen Dahlke

_____

Peter F. Biehl
Vice Provost and Dean of Graduate Studies

TABLE OF CONTENTS

LIST OF FIGURES AND TABLES

Chapter 1: Enhanced cycling of nitrogen and metals during rapid infiltration: implications for managed recharge

Chapter 2: Linking nitrate removal, carbon cycling, and mobilization of trace metals during infiltration for managed recharge

Chapter 3: Mapping suitability for managed aquifer recharge using surface and subsurface data and multi-criteria decision analysis in Santa Clara Valley, CA

ABSTRACT

Hydrologic and biogeochemical dynamics of infiltration for managed aquifer recharge and implications for groundwater management

Jennifer Pensky

Due to population growth, shifts in land use, and climate change, there is an increasing demand for fresh water worldwide. Groundwater is an increasingly critical resource used to meet demand but is facing both decreasing supply and quality. Many aquifers have the capacity to store more groundwater, and managed aquifer recharge (MAR), in which surface water in infiltrated into shallow aquifers for later use, is a strategy that can help to replenish groundwater supplies and potentially improve water quality. In order to ensure that MAR systems deliver maximum benefits, it is critical to quantify the hydrologic and biogeochemical processes that occur during infiltration. In this dissertation, I present three original studies that use field, laboratory, and analytical techniques to investigate the linkages between the hydrologic and biogeochemical cycles during infiltration for MAR and the potential implications for groundwater management. In Chapter One, plot-scale infiltration tests showed that a readily-available soil carbon amendment (wood chips) could enhance nitrate removal during rapid infiltration. In Chapter 2, linked field and laboratory studies demonstrated that another soil carbon amendment, almond shells, can promote more efficient nitrate removal than wood chips, but also can facilitate the release of geogenic trace metals. In Chapter Three, multi-criteria decision analysis (MCDA) was paired with a GIS in order to assess where recharge occurs, could occur, or could be developed through MAR

projects in Santa Clara County, California. Collectively, these studies help to further our understanding of both hydrologic and biogeochemical processes and inform sustainable water resource management.

ACKNOWLEDGEMENTS

I am very grateful to everyone who has been a part of this PhD. First, I would like to thank my advisor, Andy Fisher, for all of his guidance, support, and encouragement throughout the years. I am also thankful for my committee members – Margaret Zimmer and Helen Dahlke – for their technical input and mentorship, both of which have greatly improved this dissertation. Many collaborators have also shaped this work, in particular Chad Saltikov, Nicole Schrad, and Laura Foglia.

I also appreciate all of the contributions from the UCSC Hydrogeology group both past and present. I would especially like to thank Sarah Beganskas, Galen Gorski, Tess Weathers, Adam Price, Araceli Serrano, Kristin Dickerson, and Emily Kam for their friendship, support, and commiseration during the grad school experience, as well as all of the undergraduates and lab managers who have been instrumental to my work – Sarah Faraola, Paige Borges, Hannah Dailey, Victor Bautista, Leslie Serafin, Raymond Hess, and many others.

This research would also not be possible without the field and laboratory assistance of Rob Franks, Brian Dreyer, Colin Carney, Dan Sampson, Andrew Calderwood, and Samantha Ying. Additionally, our EPS Department would not run without Jennifer Fish, Amy Kornberg, Grace Caslavka, and Lisa Stipanovich, and I am thankful for all of their help.

Finally, I would like to thank my family and my partner, Adam, for their support throughout my academic journey. I could not have done this without you all.

Chapter One

ENHANCED CYCLING OF NITROGEN AND METALS DURING RAPID INFILTRATION: IMPLICATIONS FOR MANAGED RECHARGE

Abstract

We present results from a series of plot-scale field experiments to quantify physical infiltration dynamics and the influence of adding a carbon-rich, permeable reactive barrier (PRB) for the cycling of nitrogen and associated trace metals during rapid infiltration for managed aquifer recharge (MAR). Recent studies suggest that adding a bio-available carbon source to soils can enhance denitrification rates and associated N load reduction during moderate-to-rapid infiltration (≤ 1 m/day). We examined the potential for N removal during faster infiltration (>1 m/day), through coarse and carbon-poor soils, and how adding a carbon-rich PRB (wood chips) affects subsurface redox conditions and trace metal mobilization. During rapid infiltration, plots amended with a carbon-rich PRB generally demonstrated modest increases in subsurface loads of dissolved organic carbon, nitrite, manganese and iron, decreases in loads of nitrate and ammonium, and variable changes in arsenic. These trends differed considerably from those seen during infiltration through native soil without a carbon-rich PRB. Use of a carbon-rich soil amendment increased the fraction of dissolved N species that was removed at equivalent inflowing N loads. There is evidence that N removal took place primarily via denitrification. Shifts in microbial ecology following infiltration in all of the plots included increases in the relative abundances of microbes in the families *Comamonadaceae*, *Pseudomonadaceae*, *Methylophilaceae*, *Rhodocyclaceae* and *Sphingomonadaceae*, all of which contain genera capable of carrying out denitrification. These results, in combination with studies that have tested other soil types, flow rates, and system scales, show how water quality can be improved during

infiltration for managed recharge, even during rapid infiltration, with a carbon-rich soil amendment.

1.1 Introduction

More than 2 billion people (35% of Earth's population) currently face water stress (Wada et al., 2010), while population growth, shifts in land use, and climatic change are all increasing global demand for fresh water. Groundwater is increasingly used to meet this demand in some areas, particularly in times of drought when surface water resources are scarce. This has led to aquifer overdraft in many regions, contributing negative consequences such as land subsidence and a loss of storage capacity (Bouwer, 1977; Herrera-García et al., 2021). Aquifer overdraft has also contributed to reduced water quality. Seawater intrusion is common in coastal regions and depleted aquifers can serve as terminal sinks for salts, nutrients, and metals that were previously flushed out by groundwater discharge (Konikow and Kendy, 2005; Werner et al., 2013).

Many aquifers have the capacity to store more water, and managed aquifer recharge (MAR), in which excess water is infiltrated into shallow aquifers, is a strategy that can help to replenish groundwater supplies (Bouwer, 2002; Bouwer et al., 1999; Wendt et al., 2021). Source water quality varies and can potentially contain or mobilize contaminants that threaten groundwater quality (Fakhreddine et al., 2021; Tedoldi et al., 2016). However, MAR systems can also potentially improve groundwater quality through dilution and/or biogeochemical cycling of contaminants (Alam et al., 2021; Hartog and Stuyfzand, 2017; Hellauer et al., 2017). The infiltration rate and associated

fluid residence time during MAR can influence redox conditions, carbon utilization, and nitrogen cycling in the shallow subsurface (Greenan et al., 2009; Halaburka et al., 2017; Hoover et al., 2016).

Nitrogen contamination is particularly of concern, as nitrate is the most ubiquitous nonpoint-source groundwater contaminant worldwide and is well-known to pose ecological and human health risks (Burri et al., 2019; Van Drecht et al., 2003). Nitrogen cycling during infiltration is complex and involves many pathways, including nitrification, denitrification, anaerobic ammonium oxidation (anammox), and dissimilatory nitrate reduction to ammonium (DNRA) (Chen et al., 2014; Li et al., 2017; Lloréns et al., 2021; Sebilo et al., 2013). Of the numerous pathways that transform nitrogen, anammox and denitrification are of particular interest because they result in net, quasi-permanent removal of nitrogen from the hydrologic cycle (Long et al., 2013; Shan et al., 2016).

Anammox is a microbially-mediated process in which nitrite and ammonium are transformed into inert N_2 gas and water under anaerobic conditions. Five genera of the phylum *Planctomyecetes* are known to carry out anammox (Strous et al., 1999). Anammox has been observed in a variety of settings, including marine sediments, floodplain soils, and wastewater treatment systems, but has not been extensively studied in MAR systems (Hoagland et al., 2019; Silver et al., 2018; Welti et al., 2012). Microbially mediated denitrification also has been observed in diverse environments, including in MAR systems, under sub-oxic conditions (Ginige et al., 2013; Yuan et al., 2016). During complete denitrification, NO_3^- is converted to inert N_2 gas. This can

occur when microbes oxidize organic carbon using nitrate as a terminal electron acceptor, with NO_2^-, NO, and N_2O as intermediate products (Korom, 1992).

Recent MAR studies, with infiltration rates ≤1 m/day, have shown that nitrate removal via denitrification can occur during managed recharge (Gorski et al., 2020, 2019; Grau-Martínez et al., 2018a; Schmidt et al., 2011). However, more rapid infiltration for MAR (infiltration rates >1 m/day) can entrain oxygen in the subsurface and reduce the hydraulic retention time in saturated soils, contributing to oxic conditions that potentially hinder both denitrification and anammox (Hellauer et al., 2018a, 2017; Regnery et al., 2016a). Carbon-rich permeable reactive barriers (PRBs) can increase denitrification and nitrate load removal during infiltration for managed recharge and groundwater flow (Beganskas et al., 2018; Gorski et al., 2019; Grau-Martínez et al., 2018b; Robertson et al., 2005).

In addition to nitrogen species, infiltration can also affect the cycling of redox-sensitive metals. As oxygen content decreases, first manganese is reduced from MnO_2 to Mn^{2+}, then iron is reduced from $Fe(OH)_3$ to Fe^{2+} (Rivett et al., 2008). During rapid infiltration, subsurface conditions may not become sufficiently reducing to dissolve Mn and Fe solid phases and mobilize these metals. As such, the concentrations of redox-sensitive elements such as Mn^{2+} and Fe^{2+}, along with nitrogen species, can serve as indicators of redox conditions in the subsurface.

While anoxic environments with high dissolved organic carbon (DOC) concentrations are favorable for nitrogen removal, they can also facilitate the release of trace contaminants such as arsenic (As). Arsenic poses a particular risk for MAR

systems due to its naturally-occurring ubiquity in soils and sediments and high toxicity at trace concentrations, with a World Health Organization (WHO) recommended limit of 10 ug/L (Fakhreddine et al., 2015; Smedley and Kinniburgh, 2002; World Health Organization, 2017). Under anoxic conditions, the reductive dissolution of geogenic Fe (oxyhydr)oxides can cause the concomitant release of adsorbed As (Fendorf et al., 2010). Additionally, the presence of DOC can lead to faster consumption of dissolved oxygen, promoting reducing conditions and hastening As release. Arsenic contamination has been documented in MAR projects, most notably in aquifer storage and recovery operations using injection wells due to the abrupt introduction of recharge water and the associated strong contrast in redox potential with native groundwater, but can also be a concern in infiltration basins (Fakhreddine et al., 2021, 2015).

Here we investigate how the presence of a carbon-rich PRB affects both nitrogen and trace metal cycling during rapid infiltration for managed recharge. By investigating nitrogen and trace metal cycling concurrently, we develop a more holistic understanding of how MAR systems can impact water quality, and how carbon amendments may be used to improve resource conditions.

1.2 Materials and methods

1.2.1 Study site

This study was conducted at Kitayama Ranch (KTYA) in the Pajaro Valley groundwater basin, central coast California, at a site that is being considered for a new MAR basin to be operated by the Pajaro Valley Water Management Agency (PVWMA). The regional aquifer system is in overdraft, and both supply and demand

management efforts are underway to bring the basin into hydrologic balance (Pajaro Valley Water Management Agency, 2021, 2014). The site is located on a combination of eolian, fluvial, and alluvial deposits, adjacent to Monterey Bay (Figure 1-1), with shallow soils classified as loamy sand (SSURGO, 2014). Several recharge projects in the Pajaro Valley are currently being operated, including Kelly-Thompson Ranch (KTR), Storrs Winery (STR), and Harkins Slough (HSP), all located within 15 km of KTYA (Figure 1-1) (Beganskas and Fisher, 2017; Hanson et al., 2010; Kiparsky et al., 2018; Racz et al., 2012).

1.2.2 Plot construction and instrumentation

Infiltration plots were used to emulate a period of continuous infiltration lasting two weeks, as would occur in regional MAR infiltration basins during typical operations (e.g., Racz et al., 2012; Schmidt et al., 2011; Beganskas and Fisher, 2017). Infiltration was controlled during these experiments using a system design developed and discussed in earlier studies (Figure 1; Beganskas et al., 2018; Gorski et al., 2019) and summarized briefly in this section. Infiltration tests are commonly run using single- or double-ring infiltrometers (ASTM:D3385-94, 2009; Bouwer, 2002a). Infiltrometers tend to be relatively small (which contributes to extensive lateral flow), but the larger the infiltration area tested, the greater the fraction of vertical flow expected to occur; this understanding has motivated numerous infiltration tests using plots larger than standard ring and disk infiltrometers (Heeren et al., 2013; Khodaverdiloo et al., 2017; Lucke et al., 2014; Youngs, 1991). However, larger test areas present practical challenges, including greater construction effort and cost and a larger water supply; the

latter is a particular concern for tests that run for days to weeks, especially in soils with a high infiltration capacity.

Infiltration plots used in the present study were designed with these considerations in mind, having a footprint larger than many infiltrometers, and allowing independent measurements of vertical and total flow (Figure 1-1).

Plots with an area of 1 x 1 m were hand excavated to a depth of 1 m below ground surface (bgs). To reduce lateral flow during infiltration, fiberglass walls were installed along plot edges and caulked at corner joints, with the annulus around the walls sealed with water-activated bentonite. Additionally, instrumentation was installed as close as possible to the center of each plot, where vertical flow should be most consistent.

Plots were instrumented to measure bulk (total) and vertical infiltration rates. A stilling well was installed in each plot to measure the water level with an automated pressure logger. Bulk infiltration rates (IR_B) were calculated by volume balance based on the change in water level over time when there was no inflow. Vertical infiltration rates (IR_V) were measured in each plot using a time-series method with heat as a tracer (Hatch et al., 2006; Racz et al., 2012). The water level in the plots was controlled using an automated inflow system, including a solenoid on/off valve and float switch. This helped to maintain saturated subsurface conditions during infiltration and limited the plot water level to a defined range, based on travel of the float, so that tests could be run continuously for ≥15 days without having personnel on site at all times.
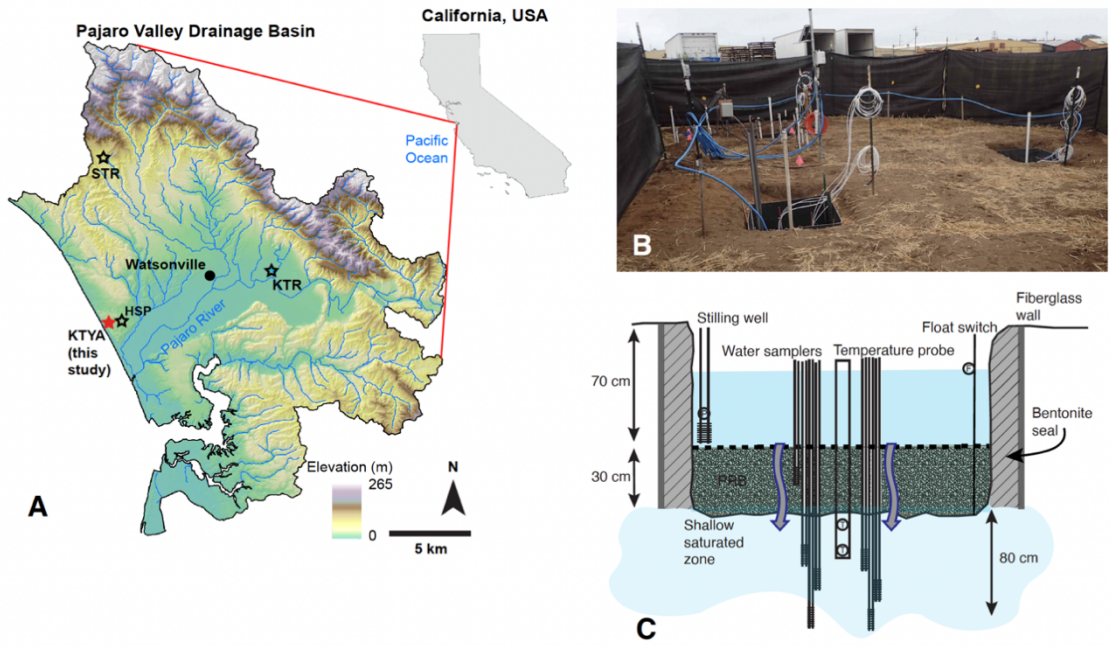
Figure 1-1 Site map where plot studies were conducted at Kitayama Ranch (KTYA), and where previous plot and core studies were conducted at Storrs Winery (STR), Kelly Thompson Ranch (KTR), and Harkins Slough (HSP) (A). Photo (B) and schematic (C) of the instrumentation installed in each plot indicate the location of temperature probes, water samplers, stilling well, and float switch in each plot.

Water for the experiments was diverted into the plots from an irrigation spigot that received flows from a mixture of an on-site groundwater well and delivered water from a system operated by the PVWMA and the City of Watsonville. Delivered water was a blend of groundwater recovered from an inland well and recycled wastewater from a nearby MAR system operated by the agency (Pajaro Valley Water Management Agency, 2021, 2014). As a consequence of using this mixture of water sources, influent water chemistry tended to have elevated solute concentrations (as can occur during MAR using non-standard water sources), allowing assessment of loads and reactions during rapid infiltration. In addition, influent chemistry was highly variable on an hourly to daily basis during the experiments because source mixtures changed over time, and experiments in the plots were run serially rather than simultaneously.

One plot was left unamended at the base as a control to test native soil conditions. Two plots were amended with a carbon-rich PRB, one with a 30-cm layer of redwood chips, obtained from a local landscape supply, and one with a 30-cm layer comprising a 1:1 mixture of redwood chips and soil by volume.

1.2.3 Soil sampling and analysis

Sediment samples were collected from beneath the base of each plot before and after infiltration experiments. Samples were collected at 10 cm intervals to a depth of 1 m below plot base (2 m bgs) and analyzed for soil texture, total organic carbon (TOC), total nitrogen (TN), and phylogenetic sequencing of microbial DNA. Microbial samples were collected using sterile techniques and were immediately placed in a liquid

nitrogen field dewar for storage, then transported back to the laboratory for storage. DNA samples were kept at -80°C until extraction.

1.2.4 Fluid sampling and analysis

Two nests of fluid sampling piezometers were installed in each plot, with screens placed just above the plot base, and at depths of 30 cm, 55 cm, and 80 cm below plot base. An additional fluid sampling piezometer was placed within the PRB layers in the amended plots (Figure 1-1C). After infiltration began in each plot, fluid samples were collected every 1-2 days from the surface and subsurface to analyze for selected nitrogen species (NO_3^-, NO_2^-, NH_4^+), dissolved organic carbon (DOC), stable isotopes of NO_3^- ($\delta^{15}N$ and $\delta^{18}O$), and metals (As, Fe, and Mn). Samples were field filtered at 0.45 μm and samples collected for nitrate isotope analyses were filtered again in the lab to 0.2 μm. All fluid samples were stored at -4° C prior to analysis.

Nutrient samples were analyzed using a Lachat QuickChem with three channels to simultaneously measure NO_3^-, NO_2^-, and NH_4^+ using colorimetry. DOC samples were analyzed using a Shimadzu TOC Analyzer. Analysis of sample duplicates, blanks, and laboratory standards indicated that both instruments were accurate within 2-5%. Selected samples were sent to the UC Davis Stable Isotope Facility for analysis of NO_3^- isotopes. Samples were prepared using the bacterial method and isotopes were measured using a Thermo Scientific Delta V Plus IRMS (Casciotti et al., 2002).

Metals samples were preserved with 2% HNO_3 prior to analysis. Metals samples were analyzed using a Thermo ElementXR High Resolution Inductively Coupled Mass Spectrometer. Analysis of sample duplicates, blanks, laboratory

standards, and standard reference materials (SRM) indicated accuracy for metals of ≤5%.

Net differences in solute loads, ΔX_L (g-N/m^{2}day^{-1}), were calculated for each day as:

$$\Delta X_L = [X]_{depth}\, IR_V - [X]_{surface}\, IR_V \qquad\qquad [1]$$

where [X] is solute concentration and IR_v is the vertical infiltration rate. "Surface" and "depth" subscripts refer to the inflowing water and the deepest piezometer sampled, respectively. Differences in solute loads with depth for samples collected during a single day are interpreted in terms of changes during transport, based on repeated sampling of fluid parcels at multiple depths (e.g., Lagrangian approach). $\Delta X_L > 0$ indicates a net load increase, whereas $\Delta X_L < 0$ indicates net load reduction. When discussing nitrogen species, the aggregate nitrogen load in solution is defined as: $[N]_L$ = $[NO_3]_L$ +$[NO_2]_L$ +$[NH_4]_L$. Net differences in solute concentration were also calculated.

For subsurface samples in each plot, reported values of both solute loads and concentrations are generally the average of two samples collected at each depth, one from each fluid sampling piezometer. Figures showing cumulative load reduction show the range of values measured when there were multiple samples collected from separate piezometers. The variability shown with this range exceeds analytical errors associated with individual to be significant if $p < 0.05$ (Tables S1-3-S1-7).

1.2.5 DNA extraction and phylogenetic sequencing

Methods for microbial analysis of soil samples were similar to those described in previous studies (Beganskas et al., 2018; Gorski et al., 2020, 2019). Briefly, soil DNA was extracted with a PowerSoil DNA Isolation Kit (QIAGEN). The Qubit 4 Fluorometer (Invitrogen) was used to quantify DNA extracts. PCR amplicons (~550 bp) with soil DNA and 16S rRNA gene primers targeting the V4 and V5 variable regions. The PCR amplicon sequencing pipeline used in this study was adapted from Illumina MiSeq platform protocol for 16S metagenomic libraries (Beganskas et al., 2018). The overall pipeline included steps for the primary PCR using 16S rRNA primers (Parada et al., 2016), PCR clean-up, library preparation (adding unique sequencing indices [barcodes] to each PCR amplicon), normalizing DNA concentrations of each library, and library pooling. The pooled library was sequenced on the Illumina MiSeq (600 cycles v3 PE300 flow cell kit) at the University of California, Davis Genome Center. The raw sequence reads have been uploaded to the National Center for Biotechnology Information Sequence Read Archive (accession number: PRJNA787642).

Sequence reads were separated into amplicon sequence variants (ASVs) using the DADA2 algorithm and assigned taxonomy using the QIIME database. Soil samples were grouped by treatment (native soil, wood chips, and 1:1 mixture) and timing (collected before infiltration began or after infiltration was completed) in order to analyze for differences with location and treatment and changes with time. The phyloseq package (v. 1.22.3) in R (v. 3.4.3) was used to calculate and visualize beta (between sample) diversity.

1.3 Results

1.3.1 Infiltration rates and dynamics

Bulk infiltration rates were highest at the start of each test (up to 30 m/day in native soil, 24 m/day in wood chips, and 22 m/day in the 1:1 mixture) and tended to decrease over time (Figure 1-2). The higher initial bulk infiltration rates likely resulted, in part, from saturation of shallow pores after the start of infiltration and rapid lateral flow below the walls of the plots at later times. Over the duration of the tests, average bulk infiltration rates were highest in the native soil and wood chip plots, 14.3±7.2 and 14.3±2.2 m/day, respectively, whereas significantly lower bulk infiltration rates were observed in the plot with the 1:1 mixture PRB, 7±1.0 m/day (Tables S1-1, S1-3).

Vertical infiltration rates (IR_V) as measured with thermal probes were rapid, although considerably lower than bulk infiltration rates. The highest IR_V values were ~4 m/day in the native soil and 1:1 mixture plots, and ~3 m/day in the wood chip PRB plot (Figure 1-2). Over the duration of the tests, average vertical infiltration rates were essentially identical for the three treatments: 2.2±0.7 m/day for native soil, 1.9±0.4 m/day for the wood chip PRB, and 2.2±0.8 m/day for the 1:1 mixture PRB (Table S1-1). Vertical infiltration rates were ~15-25% of bulk rates, indicating a large component of lateral flow in shallow soils below the base of plot walls. This last observation is consistent with earlier plot-scale studies (e.g. Beganskas et al., 2018; Gorski et al., 2019) and for infiltration testing more broadly (Bouwer, 1986; Rice et al., 2013). In inundated fields and in operating MAR infiltration basins that are much wider than
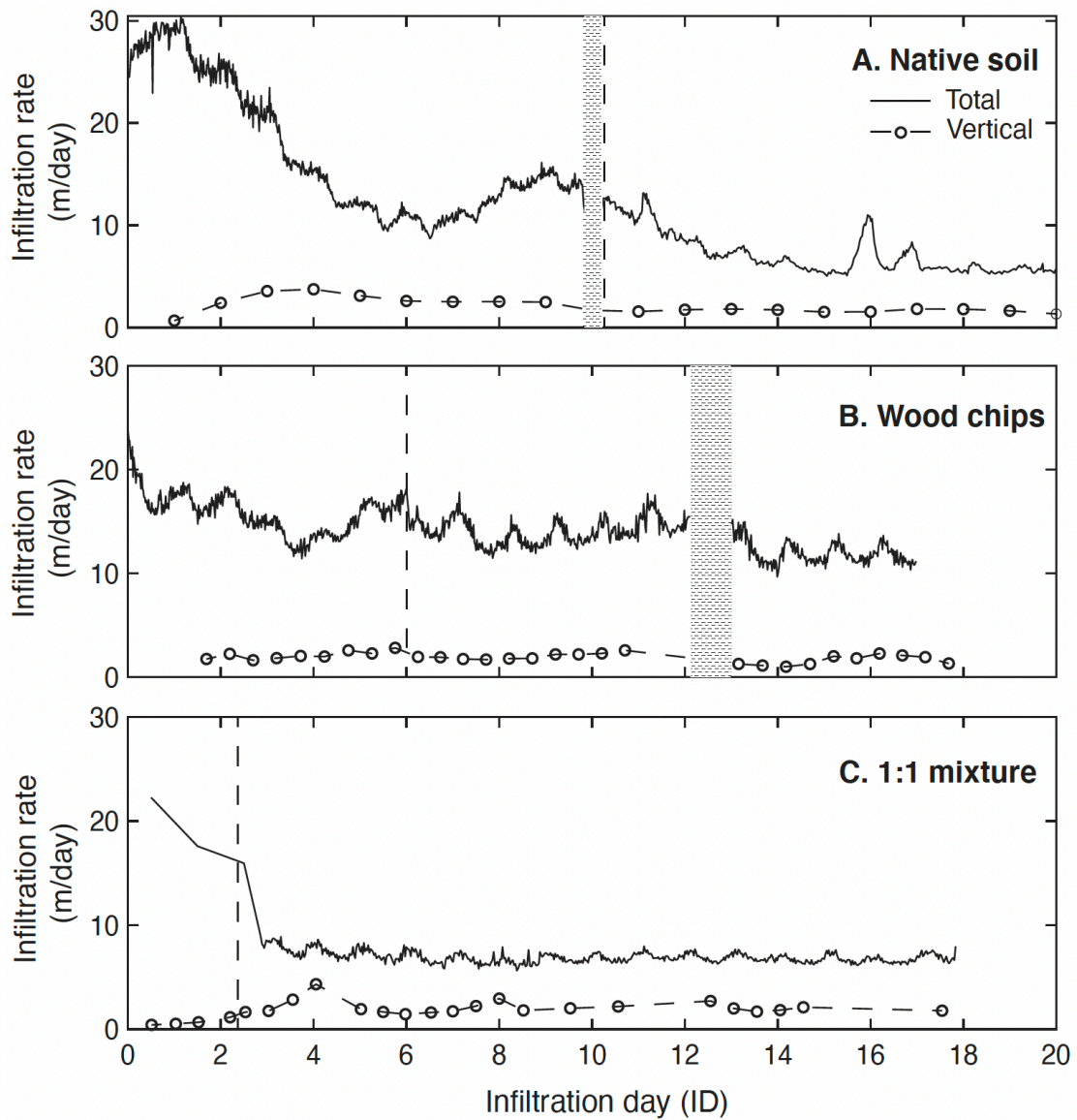
Figure 1-2 Infiltration Rates Total (bulk) and vertical infiltration rates for the native soil (A), wood chip (B), and 1:1 mixture (C) plots. The solid black line indicates the total infiltration rate, while the dashed line indicates vertical infiltration rates. The dashed vertical lines indicate times when the float switch was lowered. Vertical gray bars indicate times when the plot went dry due to float switch failure.

deep, vertical flow is expected to dominate, except adjacent to basin edges and/or where there is extensive textural layering of shallow soils (e.g., Bouwer, 2002).

1.3.2 Soil characterization

Soil properties were generally consistent beneath all three of the plots. Soil samples were coarse, ≥80% sand (Figure S1-2), consistent with soil maps for the field site. TN was very low in all samples, ≤0.05% and with little difference between samples collected before and after infiltration (Figure S1-3). TOC was also low in all samples, with values of 0.05% to 2.0% (Figure S1-3). The soil samples collected below both of the carbon-amended plots after infiltration were generally 0.01-0.05% higher in TOC than were samples collected before infiltration.

1.3.3 Variations in DOC and N load reductions with depth

The chemistry of infiltrating water varied across plots and with depth over time, along with infiltration dynamics and redox conditions (Figures S1-4 and S1-5). There was little change in dissolved organic carbon load ($\Delta[DOC]_L$) in the native soil, whereas there were clear increases in $\Delta[DOC]_L$ in both carbon-amended plots (Figures 1-3A, S1-6). In the native soil plot, daily $\Delta[DOC]_L$ values were small and varied from day to day between addition and removal, with an average of 2.01 g-DOC/m^2 cumulatively removed over 20 days (Figure 1-3A). In the wood chip plot, $\Delta[DOC]_L$ was significantly greater than in native soil (p-value = 0.05), averaging 0.30 g-DOC/m^2/day and accumulating 4.20 g-DOC/m^2 during the full test (Figure 1-3A). The 1:1 mixture plot had higher influent [DOC] than the other two plots (average ~ 4.7 g-DOC/m^2/day compared to 3.1 and 2.6 g-DOC/m^2/day in the native soil and wood chip
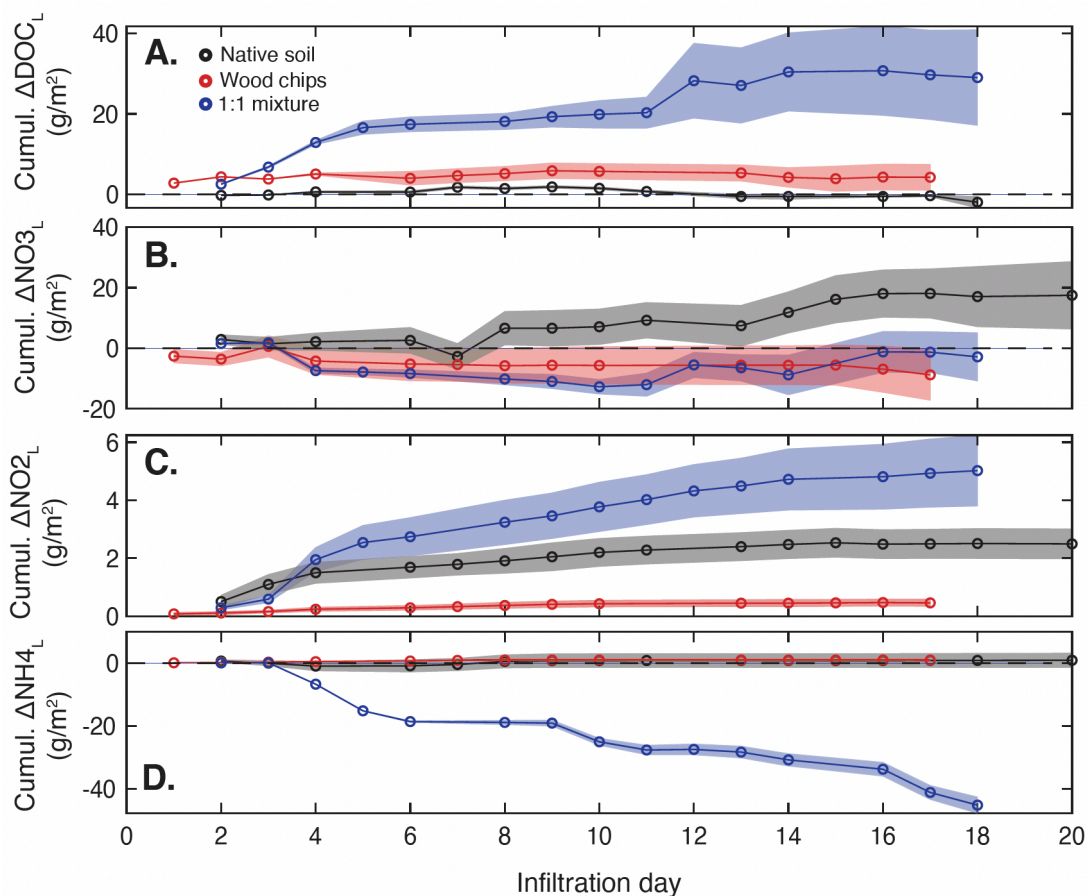
Figure 1-3 Nutrient and DOC load changes Cumulative DOC load (A), NO3-N load (B), NO2-N load (C), and NH4-N load (D) changes over the duration of the percolation experiments for each treatment. The solid lines represent the average cumulative solute load from the two samples collected at each depth. The shaded region shows the range between the highest and lowest cumulative load values from the two samples collected at each depth. Daily variations for these analytes are shown in Figure S1-6.

treatments, respectively). The 1:1 mixture plot also had the most consistently positive $\Delta[DOC]_L$, averaging ~1.9 g-DOC/m^2/day and accumulating 29.0 g-DOC/m^2 over the full test (Figure 3A), more than a 6-fold increase over the wood chip plot.

Daily $\Delta[NO_3^-]_L$ was variable in the native soil plot, with most days resulting in positive values and an average of 17.5 g-NO$_3^-$/m^2 added cumulatively during the test (Figure 1-3B). In the wood chip plot, $\Delta[NO_3^-]_L$ was negative, with an average of 8.80 g-NO$_3^-$/m^2 removed cumulatively (Figure 1-3B). The majority of infiltration days had net [NO$_3$]$_L$ removal in the 1:1 mixture plot, with average daily [NO$_3^-$]$_L$ removal up to 9.21 g-NO$_3^-$/m^2/day and an average of 2.86 g-NO$_3^-$/m^2 removed cumulatively (Figure 1-3B).

Nitrite load addition was observed in all three plots, consistent with active denitrification, despite very rapid infiltration. In the native soil plot, [NO$_2^-$]$_L$ addition was highest at the beginning of the test (infiltration days 1 to 6), with 2.50 g-NO$_2^-$/m^2 of cumulative addition (Figure 1-3C). In the wood chip plot, [NO$_2^-$]$_L$ addition was consistent but modest, with an average total of 0.46 g-NO$_2^-$/m^2 added (Figure 1-3C). Nitrite load addition was highest in the 1:1 mixture plot, with [NO$_2^-$]$_L$ on all infiltration days and an average cumulative addition of 5.02 g-NO$_2^-$/m^2 over the full test (Figure 1-3C).

In the native soil and wood chip plots, [NH$_4^+$] and $\Delta[NH_4^+]_L$ were minimal on all infiltration days (Figure 1-3D), with inflowing [NH$_4^+$]$_L$ < 2.5 g-NH$_4^+$/m^2/day. However, when the test was run in the 1:1 mixture plot, inflowing [NH$_4^+$]$_L$ was much higher, with an average of 6.90 g-NH$_4^+$/m^2/day (Figure S1-6). This was likely due to

differences in the delivered water blend, a mixture of groundwater and recycled wastewater. In the 1:1 mixture plot, $[NH_4^+]_L$ removal was observed on the majority of infiltration days, with a cumulative $[NH_4^+]_L$ reduction $= 45.1$ g-NH_4^+/m^2 (Figure 1-3D).

In native soil, N load reduction for the aggregate of species measured was observed on 4 of 16 infiltration days, with a maximum of 13% N removed on ID-13 and $\Delta N_L = 1.79$ g-N/m^2/day removed on ID-7 (Figure 1-4). However, N load addition was observed for the remaining 12 infiltration days (Figure 1-4B). The cumulative N load addition for native soil was 23.7 g-N/m^2 (Figure 1-4C). The wood chip plot saw limited N load removal, with a maximum of 32% N removal and $\Delta N_L = 4.61$ g-N/m^2 removed on ID-4, and 7.38 g-N/ m^2 removed in total. The 1:1 mixture plot showed the most days with N load removal (11) and had the largest cumulative ΔN_L, 44 g-N/m^2, over 16 days (Figure 1-4). The higher N load removal in the 1:1 mixture plot resulted partly from the higher influent NH_4^+, although the fraction of load removal was greater for many days compared to other plots. Overall, N load removal was significantly greater for both the wood chip and 1:1 mixture plots than for the native soil plot (*p*-values = 0.02 and 0.006, respectively).

1.3.4 Variations in metal load with depth

There were significant changes in $[Mn]_L$ with depth in both of the carbon-amended plots (wood chips and 1:1 mixture) relative to native soil (*p*-values = 6.2E-04 and 0.001, respectively) (Figure 1-5). Native soil saw little to no difference in $[Mn]_L$ with depth, whereas the wood chip and 1:1 mixture plots saw large increases in $\Delta[Mn]_L$ (cumulative $\Delta[Mn]_L$ was 15.9 g-Mn/m^2 in the wood chip plot and 34.7 g-Mn/m^2 in the
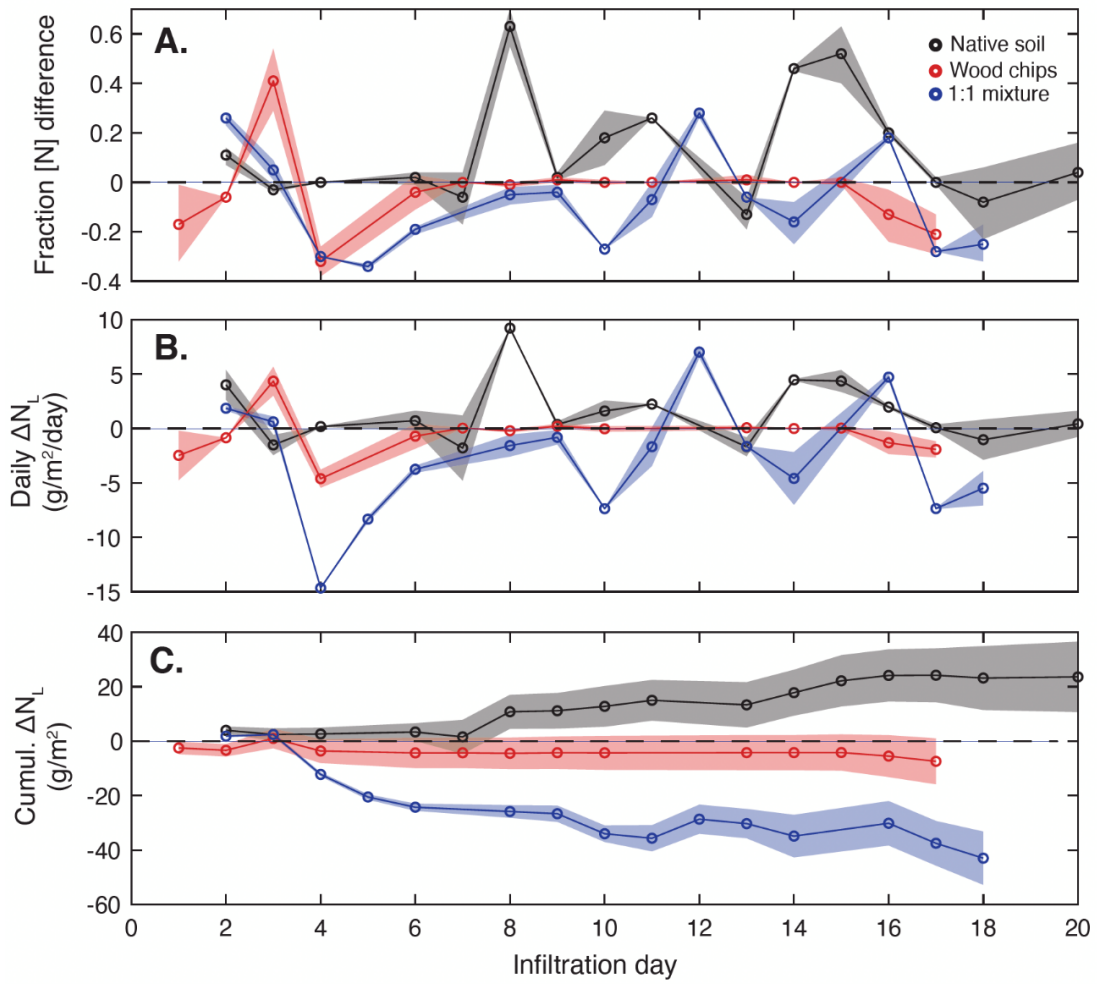
Figure 1-4 N changes The daily fraction of N difference, where positive values indicate N addition and negative values indicate N removal (A). Daily N load reduction for each treatment (B). Cumulative N load reduction of the duration of the tests for each treatment (C).
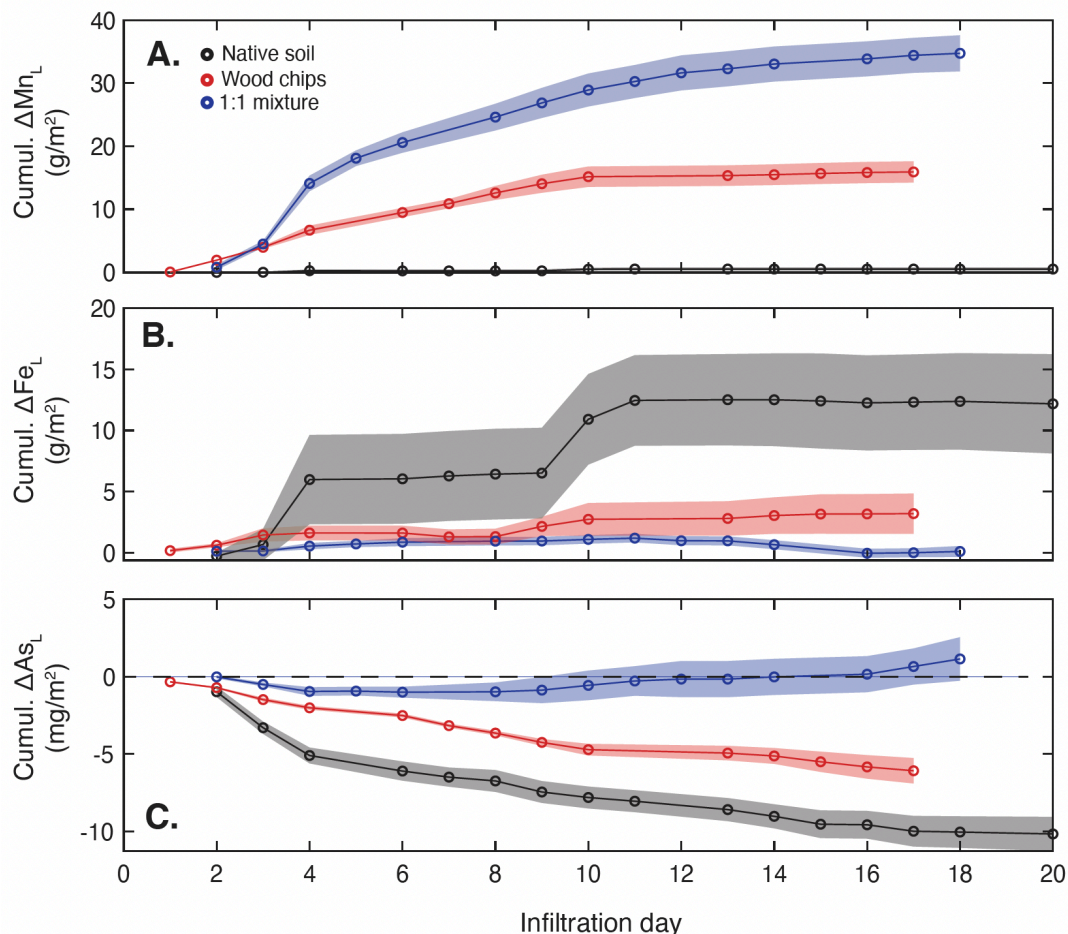
Figure 1-5 Cumulative metals load changes Cumulative Mn load (A), Fe load (B), and As load (C) changes over the duration of the percolation experiments for each treatment. The solid lines represent the average cumulative solute load from the two samples collected at each depth. The shaded region shows the range between the highest and lowest cumulative load values from the two samples collected at each depth. Daily variations for these analytes are shown in Figure 1-S8. Note different scale shown for As data.

1:1 mixture plot) (Figure 1-5A). In both carbon-amended plots, increases in [Mn] were highest during the first 10 days of the tests, then decreased, but remained elevated relative to inflowing water for the remainder of the tests (Figures 1-5 and S1-8).

The native soil plot yielded the largest increases in $[Fe]_L$ with depth (Figure 1-5B). $[Fe]_L$ increased 12.2 g-Fe/m^2/day cumulatively over the duration of the test, with much of the increase occurring on two days: ID-3 (5.31 g-Fe/m^2/day) and ID-10 (4.39 g-Fe/m^2/day) (Figures 1-5 and S1-8). $[Fe]_L$ did not increase as much or as consistently as $[Mn]_L$ in either the plots with wood chip and 1:1 mixture PRBs (Figure 5B), with cumulative values of $\Delta[Fe]_L$ = 3.2 g-Fe/m^2 and 0.1 g-Fe/m^2, respectively.

There was modest $[As]_L$ removal with depth throughout tests with both native soil ($\Delta[As]_L$ = -10 mg-As/m^2) and a wood chip PRB ($\Delta[As]_L$ = -6.1 mg-As/m^2) (Figure 1-5C). The 1:1 mixture plot initially showed $[As]_L$ removal, but there was modest $[As]_L$ addition towards the end of the test, with cumulative $\Delta[As]_L$ = 1.1 mg-As/m^2 (Figure 1-5C). Throughout the tests in all plots, [As] remained well below the WHO recommended limit of 10 μg/L. A summary of all solute load results is presented in Table S1-2.

1.3.5 Microbiological dynamics

Within the samples collected before the experiments, the ten most abundant microbial phyla comprised ~90% of total sequences (Figure 1-6A). The three most abundant phyla were *Actinobacteriota* (20.7%), *Acidobacteriota* (15.7%), and *Chloroflexi* (12.1%), which appear in similar percentages in soils below all three test plots before testing. Following infiltration, the microbial ecology shifted, with the three
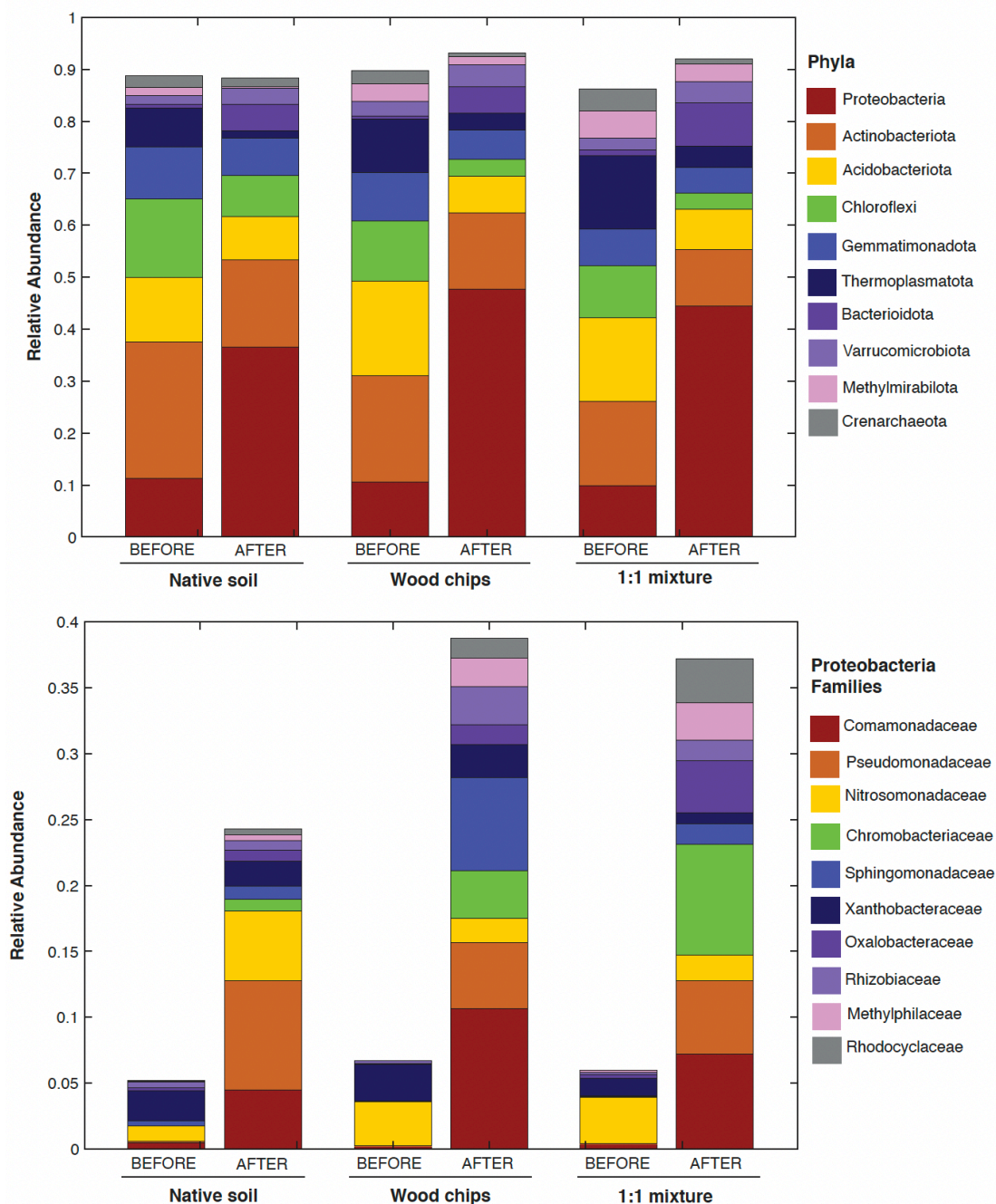
Figure 1-6 Microbiological changes Proportions of the ten most abundant phyla for each treatment before and after infiltration (A). Proportions of the ten most abundant families for each treatment within the phyla Proteobacteria, the most abundant phyla in all treatments in the samples collected after infiltration (B).

most abundant phyla being *Proteobacteria* (42.9%, up from about 10% before testing), *Actinobacteriota* (14.1%), and *Acidobacteriota* (7.78%).

The increased relative abundance in *Proteobacteria* is of particular interest because representatives of this phylum are thought to be responsible for nitrogen fixation in many soils, and are capable of utilizing the denitrification pathway under both anaerobic and aerobic conditions (e.g., Ji et al., 2015; Zumft, 1997). The relative abundance of *Proteobacteria* increased following infiltration in all three plots (Figure 1-6), with the largest increases in relative abundance occurring in the carbon-amended plots. The relative abundance of *Proteobacteria* increased by a factor of 3.2x in native soil and by a factor of 4.5x in both the wood chips and 1:1 mixture.

Within the phylum *Proteobacteria*, the most abundant families before and after infiltration were *Comamonadaceae*, *Pseudomonadaceae*, and *Nitrosomonadaceae* (Figure 1-6B). *Comamonadaceae* is a family of bacteria containing facultative organotrophs that can help to break down wood-derived carbon (Hahn et al., 2010; Nakatsu et al., 2006). After infiltration, the relative abundance of *Comamonadaceae* increased by a factor of 9.7 in the native soil plot, 49 in the wood chip plot, and 19 in the 1:1 mixture plot. *Pseudomonadaceae* includes genera known to perform denitrification and Mn reduction under anaerobic conditions (Arat et al., 2015; Nealson and Myers, 1992). The increases in relative abundance of *Pseudomonadaceae* following infiltration were even greater, with factors of 65x, 146x, and 232x in native soil, wood chip, and 1:1 mixture plots, respectively. The wood chip and 1:1 mixture plots also saw large increases in *Sphingomonadaceae*,

Methylophilaceae, and *Rhodocyclaceae* following infiltration, which all have been shown to be associated with denitrification gene presence or function (Lapidus et al., 2011; Liu et al., 2005; Palacin-Lizarbe et al., 2019; Takeuchi et al., 2001).

The relative abundance of *Nitrosomonadaceae* increased following infiltration in the native soil plot, but decreased in both the wood chip and 1:1 mixture plots. Bacteria in the family *Nitrosomonadaceae* are known to oxidize ammonia into nitrate and assist in the nitrogen fixation process (Koops et al., 1991). The decrease in *Nitrosomonadaceae* following infiltration in the carbon-amended plots is consistent with subsurface conditions that became anaerobic, serving to limit or eliminate nitrogen fixation, and thus favoring microbes that can benefit from the observed shift in redox conditions. Changes in the relative abundance of all Proteobacteria families following infiltration were consistent at all depths within the subsurface (Figure S1-10).

Bacteria of phylum *Planctomyecetes*, which are known to carry out anammox, were present in the soil of all three plots both before and after infiltration in this study, albeit at relatively low abundances (~0.01%).

1.4 Discussion

1.4.1 Mechanisms of N cycling during rapid infiltration

Experimental results from this study show an increase of N removal during infiltration through coarse soils below carbon-amended plots, with considerable variability as a consequence of initial water chemistry and infiltration rate. N cycling during infiltration likely took place via at least three pathways: denitrification, nitrification, and anammox. Denitrification was likely an important pathway for nitrate

removal below both the wood chip and 1:1 mixture plots, as the elevated DOC in water flowing through shallow soils served as a readily available electron donor, accelerating oxygen consumption and leading to more favorable conditions for denitrification. Evidence for denitrification includes the consistent presence of nitrite (Figures 1-3C and S1-6), which is generated as an intermediate product and tends to be depleted rapidly unless there is active production. Further evidence for denitrification includes changes in microbial community structure in the carbon-amended plots (Figure 1-6). Both the wood chip and 1:1 mixture plots saw increases in the relative abundances of the families *Comamonadaceae*, *Pseudomonadaceae*, *Methylophilaceae*, *Rhodocyclaceae* and *Sphingomonadaceae*, all of which contain genera capable of carrying out denitrification.

Nitrate isotopic results were mixed, with some paired measurements (at the surface and at depth) being consistent with fractionation leading to heavier isotopes in residual nitrate (particularly for 1 out of 3 days tested in native soil and 3 out of 5 days tested in the 1:1 mixture plot), but many samples from all plots showed little to no variation with depth (Figure S1-9). The inconsistency of these results may be a consequence of extremely rapid infiltration rates, allowing less opportunity for microbial selection of lighter isotopes, temperature dependence on denitrification rates, and/or overprinting of multiple cycles of nitrification and denitrification (Granger and Wankel, 2016; Osaka et al., 2018; Sebilo et al., 2019).

It is notable that the influent DOC was significantly higher in the 1:1 mixture plot than in the native soil or wood chip plots, and the 1:1 mixture had the highest

overall magnitude of N removal. Higher inflowing DOC could have potentially increased N load removal in the 1:1 mixture plot in addition to the presence of the carbon amendment. Two-way ANCOVA testing suggests that there were significant effects of treatment type (native soil, wood chips, or 1:1 mixture) on N removal ($p = 0.01$), but not the inflowing load of DOC on N load removal ($p = 0.17$), when accounting for both variables simultaneously (Table S1-8). However, the results of the two-way ANCOVA test are somewhat difficult to interpret because, according to an ANOVA test, the two covariates (treatment type and inflowing DOC load) are not independent of each other ($p = 5.6E-4$, Table S1-9). In either case, it is clear that elevated DOC, whether from the inflowing water or as a result of infiltration through the carbon amendment, was associated with elevated rates of N removal.

In addition to DOC, the 1:1 mixture plot also had significantly higher influent ammonium loads. Consequently, the higher magnitude of overall N removal in the 1:1 mixture was associated with higher rates of ammonium availability and removal during infiltration. Nitrifying bacteria and/or anaerobic oxidizing bacteria potentially contributed to observed decreases in ammonium. Like denitrification, anammox also occurs under anaerobic, reducing conditions (Mulder et al., 1995), and thus could have been enhanced by elevated DOC in infiltrating water. Bacteria of phylum *Planctomyecetes*, which are known to include microbes capable of anammox, were present in the soil both before and after infiltration in this study in all plots, albeit at relatively low abundances (~0.01%). Both denitrification and anammox pathways are

considered favorable with respect to transformation of highly reactive NO_3^- into less reactive N_2 gas.

Given the low relative abundances of *Planctomyecetes*, the majority of NH_4^+ load reduction with depth below the 1:1 mixture plot was likely accomplished via nitrification. During nitrification, NH_4^+ is oxidized to NO_3^-, also generating NO_2^- as an intermediate product. However, the majority of days in the 1:1 mixture plot had NO_3^- removal rather than addition. The nitrate produced during nitrification in oxic areas of the subsurface could have been subsequently removed by denitrification in sub-oxic areas of the subsurface, aided by the presence of high DOC in the fluid. Nitrification likely also played a role in the N cycling observed in the native soil plot. There was detectable NH_4^+ in the influent water as well as net NO_3^- and NO_2^- addition in the native soil plot over the duration of the test, which could be an indication that nitrification occurred. Additionally, the native soil plot saw an increase in the relative abundance of *Nitrosomonadaceae* following infiltration, a family of bacteria known to carry out nitrification, whereas both the wood chip and 1:1 mixture plots showed decreases in the relative abundance of *Nitrosomonadaceae* (Figure 1-6B).

The presence of a carbon amendment may promote reducing conditions and increase total N removal in infiltrating water through two primary mechanisms. First, the presence of elevated DOC can provide an electron donor, increasing dissolved oxygen consumption and leading to sub-oxic subsurface conditions that promote both denitrification and anammox. Second, the addition of a carbon-rich PRB can increase the thickness of the saturated zone, and consequently the fluid residence time within

the saturated zone where dissolved oxygen consumption and nitrogen processing, including both denitrification and anammox, can occur most efficiently (Granger et al., 2009; Lepine et al., 2016; Gorski et al., 2019). Because infiltration rates were so rapid in these experiments, DOC addition was modest even in the carbon-amended plots; nevertheless, the evidence for enhanced N cycling is clear.

1.4.2 Impact of a carbon amendment on trace metals

The higher DOC loads associated with the carbon-amended plots also impacted the cycling of As, Mn, and Fe. Persistent increases in Mn with depth were observed in both of the carbon-amended plots, but not in the native soil plot (Figures 1-5A, S1-8A). This is likely due to the development of sub-oxic conditions in the carbon-amended plots, which would both promote removal of nitrate and ammonium via denitrification and anammox, respectively, and enhance Mn release. Solubility calculations suggest that Mn-bearing soil minerals (such as $MnSO_4$(s), pyrochroite, and rhodochrosite) and other solid phases were largely undersaturated in the carbon-amended plots, which could have facilitated Mn mobilization (Tables S1-10 to S1-12). Low pH can increase the mobility of trace metals such as Mn (Appelo and Postma, 1995), but the pH of subsurface fluids was relatively consistent and neutral during all experiments, ranging from 7.4 – 7.6 (Tables S1-10-S1-12).

Fe was variable in all plots throughout the experiments, although the largest increases were observed on three sample days in the native soil plot (Figures 1-5B, S1-8D-F). It is curious that $\Delta[Fe]_L$ increased in the native soil plot during infiltration whereas $\Delta[Mn]_L$ barely changed; this pattern is the opposite of that seen below the

carbon-amended plots, where $\Delta[Mn]_L > \Delta[Fe]_L$. This could suggest that redox conditions in the native soil were more variable than were those in other plots. Both Fe and Mn oxides and hydroxides in the soil can be reduced under anoxic conditions, but the Mn reduction zone has been found to be particularly narrow in some soil-water systems, and conditions in shallow soils could be in thermodynamic disequilibrium (perhaps limited by kinetics) or subject to linked Fe-NO_3 cycling that favors Fe mobilization (Christensen et al., 2000; Desireddy and Pothanamkandathil Chacko, 2021; Hamer et al., 2020). Additionally, solubility calculations suggest that Fe-bearing soil minerals (such as siderite, vivianite, melanterite, and $Fe(OH)_2$) were undersaturated in the native soil as well as the carbon-amended plots, which could have contributed to Fe mobilization (Tables S1-10, S1-11, and S1-12). However, in the carbon-amended plots, mobilized Fe could have adsorbed to DOC, reducing the concentrations of dissolved Fe relative to the native soil (Riedel et al., 2013). These contrasting ΔMn and ΔFe results suggest that different physical and chemical controls may explain conditions below the carbon-amended and native soil plots.

Arsenic generally decreased with depth during infiltration, particularly in the native soil and wood chip plots. Arsenic removal was highest in the native soil plot, which could have resulted from somewhat more oxic (less reducing) conditions facilitating As adsorption in the shallow subsurface. The presence of a carbon amendment led to a reduction of As removal for the entirety of the test below the wood chip plot and for the majority of days below the 1:1 mixture plot. However, there were a few days during the last half of the experiment during which As increased below the

1:1 mixture plot, perhaps in response to more strongly reducing conditions (Figures 1-5C, S1-8) and/or shifts in inflowing water chemistry. A recent study of riverbank filtration found that the release of Fe and As from shallow aquifer media occurred through a combination of desorption of exchangeable Fe and As, dissolution of Fe-Mn oxides, and oxidation of Fe-bound organic matter (Bai et al., 2018; Wang et al., 2020). The inconsistency of day-to-day Fe and As during our experiments could result from rapid and highly localized shifts in redox zonation, with adjacent areas favoring contrasting conditions, microbial communities, and/or metal mobilization pathways (Hassan et al., 2015; Su et al., 2018).

We also note that although some elevated values of Mn, Fe, and As were observed in inflowing water and within the subsurface, all measured values were below WHO guidelines and did not pose a water quality concern in this setting. In addition, below an operating MAR basin, passage of infiltrating water through the underlying vadose zone (typically ≥20-m thick in this region) where oxic conditions are expected to dominate, should provide opportunities for readsorption of metals that may be mobilized during rapid infiltration through a thin zone of saturated soil. Results from the present study help to motivate investigation of the speciation of trace metals during infiltration for MAR, to elucidate specific mechanisms of Mn, Fe, and As mobilization, transport, and readsorption during managed recharge operations.

1.4.3 Impact of initial N load on water chemistry

In this section, we compare relationship between inflowing N load (N_L) and the fraction of N removed in this study to those found in previous field and laboratory

(column) experiments, using a variety of soils, in the same groundwater basin (Figure 1): Kitayama Ranch (KTYA, eolian sediments), Kelly-Thompson Ranch (KTR, flood plain and levee deposits), Harkins Slough (HSP, eolian and fluvial sediments), and Storrs Winery (STR, alluvial fan deposits) (Beganskas et al., 2018; Gorski et al., 2019; Gorski et al., 2020). Using the initial N load (N_L) as the independent variable accounts for aggregate differences in inflowing N and flow rates in the various experiments. All of these studies explored processes occurring with and without elevated DOC in infiltrating fluid.

The combined datasets, drawn from all sites tested, show an exponential decrease in N as a function of incoming load (Figure 1-7). Individual studies focused on specific sets of soil and experimental conditions, but the influence of elevated DOC appears to be relatively consistent across the sites. For tests with native soils, the fraction of N removed decreases exponentially as $N_{frac} = 1.81e^{-1.09NL}$, with minimal N removal for incoming loads >5 g-N/m^{2}day^{-1} (Figure 1-7A). With the addition of a carbon amendment and associated increases in DOC, the exponential decay of N_{frac} versus load is more gradual, with $N_{frac} = 1.34e^{-0.44NL}$ for a wood chip PRB (Figure 1-7B) and $N_{frac} = 1.58^{-0.51NL}$ for a PRB comprising a 1:1 mixture of wood chips and native soil (Figure 1-7C). In both sets of tests with carbon-amended soils, response curves are shifted to the right (higher incoming loads) with measurable benefits in N removal extending up to ~10 g-N/ m^{2}day^{-1}, about twice the limit for N removal in native soils. The 1:1 mixture treatment in the current study was accompanied by somewhat elevated DOC in inflowing water, but other studies had low influent DOC and still saw
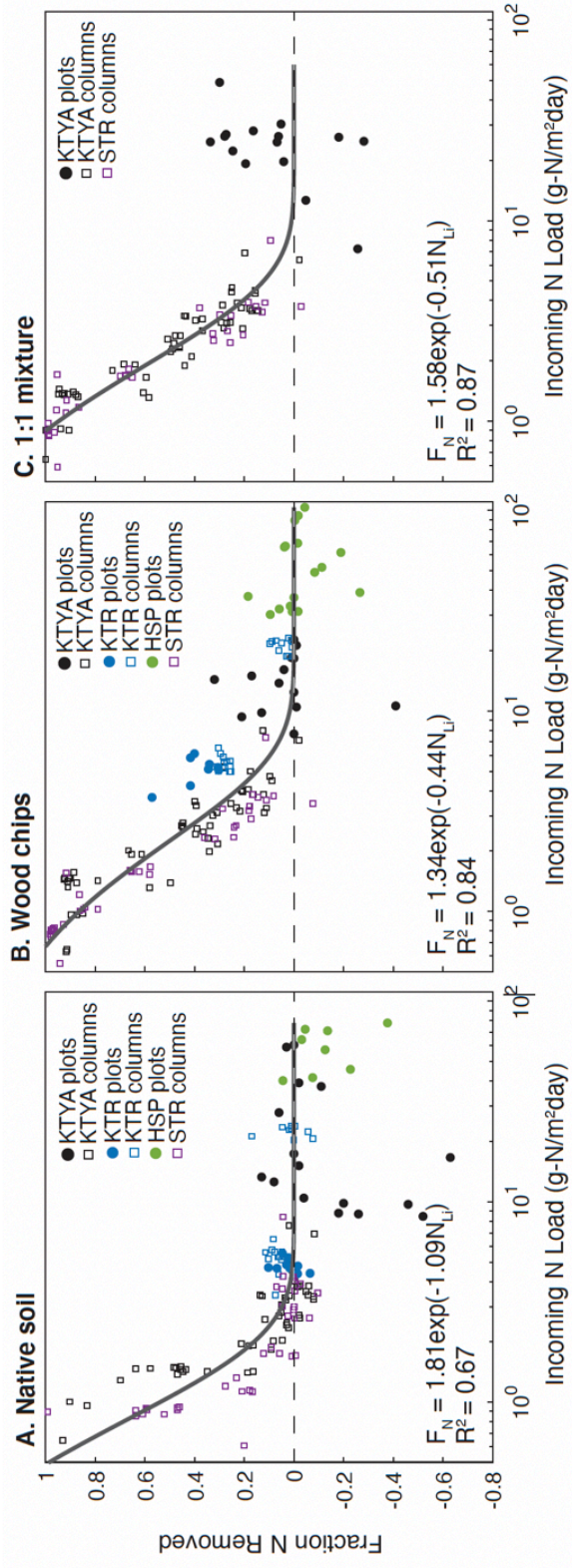
Figure 1-7 Effect of inflowing N load by treatment The fraction of N removed as a function of incoming N load (inflowing mass of N x vertical infiltration rate) for this and previous studies for different treatments – native soil (A), wood chips (B), and 1:1 mixture of wood chips and native soil (C). Grey lines on each panel show exponential fits with fitted constants shown, where F_N is the fraction of N removed and N_{Li} is the incoming N load.

33

systematic shifts in the fraction of N removed. Thus, the application of a carbon-rich soil amendment, as either a woodchip PRB or a 1:1 mixture of woodchips and native soil, appears to increase the fraction of N that can be removed at equivalent incoming N loads, suggesting the potential to enhance the quality of water infiltrated for MAR (Figure 1-8). Data from the present study are consistent with the overall trends defined by the data compilation, although results are more variable, which is not surprising given the high infiltration rates involved (≥ 1 m/day).

This composite analysis with samples and data from multiple sites suggests that the incoming N load can be considered a fundamental control on the extent of N removal during infiltration under a range of physical and geochemical conditions, provided there is sufficient DOC present to allow development of appropriate redox conditions. The load tests the capacity of soil microbial communities to keep up with delivery of carbon and nutrients. Slower infiltration rates (associated with lower incoming N loads) increase the fluid residence time and allow for more extensive development of sub-oxic to anoxic conditions in the shallow subsurface, which enhances N removal processes such as denitrification and annamox. With faster infiltration, soil microbes have a harder time removing greater amounts of entrained oxygen, and redox conditions remain more oxic and/or more variable, with isolated zones of modestly elevated N processing.

1.4.4 Linking infiltration, geochemistry, and microbial ecology during MAR

Experimental results from this study demonstrate the benefits of increasing DOC in infiltrating fluids during MAR, and points to complexity in relationships
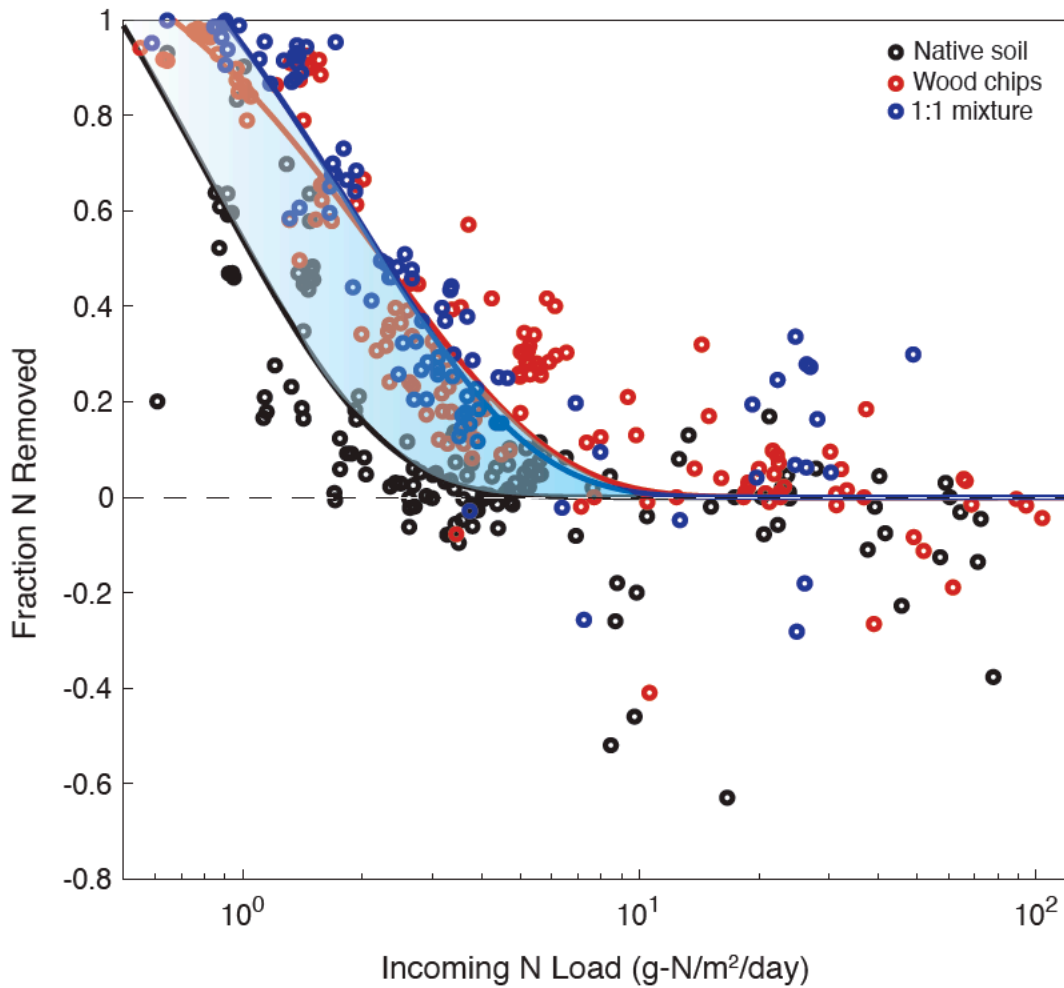
Figure 1-8 Effect of inflowing N load, all studies and settings (field, laboratory)
The fractions of N removed as a function of inflowing N load (inflowing mass of N x vertical infiltration rate) for this and previous studies, where all studies are grouped by treatment (native soil, wood chips, and 1:1 mixture). Positive fractions of N values indicate N removal, while negative fractions of N values indicate N addition. Solid lines for each treatment show the exponential fit. Shaded blue area indicates the enhanced fraction N removed benefit when applying a carbon amendment (wood chips or 1:1 mixture).

between use of a PRB, infiltration rate, substrate composition, water chemistry, and soil microbial ecology. As with non-traditional water sources generally, there was considerable variability in the geochemistry of the inflowing water. Nonetheless, the impacts observed are large enough to be clearly expressed, whether higher DOC occurs within incoming fluid or is provided by a carbon-rich PRB. Soil sample analyses indicated that microbes capable of carrying out N removal were present in the soil prior to infiltration and increased in relative abundance as a consequence of infiltration. The increase in putative denitrifying taxa in all three plots indicates that these soils likely have the potential for more extensive NO_3^- removal at lower infiltration rates, which commonly develop over time in operating recharge basins due to compaction, sediment accumulation, and other processes (Bouwer, 2002; Beganskas and Fisher, 2017; Zaidi et al., 2020).

Microbes of the phylum *Planctomycetes*, which are capable of carrying out anammox, were also present in the soil both before and after infiltration in all plots and may have facilitated rapid NH_4^+ removal in the plot with the 1:1 mixture amendment, which had elevated NH_4^+ in inflowing water. Although enhanced N cycling was accompanied in some cases by mobilization of metals from shallow soils, elevations of metals concentrations were modest, and there should be opportunity for oxidation and readsorption in the vadose zone above the regional water table. Overall, the higher loads of DOC in infiltrating water, either as inflow or with the addition of a bio-available carbon from a PRB, allowed for a greater range of infiltration rates under which water quality improvement was possible. This is important for managed recharge

systems in which there are rapid infiltration rates and non-traditional surface water sources (e.g., stormwater, recycled water) that would benefit from water quality improvement.

Understanding the relationship between infiltration, geochemistry, and microbial ecology is critical for optimizing the performance and operation of managed recharge systems. The present study was completed at a single site and at a plot scale, but other studies have found similar results from plot studies and at larger and smaller scales (Gorski et al., 2019; Grau-Martínez et al., 2018a; Schmidt et al., 2012, 2011). At the scale of an operating MAR infiltration basin, one should expect considerable soil heterogeneity (Beganskas and Fisher, 2017; Racz et al., 2012), which is likely to cause to differences in both rates of infiltration and contaminant cycling. When there are goals for improving both water supply and water quality, these systems might benefit from greater control of infiltration rates, to increase the fluid residence time and encourage development of a thicker and more reactive shallow soil layer. As a practical matter, creating a carbon-rich PRB in an operating MAR basin is relatively inexpensive and simple, mainly requiring spreading and disking-in of a suitable material that is locally available. Maintenance for a MAR system that uses a PRB with a mixture of soil and supplemental carbon, such as wood chips, is also relatively easy, as this approach permits scraping using standard agricultural equipment followed by disking to open up soil pores. Additional carbon can be added over time as may be needed.

There are challenges associated with optimization of MAR systems for improvement to water quality. Slower infiltration rates can enhance N removal, but can

also mobilize geogenic contaminants such as trace metals (Fakhreddine et al., 2021). Complex interactions between soil type and properties, bio-available carbon, infiltration rates, and additional factors require care in designing and operating MAR systems to achieve multiple goals and avoid degradation of essential resources. This study helps to motivate additional work in operating MAR systems that will help to define the range of conditions under which benefits during MAR can be generated and degradation to water quality can be avoided.

1.5 Conclusions

This study has shown how elevated DOC, including that released by a carbon-rich PRB, encourages nitrogen and trace metal cycling, in association with shifts in soil microbial ecology, during infiltration at rapid infiltration rates (>1 m/day) through coarse and carbon-poor soil. Experimental plots that used carbon-rich PRBs resulted in higher pore-fluid dissolved organic carbon concentrations and loads, and lower N loads, compared to results in native soil under similar hydrologic conditions. Experimental results were highly dynamic from day to day, with changes in inflowing fluid chemistry and as redox conditions likely shifted from oxic to sub-oxic or anoxic over short length and time scales. Nevertheless, cumulative calculations show that the introduction of bio-available carbon during rapid infiltration can help to improve water quality. The application of a carbon amendment increased the fraction of N that can be removed at equivalent inflowing N loads at rates consistent with findings from previous studies. Notably, a 1:1 mixture of native soil and wood chips appeared to be similarly efficient for N removal compared to wood chips alone, despite the mixed layer

containing a smaller volume of wood chips. This suggests that in both of the carbon-amended plots, there was no DOC limitation for N cycling in infiltrating water below the PRB (whether this DOC came from inflowing water or the PRB). These results also suggest that there may be benefits to keeping the PRB carbon source in close proximity to soil microbial communities, as was achieved with a PRB comprising a mixture of native soil and a carbon amendment.

These experiments also showed that, in additional to enhancing N cycling, shifting redox conditions can contribute to mobilization of Mn and (to a lesser extent) Fe and As in the soils tested. Concentrations of these metals in soil pore fluid remained well below actionable levels in this study, but under slower infiltration and/or more reducing conditions, additional metal mobilization could occur. This illustrates challenges inherent in operating MAR systems for improvement to multiple water quality parameters: improvement in one could contribute to degradation in another.

Experimental results from this and related studies indicate that both water quality and quantity can be improved during managed recharge, even during rapid infiltration. Mixing in an inexpensive carbon amendment, such as wood chips, can be particularly helpful in removing nitrogen species, which are common contaminants in surface water and groundwater in basins developed for agriculture. Given increased threats to groundwater supply and quality facing water-stressed regions worldwide, incorporating bio-available carbon as part of designing and operating managed infiltration projects should be assessed as a more common practice.

REFERENCES

Abusallout, I., Hua, G., 2017. Characterization of dissolved organic carbon leached from a woodchip bioreactor. Chemosphere 183, 36–43. https://doi.org/10.1016/j.chemosphere.2017.05.066

Addy, K., Gold, A.J., Christianson, L.E., David, M.B., Schipper, L.A., Ratigan, N.A., 2016. Denitrifying bioreactors for nitrate removal: A meta-analysis. J. Environ. Qual. 45, 873–881. https://doi.org/10.2134/jeq2015.07.0399

Alam, S., Borthakur, A., Ravi, S., Gebremichael, M., Mohanty, S.K., 2021. Managed aquifer recharge implementation criteria to achieve water sustainability. Sci. Total Environ. 768, 144992. https://doi.org/10.1016/J.SCITOTENV.2021.144992

Appelo, C.A.J., Postma, D., 1995. Geochemsitry, Groundwater, and Pollution, 2nd Editio. ed. CRC Press, London.

Arat, S., Bullerjahn, G.S., Laubenbacher, R., 2015. A network biology approach to denitrification in Pseudomonas aeruginosa. PLoS One 10, 1–12. https://doi.org/10.1371/journal.pone.0118235

ASTM:D3385-94, 2009. Standard Test Method for Infiltration Rate of Soils in Field Using Double-Ring Infiltrometer. ASTM Stand. Int. D3385-09, 1–7. https://doi.org/10.1520/D3385-09.responsibility

Bachand, P.A.M., Roy, S.B., Choperena, J., Cameron, D., Horwath, W.R., 2014. Implications of using on-farm flood flow capture to recharge groundwater and mitigate flood risks along the Kings River, CA. Environ. Sci. Technol. 48, 13601–13609. https://doi.org/10.1021/es501115c

Bai, J., Su, X., Yuan, W., 2018. Release of arsenic and iron in aquifer to groundwater under the variation of REDOX environment during bank infiltration: a case study in Huangjia groundwater source area, Northeastern China. Hum. Ecol. Risk Assess. An Int. J. 25, 1594–1614.

Baskaran, V., Patil, P.K., Antony, M.L., Avunje, S., Nagaraju, V.T., Ghate, S.D., Nathamuni, S., Dineshkumar, N., Alavandi, S. V., Vijayan, K.K., 2020.

Microbial community profiling of ammonia and nitrite oxidizing bacterial enrichments from brackishwater ecosystems for mitigating nitrogen species. Sci. Rep. 10, 1–11. https://doi.org/10.1038/s41598-020-62183-9

Beganskas, S., Fisher, A.T., 2017. Coupling distributed stormwater collection and managed aquifer recharge: Field application and implications. J. Environ. Manage. 200, 366–379. https://doi.org/10.1016/j.jenvman.2017.05.058

Beganskas, S., Gorski, G., Weathers, T., Fisher, A.T., Schmidt, C., Saltikov, C., Redford, K., Stoneburner, B., Harmon, R., Weir, W., 2018. A horizontal permeable reactive barrier stimulates nitrate removal and shifts microbial ecology during rapid infiltration for managed recharge. Water Res. 144, 274–284. https://doi.org/10.1016/j.watres.2018.07.039

Böhlke, J.K., Wanty, R., Tuttle, M., Delin, G., Landon, M., 2002. Denitrification in the recharge area and discharge area of a transient agricultural nitrate plume in a glacial outwash sand aquifer, Minnesota. Water Resour. Res. 38, 10-1-10–26. https://doi.org/10.1029/2001wr000663

Borch, T., Kretzscmar, R., Kappler, A., Van Cappellen, P., Ginder-Vogel, M., Voegelin, A., Campbell, K., 2010. Biogeochemical Redox Processes and their Impact on Contaminant Dynamics. Environ. Sci. Technol. 44, 15–23.

Bouwer, H., 2002a. Artificial recharge of groundwater: Hydrogeology and engineering. Hydrogeol. J. 10, 121–142. https://doi.org/10.1007/s10040-001-0182-4

Bouwer, H., 2002b. Artificial recharge of groundwater: hydrogeology and engineering. Hydrogeol. J. 121–142.

Bouwer, H., 1986. Intake Rate: Cylinder Infiltrometer. Methods Soil Anal. Part 1 Phys. Mineral. Methods 825–855.

Bouwer, H., 1977. Land Subsidence and Cracking Due to Groundwater Depletion. Ground Water 15, 358–364.

Bouwer, H., Back, J.T., Oliver, J.M., 1999. Predicting infiltration and ground-water mounds for artificial recharge.

Burri, N.M., Weatherl, R., Moeck, C., Schirmer, M., 2019. A review of threats to groundwater quality in the anthropocene. Sci. Total Environ. 684, 136–154. https://doi.org/10.1016/j.scitotenv.2019.05.236

Casciotti, K.L., Sigman, D.M., Hastings, M.G., Bohlke, J.K., Hilkert, A., 2002. Measurement of the oxygen isotopic composition of nitrate in seawater and freshwater using the denitrifier method. Anal. Chem. 74, 4905–4912.

CH2M Hill, 1992. Santa Clara Valley Groundwater Model Project - Basin Groundwater Flow Model.

Chen, P.Z., Cui, J.Y., Hu, L., Zheng, M.Z., Cheng, S.P., Huang, J.W., Mu, K.G., 2014. Nitrogen removal improvement by adding peat in deep soil of subsurface wastewater infiltration system. J. Integr. Agric. 13, 1113–1120. https://doi.org/10.1016/S2095-3119(13)60401-3

Christensen, T.H., Bjerg, P.L., Banwart, S.A., Jakobsen, R., Heron, G., Albrechtsen, H.J., 2000. Characterization of redox conditions in groundwater contaminant plumes. J. Contam. Hydrol. 45, 165–241. https://doi.org/10.1016/S0169-7722(00)00109-1

Chu, L., Wang, J., 2017. Denitrification of groundwater using a biodegradable polymer as a carbon source: Long-term performance and microbial diversity. RSC Adv. 7, 53454–53462. https://doi.org/10.1039/c7ra11151g

City of Santa Cruz Water Department, 2021. City of Santa Cruz Water Department Consumer Confidence Report 2021.

Dahlke, H.E., Brown, A.G., Orloff, S., Putnam, D.H., O'Geen, T., 2018a. Managed winter flooding of alfalfa recharges groundwater with minimal crop damage. Calif. Agric. 72, 65–75.

Dahlke, H.E., LaHue, G.T., Mautner, M.R.L., Murphy, N.P., Patterson, N.K., Waterhouse, H., Yang, F., Foglia, L., 2018b. Chapter 8 - Managed Aquifer Recharge as a Tool to Enhance Sustainable Groundwater Management in California: Examples from Field and Modeling Studies. Adv. Chem. Pollution, Environ. Manag. Prot. 3, 215–275.

Desireddy, S., Pothanamkandathil Chacko, S., 2021. A review on metal oxide (FeOx/MnOx) mediated nitrogen removal processes and its application in wastewater treatment, Reviews in Environmental Science and Biotechnology. Springer Netherlands. https://doi.org/10.1007/s11157-021-09581-1

Dillon, P., 2005. Future management of aquifer recharge. Hydrogeol. J. 13, 313–316. https://doi.org/10.1007/s10040-004-0413-6

Dillon, P., Pavelic, P., Toze, S., Rinck-Pfeiffer, S., Martin, R., Knapton, A., Pidsley, D., 2006. Role of aquifer storage in water reuse. Desalination. https://doi.org/10.1016/j.desal.2005.04.109

Doussan, C., Ledoux, E., Detay, M., 1998. River-Groundwater Exchanges, Bank Filtration, and Groundwater Quality: Ammonium Behavior. J. Environ. Qual. 27, 1418–1427. https://doi.org/10.2134/jeq1998.00472425002700060019x

Exner, M.E., Hirsh, A.J., Spalding, R.F., 2014. Nebraska's groundwater legacy: Nitrate contamination beneath irrigated cropland. Water Resour. Res. 50, 4474–4489. https://doi.org/10.1002/2013WR015073.Received

Fakhreddine, S., Dittmar, J., Phipps, D., Dadakis, J., Fendorf, S., 2015. Geochemical Triggers of Arsenic Mobilization during Managed Aquifer Recharge. Environ. Sci. Technol. 49, 7802–7809. https://doi.org/10.1021/acs.est.5b01140

Fakhreddine, S., Prommer, H., Scanlon, B.R., Ying, S.C., Nicot, J.P., 2021. Mobilization of arsenic and other naturally occurring contaminants during managed aquifer recharge: A critical review. Environ. Sci. Technol. 55, 2208–2223. https://doi.org/10.1021/acs.est.0c07492

Fendorf, S., Nico, P.S., Kocar, B.D., Masue, Y., Tufano, K.J., 2010. Arsenic Chemistry in Soils and Sediments. Dev. Soil Sci. 34, 357–378. https://doi.org/10.1016/S0166-2481(10)34012-8

Fryar, A.E., Macko, S.A., Mullican, W.F., Romanak, K.D., Bennett, P.C., 2000. Nitrate reduction during ground-water recharge, Southern High Plains, Texas. J. Contam. Hydrol. 40, 335–363. https://doi.org/10.1016/S0169-7722(99)00059-5

Ginige, M.P., Kaksonen, A.H., Morris, C., Shackelton, M., Patterson, B.M., 2013.

Bacterial community and groundwater quality changes in an anaerobic aquifer during groundwater recharge with aerobic recycled water. FEMS Microbiol. Ecol. 85, 553–567. https://doi.org/10.1111/1574-6941.12137

Gorski, G., Dailey, H., Fisher, A.T., Schrad, N., Saltikov, C., 2020. Denitrification during infiltration for managed aquifer recharge: Infiltration rate controls and microbial response. Sci. Total Environ. 727. https://doi.org/10.1016/j.scitotenv.2020.138642

Gorski, G., Fisher, A.T., Beganskas, S., Weir, W.B., Redford, K., Schmidt, C., Saltikov, C., 2019. Field and Laboratory Studies Linking Hydrologic, Geochemical, and Microbiological Processes and Enhanced Denitrification during Infiltration for Managed Recharge. Environ. Sci. Technol. 53, 9491–9501. https://doi.org/10.1021/acs.est.9b01191

Granger, J., Wankel, S.D., 2016. Isotopic overprinting of nitrification on denitrification as a ubiquitous and unifying feature of environmental nitrogen cycling. Proc. Natl. Acad. Sci. U. S. A. 113, E6391–E6400. https://doi.org/10.1073/pnas.1601383113

Grau-Martínez, A., Folch, A., Torrentó, C., Valhondo, C., Barba, C., Domènech, C., Soler, A., Otero, N., 2018a. Monitoring induced denitrification during managed aquifer recharge in an infiltration pond. J. Hydrol. https://doi.org/10.1016/j.jhydrol.2018.03.044

Grau-Martínez, A., Folch, A., Torrentó, C., Valhondo, C., Barba, C., Domènech, C., Soler, A., Otero, N., 2018b. Monitoring induced denitrification during managed aquifer recharge in an infiltration pond. J. Hydrol. 561, 123–135. https://doi.org/10.1016/j.jhydrol.2018.03.044

Greenan, C.M., Moorman, T.B., Parkin, T.B., Kaspar, T.C., Jaynes, D.B., 2009. Denitrification in Wood Chip Bioreactors at Different Water Flows. J. Environ. Qual. 38, 1664–1671.

Hahn, M.W., Kasalický, V., Jezbera, J., Brandt, U., Šimek, K., 2010. Limnohabitans australis sp. nov., isolated from a freshwater pond, and emended description of

the genus Limnohabitans. Int. J. Syst. Evol. Microbiol. 60, 2946–2950. https://doi.org/10.1099/ijs.0.022384-0

Halaburka, B.J., Lefevre, G.H., Luthy, R.G., 2017. Evaluation of Mechanistic Models for Nitrate Removal in Woodchip Bioreactors. Environ. Sci. Technol. 51, 5156–5164.

Hamer, K., Gudenschwager, I., Pichler, T., 2020. Manganese (Mn) concentrations and the mn-fe relationship in shallow groundwater: Implications for groundwater monitoring. Soil Syst. 4, 1–19. https://doi.org/10.3390/soilsystems4030049

Hanson, R.T., Schmid, W., Faunt, C.C., Lockwood, B., 2010. Simulation and Analysis of Conjunctive Use with MODFLOW's Farm Process. Ground Water 48, 674–689.

Hartog, N., Stuyfzand, P.J., 2017. Water quality considerations on the rise as the use of managed aquifer recharge systems widens. Water (Switzerland) 9. https://doi.org/10.3390/w9100808

Hassan, Z., Sultana, M., van Breukelen, B.M., Khan, S.I., Roling, W.F.M., 2015. Diverse arsenic- and iron-cycling microbial communities in arsenic-contaminated aquifers used for drinking water in Bangladesh. FEMS Microbiol. Ecol. 91.

Hatch, C.E., Fisher, A.T., Revenaugh, J.S., Constantz, J., Ruehl, C., 2006. Quantifying surface water-groundwater interactions using time series analysis of streambed thermal records: Method development. Water Resour. Res. 42, 1–14. https://doi.org/10.1029/2005WR004787

Heeren, D.M., Fox, G.A., Storm, D.E., 2013. Berm Method for Quantification of Infiltration at the Plot Scale in High Conductivity Soils. J. Hydrol. Eng. 19, 457–461. https://doi.org/10.1061/(asce)he.1943-5584.0000802

Hellauer, K., Karakurt, S., Sperlich, A., Burke, V., Massmann, G., Hübner, U., Drewes, J.E., 2018a. Establishing sequential managed aquifer recharge technology (SMART) for enhanced removal of trace organic chemicals: Experiences from field studies in Berlin, Germany. J. Hydrol.

https://doi.org/10.1016/j.jhydrol.2017.09.044

Hellauer, K., Karakurt, S., Sperlich, A., Burke, V., Massmann, G., Hübner, U., Drewes, J.E., 2018b. Establishing sequential managed aquifer recharge technology (SMART) for enhanced removal of trace organic chemicals: Experiences from field studies in Berlin, Germany. J. Hydrol. 563, 1161–1168. https://doi.org/10.1016/j.jhydrol.2017.09.044

Hellauer, K., Mergel, D., Ruhl, A.S., Filter, J., Hübner, U., Jekel, M., Drewes, J.E., 2017. Advancing sequential managed aquifer recharge technology (SMART) using different intermediate oxidation processes. Water 9, 1–14. https://doi.org/10.3390/w9030221

Hellman, M., Bonilla-Rosso, G., Widerlund, A., Juhanson, J., Hallin, S., 2019. External carbon addition for enhancing denitrification modifies bacterial community composition and affects CH4 and N2O production in sub-arctic mining pond sediments. Water Res. 158, 22–33. https://doi.org/10.1016/j.watres.2019.04.007

Hellman, M., Valhondo, C., Martínez-Landa, L., Carrera, J., Juhanson, J., Hallin, S., 2022. Nitrogen Removal Capacity of Microbial Communities Developing in Compost- and Woodchip-Based Multipurpose Reactive Barriers for Aquifer Recharge With Wastewater. Front. Microbiol. 13, 1–11. https://doi.org/10.3389/fmicb.2022.877990

Herrera-García, G., Ezquerro, P., Tomas, R., Béjar-Pizarro, M., López-Vinielles, J., Rossi, M., Mateos, R.M., Carreón-Freyre, D., Lambert, J., Teatini, P., Cabral-Cano, E., Erkens, G., Galloway, D., Hung, W.C., Kakar, N., Sneed, M., Tosi, L., Wang, H., Ye, S., 2021. Mapping the global threat of land subsidence. Science (80-.). 371, 34–36. https://doi.org/10.1126/science.abb8549

Hiscock, K.M., Bense, V.F., 2014. Chapter 2, in: Hydrogeology: Principles and Practice. Wiley, pp. 34–35.

Hoagland, B., Schmidt, C., Russo, T.A., Adams, R., Kaye, J., 2019. Controls on nitrogen transformation rates on restored floodplains along the Cosumnes River,

California. Sci. Total Environ. 649, 979–994. https://doi.org/10.1016/j.scitotenv.2018.08.379

Holtman, K.M., Offeman, R.D., Franqui-Villanueva, D., Bayati, A.K., Orts, W.J., 2015. Countercurrent extraction of soluble sugars from almond hulls and assessment of the bioenergy potential. J. Agric. Food Chem. 63, 2490–2498. https://doi.org/10.1021/jf5048332

Hoover, N.L., Bhandari, A., Soupir, M.L., Moorman, T.B., 2016. Woodchip Denitrification Bioreactors: Impact of Temperature and Hydraulic Retention on Nitrate Removal. J. Environ. Qual. 45, 803–812.

Jessen, S., Postma, D., Thorling, L., Muller, S., Leskela, J., Engesgaard, P., 2017. Decadal variations in groundwater quality: A legacy from nitrate leaching and denitrification by pyrite in a sandy aquifer. Water Resour. Res. 53, 184–198. https://doi.org/10.1111/j.1752-1688.1969.tb04897.x

Ji, B., Yang, K., Zhu, L., Jiang, Y., Wang, H., Zhou, J., Zhang, H., 2015. Aerobic denitrification: A review of important advances of the last 30 years. Biotechnol. Bioprocess Eng. 20, 643–651. https://doi.org/10.1007/s12257-015-0009-0

Katz, B.G., 2020. Groundwater Contamination from Reactive Nitrogen, in: Nitrogen Overload. pp. 119–154. https://doi.org/10.1002/9781119513933.ch7

Khodaverdiloo, H., Khani Cheraghabdal, H., Bagarello, V., Iovino, M., Asgarzadeh, H., Ghorbani Dashtaki, S., 2017. Ring diameter effects on determination of field-saturated hydraulic conductivity of different loam soils. Geoderma 303, 60–69. https://doi.org/10.1016/j.geoderma.2017.04.031

Kiparsky, M., Fisher, A.T., Hanemann, W.M., Bowie, J., Kantor, R., Coburn, C., Lockwood, B., 2018. Recharge Net Metering to Enhance Groundwater Sustainability.

Kleber, M., 2010. What is recalcitrant soil organic matter? Environ. Chem. 7, 320–332. https://doi.org/10.1071/EN10006

Kocis, T.N., Dahlke, H.E., 2017. Availability of high-magnitude streamflow for groundwater banking in the Central Valley, California. Environ. Res. Lett. 12.

https://doi.org/10.1088/1748-9326/aa7b1b

Konikow, L.F., Kendy, E., 2005. Groundwater depletion: A global problem. Hydrogeol. J. 13, 317–320. https://doi.org/10.1007/s10040-004-0411-8

Koops, H.-P., Böttcher, B., Möller, U.C., Pommerening-Röser, a, Stehr, G., 1991. Classification of eight new species of ammonia-oxidizing bacteria. J. Gen. Microbiol. 137, 1689–1699.

Korom, S.F., 1992. Natural denitrification in the saturated zone: A review. Water Resour. Res. 28, 1657–1668. https://doi.org/10.1029/92WR00252

Lapidus, A., Clum, A., LaButti, K., Kaluzhnaya, M.G., Lim, S., Beck, D.A.C., Glavina del Rio, T., Nolan, M., Mavromatis, K., Huntemann, M., Lucas, S., Lidstrom, M.E., Ivanova, N., Chistoserdova, L., 2011. Genomes of Three Methylotrophs from a Single Niche Reveal the Genetic and Metabolic Divergence of the Methylophilaceae. J. Bacteriol. 193, 3757–3764.

Li, Y. hua, Li, H. bo, Xu, X. yang, Xiao, S. yao, Wang, S. qi, Xu, S. cong, 2017. Fate of nitrogen in subsurface infiltration system for treating secondary effluent. Water Sci. Eng. 10, 217–224. https://doi.org/10.1016/j.wse.2017.10.002

Liu, Z.P., Wang, B.J., Liu, Y.H., Liu, S.J., 2005. Novosphingobium taihuense sp. nov., a novel aromatic-compound-degrading bacterium isolated from Taihu Lake, China. Int. J. Syst. Evol. Microbiol. 55, 1229–1232. https://doi.org/10.1099/ijs.0.63468-0

Lloréns, M., Aguilar, M.I., Sáez, J., Ortuño, J.F., Meseguer, V.F., 2021. Nitrogen transformation in two vertical subsurface flow pilot plants 1–30.

Long, A., Heitman, J., Tobias, C., Philips, R., Song, B., 2013. Co-occurring anammox, denitrification, and codenitrification in agricultural soils. Appl. Environ. Microbiol. 79, 168–176. https://doi.org/10.1128/AEM.02520-12

Lucke, T., Boogaard, F., van de Ven, F., 2014. Evaluation of a new experimental test procedure to more accurately determine the surface infiltration rate of permeable pavement systems. Urban Plan. Transp. Res. 2, 22–35.

Marr, J., Arrate, D., Maendly, R., Dhillon, D., Stygar, S., 2018. FLOOD-MAR: Using

Flood Water for Managed Aquifer Recharge to Support Sustainable Water Resources.

Mulder, A., van de Graaf, A.A., Robertson, L.A., Kuenen, J.G., 1995. Anaerobic ammonium oxidation discovered in a denitrifying fluidized bed reactor. FEMS Microbiol. Ecol. 16, 177–183. https://doi.org/10.1016/0168-6496(94)00081-7

Nakatsu, C.H., Hristova, K., Hanada, S., Meng, X.Y., Hanson, J.R., Scow, K.M., Kamagata, Y., 2006. Methylibium petroleiphilum gen. nov., sp. nov., a novel methyl tert-butyl ether-degrading methylotroph of the Betaproteobacteria. Int. J. Syst. Evol. Microbiol. 56, 983–989. https://doi.org/10.1099/ijs.0.63524-0

Nealson, K.H., Myers, C.R., 1992. Microbial reduction of manganese and iron: New approaches to carbon cycling. Appl. Environ. Microbiol. 58, 439–443. https://doi.org/10.1128/aem.58.2.439-443.1992

Nordström, A., Hellman, M., Hallin, S., Herbert, R.B., 2021. Microbial controls on net production of nitrous oxide in a denitrifying woodchip bioreactor. J. Environ. Qual. 50, 228–240. https://doi.org/10.1002/jeq2.20181

Nordström, A., Herbert, R.B., 2018. Determination of major biogeochemical processes in a denitrifying woodchip bioreactor for treating mine drainage. Ecol. Eng. 110, 54–66. https://doi.org/10.1016/j.ecoleng.2017.09.018

O'Geen, A.T., Saal, M.B.B., Dahlke, H., Doll, D., Elkins, R., Fulton, A., Fogg, G., Harter, T., Hopmans, J.W., Ingels, C., Niederholzer, F., Solis, S.S., Verdegaal, P., Walkinshaw, M., 2015. Soil suitability index identifies potential areas for groundwater banking on agricultural lands. Calif. Agric. 69, 75–84. https://doi.org/10.3733/ca.v069n02p75

Orlygsson, J., Krisstjansson, J.K., 2014. The Family Hydrogenophilaceae, in: The Prokaryotes. pp. 859–868.

Osaka, K., Nakajima, Y., Suzuki, K., Eguchi, S., Katou, H., 2018. Nitrogen and oxygen isotope enrichment factors of nitrate at different denitrification rates in an agricultural soil. Soil Sci. Plant Nutr. 64, 558–565. https://doi.org/10.1080/00380768.2018.1504321

Pabich, W.J., Valiela, I., Hemond, H.F., 2001. Relationship between DOC concentration and vadose zone thickness and depth below water Pabich, W.J., Valiela, I., Hemond, H.F., 2001. Relationship between DOC concentration and vadose zone thickness and depth below water table in groundwater of Cape Cod, . Biogeochemistry 55, 247–268.

Pajaro Valley Water Management Agency, 2021. Pajaro Valley Basin Management Plan Groundwater Sustainability Update 2022.

Pajaro Valley Water Management Agency, 2014. Pajaro Valley Water Management Agency Basin Management Plan Update.

Palacin-Lizarbe, C., Camarero, L., Hallin, S., Jones, C.M., Cáliz, J., Casamayor, E.O., Catalan, J., 2019. The DNRA-denitrification dichotomy differentiates nitrogen transformation pathways in mountain lake benthic habitats. Front. Microbiol. 10, 1–15. https://doi.org/10.3389/fmicb.2019.01229

Parada, A.E., Needham, D.M., Fuhrman, J.A., 2016. Every base matters: Assessing small subunit rRNA primers for marine microbiomes with mock communities, time series and global field samples. Environ. Microbiol. 18, 1403–1414. https://doi.org/10.1111/1462-2920.13023

Pavelic, P., Dillon, P.J., Barry, K.E., Gerges, N.Z., 2006. Hydraulic evaluation of aquifer storage and recovery (ASR) with urban stormwater in a brackish limestone aquifer. Hydrogeol. J. 14, 1544–1555. https://doi.org/10.1007/s10040-006-0078-4

Pensky, J., Fisher, A.T., Gorski, G., Schrad, N., Dailey, H., Beganskas, S., Saltikov, C., 2022. Enhanced cycling of nitrogen and metals during rapid infiltration: Implications for managed recharge. Sci. Total Environ. 838, 156439. https://doi.org/10.1016/j.scitotenv.2022.156439

Porcal, P., Koprivnjak, J.F., Molot, L.A., Dillon, P.J., 2009. Humic substances-part 7: The biogeochemistry of dissolved organic carbon and its interactions with climate change. Environ. Sci. Pollut. Res. 16, 714–726. https://doi.org/10.1007/s11356-009-0176-7

Racz, A.J., Fisher, A.T., Schmidt, C.M., Lockwood, B.S., Huertos, M.L., 2012.
Spatial and Temporal Infiltration Dynamics During Managed Aquifer Recharge.
Ground Water 50, 562–570. https://doi.org/10.1111/j.1745-6584.2011.00875.x

Regnery, J., Wing, A.D., Kautz, J., Drewes, J.E., 2016a. Introducing sequential
managed aquifer recharge technology (SMART) - From laboratory to full-scale
application. Chemosphere 154, 8–16.
https://doi.org/10.1016/j.chemosphere.2016.03.097

Regnery, J., Wing, A.D., Kautz, J., Drewes, J.E., 2016b. Introducing sequential
managed aquifer recharge technology (SMART) - From laboratory to full-scale
application. Chemosphere 154, 8–16.
https://doi.org/10.1016/j.chemosphere.2016.03.097

Rice, R., Milczarek, M., Keller, J., 2013. A Comparison of single and double ring
infiltrometer methods for measuring infiltration rates. Proc. Arizona Hydrol.
Soc. 2013 Symp. 104.

Riedel, T., Zak, D., Biester, H., Dittmar, T., 2013. Iron traps terrestrially derived
dissolved organic matter at redox interfaces. Proc. Natl. Acad. Sci. U. S. A. 110,
10101–10105. https://doi.org/10.1073/pnas.1221487110

Rivett, M.O., Buss, S.R., Morgan, P., Smith, J.W.N., Bemment, C.D., 2008. Nitrate
attenuation in groundwater: A review of biogeochemical controlling processes.
Water Res. 42, 4215–4232. https://doi.org/10.1016/j.watres.2008.07.020

Robertson, W.D., 2010. Nitrate removal rates in woodchip media of varying age.
Ecol. Eng. 36, 1581–1587. https://doi.org/10.1016/j.ecoleng.2010.01.008

Robertson, W.D., Yeung, N., VanDriel, P.W., Lombardo, P.S., 2005. High-
permeability layers for remediation of ground water; go wide, not deep. Ground
Water 43, 574–581. https://doi.org/10.1111/j.1745-6584.2005.0062.x

Schmidt, C.M., Fisher, A.T., Racz, A., Wheat, C.G., Los Huertos, M., Lockwood, B.,
2012. Rapid nutrient load reduction during infiltration of managed aquifer
recharge in an agricultural groundwater basin: Pajaro Valley, California. Hydrol.
Process. 26, 2235–2247. https://doi.org/10.1002/hyp

Schmidt, C.M., Fisher, A.T., Racz, A.J., Lockwood, B.S., Los Huertos, M., 2011. Linking Denitrification and Infiltration Rates during Managed Groundwater Recharge. Environ. Sci. Technol. 45, 9634–9640.

Sebilo, M., Aloisi, G., Mayer, B., Perrin, E., Vaury, V., Mothet, A., Laverman, A.M., 2019. Controls on the Isotopic Composition of Nitrite ($\delta 15N$ and $\delta 18O$) during Denitrification in Freshwater Sediments. Sci. Rep. 9, 1–14. https://doi.org/10.1038/s41598-019-54014-3

Sebilo, M., Mayer, B., Nicolardot, B., Pinay, G., Mariotti, A., 2013. Long-term fate of nitrate fertilizer in agricultural soils. Proc. Natl. Acad. Sci. U. S. A. 110, 18185–18189. https://doi.org/10.1073/pnas.1305372110

Shan, J., Zhao, X., Sheng, R., Xia, Y., Ti, C., Quan, X., Wang, S., Wei, W., Yan, X., 2016. Dissimilatory Nitrate Reduction Processes in Typical Chinese Paddy Soils: Rates, Relative Contributions, and Influencing Factors. Environ. Sci. Technol. 50, 9972–9980. https://doi.org/10.1021/acs.est.6b01765

Silver, M., Knöller, K., Schlögl, J., Kübeck, C., Schüth, C., 2018. Nitrogen cycling and origin of ammonium during infiltration of treated wastewater for managed aquifer recharge. Appl. Geochemistry 97, 71–80. https://doi.org/10.1016/j.apgeochem.2018.08.003

Smedley, P.L., Kinniburgh, D.G., 2002. A review of the source, behaviour and distribution of arsenic in natural waters. Appl. Geochemistry 17, 517–568. https://doi.org/10.1016/S0883-2927(02)00018-5

Soil Survey Staff, 2014. Soil Survey Geographic (SSURGO) Database.

Strous, M., Fuerst, J.A., Kramer, E.H.M., Logemann, S., Muyzer, G., Van De Pas-Schoonen, K.T., Webb, R., Kuenen, J.G., Jetten, M.S.M., 1999. Missing lithotroph identified as new planctomycete. Nature 400, 446–449. https://doi.org/10.1038/22749

Su, X., Lu, S., Yuan, W., Woo, N.C., Dai, Z., Dong, W., Du, S., Zhang, X., 2018. Redox zonation for different groundwater flow paths during bank filtration: a case study at Liao River, Shenyang, northeastern China. Hydrogeol. J. 26, 1573–

1589.

Takeuchi, M., Hamana, K., Hiraishi, A., 2001. Proposal of the genus Sphingomonas sensu stricto and three new genera, Sphingobium, Novosphingobium and Sphingopyxis, on the basis of phylogenetic and chemotaxonomic analyses. Int. J. Syst. Evol. Microbiol. 51, 1405–1417. https://doi.org/10.1099/00207713-51-4-1405

Tedoldi, D., Chebbo, G., Pierlot, D., Kovacs, Y., Gromaire, M.C., 2016. Impact of runoff infiltration on contaminant accumulation and transport in the soil/filter media of Sustainable Urban Drainage Systems: A literature review. Sci. Total Environ. 569–570, 904–926. https://doi.org/10.1016/j.scitotenv.2016.04.215

Valhondo, C., Carrera, J., Ayora, C., Barbieri, M., Nödler, K., Licha, T., Huerta, M., 2014. Behavior of nine selected emerging trace organic contaminants in an artificial recharge system supplemented with a reactive barrier. Environ. Sci. Pollut. Res. 21, 11832–11843. https://doi.org/10.1007/s11356-014-2834-7

Valhondo, C., Carrera, J., Ayora, C., Tubau, I., Martinez-Landa, L., Nödler, K., Licha, T., 2015. Characterizing redox conditions and monitoring attenuation of selected pharmaceuticals during artificial recharge through a reactive layer. Sci. Total Environ. 512–513, 240–250. https://doi.org/10.1016/j.scitotenv.2015.01.030

Valhondo, C., Martínez-Landa, L., Carrera, J., Díaz-Cruz, S.M., Amalfitano, S., Levantesi, C., 2020. Six artificial recharge pilot replicates to gain insight into water quality enhancement processes. Chemosphere 240. https://doi.org/10.1016/j.chemosphere.2019.124826

Valley Water, 2021. One Water Santa Clara Countywide Framework: An Integrated Approach to Water Resources Management Draft Report.

Van Drecht, G., Bouwman, A.F., Knoop, J.F., Beusen, H.W., Meinardi, C.R., 2003. Global modeling of the fate of nitrogen from point and nonpoint sources in soils, groundwater, and surface water. Global Biogeochem. Cycles 17, 1115.

Van Meter, K.J., Basu, N.B., Veenstra, J.J., Burras, C.L., 2016. The nitrogen legacy:

Emerging evidence of nitrogen accumulation in anthropogenic landscapes. Environ. Res. Lett. 11. https://doi.org/10.1088/1748-9326/11/3/035014

Wada, Y., Van Beek, L.P.H., Van Kempen, C.M., Reckman, J.W.T.M., Vasak, S., Bierkens, M.F.P., 2010. Global depletion of groundwater resources. Geophys. Res. Lett. 37, 1–5. https://doi.org/10.1029/2010GL044571

Wang, J., Yan, Y., Bai, J., Su, X., 2020. Influences of riverbed siltation on redox zonation during bank filtration: A case study of Liao River, Northeast China. Hydrol. Res. 51, 1478–1489. https://doi.org/10.2166/nh.2020.107

Weishaar, J.L., Aiken, G.R., Bergamaschi, B.A., Fram, M.S., Fujii, R., Mopper, K., 2003. Evaluation of specific ultraviolet absorbance as an indicator of the chemical composition and reactivity of dissolved organic carbon. Environ. Sci. Technol. 37, 4702–4708. https://doi.org/10.1021/es030360x

Welti, N., Bondar-Kunze, E., Singer, G., Tritthart, M., Zechmeister-Boltenstern, S., Hein, T., Pinay, G., 2012. Large-scale controls on potential respiration and denitrification in riverine floodplains. Ecol. Eng. 42, 73–84. https://doi.org/10.1016/j.ecoleng.2012.02.005

Wendt, D.E., van Loon, A.F., Scanlon, B.R., Hannah, D.M., 2021. Managed aquifer recharge as a drought mitigation strategy in heavily-stressed aquifers. Environ. Res. Lett. 16. https://doi.org/10.1088/1748-9326/abcfe1

Werner, A.D., Bakker, M., Post, V.E.A., Vandenbohede, A., Lu, C., Ataie-Ashtiani, B., Simmons, C.T., Barry, D.A., 2013. Seawater intrusion processes, investigation and management: Recent advances and future challenges. Adv. Water Resour. 51, 3–26. https://doi.org/10.1016/j.advwatres.2012.03.004

World Health Organization, 2017. Guidelines for drinking-water quality: fourth edition incorporating the first addendum.

Ying, S.C., Schaefer, M. V., Cock-Esteb, A., Li, J., Fendorf, S., 2017. Depth Stratification Leads to Distinct Zones of Manganese and Arsenic Contaminated Groundwater. Environ. Sci. Technol. 51, 8926–8932. https://doi.org/10.1021/acs.est.7b01121

Youngs, E.G., 1991. Infiltration Measurements - A Review. Hydrol. Process. 5, 309–320.

Yuan, J., Van Dyke, M.I., Huck, P.M., 2016. Water reuse through managed aquifer recharge (MAR): Assessment of regulations/guidelines and case studies. Water Qual. Res. J. Canada 51, 357–376. https://doi.org/10.2166/wqrjc.2016.022

Zaidi, M., Ahfir, N.D., Alem, A., El Mansouri, B., Wang, H., Taibi, S., Duchemin, B., Merzouk, A., 2020. Assessment of clogging of managed aquifer recharge in a semi-arid region. Sci. Total Environ. 730, 139107. https://doi.org/10.1016/J.SCITOTENV.2020.139107

Zumft, W.G., 1997. Cell biology and molecular basis of denitrification. Microbiol. Mol. Biol. Rev. 61, 533–616.

Treatment	Test duration (days)	Analysis period (ID) [a]	IR_B (m/day) [b]	IR_V (m/day) [b]
Native soil	20	5 – 20	14.4 ± 7.3	2.2 ± 0.7
Wood chips	18	4 – 18	14.3 ± 2.2	1.9 ± 0.4
1:1 mixture	18	4 – 18	7.0 ± 1.0	2.2 ± 0.8

[a] ID = infiltration day. Analyses focused on results following a start-up period of 3-4 days, after which dominantly saturated hydrologic conditions were established.

[b] IR_B = bulk infiltration rate, IR_V = vertical infiltration rate. Mean ± standard deviation are for daily values.

Table S1-1. Summary of experimental conditions.

Treatment	$\Delta[NO_3^-]_L$ (g/m²day)	$\Delta[NO_2^-]_L$ (g/m²day)	$\Delta[NH_4^+]_L$ (g/m²day)	$\Delta[DOC]_L$ (g/m²day)	$\Delta[Mn]_L$ (g/m²day)	$\Delta[Fe]_L$ (g/m²day)	$\Delta[As]_L$ (mg/m²day)
Native soil	1.09 ± 3.25	0.16 ± 0.18	0.05 ± 0.44	-0.18 ± 0.75	0.03 ± 0.09	0.76 ± 1.67	-0.64 ± 0.63
Wood chips	-0.63 ± 1.96	0.03 ± 0.03	0.07 ± 0.08	0.30 ± 1.06	1.14 ± 1.01	0.23 ± 0.33	-0.43 ± 0.17
1:1 mixture	-0.19 ± 3.81	0.33 ± 0.32	-3.01 ± 2.95	1.93 ± 2.67	2.32 ± 2.39	0.08 ± 0.25	0.08 ± 0.28

[a] Solute loads are mean ± standard deviation from samples collected every 1-2 days.

Table S1-2. Summary of daily solute load results.

			Total Infiltration Rates (m/day)		Vertical Infiltration Rates (m/day)	
Comparison	Type	Tails	p.value	sig @ 0.05	p.value	sig @ 0.05
NS > WC	3	1	0.4	0	0.08	0
NS > MIX	3	1	<2.2e-16	1	0.46	0
WC > MIX	3	1	<2.2e-16	1	0.08	0

Table S1-3. Single-tailed t-test results comparing total and vertical infiltration rates between treatments.

			$\Delta NO3_L$ $(gNO_3/m^2/d)$		$\Delta NO2_L$ $(gNO_2/m^2/d)$		$\Delta NH4_L$ $(gNH_4/m^2/d)$		ΔN_L $(gN/m^2/d)$	
Comparison	Type	Tails	p.value	sig @ 0.05	p.value	sig @ 0.05	p.value	sig @ 0.05	p.value	sig @ 0.05
NS > WC	3	1	0.05	1	0.01	1	0.56	0	0.02	1
NS > MIX	3	1	0.18	0	0.96	0	0.001	1	0.006	1
WC > MIX	3	1	0.65	0	0.99	0	0.001	1	0.07	0

Table S1-4. Single-tailed t-test results comparing N species load and total N load addition between treatments.

			ΔDOC_L $(gDOC/m^2/d)$		ΔMn_L $(gMn/m^2/d)$		ΔFe_L $(gFe/m^2/d)$		ΔAs_L $(gAs/m^2/d)$	
Comparison	Type	Tails	p.value	sig @ 0.05	p.value	sig @ 0.05	p.value	sig @ 0.05	p.value	sig @ 0.05
NS < WC	3	1	0.05	1	6.2E-4	1	0.89	0	0.12	0
NS < MIX	3	1	0.006	1	0.001	1	0.95	0	2.6E-4	1
WC < MIX	3	1	0.03	1	0.05	1	0.97	0	2.1E-6	1

Table S1-5. Single-tailed t-test results comparing DOC load and metals load addition between treatments.

	NO3$_{In}$ (gNO$_3$/m^2/d)		NO2$_{In}$ (gNO$_2$/m^2/d)		NH4$_{In}$ (gNH$_4$/m^2/d)		N$_{In}$ (gN/m^2/d)	
Comparison	p.value	sig @ 0.05	p.value	sig @ 0.05	p.value	sig @ 0.05	p.value	sig @ 0.05
NS > WC	0.04	1	0.01	1	0.03	1	0.04	1
NS < MIX	0.81	0	0.03	1	1.2E-6	1	0.32	0
WC < MIX	0.05	1	5.1E-4	1	8.2E-7	1	2.4E-4	1

Table S1-6. Single-tailed t-test results comparing inflowing N species and inflowing total N loads between treatments.

	DOC$_{In}$ (gDOC/m^2/d)		Mn$_{In}$ (gMn/m^2/d)		Fe$_{In}$ (gFe/m^2/d)		As$_{In}$ (gAs/m^2/d)	
Comparison	p.value	sig @ 0.05	p.value	sig @ 0.05	p.value	sig @ 0.05	p.value	sig @ 0.05
NS > WC	0.11	0	0.86	0	0.15	0	0.05	1
NS < MIX	0.006	1	6.5E-4	1	0.79	0		
NS > MIX							0.03	1
WC < MIX	4.1E-4	1	1.3E-4	1	0.44	0	0.74	0

Table S1-7. Single-tailed t-test results comparing inflowing DOC, Mn, Fe, and As loads between treatments.

ANCOVA Response: N load removal		
Variable	F-value	p-value
Carbon amendment type	5.31	0.009
Inflowing DOC load	1.94	0.17
Carbon amendment type: Inflowing DOC load	0.84	0.44

Table S1-8. Two-way ANCOVA test results comparing the effects of carbon amendment type and inflowing DOC load, carbon amendment type, and the interaction between the two on N load removal when accounting for both variables simultaneously.

ANOVA Numeric variable: Inflowing DOC load		
Categorical variable	F-value	p-value
Carbon amendment type	9.07	5.6E-4

Table S1-9. ANOVA results testing the correlation between inflowing DOC load (numeric) and carbon amendment type (categorical).

	Native soil					
	180709_000	180709_030	180709_055	180720_000	180720_030	180720_055
pH (Measured)	7.40	7.40	7.40	7.50	7.40	7.50
Minerals (Saturation Index)						
As2O5(s)	-35.16	-36.18	-36.10	-35.64	-35.60	-36.00
Fe(OH)2 (am)	-5.93	-5.10	-5.55	-4.57	-4.80	-4.48
Fe(OH)2 (c)	-5.06	-4.22	-4.67	-3.70	-3.93	-3.61
Melanterite	-7.97	-7.13	-7.58	-6.87	-6.90	-6.77
Mn3(AsO4)2:8H2O(s)	-17.67	-18.62	-22.80	-45.42	-45.96	-45.78
Mn3(PO4)2(s)	-40.10	-40.03	-44.27	-67.68	-67.90	-67.65
MnCl2:4H2O(s)	-14.94	-14.93	-16.34	-24.44	-24.42	-24.42
MnCO3 (am)	-2.06	-2.03	-3.44	-11.20	-11.29	-11.20
MnHPO4(s)	-10.49	-10.47	-11.88	-19.74	-19.75	-19.72
MnSO4(s)	-13.02	-13.00	-14.41	-22.37	-22.36	-22.36
Pyrochroite	-7.66	-7.63	-9.05	-16.75	-16.94	-16.74
Rhodochrosite	-1.56	-1.54	-2.94	-10.70	-10.79	-10.70
Siderite	-1.98	-1.15	-1.59	-0.68	-0.80	-0.58
Vivianite	-26.16	-23.66	-25.00	-22.40	-22.73	-22.10

Table S1-10. pH values and simulated saturation indices for soil solid phases in the native soil from two fluid sampling days. Sample names indicate the date the sample was collected and the depth at which it was collected in centimeters below plot base, in the format "YYMMDD_XXX."

	Wood chips					
	180727_000	180727_030	180727_055	180809_000	180809_030	180809_055
pH (Measured)	7.50	7.40	7.50	7.70	7.60	7.60
Minerals (Saturation Index)						
As2O5(s)	-35.69	-36.09	-37.06	-36.60	-36.80	-36.61
Fe(OH)2 (am)	-4.56	-4.68	-4.77	-5.50	-5.25	-5.53
Fe(OH)2 (c)	-3.69	-3.81	-3.89	-4.62	-4.38	-4.65
Melanterite	-6.88	-6.80	-7.08	-8.35	-7.90	-8.18
Mn3(AsO4)2:8H2O(s)	-45.47	-14.70	-12.58	-20.62	-18.46	-17.16
Mn3(PO4)2(s)	-67.66	-36.14	-33.42	-42.64	-39.91	-38.79
MnCl2:4H2O(s)	-24.51	-13.92	-13.09	-16.54	-15.56	-15.19
MnCO3 (am)	-11.18	-0.69	0.24	-2.79	-1.91	-1.54
MnHPO4(s)	-19.73	-9.16	-8.32	-11.51	-10.54	-10.17
MnSO4(s)	-22.39	-11.80	-10.97	-14.34	-13.34	-12.98
Pyrochroite	-16.74	-6.35	-5.32	-8.16	-7.37	-7.00
Rhodochrosite	-10.69	-0.20	0.73	-2.29	-1.41	-1.04
Siderite	-0.65	-0.67	-0.86	-1.78	-1.44	-1.71
Vivianite	-22.35	-22.36	-22.98	-25.90	-24.79	-25.62

Table S1-11. pH values and saturation indices for soil solid phases in the wood chips from two fluid sampling days. Sample names indicate the date the sample was collected and the depth at which it was collected in centimeters below plot base, in the format "YYMMDD_XXX."

	1:1 mixture					
	180821_000	180821_030	180821_055	180828_000	180828_030	180828_055
pH (Measured)	7.40	7.40	7.40	7.40	7.40	7.40
Minerals (Saturation Index)						
As2O5(s)	-35.71	-35.57	-35.54	-35.75	-35.94	-35.29
Fe(OH)2 (am)	-5.71	-5.39	-5.06	-5.68	-5.76	-5.33
Fe(OH)2 (c)	-4.84	-4.52	-4.18	-4.81	-4.88	-4.46
Melanterite	-7.76	-7.44	-7.11	-7.71	-7.79	-7.36
Mn3(AsO4)2:8H2O(s)	-18.36	-14.19	-12.39	-19.54	-16.13	-13.44
Mn3(PO4)2(s)	-40.20	-16.12	-34.40	-41.35	-17.71	-15.67
MnCl2:4H2O(s)	-15.20	-13.87	-13.26	-15.53	-14.33	-13.65
MnCO3 (am)	-2.00	-0.66	-0.07	-2.34	-1.15	-0.47
MnHPO4(s)	-10.52	0.85	-8.59	-10.90	0.32	1.00
MnSO4(s)	-13.08	-11.73	-11.15	-13.43	-12.23	-11.55
Pyrochroite	-7.70	-6.36	-5.77	-8.08	-6.88	-6.20
Rhodochrosite	-1.51	-0.16	0.43	-1.85	-0.66	0.03
Siderite	-1.66	-1.35	-1.01	-1.59	-1.68	-1.25
Vivianite	-25.47	-4.47	-23.51	-25.38	-5.58	-4.30

Table S1-12. pH values and saturation indices for soil solid phases in the 1:1 mixture from two fluid sampling days. Sample names indicate the date the sample was collected and the depth at which it was collected in centimeters below plot base, in the format "YYMMDD_XXX."
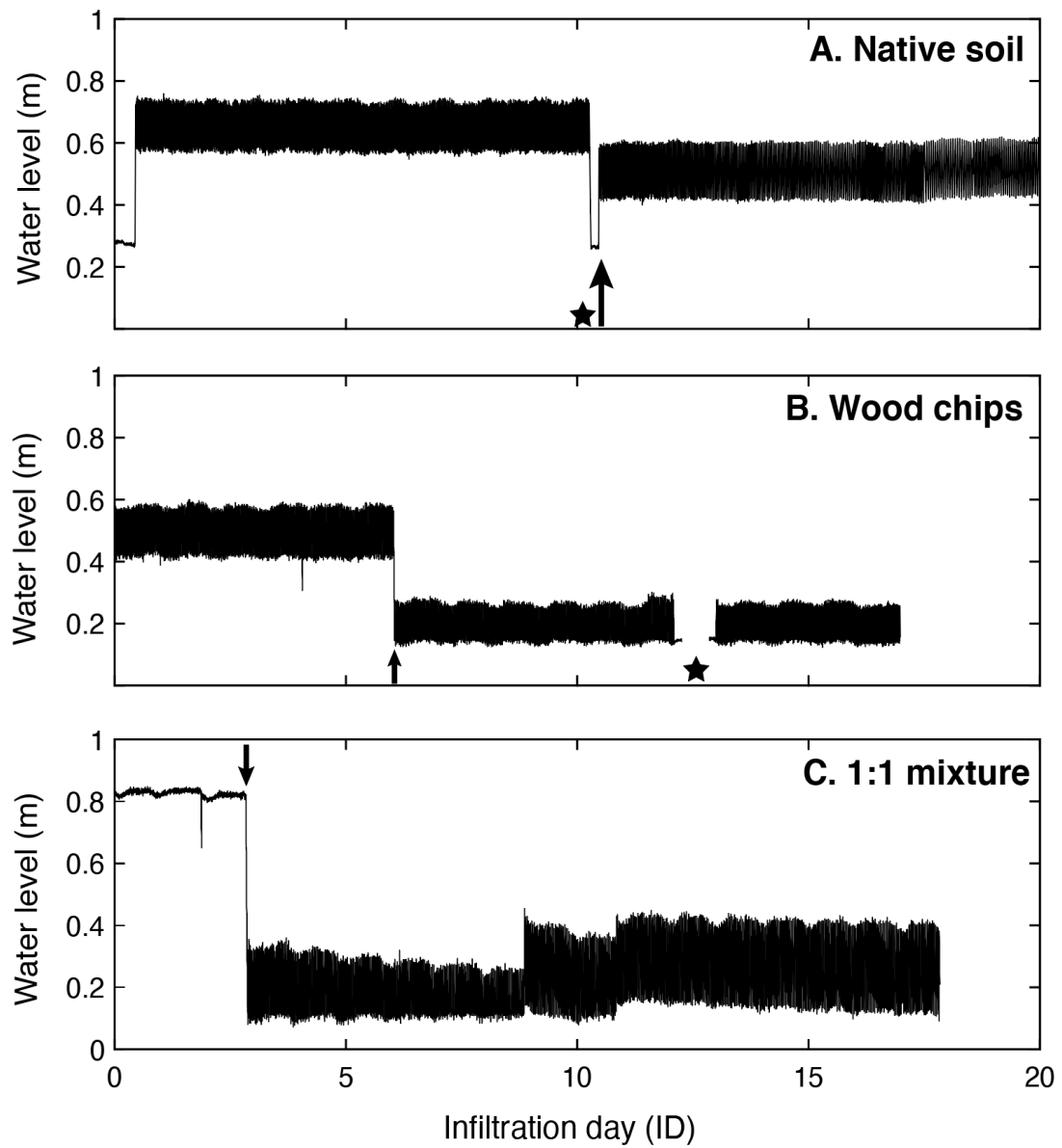
Figure S1-1. Water level records for each plot (A – native soil, B – wood chips, C – 1:1 mixture) over the duration of the test. Black arrows indicate times that the float switch in the plot was lowered. Stars indicate times when the plot went dry.
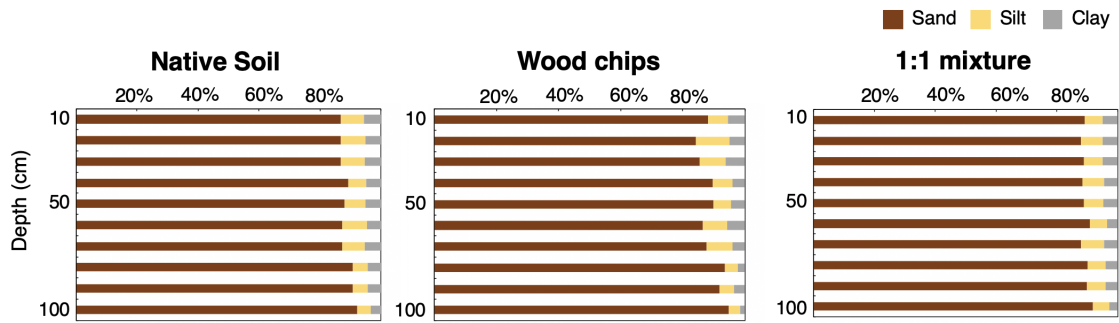
Figure S1-2. Soil grain size for each plot.

Figure S1-3. Soil TN and TOC (percent weight) for each plot. Filled circles represent soil samples collected before infiltration, while open circles represent soils collected after infiltration.
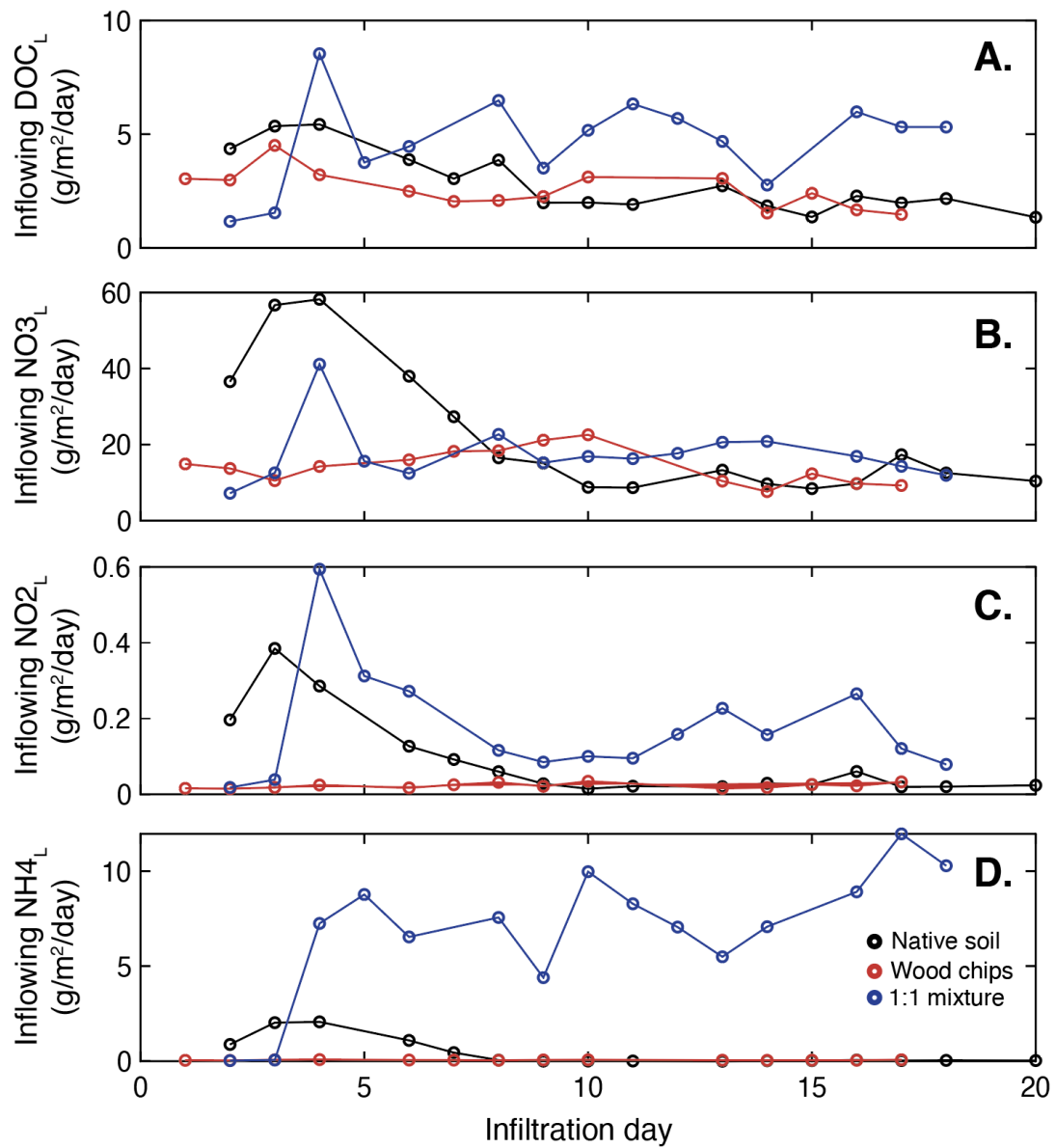
Figure S1-4. Inflowing DOC load (A), NO3-N load (B), NO2-N load (C), and NH4-N load (D) changes over the duration of the percolation experiments for each treatment.
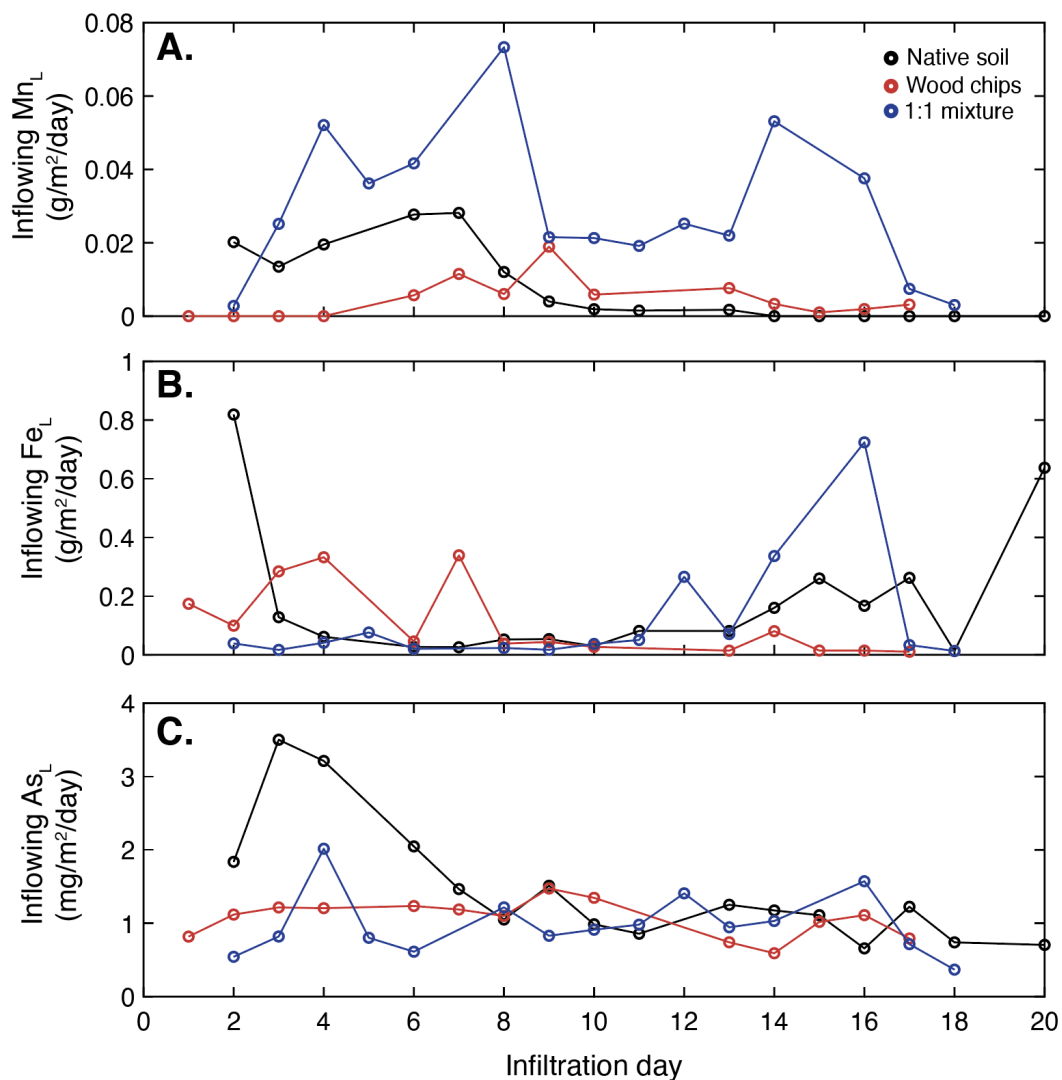
Figure S1-5. Inflowing Mn load (A), Fe load (B), and As load (C) changes over the duration of the percolation experiments for each treatment. Note different scale shown for As data.
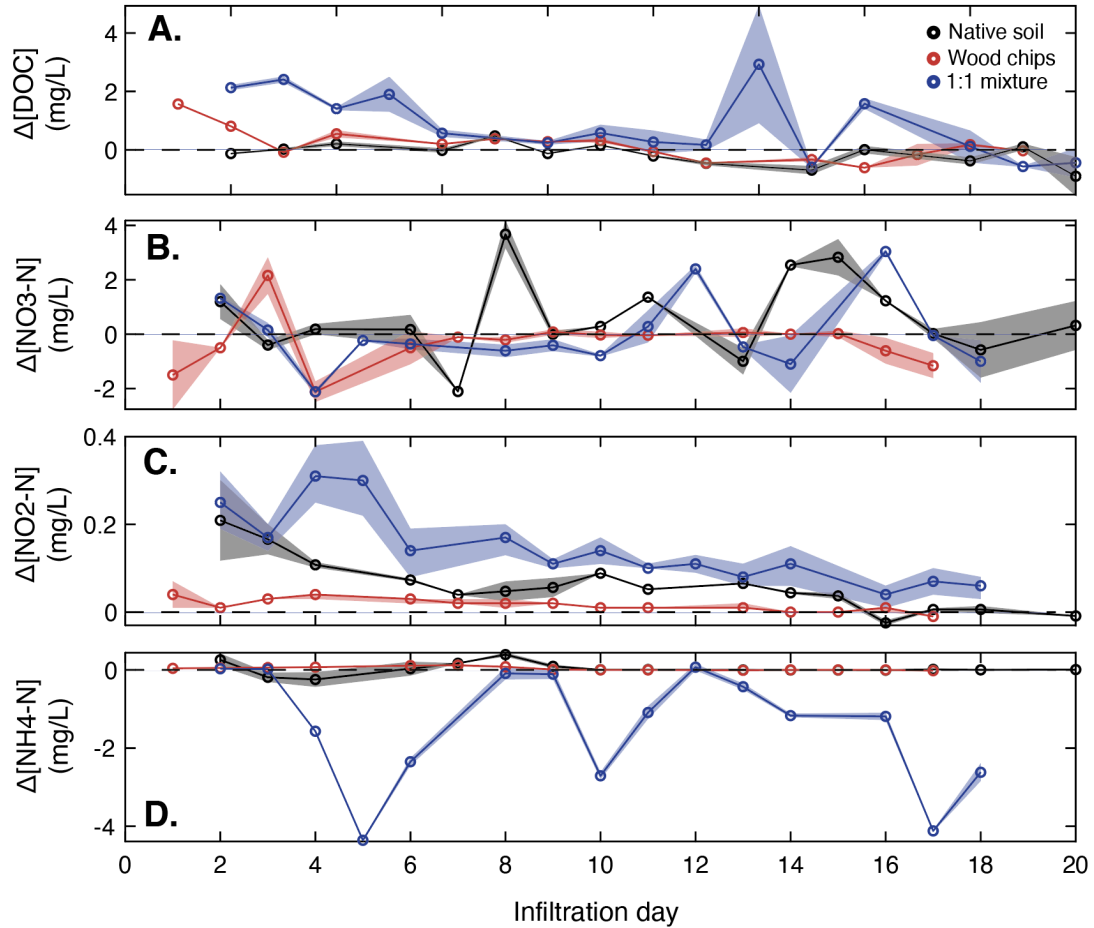
Figure S1-6. Net concentration change with depth (surface sample concentration – deepest sample concentration) of DOC (A) and N-species (B, C, and D) in fluid samples collected from each of the treatments (native soil, wood chips, and 1:1 mixture). The solid lines represent the average concentration from the two samples collected at each depth. The shaded region shows the range between the highest and lowest concentrations from the two samples collected at each depth.
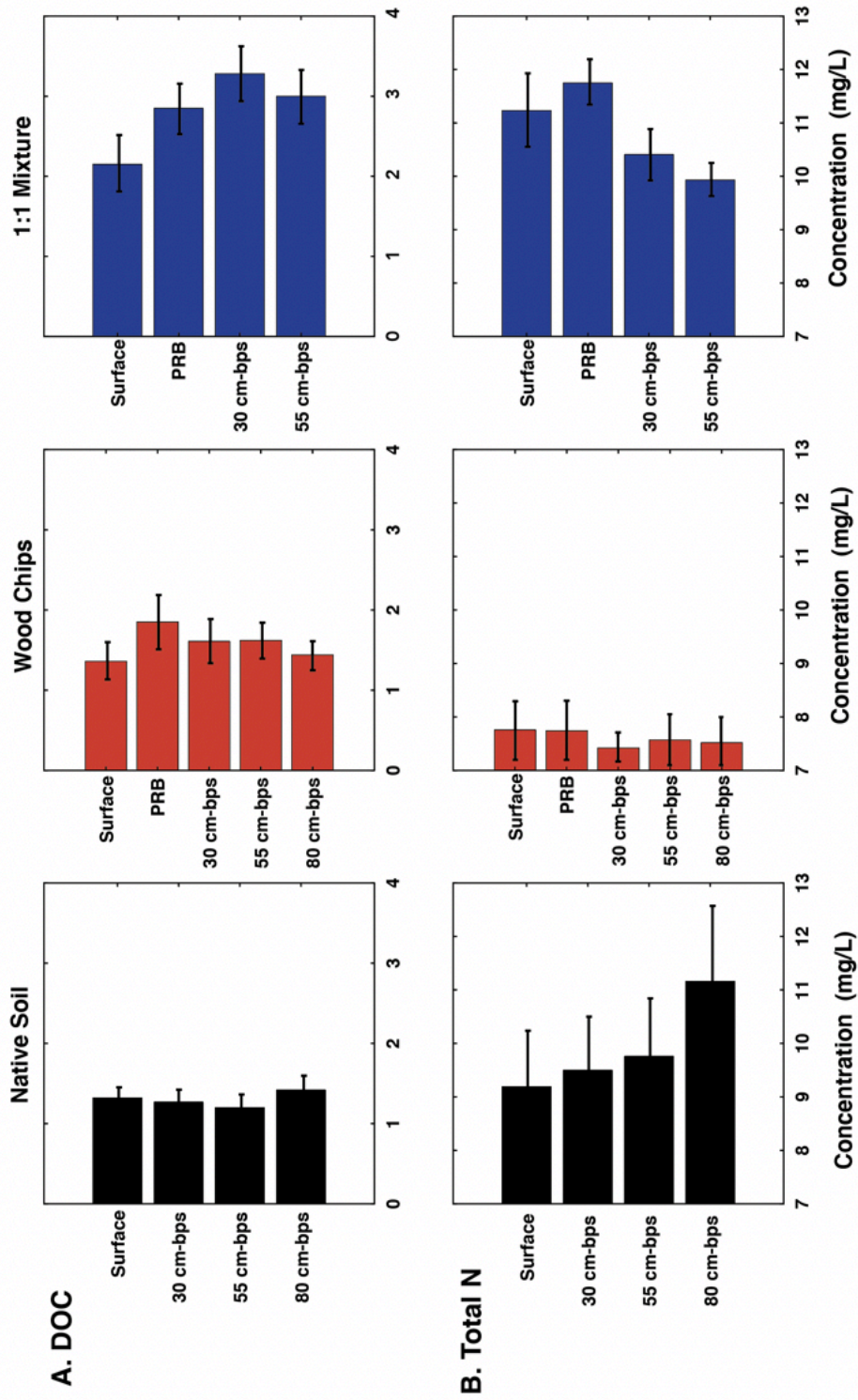
Figure S1-7. The average concentration of DOC in pore fluids over the duration of the percolation tests at each of the depths sampled in the native soil, wood chips, and 1:1 mixture plots (**A**). The average concentration of N in pore fluids over the duration of the percolation tests at each of the depths sampled in the native soil, wood chips, and 1:1 mixture plots (**B**). Error bars indicate a 95% confidence interval.
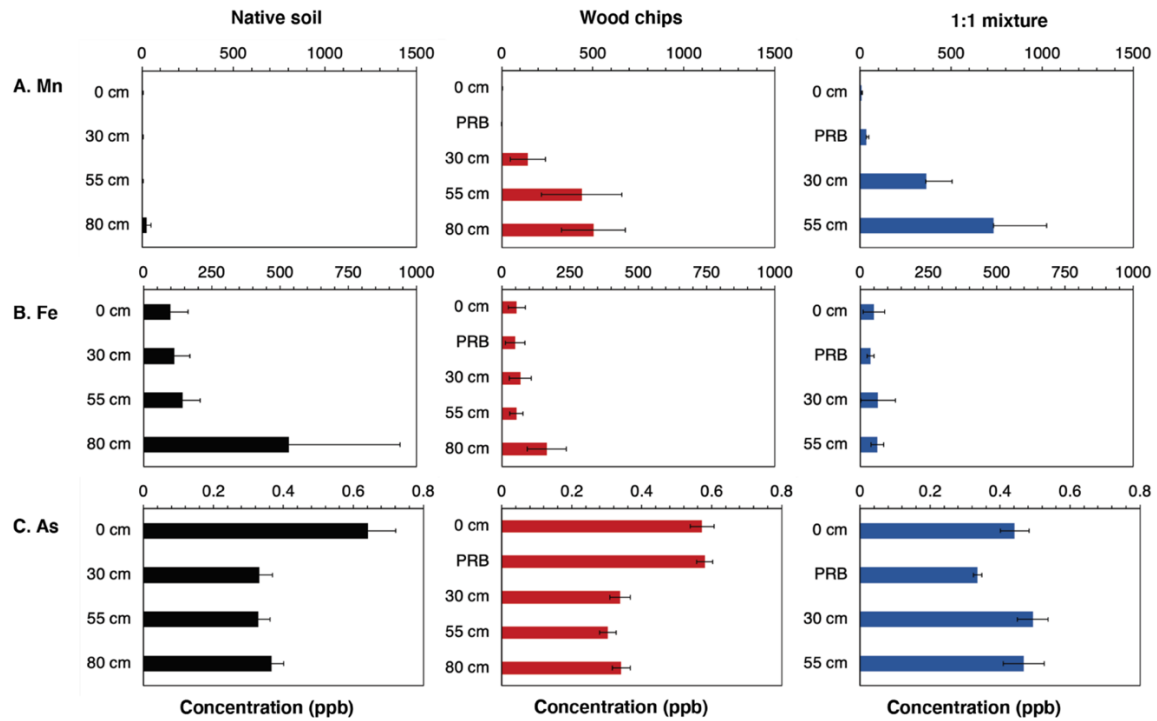
Figure S1-8. The average concentration of Mn in pore fluids over the duration of the percolation tests at each of the depths sampled in the native soil, wood chips, and 1:1 mixture plots (**A**). The average concentration of Fe in pore fluids over the duration of the percolation tests at each of the depths sampled in the native soil, wood chips, and 1:1 mixture plots (**B**). The average concentration of As in pore fluids over the duration of the percolation tests at each of the depths sampled in the native soil, wood chips, and 1:1 mixture plots (**C**). Error bars indicate a 95% confidence interval.
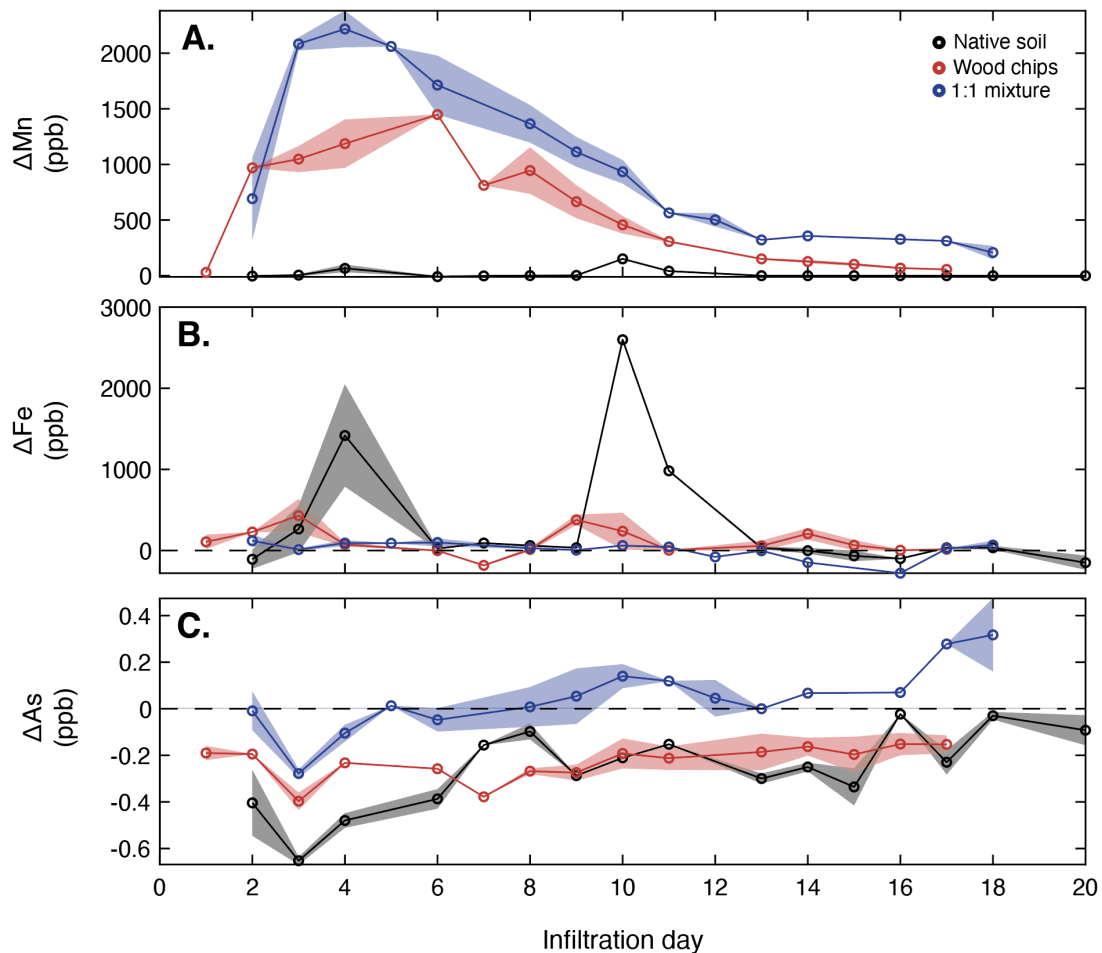
Figure S1-9. Net concentration change with depth (surface sample concentration – deepest sample concentration) of Mn, Fe, and As in fluid samples collected from each of the treatments (native soil, wood chips, and 1:1 mixture). The solid lines represent the average concentration from the two samples collected at each depth. The shaded region shows the range between the highest and lowest concentrations from the two samples collected at each depth.
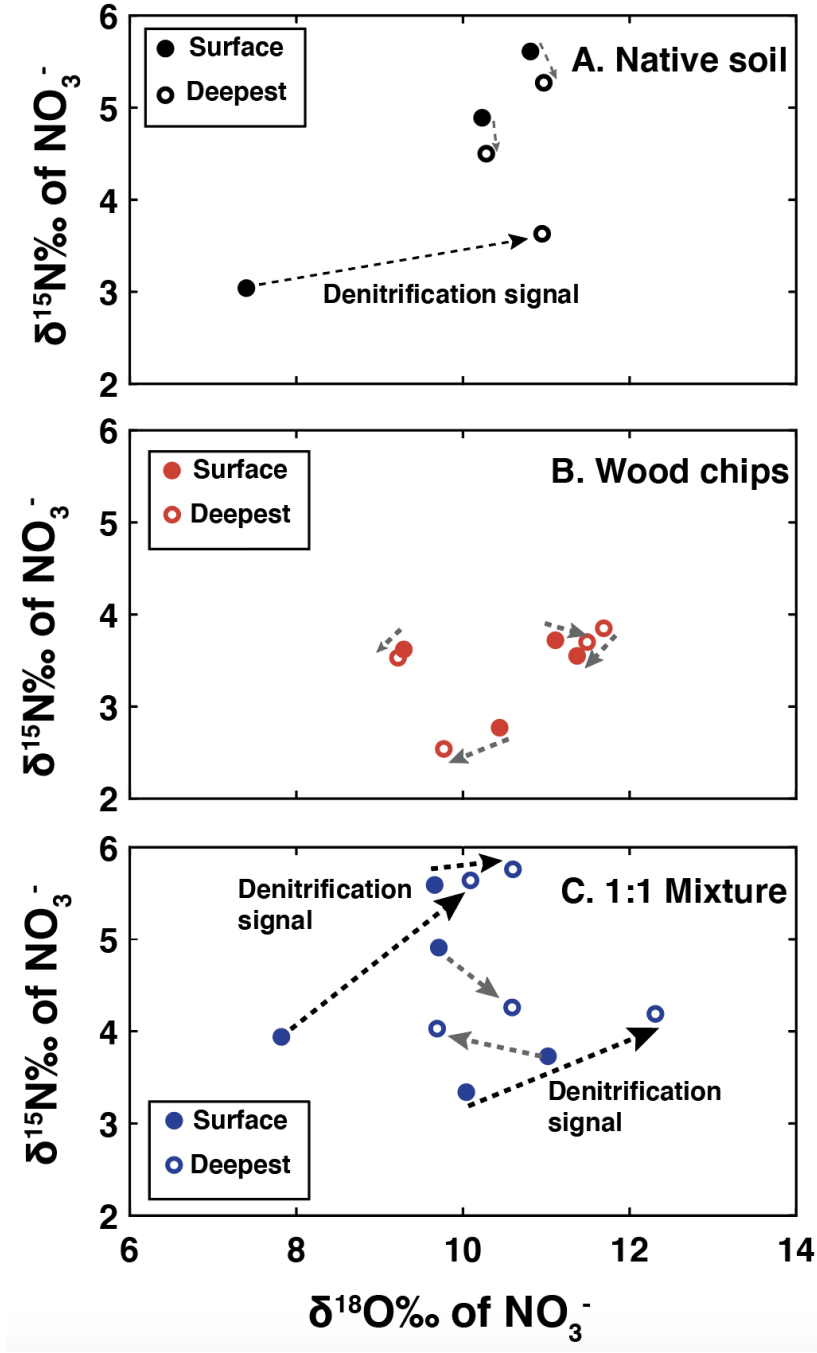
Figure S1-10. δ15N values of nitrate plotted against δ18O values of nitrate for each treatment on days in which NO3- removal was detected. The arrows connect surface and deepest samples from the same infiltration day. Black arrows indicate enrichment indicative of a denitrification signal.
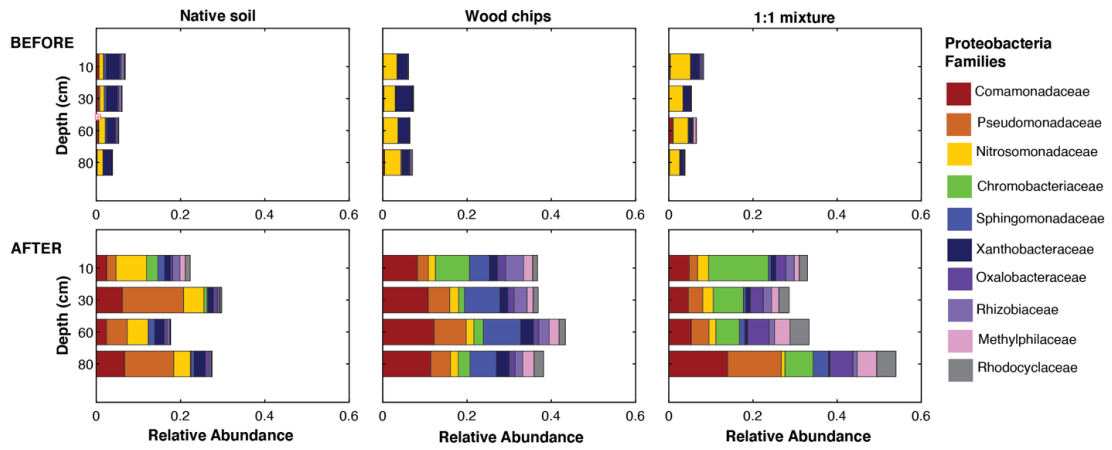
Figure S1-11. The relative abundance of Proteobacteria in soil samples from each treatment by depth before and after infiltration was completed.

Chapter Two

**LINKING NITRATE REMOVAL, CARBON CYCLING, AND
MOBILIZATION OF TRACE METALS DURING INFILTRATION FOR
MANAGED RECHARGE**

Abstract

We present results from a series of laboratory column studies investigating the impacts of infiltration dynamics and the addition of a soil-carbon amendment (wood mulch or almond shells) on water quality during infiltration for flood-managed aquifer recharge (flood-MAR). Recent studies suggest that nitrate removal could be enhanced during infiltration for MAR through the application of a wood chip permeable reactive barrier (PRB). However, less is understood about how other readily available carbon sources, such as almond shells, could be used as a PRB material, and how carbon amendments could impact other solutes, such as trace metals. Here we show that the presence of a carbon amendment increases nitrate removal relative to native soil, and that there is greater nitrate removal in association with longer fluid retention times (slower infiltration rates). Almond shells promoted more efficient nitrate removal than wood mulch or native soil, but also promoted the mobilization of geogenic trace metals (Mn, Fe, and As) during experiments. Almond shells in a PRB likely enhanced nitrate removal and trace metal cycling by releasing labile carbon, promoting reducing conditions, and providing habitat for microbial communities, the composition of which shifts in response. These results suggest that limiting the amount of bioavailable carbon released by a carbon-rich PRB may be preferred where geogenic trace metals are common in soils. Given the dual threats to groundwater supplies and quality worldwide, incorporating a suitable carbon source into the soil for managed infiltration projects could help to generate co-benefits and avoid undesirable results.

2.1 Introduction

More than 2 billion people worldwide face water stress and are increasingly reliant on groundwater to meet demand (Wada et al., 2010). Managed aquifer recharge (MAR) is a suite of techniques that can replenish groundwater supplies by collecting and infiltrating excess surface water into underlying aquifers (Bouwer, 2002b; Dillon, 2005; Dillon et al., 2006). MAR strategies include dedicated infiltration basins, injection wells, and stream bank filtration (Doussan et al., 1998; Pavelic et al., 2006). More recently, flood-managed aquifer recharge (flood-MAR) has been of particular interest in California, where precipitation is highly seasonal and varies year by year, major rivers tend to flood periodically, and there is abundant agricultural land on which infiltration can occur (Dahlke et al., 2018a; O'Geen et al., 2015).

Flood-MAR uses excess water from high magnitude winter flows in major rivers for recharge on open and working lands to simultaneously enhance groundwater recharge and manage flood waters. There are several potential benefits to implementing flood-MAR, including flood risk reduction, flood-plain reclamation, aquifer replenishment, drought preparedness, subsidence mitigation, and climate change adaptation (Marr et al., 2018). Field and modeling studies suggest that there is abundant surface water (i.e. high-magnitude stream flow) available for on-farm flooding, and that many crops are resilient to inundation (Dahlke et al., 2018b; Kocis and Dahlke, 2017). However, questions remain about the hydrogeologic and geochemical consequences of using flood-MAR as a water management strategy, particularly the potential impacts of flood-MAR on water quality.

During flood-MAR, contaminants can be introduced from the infiltrating water, past agricultural practices, or leaching of geogenic contaminants from soils (Exner et al., 2014; Fakhreddine et al., 2021). Because many proposed flood-MAR projects are on active or historical agricultural land, nitrogen contamination is of particular concern (Bachand et al., 2014; Katz, 2020). Nitrogen is the most ubiquitous nonpoint-source groundwater contaminant worldwide, and is well-known to pose ecological and human health risks (Burri et al., 2019; Van Drecht et al., 2003). In addition, long transport pathways and the legacy of past practices can result in nitrogen contamination that takes decades to occur or be recognized (Böhlke et al., 2002; Jessen et al., 2017; Sebilo et al., 2013; Van Meter et al., 2016).

Nitrogen cycling during infiltration is complex and involves many pathways, including nitrification, denitrification, anaerobic ammonium oxidation (annamox), and dissimilatory nitrate reduction to ammonium (DNRA) (Chen et al., 2014; Hellman et al., 2019; Li et al., 2017; Lloréns et al., 2021; Sebilo et al., 2013). Of these pathways, denitrification is of particular interest because it results in net, quasi-permanent removal of nitrogen from the system (Long et al., 2013; Shan et al., 2016). During denitrification, NO_3^- is converted to N_2 gas, with NO_2^-, NO, and N_2O as intermediate products, and typically requires an abundance of nitrate, anaerobic conditions, and the presence of an electron donor, often in the form of organic carbon (Korom, 1992). Carbon amendments in soils can enhance nitrogen removal during infiltration by stimulating denitrification (Beganskas et al., 2018; Gorski et al., 2020; Grau-Martínez et al., 2018b; Nordström and Herbert, 2018; Pensky et al., 2022). Traditional carbon

amendment materials include wood chips, alfalfa, biochar, and other organic, carbon-rich substrates (Addy et al., 2016; Gorski et al., 2019; Pensky et al., 2022; Schmidt et al., 2012). In regions where almond trees are abundant, almond shells could also be an effective, low-cost soil-carbon amendment.

While carbon amendments can aid in removal of nitrate, they could also contribute to the mobilization and cycling of geogenic trace metals associated with shallow soils and aquifers. High amounts of DOC will consume available oxygen and drive to anoxic environments that facilitate the release of trace contaminants such as manganese (Mn), iron (Fe), and arsenic (As) (Borch et al., 2010). The release of reduced Mn and Fe has been observed in previous MAR projects that used carbon reactive barriers (Valhondo et al., 2015, 2014). Additionally, arsenic poses a particular risk due to its naturally-occurring ubiquity in soils and sediments and high toxicity at trace concentrations, with a World Health Organization (WHO) recommended limit of 10 ug/L (Fakhreddine et al., 2015; Smedley and Kinniburgh, 2002; World Health Organization, 2017). Under anoxic conditions, the reductive dissolution of geogenic Fe(oxyhydr)oxides can cause the concomitant release of adsorbed As (Fendorf et al., 2010). Arsenic contamination has been documented in MAR projects, most notably in aquifer storage and recovery operations using injection wells (Fakhreddine et al., 2021, 2015), but could potentially be of concern for flood-MAR systems if conditions were consistently saturated and remained highly reducing for extended periods of time.

While many studies have demonstrated that carbon amendments enhance denitrification, fewer studies have investigated concurrent nitrogen and trace metal

cycling when applying a carbon amendment for managed recharge. Additionally, few studies have assessed almond shells specifically as a soil-carbon amendment. For the present study, we collected intact soil cores from a pilot flood-MAR site and conducted flow-through experiments to quantify the relationship between infiltration rates, nitrogen cycling, and trace metal cycling in the presence or absence of a carbon amendment (wood mulch, almond shells). Additionally, we instrumented the field site in order to measure infiltration rates and dynamics in the field. By investigating how different carbon amendments influence concurrent nitrogen and trace metal cycling under the hydrogeologic conditions observed in the field, this work seeks to elucidate how flood-MAR may impact both water supply and quality, and how carbon amendments could enhance benefits and/or mobilize contaminants.

2.2 Methods

2.2.1 Study site and field measurements

Three intact soil cores were collected from Teichert Ranch, a 785-acre active vineyard in California's Central Valley in Wilton, CA, located adjacent to the Cosumnes River (Figure 2-1A). This site is part of a pilot flood-MAR project, testing the conditions and processes associated with diversion and infiltration of up to 7.4 x 10^6 m^3 (6,000 acre-feet) of water per year.

In November 2019, Teichert Ranch was instrumented with 12 thermal probes (HOBO Water Temperature Pro v2 Data Logger) and 4 stilling wells with pressure gages (HOBO U20 Water Level Data Logger) in order to investigate infiltration dynamics across the site during inundation. We placed instruments along four transects
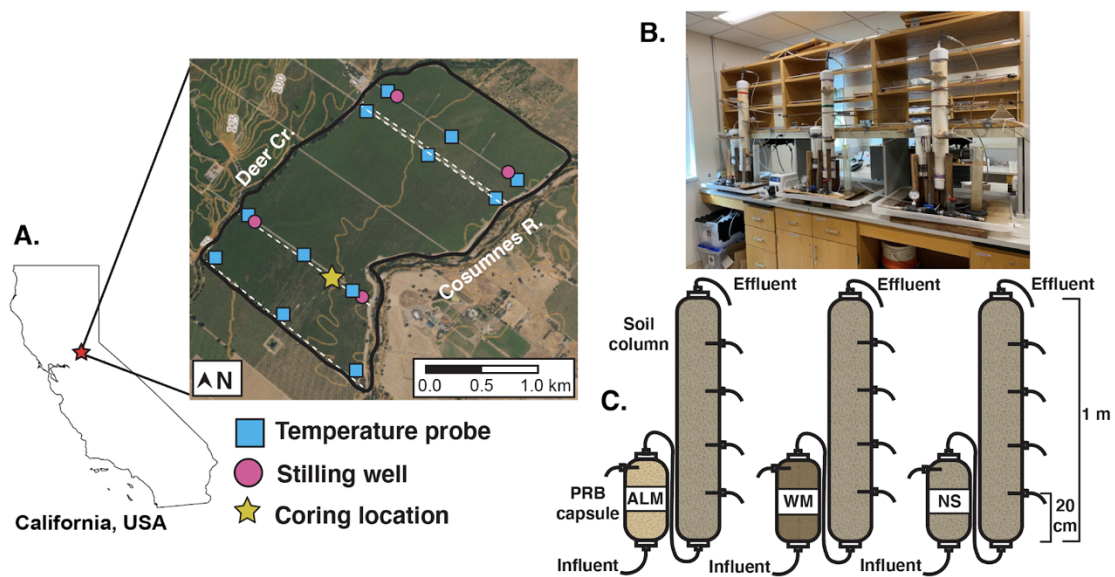
Figure 2-1 Site location Map of site location (A). A photo (B) and schematic (C) of the column configuration, including permeable reactive barrier (PRB) capsules and sampling locations.

that run roughly west-east across the site to assess conditions in the two major soil types mapped at the field site: silt loam on the northern portion of the property and sandy loam on the southern side of the property (SSURGO, 2014) (Figure 2-1A).

Each thermal probe consisted of a PVC tube with pairs of thermal sensor/loggers installed at depths of 5 cm and 20 cm below the ground surface. These tools measured a time-series of temperature of the infiltrating water at 15-minute intervals. The vertical infiltration rate can be calculated as a function of the amplitude ratio and/or phase shift of the thermal peaks between the shallow and deep temperature records in the same location (Hatch et al., 2006). Each stilling well contained a pressure gauge recording pressure measurements at 15-minute intervals, to measure the water height above the ground during a flood.

2.2.2 Soil sampling and analysis

Soil samples co-located with the sediment cores were collected at 10 cm depth intervals to 1 m below ground surface and were analyzed for texture, total carbon/nitrogen, total metals, and microbiological ecology. Following the column flow-through experiments, soil cores were deconstructed, and soil was sampled at 20 cm depth intervals for total carbon/nitrogen, total metals, and microbiological ecology to assess biogeochemical differences after infiltration. Statistical methods (single-tailed t-tests) were applied to determine the significance of observed differences before and after infiltration (Table S2-6).

2.2.3 Column experimental design

Intact soil cores were collected with a custom-built hammer-coring system and transported back to the lab for flow-through experiments. Soil cores were collected in adjacent locations (Figure 2-1) in 10 cm internal diameter (ID) polyvinylchloride (PVC) tubes, 100 cm in length. The cores were tested in the same tubes, in order to maintain the layering, structure, and microbial habitat and ecology at the field site. Micro-sampling ports were installed using ceramic 0.15 um pore size rhizon samplers for pore water collection during experiments.

Soil carbon amendments were placed in capsules plumbed in line with the columns, upstream of inflow (Figure 2-1B, 2-1C). Capsules were 30 cm in length and 10 cm in diameter, and filled with a 1:1 mixture of wood mulch and native soil by volume (WM), a 1:1 mixture of almond shells and native soil by volume (ALM), or native soil from the site (NS, as a control).

A solution of local tap water (Table S2-2) and nitrate, to simulate high nitrate conditions during infiltration, was pre-mixed with an initial concentration of $[NO_3]_{init}$ = 10 mg/L, applied for the first 120 days of the experiments. $[NO_3]_{init}$ was raised to 20 mg/L for the final 30 days of the experiments in order to assess the potential impact of higher nitrate load on the fraction of nitrate removed under otherwise similar infiltration conditions. The influent water was pumped in an upward flow direction, first through the soil amendment capsule, and then through an inverted soil core, using a peristaltic pump. Water was pumped upward through inverted cores to test a wide range of controlled flow rates under saturated conditions, without introducing air. Prior to sampling, core hydraulic properties were determined using Darcy experiments and

breakthrough tracer tests (with an inert NaCl tracer) for each core. Breakthrough test results are described in Table S2-1.

Tests of the three core treatments were run concurrently and continuously for 150 days, with temporal results reported in terms of infiltration days (ID) which began once the columns were fully saturated. The infiltration rate was varied incrementally to determine its influence on DOC, NO_3 and metal cycling, and flow rates were repeated to assess the potential influences of hysteresis and infiltration time. Infiltration rates were started at 0.2-0.3 m/day (volume/area/time) and increased to 1.3 m/day at intervals of ~0.3 m/day, and then decreased back down to 0.3 m/day at intervals of ~0.3 m/day (Figure S2-3). Every 1-2 days, infiltration rates were measured, and fluid samples were collected from each core. For each infiltration rate, the system was allowed to equilibrate for at least 24 hours before sampling, and a minimum of 3 daily samples were collected at each rate. For purposes of presentation and discussion, we divide the experiment into 7 infiltration periods based on the manipulation of infiltration rates (Table 2-1).

2.4 Fluid sampling and analysis

Influent and effluent samples were collected from each column, and pore fluids were extracted from the carbon amendment capsule and at soil depths of 20 cm, 40 cm, 60 cm, and 80 cm along each column. Fluid samples were analyzed for concentrations of selected nitrogen species ($[NO_3^-]$, $[NO_2^-]$, $[NH_4^+]$), dissolved organic carbon (DOC), specific UV absorbance at 254 nm (SUVA), stable isotopes of NO_3^- ($\delta^{15}N$ and $\delta^{18}O$),

Table 2-1. Experimental conditions. Infiltration rate, residence time (RT), and influent [N-NO3] and [DOC] are mean values over the specified infiltration days (IDs) for each of the treatments (NS, WM, and ALM). Influent [Mn], [Fe], and [As] values were all negligible.

Infiltration period (IP)	Infiltration day (ID)	Infiltration rate[a]	RT in PRB[a]	RT in column[a]	Influent [NO3-N][a]	Influent [DOC][a]
		m/day	hrs	hrs	mg/L	mg/L
1	1-12	0.31 (0.07)	24.6 (6.1)	82.0 (20.4)	10.6 (0.87)	0.33 (0.34)
2	36-43	0.32 (0.02)	22.4 (0.91)	74.6 (3.0)	10.4 (0.36)	1.50 (0.08)
3	44-55	0.62 (0.10)	11.9 (2.0)	39.6 (6.6)	10.4 (0.48)	1.60 (0.21)
4	56-85	1.14 (0.16)	6.44 (0.83)	21.5 (2.8)	9.98 (0.44)	1.71 (0.25)
5	86-96	0.60 (0.10)	12.2 (2.0)	40.8 (6.5)	11.1 (0.21)	1.79 (0.07)
6	97-114	0.33 (0.03)	22.2 (2.7)	74.0 (9.0)	10.8 (1.06)	1.62 (0.18)
7	127-148	0.56 (0.09)	13.2 (1.8)	44.1 (6.0)	21.9 (0.64)	1.57 (0.80)

[a] Values listed are mean (standard deviation) for each infiltration period.

and metals (As, Fe, and Mn). Samples were filtered at 0.2 µm and stored at -4° C prior to analysis.

Nutrient samples were analyzed using a Lachat QuickChem with three channels to simultaneously measure NO_3^-, NO_2^-, and NH_4^+ using colorimetry. DOC samples were analyzed using a Shimadzu TOC Analyzer. Analysis of sample duplicates, blanks, and laboratory standards indicated that both instruments were accurate within 2-5%. SUVA was determined by measuring the specific UV absorbance at 254 nm using an Orion AquaMate 8100 UV-Visible Spectrophotometer, and dividing that value by the DOC concentration measured in the same sample (Weishaar et al., 2003). SUVA is reported in units of L/mg-m. Selected samples were sent to the UC Davis Stable Isotope Facility for analysis of NO_3^- isotopes. Nitrate isotopic analyses were completed using the bacterial method (Casciotti et al., 2002) with a Thermo Scientific Delta V Plus IRMS.

Metals samples were preserved with 2% HNO_3 prior to analysis, then analyzed using a Thermo ElementXR High Resolution Inductively Coupled Mass Spectrometer. Analysis of sample duplicates, blanks, laboratory standards, and standard reference materials (SRM) indicated accuracy for metals concentrations of ≤5%. Influent and effluent chemistry data for all solutes and samples at each infiltration rate are listed in Tables S2-2-S2-3.

Net differences in solute concentrations, ΔX (mg/L or ug/L), were calculated for each day as:

$$\Delta X = [X]_{effluent} - [X]_{influent} \qquad [1]$$

Net differences in solute loads, ΔX_L (g-X/m^{2}day^{-1}), were calculated for each day as:

$$\Delta X_L = [X]_{\text{effluent}} \, IR_V - [X]_{\text{influent}} \, IR_V \qquad [2]$$

where [X] is solute concentration and IR_v is the vertical infiltration rate. "Influent" and "effluent" subscripts refer to the inflowing water and the outflowing water, respectively. Differences in solute concentrations and loads with depth for samples collected during a single day are interpreted in terms of changes during transport, based on repeated sampling of fluid parcels at multiple depths (e.g., Lagrangian approach). $\Delta X_L > 0$ indicates a net load increase, whereas $\Delta X_L < 0$ indicates net load reduction. Statistical methods (single-tailed t-tests) were applied to determine the significance of observed differences between treatments (Tables S2-7-S2-8).

2.2.5 DNA extraction and phylogenetic sequencing

Methods for microbial analysis of soil samples were similar to those applied in earlier studies (e.g., Beganskas et al., 2018). Briefly, soil DNA was extracted with a PowerSoil DNA Isolation Kit (QIAGEN). The Qubit 4 Fluorometer (Invitrogen) was used to quantify DNA extracts. PCT amplicons (~550 bp) were generated from PCRs with soil DNA and 16S rRNA gene primers targeting the V4 and V5 variable regions.

2.3 Results

2.3.1 Variations in organic carbon in pore fluid

Concentrations of DOC in pore fluid varied between treatments, with depth, and over time. During the first infiltration period (IP 1), DOC concentrations were higher in effluent from the carbon amended columns than in the native soil, with

concentrations up to 10.9 mg/L and 4.64 mg/L in the ALM and WC effluent, respectively, compared to a maximum of 2.50 mg/L in the NS effluent (Figure 2-2A, Figure 2-3A-C). During this time, elevated DOC in the carbon-amended columns was particularly notable in fluid samples collected from the PRB capsule, with average DOC concentrations of 4.18 ± 0.71 mg/L in the WC PRB and 16.0 ± 7.1 mg/L in the ALM PRB (Figure 2-3B-C). In contrast, during IP 1 in the NS column, average DOC concentrations were 0.55 ± 0.54 mg/L within the control PRB capsule and 1.24 ± 0.77 mg/L in the effluent (Figure 2-3A). Concentrations of DOC in fluids in the carbon amended columns decreased with time during the experiments, resulting in modest increases in DOC concentration within both the PRB capsules and in effluent from the WM and ALM columns after IP 1 (Figure S2-6D-F). During the remainder of the test (IP 2 to IP 7, ID 35 to ID 150), DOC values ranged from 1.49 to 3.22 mg/L in the ALM effluent, 1.51 to 3.58 mg/L in the WC effluent, and 1.09 to 1.99 mg/L in the NS effluent (Figure 2-2A).

The nature of the DOC measured also changed over time, particularly in the native soil. SUVA values of fluids collected from NS column were highest at the beginning of the test during IP1 (up to 112 L/mg-m) and decreased over time (Figure 2-3D). In the WM and ALM columns, SUVA values were lower, ranging from 0.6 to 30.1 L/mg-m, and were lowest in the ALM column (Figure 2-3E-D). During the remainder of the test (ID 36 to 150), SUVA values were similar for all treatments, ranging from 3.1 to 6.4 L/mg-m.
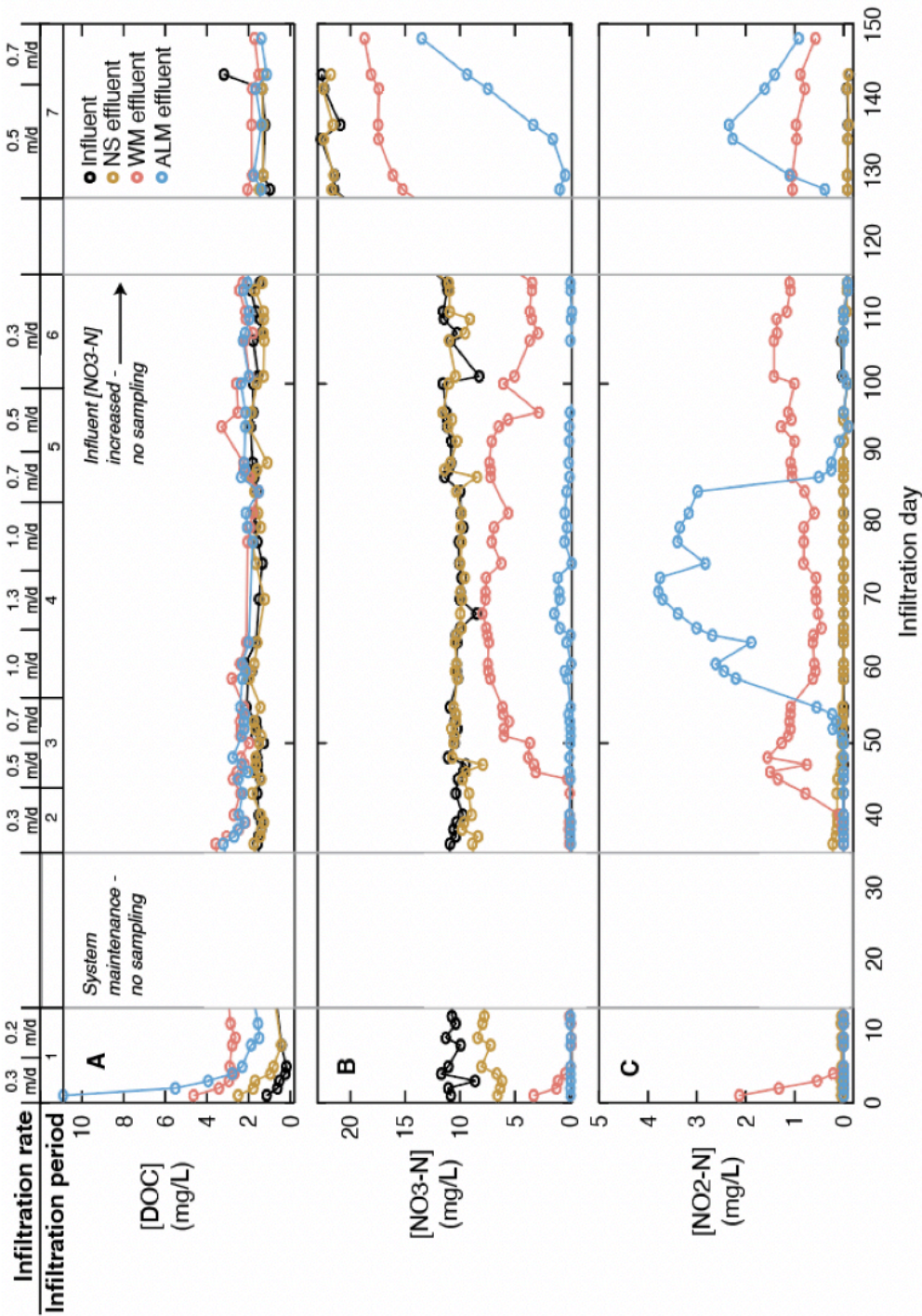
Figure 2-2 N-species and DOC influent and effluent DOC (A), NO3-N (B), and NO2-N (C) concentrations of the column influent and effluent for each treatment over the duration of the column experiments, with the corresponding infiltration rate.
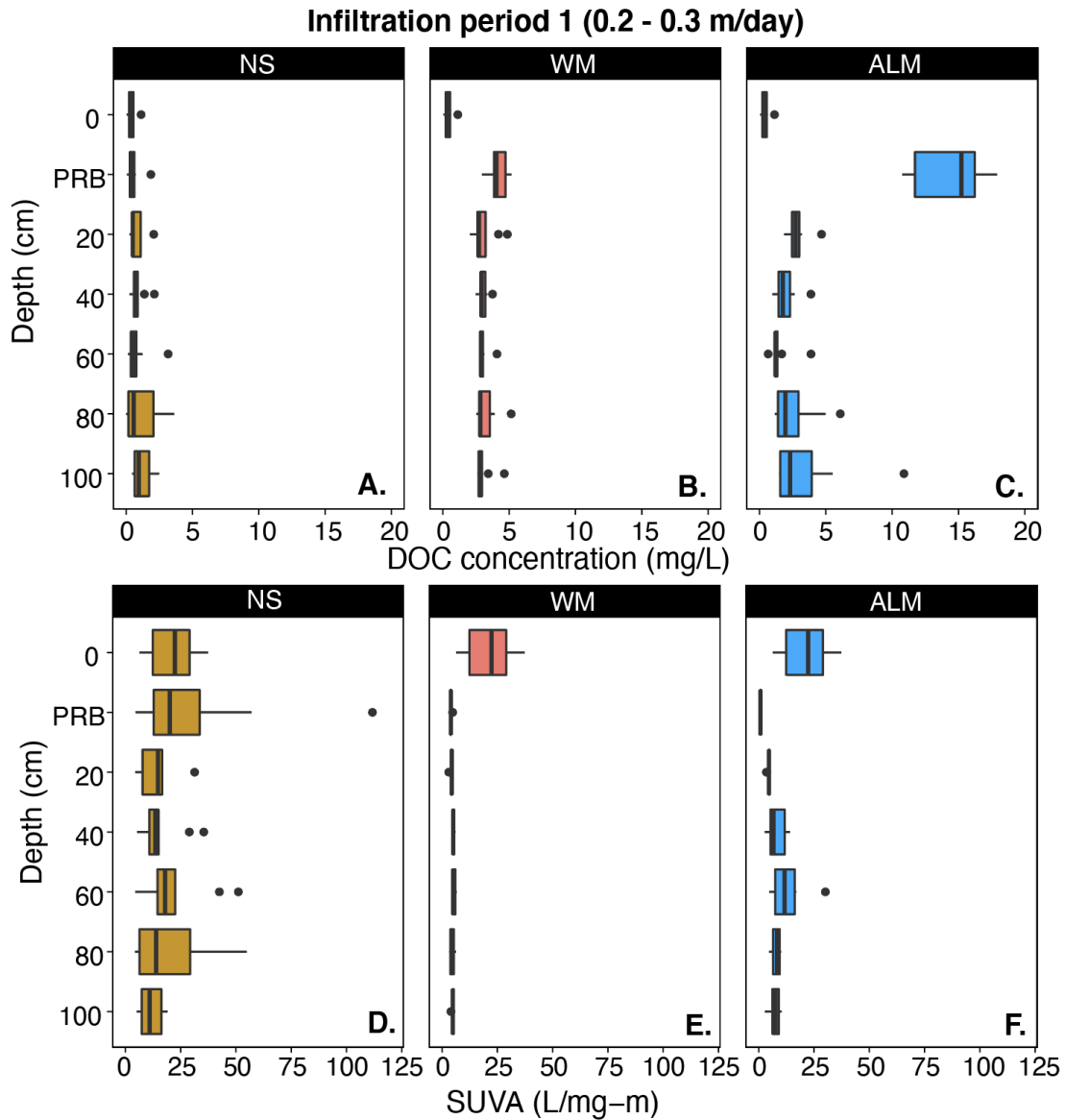
Figure 2-3 Initial DOC and SUVA Box-and-whisker plots of [DOC] (A-C) and SUVA (D-F) with depth during the initial infiltration period (IP 1), soon after soils were initially saturated for each treatment (NS, WM, and ALM).

2.3.2 Nitrogen transformations in pore fluid

There were substantial differences in nitrogen transformations between the three treatments, with depth, and at varying infiltration rates. At the slowest infiltration rates (0.2-0.4 m/day, IPs 1, 2, and 6), there were reductions of [NO_3-N] with depth in all three columns. In the NS column, the concentration of [NO_3-N] in the effluent was as low as 6.18 mg/L, with an average of 8.78 ± 1.57 mg/L (Figure 2-2B; Figure 2-4A). However, at higher infiltration rates, there were no apparent reductions in [NO_3-N] with depth in the NS column (Figure 2-2B; Figure 2-4D). In both the WM and ALM columns, there were reductions of [NO_3-N] at all infiltration rates, with a higher fraction of [NO_3-N] removed at lower infiltration rates and the majority of removal occurring within the PRB capsules (Figure 2-2B; Figure 2-5A). With influent [NO_3-N] ~10 mg/L, the [NO_3-N] in the WM effluent ranged from ND (no detect) to 6.05 mg/L at slower infiltration rates (< 0.4 m/day, Figure 2-4B) and 2.82 to 7.97 mg/L at more rapid infiltration rates (> 0.4 m/day, Figure 2-4E). When influent [NO_3-N] was increased to 20 mg/L (IP 7), effluent [NO_3-N] from the WM treatment ranged from 15.2 to 8.7 mg/L (Figure 2-2B).

The ALM treatment resulted in the most consistent and efficient [NO_3-N] removal, with the majority of removal occurring within the PRB capsule. At infiltration rates <1.3 m/day and influent [NO_3-N] ~10 mg/L, there was no detected [NO_3-N] from the ALM PRB capsule or any soil depth (Figure 2-2B; Figure 2-4C; Figure 2-5A). At infiltration rates ≥1.3 m/day, concentrations of [NO_3-N] in the ALM effluent ranged from 0.90 to 1.40 mg/L, comprising a removal of ~86 to 91%. When the concentration
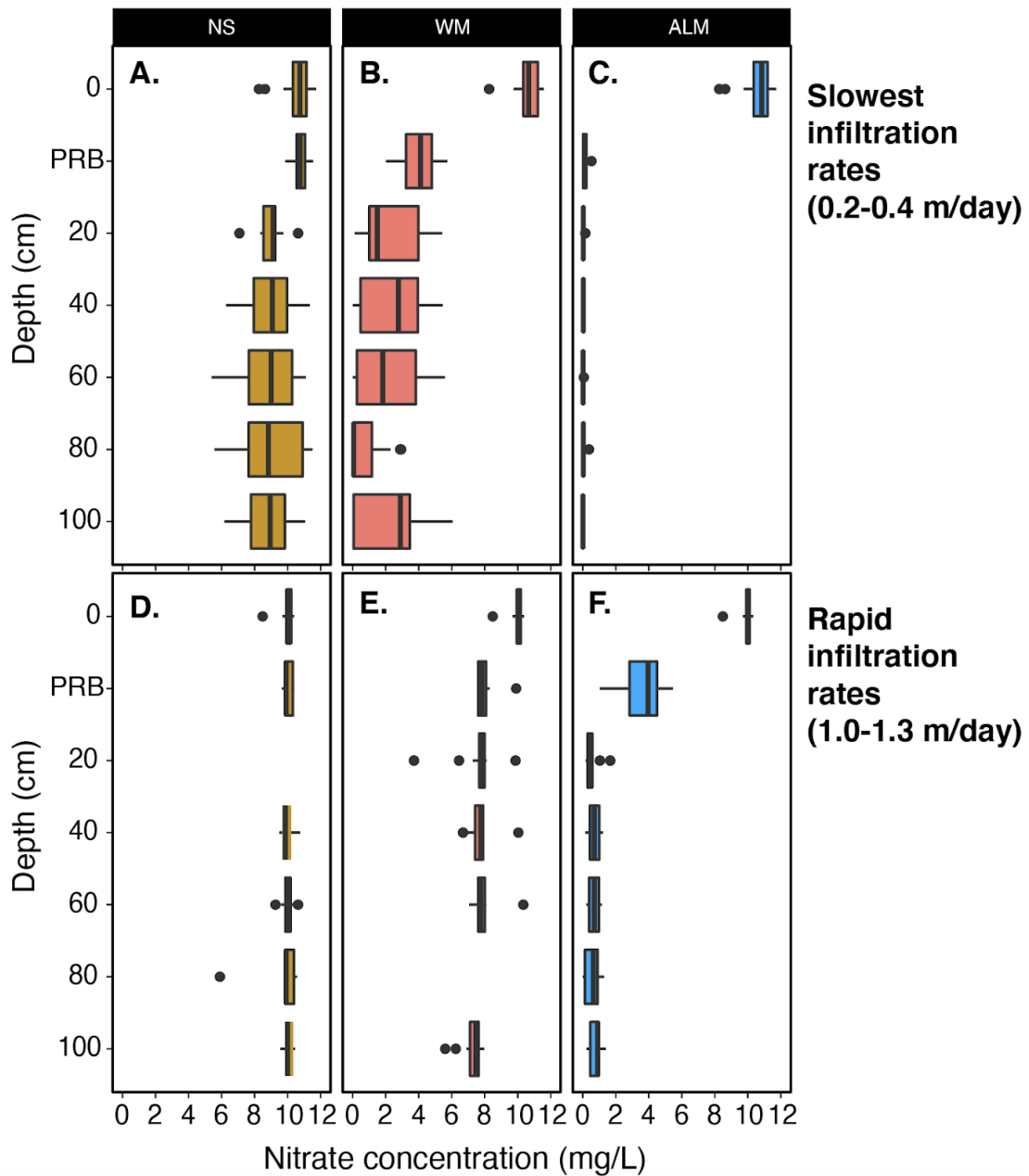
Figure 2-4 Nitrate with depth Box-and-whisker plots of [NO$_3$-N] with depth at the slowest (A) and most rapid (B) infiltration rates measured for each treatment (NS, WM, and ALM). Slowest infiltration rates (A) occurred during infiltration periods 1, 2, and 6. Most rapid infiltration rates (B) occurred during infiltration period 4. No data was available at the 20 cm depth in panel D and the 80 cm depth in panel E due to sampling issues.
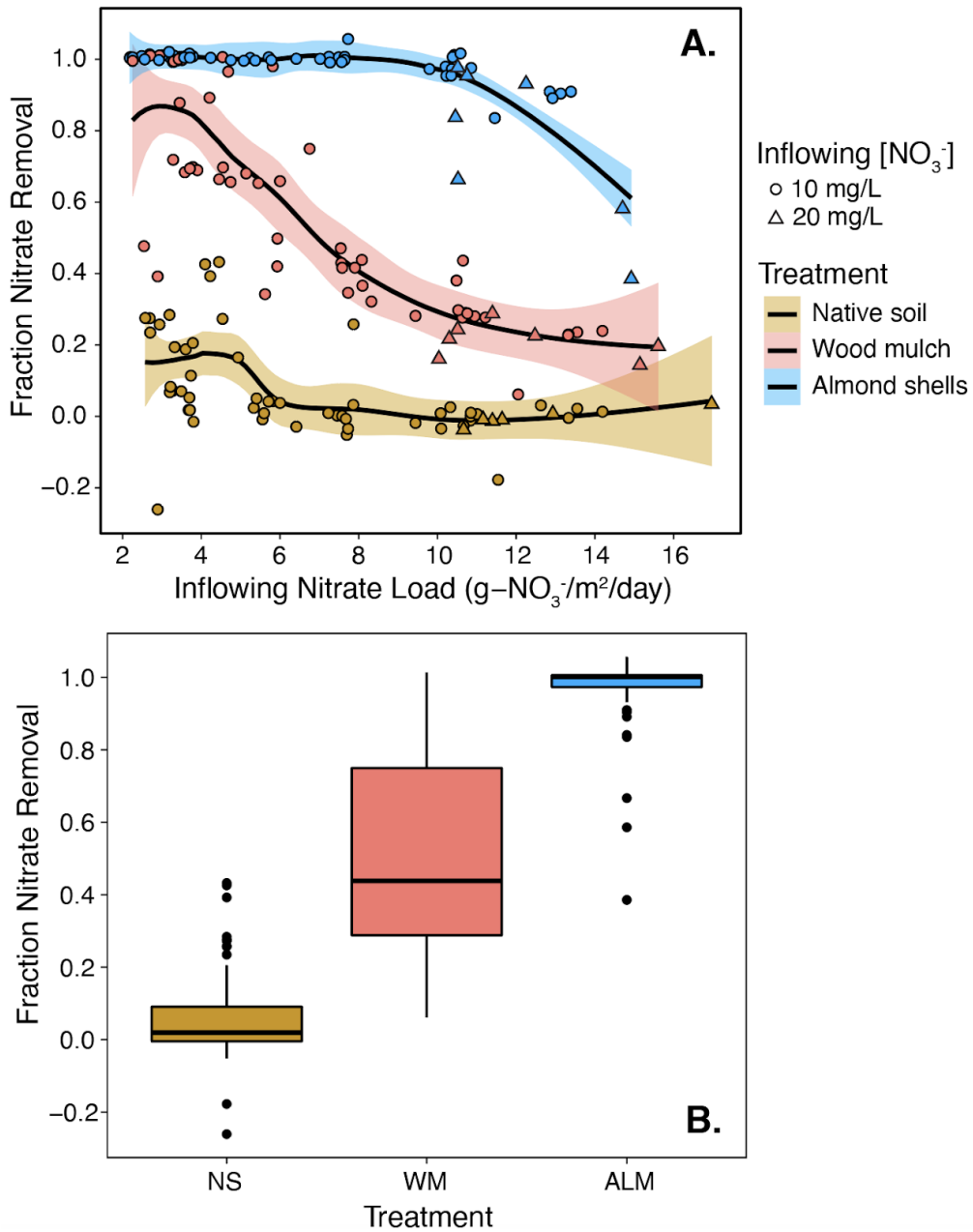
Figure 2-5 Fraction of nitrate removed as a function of the inflowing nitrate load (infiltration rate x influent NO3 concentration) for all three treatments, with a locally weighted least squares regression fit. The shaded region represents the standard error for the regression (A). Box and whisker plots of the fraction of nitrate removed over the duration of the entire experiment, inclusive of all infiltration rates, for each treatment (B).

of influent [NO_3-N] was increased to 20 mg/L, [NO_3-N] in the ALM effluent was less consistent, ranging from 0.41 to 13.5 mg/L (removal of ~39 to 98%). Over the full experiment, both carbon amended columns (WM and ALM) had significantly higher nitrate load reduction ([NO_3-N]$_L$) compared to native soil, and the ALM column had significantly higher [NO_3-N]$_L$ reduction than did the WM column (Table S2-7).

In the NS column, there was no change in [NO_2-N] with depth, and no [NO_2-N] detected in the NS effluent (Figure 2-2C). In the WM column, effluent [NO_2-N] was elevated on the majority of infiltration days, with typical values of ~1 to 2 mg/L. In the ALM column, effluent [NO_2-N] increased during IP 3, when the infiltration rate was ≥ 0.6 m/day. Concentrations of [NO_2-N] in the ALM effluent ranged from 1.89 to 3.79 mg/L at the most rapid infiltration rates during IP 4. [NO_2-N] began decreasing in the ALM column during IP 5, in association with a decrease in infiltration rate. When influent [NO_3-N] was increased to 20 mg/L, [NO_2-N] in the effluent of the ALM treatment increased to a maximum of 2.34 mg/L. NO_2-N is a short-lived intermediate product created during denitrification, and thus finding elevated [NO_2-N] during periods having elevated influent NO_3-N loads suggests that NO_2-N production may be more rapid than consumption, at least temporarily.

There was substantially more [NH_4-N] in the effluent of the carbon amended columns than in the native soil effluent, with an average of 0.24 ± 0.15 mg/L from the ALM treatment, 0.13 ± 0.09 mg/L from the WM treatment, and $0.0.09 \pm 0.07$ mg/L from the NS treatment, compared to an average of 0.07 ± 0.05 mg/L in the influent (Figure S2-7). Higher NH4-N generation in the carbon-amended columns could be the

result of DNRA, which is a more prevalent nitrogen transformation pathway when C/N ratios are higher, as they are in the WM and ALM PRB materials (Figure S2-11) (Nordström et al., 2021; Nordström and Herbert, 2018). However, changes in [NH4-N] were much smaller in magnitude than changes observed for both [NO3-N] and [NO2-N], suggesting that the presence of a carbon amendment did not impact pathways resulting in generation of NH4-N as substantially as those involving NO3-N and NO2-N.

Nitrogen and oxygen stable isotopes of nitrate show a progressive enrichment with distance past the PRB in both of the carbon amended columns, but not in the native soil. Cross plotting $\delta^{15}N$ and $\delta^{18}O$ showed a strong (often linear) enrichment in both isotopes for all days analyzed in fluids from both the WM and ALM treatments (Figure S2-8). Observed enrichment factors were $\varepsilon_N = 21.2$ and $\varepsilon_O = 8.67$ ($\varepsilon_N/\varepsilon_O = 2.6$) for the wood mulch treatment, and $\varepsilon_N = 19.5$ and $\varepsilon_O = 3.74$ ($\varepsilon_N/\varepsilon_O = 6.77$) for the almond shell treatment. In contrast, there were no consistent enrichment trends for fluid samples collected from the native soil column. Commonly reported N-enrichment factors for field studies of denitrification are often $\varepsilon_N \sim 4$ to 30 (Pauwels et al., 2000; Vogel et al., 1981), consistent with results from the wood mulch and almond shell treatments in this study, but observed $\varepsilon_N/\varepsilon_O$ ratios are somewhat higher than values of 0.9 to 2.1 found on other aquatic systems (Bottcher, 1990; Otero et al., 2009).

2.3.3 Trace metals in pore fluid

There were notable increases in dissolved Mn concentrations in pore fluids for all three treatments, particularly during the first half of the experiments (Figure 2-6A).
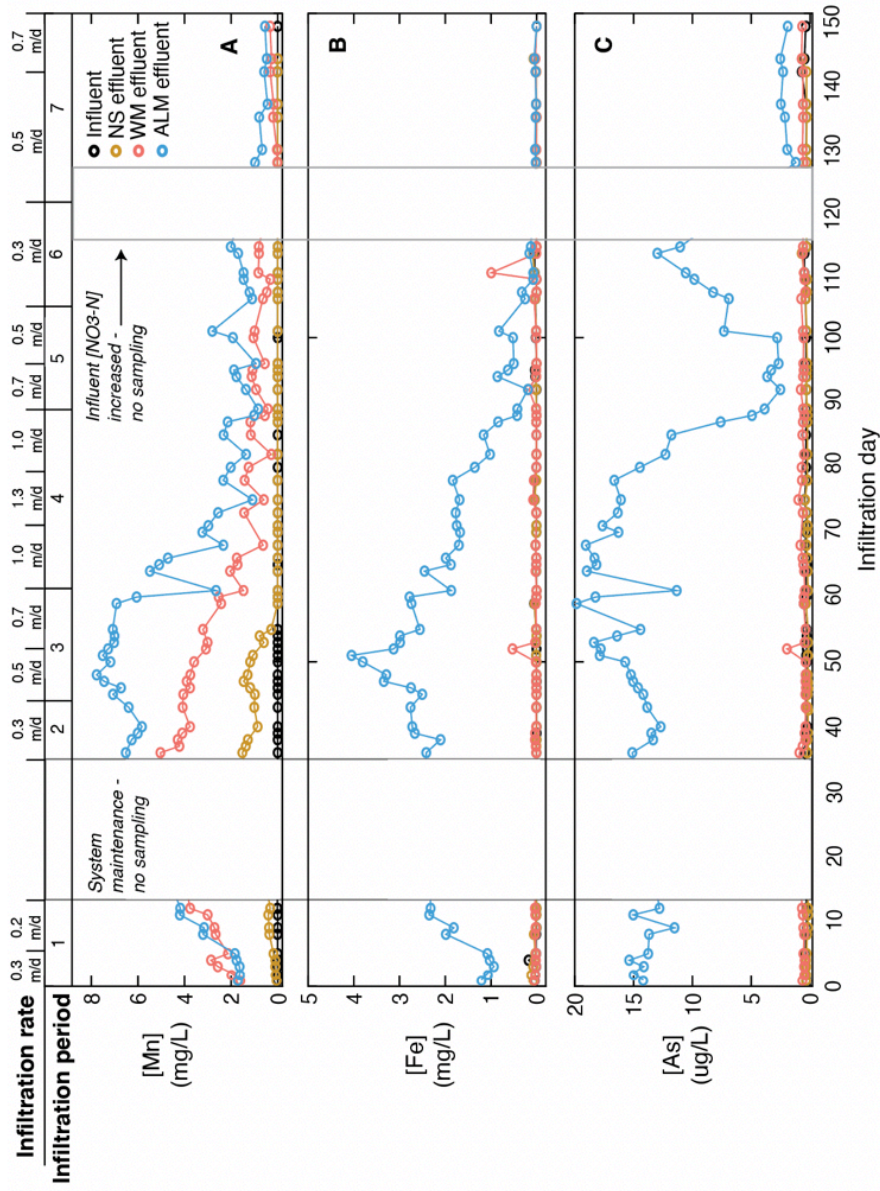
Figure 2-6 Metals influent and effluent Mn (A), Fe (B), and As (C) concentrations of the column influent and effluent for each treatment over the duration of the column experiments, with the corresponding infiltration rate and infiltration period shown along upper *X*-axis. Note difference in scale for [As].

Effluent from the NS treatment had elevated [Mn] concentrations during the first three infiltration periods, with flow rates of ~0.2 to 0.5 m/day (ID 3 to ID 51), with a maximum [Mn] = 1.46 mg/L, but there was little or no elevation in [Mn] during later flow periods. Both of the carbon amended columns saw elevated [Mn] in effluent relative to the NS control, particularly for the ALM treatment (Figure 2-6A; Figure 2-7A). In the WM treatment, [Mn] peaked at 5.02 mg/L on ID 36, then decreased to an average of 1.68 ± 1.41 mg/L for the rest of the test. [Mn] in effluent from the ALM treatment peaked on ID 48 at [Mn] = 7.77 mg/L, then decreased for the rest of the test, with an average [Mn] = 2.84 ± 2.31 mg/L.

There was an increase in dissolved [Fe] in the pore fluid effluent from the ALM treatment, but not in the NS or (with minor exceptions) WC treatments (Figure 2-6B; Figure 2-7B). [Fe] in effluent from the ALM treatment was initially ~1 mg/L, increased to a maximum of 4.05 mg/L on ID 51, then decreased to non-detect levels after ID 114. Similar to Fe, there was little to no dissolved As observed in the effluent of the NS or WM columns, but As was ubiquitous in effluent from the ALM treatment (Figure 2-6C; Figure 2-7C). [As] in the ALM effluent was generally 10-20 µg/L through IP 1-3 (average 14.7 ± 1.65 ug/L), then decreased during IP 4-6 (average 11.5 ± 5.86 ug/L) and IP 7 (2.07 ± 0.45 ug/L (Figure 2-8). Concentrations of As in the ALM column also varied with depth, with the highest [As] observed at 40 and 60 cm depths, particularly at the beginning of the test, and lower [As] at greater depths and in effluent. In aggregate and data from all sampling days, the ALM effluent had significantly higher
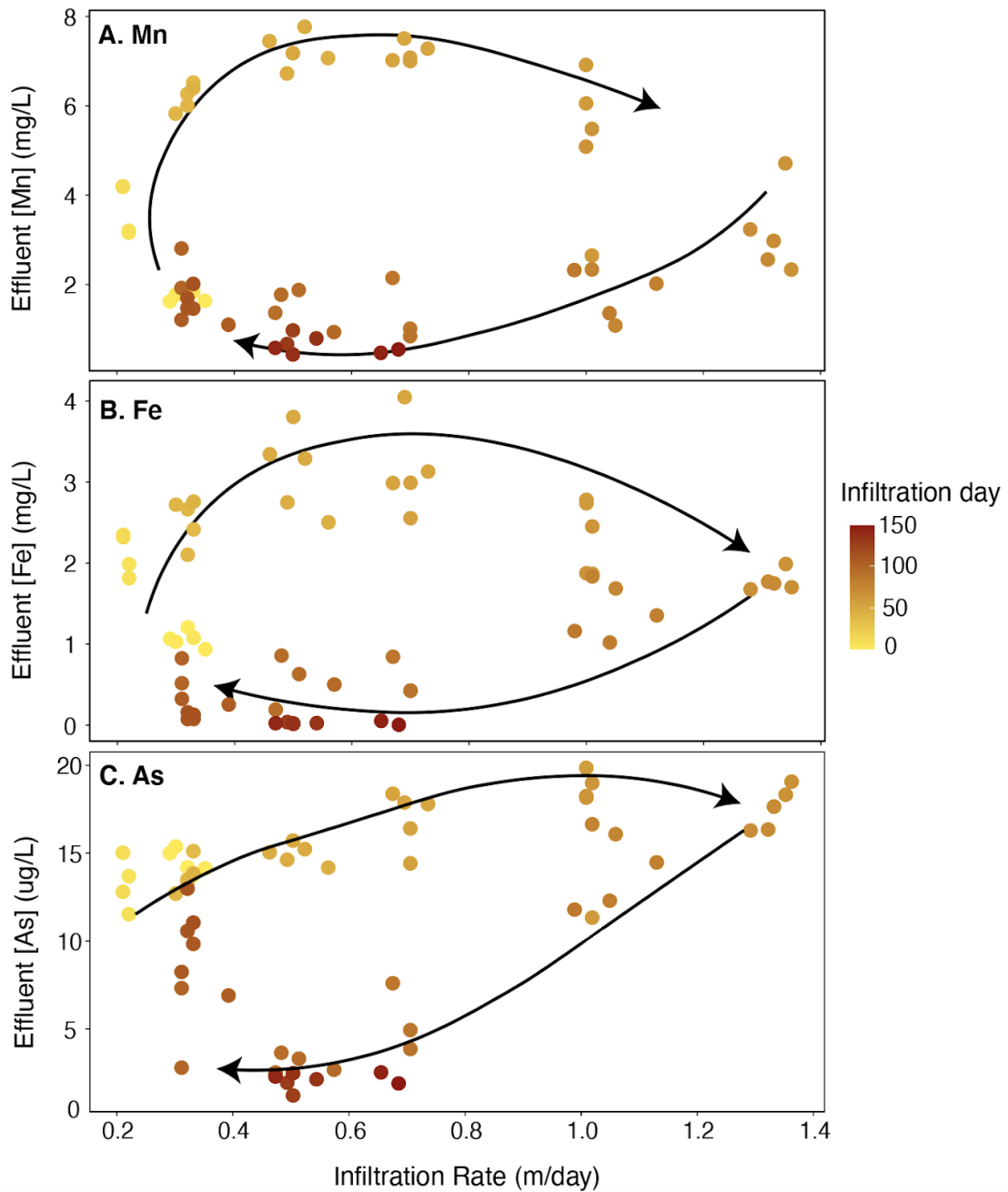
Figure 2-7 Metals as a function of infiltration rate Mn (A), Fe (B), and As (C) concentrations of the ALM column effluent as a function of the infiltration rate over the duration of the column experiments, with color representing the infiltration day and arrows illustrating hysteretic behavior.
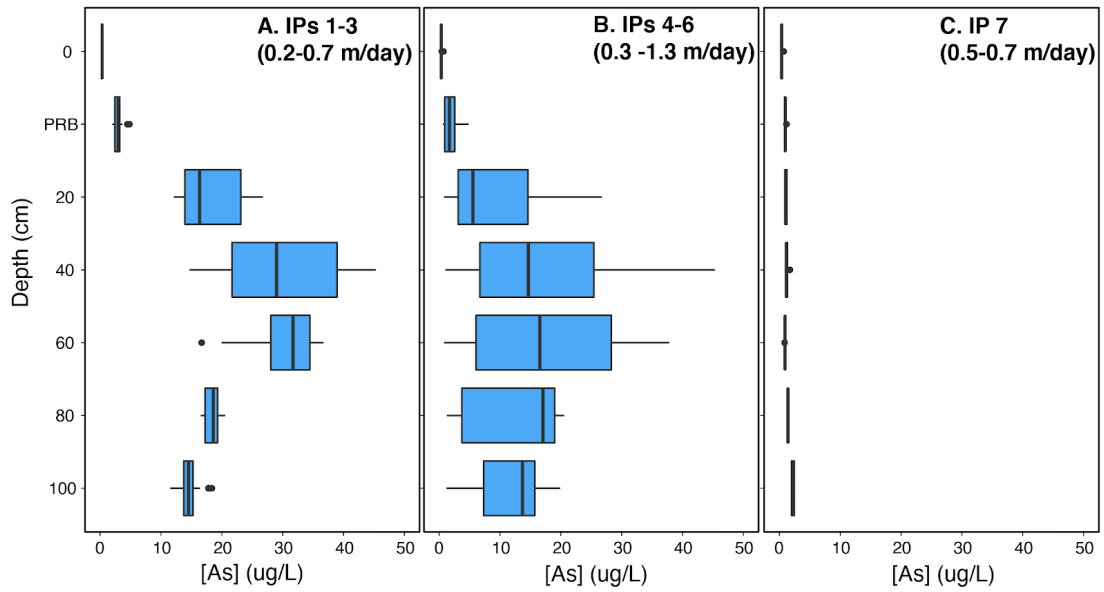
Figure 2-8 Arsenic in the ALM column Arsenic concentrations with depth in fluid samples collected from the almond shell (ALM) column at 3 different timesteps: infiltration periods (IPs) 1 to 3, IPs 4 to 6, and IP 7.

trace metal loads (Mn, Fe, and As) than either the WM effluent or NS effluent (Table S2-5).

2.3.4 Trace metals in soils

Concentrations of Mn in soil samples collected after infiltration were lower than concentrations of Mn in soil samples collected from the field site before infiltration, and were lowest in soils from the carbon amended columns (Figure 2-9A). Concentrations of Fe in all soil samples were high, ranging from 1.0 to 6.3%, and post-infiltration results were mixed: NS samples were slightly elevated, median WM samples were lower, and median ALM samples were more elevated but variable (Figure 2-9B). Concentrations of As were usually lower in soil samples collected after infiltration than in soils collected before infiltration, and were lowest in the almond shell column (Figure 2-9C). It is likely that the decreases in Mn and As in the soils following infiltration were due to leaching, with more trace metals leached from soils amended with carbon than from the native soil, and variability in soil Fe in the column samples after infiltration may result irregular leaching and net transport from the capsule.

2.3.5 Shifts in soil microbiology following infiltration

Within the samples collected from the same field site before the experiments, the 11 most abundant phyla comprised ~94% of total sequences (Figure 2-10A). The three most abundant phyla prior to infiltration were *Actinobacteriota* (22.7%), *Proteobacteria* (20.6%), and *Firmicutes* (14.1%). In samples collected after infiltration, there were decreases in the relative abundance of *Actinobacteriota* and
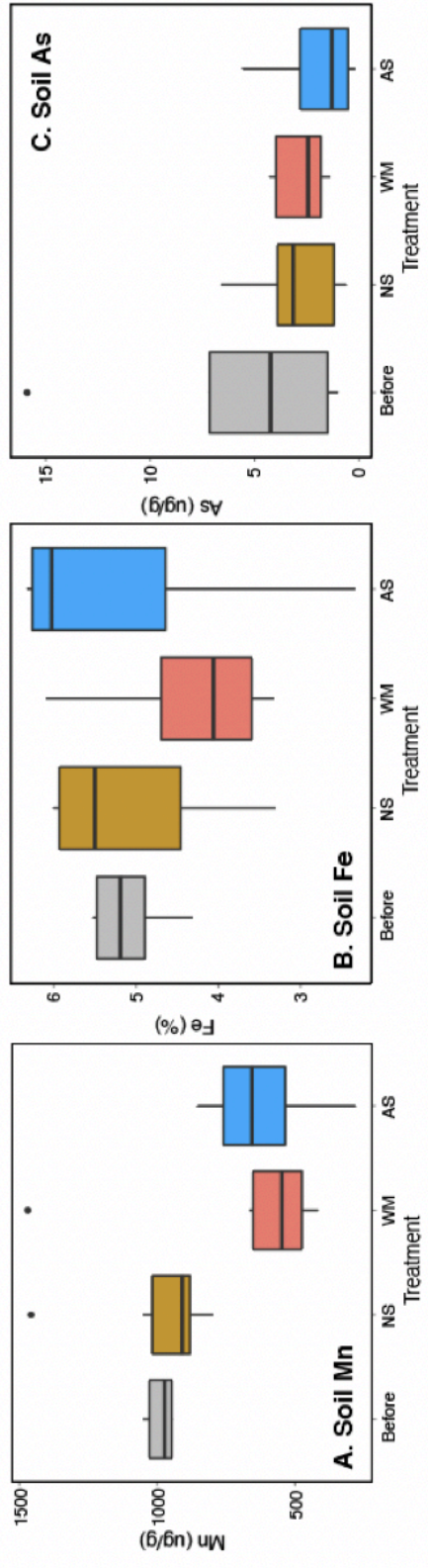
Figure 2-9 Soil metals concentrations before and after infiltration experiments. Box plots show average Mn (A), Fe (B), and As (C) concentrations in soil samples.

99
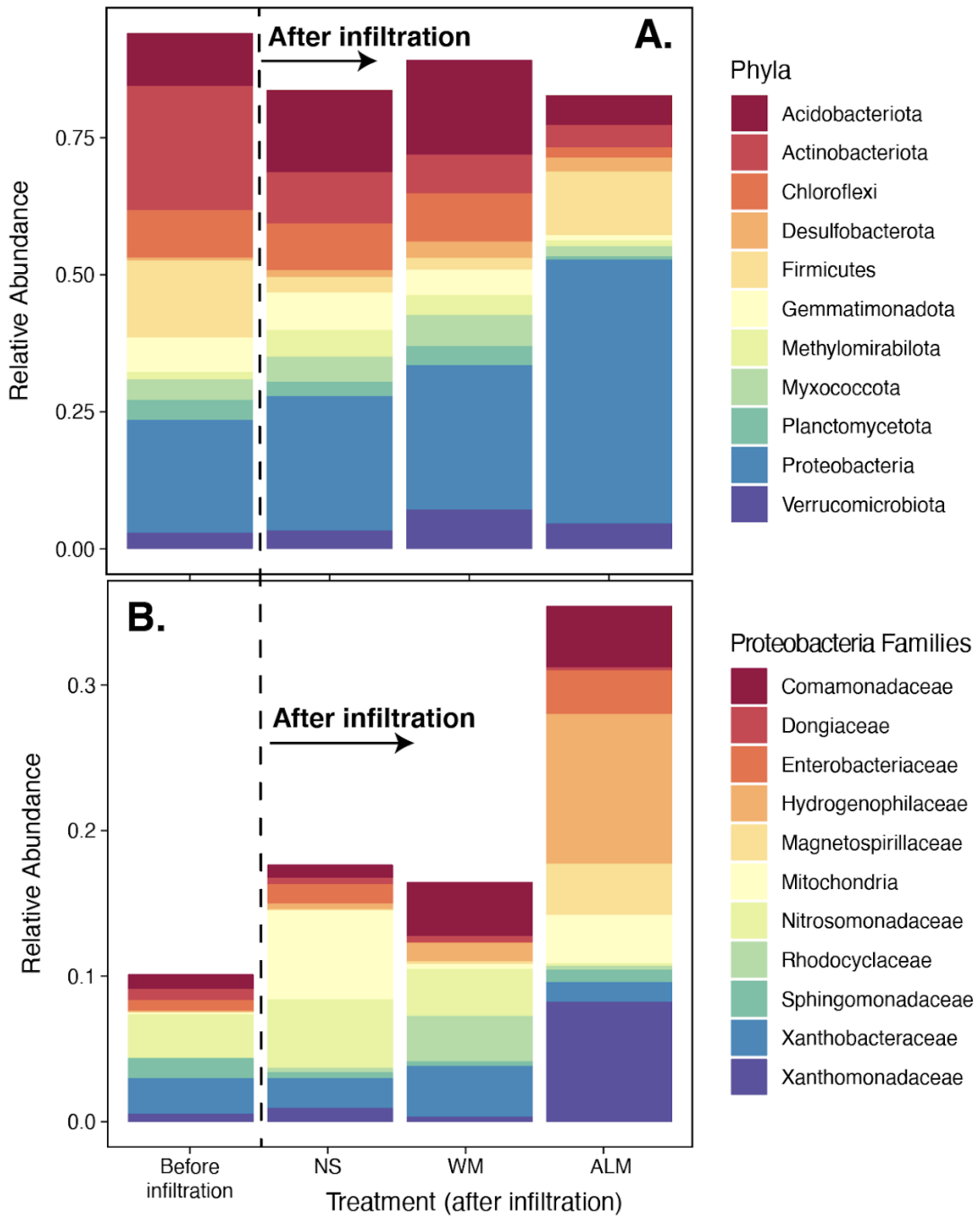
Figure 2-10 Changes in microbial community structure Microbial communities' response to different carbon amendments at the phylum level (A) and changes in Proteobacteria at the family level (B) before and after infiltration.

Firmicutes. However, all samples collected after infiltration had increases in the relative abundance of *Proteobacteria*, with the highest increases found in soils from the column below the ALM treatment. The relative abundance of *Proteobacteria* was 24.5% in the NS column, 26.4% in the WM column, and 48.1% in the ALM column.

Microbes within the phylum *Proteobacteria* are of particular interest because they include families responsible for nitrogen fixation and capable of utilizing the denitrification pathway (Ji et al., 2015; Zumft, 1997). Within the phylum *Proteobacteria*, the most abundant families were identified for each column before and after infiltration (Figure 2-10B). In soils collected before infiltration, the three most abundant *Proteobacteria* families were *Nitrosomonadaceae* (3.0%), *Xanthobacteraceae* (2.4%), and *Sphingomonadaceae* (1.4%). Following infiltration, the three most abundant Proteobacteria families were *Nitrosomonadaceae* (4.7%), *Xanthobacteraceae* (2.1%), and *Enterobacteriaceae* (1.3%) in the NS soils; *Comamonadaceae* (3.7%), *Xanthobacteraceae* (3.5%), and *Nitrosomonadaceae* (3.2%) in the WM soils; and *Hydrogenophilaceae* (10.3%), *Xanthomonadaceae* (8.2%), and *Comamonadaceae* (4.2%) in the ALM soils. Additionally, NMDS analyses indicate that the microbial communities were notably different following infiltration and between treatments (Figure S2-9), with native soil being the least different and soil below the ALM treatment being the most different.

2.4 Discussion

2.4.1 Linkages between carbon amendments and water quality

The presence of a carbon-rich soil amendment significantly increased nitrate removal and trace metal addition relative to the native soil (Tables S2-7-S2-8). Across all infiltration days, the WM and ALM treatments removed a higher fraction of NO_3-N than seen in native soil (Figure 2-5B). In particular, the ALM column saw 100% nitrate removal even at flow rates up to 1 m/day and inflowing N loads up to 10 $g/m^2/day$. However, the ALM column also saw the highest increases in trace metals concentrations in pore fluids, [Mn], [Fe], and [As]. The presence of a carbon amendment likely enhanced denitrification and trace metal mobilization through three primary mechanisms: releasing labile carbon, promoting reducing conditions, and providing habitat for microbial communities.

The effluents from both the WM and ALM columns had significantly higher DOC loads than the native soil over the duration of the tests (Table S2-8). During the first 12 days of the tests, this difference was particularly pronounced, with the ALM treatment having the highest concentrations of DOC, followed by the WM treatment. The addition of high amounts of DOC from the WM and ALM treatments likely facilitated the development of anoxic, reducing conditions, which facilitated the consumption of NO3-N and the release of Mn and Fe.

Additionally, the carbon amendments likely released much higher amounts of DOC than measured, since some DOC must have been consumed by reducing dissolved oxygen, NO_3-N, Mn-oxides, and Fe-(oxyhydr)oxides by the time the water in the PRB

was sampled. The total amount of DOC released by the carbon amendments can be estimated by considering the redox reactions for aerobic respiration, denitrification, manganese-reduction, and iron-reduction. For example, during infiltration period 7, when the amount of influent NO_3-N was highest, it would have taken ~8 mg/L DOC release by the WM treatment and ~20 mg/L DOC released by the ALM treatment in order to achieve the geochemical transformations measured from the influent to the outflow (Table S2-5). While these DOC values are higher than those measured (Table S2-6), the almond shells and wood mulch are likely producing at least that much carbon, but it's being consumed by the time the fluid reaches the first sampling point (the PRB outlet). Previous studies measured long-term DOC releases from wood chip amendments up to ~40 mg/L and subsequent high nitrate removal rates (Greenan et al., 2009; Robertson, 2010). In addition, leaching experiments with the carbon materials used in this study that are not underway show up to ~1,500 mg/L of DOC released from almond shells and up to ~250 mg/L of DOC released from wood mulch when in contact with low ionic (MilliQ) water for 1-24 hours (pers comms, A. Serrano). The large amount of DOC leached from the almond shells is consistent with strong indications of reducing conditions in soils of the underlying ALM column (Figs. 2-2, 2-4, and 2-6).

The nature of DOC compounds can also influence impacts on water quality, with more humic, recalcitrant forms of DOC being less bioavailable to microbes carrying out nitrogen and trace metal cycling (Kleber, 2010; Porcal et al., 2009). Lower SUVA values in fluid samples collected from the WM and ALM columns indicate that there was less humic matter, meaning that the DOC was less recalcitrant and more

bioavailable compared to DOC in the NS column (Weishaar et al., 2003). The WM and ALM columns had similar SUVA values, but yielded substantially different geochemical results (Figs. 2-2, 2-5 and 2-6). Previous studies have found that almond shells include a significant fraction of water-soluble fermentable sugars such as sucrose and fructose, whereas wood mulch leaches more hydrophobic and high molecular weight compounds (Abusallout and Hua, 2017; Holtman et al., 2015). Future work to understand differences in DOC released from candidate carbon sources should explore the nature of specific organic compounds in solution during infiltration.

Soil samples collected from below the ALM treatment following the flow experiment contained a significantly different microbial community compared to that seen both before flow and after flow with other treatments (Figs. 2-10 and S2-9). The ALM soils had the highest increase in relative abundance of Proteobacteria, a phylum known for denitrification (Ji et al., 2015; Zumft, 1997). Among Proteobacteria, there were elevated abundances of *Hydrogenophilaceae*, *Comamonadaceae*, and *Xanthomonadaceae*. *Hydrogenophilaceae* is a family of bacteria known to be sulfur reducers and found commonly in reducing environments such as water treatment digesters and hot springs (Orlygsson and Krisstjansson, 2014). *Comamonadaceae* is a family of bacteria containing facultative organotrophs that degrade carbon and also can be responsible for denitrification (Chu and Wang, 2017; Hahn et al., 2010; Nakatsu et al., 2006). *Xanthomonadaceae* are known to participate in the nitrogen cycle as well, including nitrate reduction (Baskaran et al., 2020). The increase in the relative

abundance of these families suggests that the almond shells promote more microbial reduction of carbon, nitrogen, and trace metals, leading to more reducing conditions.

These results suggest that, when considering the addition of a carbon amendment, the nature and quantity of carbon added is important for understanding and anticipating water quality impacts. In the present study, wood mulch and almond shells had similar weight percentages of carbon (Figure S2-10), but the almond shell treatment was associated with more nitrate removal and greater trace metal addition. These findings also add to a growing body of literature demonstrating that carbon amendments can enhance nitrate removal, but can also facilitate the mobilization of redox-sensitive elements (Hellman et al., 2022, 2019; Valhondo et al., 2020, 2015, 2014).

2.4.2 Linkages between infiltration dynamics and water quality

All treatments in this study showed a decrease in the fraction of nitrate removed as the flow rate and corresponding inflowing nitrate load increased (Figure 2-5). The rate at which the fraction of nitrate removal decreased was dependent on the treatment type, with the almond shells and wood mulch-amended columns removing significantly more nitrate even when the inflowing nitrate loads approached 15 $g\text{-}NO_3\text{-}N/m^2/day$ (Figure 2-5A). Slower infiltration rates favor development of anoxic conditions in the shallow subsurface, which favors nitrate removal processes like denitrification. Importantly, slower infiltration rates increase the residence time of the influent water in the subsurface, which allows more time for microbial processing. However, high inflowing nitrate concentrations can overwhelm the microbial capacity for

denitrification, even with longer retention times, resulting in a smaller fraction of nitrate being removed.

There is evidence for active denitrification within the PRB capsules and in the soils below both the wood mulch and almond shell treatments. Both PRB-treated columns had elevated nitrite, which is generated as an intermediate product along the denitrification pathway, for flow rates ≥ 0.7 m/day for the almond shell treatment and ≥ 0.3 m/day for the wood mulch treatment (Figure 2-2). When the inflowing nitrate load is low (with low concentration and/or slow flow rate), complete denitrification is possible and intermediate nitrite is depleted as quickly as it is produced. However, as the inflowing nitrate load increases, the delivery of nitrate overwhelms the capacity of soil microbes to keep up with all steps in the denitrification process, resulting in a standing stock on nitrite despite relatively rapid processing.

While the infiltration rate appeared to be a primary control on the extent of nitrate removal, for a given PRB treatment, infiltration rate was not as strong of a control on trace metal cycling. The release of trace metals was much more strongly correlated with the presence of a carbon amendment, the carbon amendment type, and the history of past infiltration (Figure 2-6, Tables S2-10-S2-11). The type of carbon amendment had the most notable impact on trace metal release, with the ALM effluent having significantly higher loads of Mn, Fe, and As compared to the WM or NS columns (Table S2-8). However, the concentration of trace metals in the column effluent generally increased the most during the first 50-60 days of flow, then decreased, regardless of the change in infiltration rate. This apparently hysteretic behavior (Figure

2-7) is likely a consequence of the trace metals being geogenic, rather than introduced with the fluids, providing a limited pool of mobile trace metals in the soils that is depleted over time. It is also unlikely that the carbon amendment materials (wood mulch and almond shells) were the sources of the trace metals, as both the wood mulch and almond shells had significantly lower metal (Mn, Fe, and As) concentrations than the soils (Figure S2-12; Table S2-9). This result is encouraging for the long-term application of carbon amendments during MAR, because after an initial pulse of trace metal release, metal loading should decrease. In addition, oxic conditions are likely to occur deeper within the vadose zone and in many shallow aquifers (Böhlke et al., 2002; Fryar et al., 2000; Pabich et al., 2001), which should limit trace metal mobility and subsequent transport (Ying et al., 2017).

2.4.3 Implications for managed recharge field studies

Results from this study suggest that there are tradeoffs between nitrate removal and metals mobilization during managed recharge. As such, care should be taken when applying a carbon amendment for MAR operations with considerations of water quality targets and potential infiltration rates. At infiltration rates measured at Teichert Ranch (0.01-0.2 m/day), native soil, wood mulch, and almond shells all promote NO3-N removal. However, using almond shells as a soil carbon amendment might also enhance leaching from soils of geogenic trace metals (Mn, Fe, and As) by promoting strongly reducing conditions. In this study, the influence of soil leaching decreases over time and with depth (distance), with the lowest trace metal concentrations in pore waters found at the end of flow experiments (Figs. 2-6, 2-7, and 2-8). At an operating flood-

MAR site that experiences periodic inundation and drying, highly reducing conditions are likely to be short-lived, with the shallowest soil being saturated days or a few weeks following a rain event, then draining and becoming more oxic over time. Additionally, oxic conditions are expected to dominate as water flows through the vadose zone underlying an infiltration basin, providing opportunities for the readsorption of metals that were initially mobilized.

If the primary concerns at a managed recharge project site are decreasing nitrate concentrations, and there is periodic wetting and drying of the system, a very labile carbon source, such as almond shells, may be the most appropriate. Periodic wetting/drying cycles will allow the temporary development of suboxic conditions that promote nitrate removal while also preventing the development of highly reducing conditions that lead to trace metal release. This has been demonstrated in sequential managed aquifer recharge technologies (SMART), which utilize sequential treatment zones characterized by carbon-rich, reducing zones followed by carbon-depleted, oxic zones to address multiple redox-sensitive contaminants (Hellauer et al., 2018b, 2017; Regnery et al., 2016b). However, if a managed recharge project is expected to have consistently saturated conditions, then wood mulch (or a limited application of almond shells) may be a preferable amendment. Additionally, adding somewhat less bioavailable carbon may be preferred compared to almond shells where trace contaminants such as arsenic are present at high concentrations in shallow soils. In the present study, wood mulch promoted considerable nitrate removal, but did not lead to as strong of reducing conditions and associated trace metal release compared to almond

shells. This study helps to motivate additional work to better understand the mechanisms by which different carbon sources impact water quality during managed recharge, including the nature of DOC compounds, so that MAR systems can be optimized to provide maximum water supply and quality benefits.

2.5 Conclusions

Experimental results from this study demonstrate the benefits of applying a carbon amendment during flood-MAR, and illustrates the complexity in relationships between infiltration rates, water chemistry, soil microbial ecology, and the nature of the applied carbon source. Of the two carbon amendments tested, almond shells promoted more efficient nitrate removal than did wood mulch, but also resulted in greater release of trace metals from soils under some conditions. As a result, wood mulch or a smaller quantity of almond shells may be a preferred soil amendment for managed recharge where consistently saturated conditions are expected and/or where geogenic trace metals in the soil are a concern. The amount of geogenic metals released during infiltration for MAR ultimately depends on the amount and form of reactive metal compounds associated with soil grains; once the soil reservoir of mobile metals is depleted, geogenic metals should be less of a concern for ongoing MAR operations. Given the dual threats to groundwater supply and quality that water-stressed regions worldwide are facing, incorporating a soil carbon source into the design of managed recharge projects should be considered as a means to generate multiple benefits for associated water resources and aquatic systems.

ACKNOWLEDGEMENTS

REFERENCES

Abusallout, I., Hua, G., 2017. Characterization of dissolved organic carbon leached from a woodchip bioreactor. Chemosphere 183, 36–43. https://doi.org/10.1016/j.chemosphere.2017.05.066

Addy, K., Gold, A.J., Christianson, L.E., David, M.B., Schipper, L.A., Ratigan, N.A., 2016. Denitrifying bioreactors for nitrate removal: A meta-analysis. J. Environ. Qual. 45, 873–881. https://doi.org/10.2134/jeq2015.07.0399

Bachand, P.A.M., Roy, S.B., Choperena, J., Cameron, D., Horwath, W.R., 2014. Implications of using on-farm flood flow capture to recharge groundwater and mitigate flood risks along the Kings River, CA. Environ. Sci. Technol. 48, 13601–13609. https://doi.org/10.1021/es501115c

Baskaran, V., Patil, P.K., Antony, M.L., Avunje, S., Nagaraju, V.T., Ghate, S.D., Nathamuni, S., Dineshkumar, N., Alavandi, S. V., Vijayan, K.K., 2020. Microbial community profiling of ammonia and nitrite oxidizing bacterial enrichments from brackishwater ecosystems for mitigating nitrogen species. Sci. Rep. 10, 1–11. https://doi.org/10.1038/s41598-020-62183-9

Beganskas, S., Gorski, G., Weathers, T., Fisher, A.T., Schmidt, C., Saltikov, C., Redford, K., Stoneburner, B., Harmon, R., Weir, W., 2018. A horizontal permeable reactive barrier stimulates nitrate removal and shifts microbial ecology during rapid infiltration for managed recharge. Water Res. 144, 274–284. https://doi.org/10.1016/j.watres.2018.07.039

Böhlke, J.K., Wanty, R., Tuttle, M., Delin, G., Landon, M., 2002. Denitrification in the recharge area and discharge area of a transient agricultural nitrate plume in a glacial outwash sand aquifer, Minnesota. Water Resour. Res. 38, 10-1-10–26. https://doi.org/10.1029/2001wr000663

Borch, T., Kretzscmar, R., Kappler, A., Van Cappellen, P., Ginder-Vogel, M., Voegelin, A., Campbell, K., 2010. Biogeochemical Redox Processes and their Impact on Contaminant Dynamics. Environ. Sci. Technol. 44, 15–23.

Bouwer, H., 2002. Artificial recharge of groundwater: hydrogeology and engineering.

Hydrogeol. J. 121–142.

Burri, N.M., Weatherl, R., Moeck, C., Schirmer, M., 2019. A review of threats to groundwater quality in the anthropocene. Sci. Total Environ. 684, 136–154. https://doi.org/10.1016/j.scitotenv.2019.05.236

Chen, P.Z., Cui, J.Y., Hu, L., Zheng, M.Z., Cheng, S.P., Huang, J.W., Mu, K.G., 2014. Nitrogen removal improvement by adding peat in deep soil of subsurface wastewater infiltration system. J. Integr. Agric. 13, 1113–1120. https://doi.org/10.1016/S2095-3119(13)60401-3

Chu, L., Wang, J., 2017. Denitrification of groundwater using a biodegradable polymer as a carbon source: Long-term performance and microbial diversity. RSC Adv. 7, 53454–53462. https://doi.org/10.1039/c7ra11151g

Dahlke, H.E., Brown, A.G., Orloff, S., Putnam, D.H., O'Geen, T., 2018a. Managed winter flooding of alfalfa recharges groundwater with minimal crop damage. Calif. Agric. 72, 65–75.

Dahlke, H.E., LaHue, G.T., Mautner, M.R.L., Murphy, N.P., Patterson, N.K., Waterhouse, H., Yang, F., Foglia, L., 2018b. Chapter 8 - Managed Aquifer Recharge as a Tool to Enhance Sustainable Groundwater Management in California: Examples from Field and Modeling Studies. Adv. Chem. Pollution, Environ. Manag. Prot. 3, 215–275.

Dillon, P., 2005. Future management of aquifer recharge. Hydrogeol. J. 13, 313–316. https://doi.org/10.1007/s10040-004-0413-6

Dillon, P., Pavelic, P., Toze, S., Rinck-Pfeiffer, S., Martin, R., Knapton, A., Pidsley, D., 2006. Role of aquifer storage in water reuse. Desalination. https://doi.org/10.1016/j.desal.2005.04.109

Doussan, C., Ledoux, E., Detay, M., 1998. River-Groundwater Exchanges, Bank Filtration, and Groundwater Quality: Ammonium Behavior. J. Environ. Qual. 27, 1418–1427. https://doi.org/10.2134/jeq1998.00472425002700060019x

Exner, M.E., Hirsh, A.J., Spalding, R.F., 2014. Nebraska's groundwater legacy: Nitrate contamination beneath irrigated cropland. Water Resour. Res. 50, 4474–

4489. https://doi.org/10.1002/2013WR015073.Received

Fakhreddine, S., Dittmar, J., Phipps, D., Dadakis, J., Fendorf, S., 2015. Geochemical Triggers of Arsenic Mobilization during Managed Aquifer Recharge. Environ. Sci. Technol. 49, 7802–7809. https://doi.org/10.1021/acs.est.5b01140

Fakhreddine, S., Prommer, H., Scanlon, B.R., Ying, S.C., Nicot, J.P., 2021. Mobilization of arsenic and other naturally occurring contaminants during managed aquifer recharge: A critical review. Environ. Sci. Technol. 55, 2208–2223. https://doi.org/10.1021/acs.est.0c07492

Fendorf, S., Nico, P.S., Kocar, B.D., Masue, Y., Tufano, K.J., 2010. Arsenic Chemistry in Soils and Sediments. Dev. Soil Sci. 34, 357–378. https://doi.org/10.1016/S0166-2481(10)34012-8

Fryar, A.E., Macko, S.A., Mullican, W.F., Romanak, K.D., Bennett, P.C., 2000. Nitrate reduction during ground-water recharge, Southern High Plains, Texas. J. Contam. Hydrol. 40, 335–363. https://doi.org/10.1016/S0169-7722(99)00059-5

Gorski, G., Dailey, H., Fisher, A.T., Schrad, N., Saltikov, C., 2020. Denitrification during infiltration for managed aquifer recharge: Infiltration rate controls and microbial response. Sci. Total Environ. 727. https://doi.org/10.1016/j.scitotenv.2020.138642

Gorski, G., Fisher, A.T., Beganskas, S., Weir, W.B., Redford, K., Schmidt, C., Saltikov, C., 2019. Field and Laboratory Studies Linking Hydrologic, Geochemical, and Microbiological Processes and Enhanced Denitrification during Infiltration for Managed Recharge. Environ. Sci. Technol. 53, 9491–9501. https://doi.org/10.1021/acs.est.9b01191

Grau-Martínez, A., Folch, A., Torrentó, C., Valhondo, C., Barba, C., Domènech, C., Soler, A., Otero, N., 2018. Monitoring induced denitrification during managed aquifer recharge in an infiltration pond. J. Hydrol. 561, 123–135. https://doi.org/10.1016/j.jhydrol.2018.03.044

Greenan, C.M., Moorman, T.B., Parkin, T.B., Kaspar, T.C., Jaynes, D.B., 2009. Denitrification in Wood Chip Bioreactors at Different Water Flows. J. Environ.

Qual. 38, 1664–1671.

Hahn, M.W., Kasalický, V., Jezbera, J., Brandt, U., Šimek, K., 2010. Limnohabitans australis sp. nov., isolated from a freshwater pond, and emended description of the genus Limnohabitans. Int. J. Syst. Evol. Microbiol. 60, 2946–2950. https://doi.org/10.1099/ijs.0.022384-0

Hellauer, K., Karakurt, S., Sperlich, A., Burke, V., Massmann, G., Hübner, U., Drewes, J.E., 2018. Establishing sequential managed aquifer recharge technology (SMART) for enhanced removal of trace organic chemicals: Experiences from field studies in Berlin, Germany. J. Hydrol. 563, 1161–1168. https://doi.org/10.1016/j.jhydrol.2017.09.044

Hellauer, K., Mergel, D., Ruhl, A.S., Filter, J., Hübner, U., Jekel, M., Drewes, J.E., 2017. Advancing sequential managed aquifer recharge technology (SMART) using different intermediate oxidation processes. Water 9, 1–14. https://doi.org/10.3390/w9030221

Hellman, M., Bonilla-Rosso, G., Widerlund, A., Juhanson, J., Hallin, S., 2019. External carbon addition for enhancing denitrification modifies bacterial community composition and affects CH4 and N2O production in sub-arctic mining pond sediments. Water Res. 158, 22–33. https://doi.org/10.1016/j.watres.2019.04.007

Hellman, M., Valhondo, C., Martínez-Landa, L., Carrera, J., Juhanson, J., Hallin, S., 2022. Nitrogen Removal Capacity of Microbial Communities Developing in Compost- and Woodchip-Based Multipurpose Reactive Barriers for Aquifer Recharge With Wastewater. Front. Microbiol. 13, 1–11. https://doi.org/10.3389/fmicb.2022.877990

Holtman, K.M., Offeman, R.D., Franqui-Villanueva, D., Bayati, A.K., Orts, W.J., 2015. Countercurrent extraction of soluble sugars from almond hulls and assessment of the bioenergy potential. J. Agric. Food Chem. 63, 2490–2498. https://doi.org/10.1021/jf5048332

Jessen, S., Postma, D., Thorling, L., Muller, S., Leskela, J., Engesgaard, P., 2017.

Decadal variations in groundwater quality: A legacy from nitrate leaching and denitrification by pyrite in a sandy aquifer. Water Resour. Res. 53, 184–198. https://doi.org/10.1111/j.1752-1688.1969.tb04897.x

Ji, B., Yang, K., Zhu, L., Jiang, Y., Wang, H., Zhou, J., Zhang, H., 2015. Aerobic denitrification: A review of important advances of the last 30 years. Biotechnol. Bioprocess Eng. 20, 643–651. https://doi.org/10.1007/s12257-015-0009-0

Katz, B.G., 2020. Groundwater Contamination from Reactive Nitrogen, in: Nitrogen Overload. pp. 119–154. https://doi.org/10.1002/9781119513933.ch7

Kleber, M., 2010. What is recalcitrant soil organic matter? Environ. Chem. 7, 320–332. https://doi.org/10.1071/EN10006

Kocis, T.N., Dahlke, H.E., 2017. Availability of high-magnitude streamflow for groundwater banking in the Central Valley, California. Environ. Res. Lett. 12. https://doi.org/10.1088/1748-9326/aa7b1b

Korom, S.F., 1992. Natural denitrification in the saturated zone: A review. Water Resour. Res. 28, 1657–1668. https://doi.org/10.1029/92WR00252

Li, Y. hua, Li, H. bo, Xu, X. yang, Xiao, S. yao, Wang, S. qi, Xu, S. cong, 2017. Fate of nitrogen in subsurface infiltration system for treating secondary effluent. Water Sci. Eng. 10, 217–224. https://doi.org/10.1016/j.wse.2017.10.002

Lloréns, M., Aguilar, M.I., Sáez, J., Ortuño, J.F., Meseguer, V.F., 2021. Nitrogen transformation in two vertical subsurface flow pilot plants 1–30.

Long, A., Heitman, J., Tobias, C., Philips, R., Song, B., 2013. Co-occurring anammox, denitrification, and codenitrification in agricultural soils. Appl. Environ. Microbiol. 79, 168–176. https://doi.org/10.1128/AEM.02520-12

López, R., Burgos, P., Hermoso, J.M., Hormaza, J.I., González-Fernández, J.J., 2014. Long term changes in soil properties and enzyme activities after almond shell mulching in avocado organic production. Soil Tillage Res. 143, 155–163. https://doi.org/10.1016/j.still.2014.06.004

Marr, J., Arrate, D., Maendly, R., Dhillon, D., Stygar, S., 2018. FLOOD-MAR: Using Flood Water for Managed Aquifer Recharge to Support Sustainable Water

Resources.

Nakatsu, C.H., Hristova, K., Hanada, S., Meng, X.Y., Hanson, J.R., Scow, K.M., Kamagata, Y., 2006. Methylibium petroleiphilum gen. nov., sp. nov., a novel methyl tert-butyl ether-degrading methylotroph of the Betaproteobacteria. Int. J. Syst. Evol. Microbiol. 56, 983–989. https://doi.org/10.1099/ijs.0.63524-0

Nordström, A., Hellman, M., Hallin, S., Herbert, R.B., 2021. Microbial controls on net production of nitrous oxide in a denitrifying woodchip bioreactor. J. Environ. Qual. 50, 228–240. https://doi.org/10.1002/jeq2.20181

Nordström, A., Herbert, R.B., 2018. Determination of major biogeochemical processes in a denitrifying woodchip bioreactor for treating mine drainage. Ecol. Eng. 110, 54–66. https://doi.org/10.1016/j.ecoleng.2017.09.018

O'Geen, A.T., Saal, M.B.B., Dahlke, H., Doll, D., Elkins, R., Fulton, A., Fogg, G., Harter, T., Hopmans, J.W., Ingels, C., Niederholzer, F., Solis, S.S., Verdegaal, P., Walkinshaw, M., 2015. Soil suitability index identifies potential areas for groundwater banking on agricultural lands. Calif. Agric. 69, 75–84. https://doi.org/10.3733/ca.v069n02p75

Orlygsson, J., Krisstjansson, J.K., 2014. The Family Hydrogenophilaceae, in: The Prokaryotes. pp. 859–868.

Pabich, W.J., Valiela, I., Hemond, H.F., 2001. Relationship between DOC concentration and vadose zone thickness and depth below water Pabich, W.J., Valiela, I., Hemond, H.F., 2001. Relationship between DOC concentration and vadose zone thickness and depth below water table in groundwater of Cape Cod, . Biogeochemistry 55, 247–268.

Pavelic, P., Dillon, P.J., Barry, K.E., Gerges, N.Z., 2006. Hydraulic evaluation of aquifer storage and recovery (ASR) with urban stormwater in a brackish limestone aquifer. Hydrogeol. J. 14, 1544–1555. https://doi.org/10.1007/s10040-006-0078-4

Pensky, J., Fisher, A.T., Gorski, G., Schrad, N., Dailey, H., Beganskas, S., Saltikov, C., 2022. Enhanced cycling of nitrogen and metals during rapid infiltration:

Implications for managed recharge. Sci. Total Environ. 838, 156439.
https://doi.org/10.1016/j.scitotenv.2022.156439

Porcal, P., Koprivnjak, J.F., Molot, L.A., Dillon, P.J., 2009. Humic substances-part 7:
The biogeochemistry of dissolved organic carbon and its interactions with
climate change. Environ. Sci. Pollut. Res. 16, 714–726.
https://doi.org/10.1007/s11356-009-0176-7

Regnery, J., Wing, A.D., Kautz, J., Drewes, J.E., 2016. Introducing sequential
managed aquifer recharge technology (SMART) - From laboratory to full-scale
application. Chemosphere 154, 8–16.
https://doi.org/10.1016/j.chemosphere.2016.03.097

Robertson, W.D., 2010. Nitrate removal rates in woodchip media of varying age.
Ecol. Eng. 36, 1581–1587. https://doi.org/10.1016/j.ecoleng.2010.01.008

Schmidt, C.M., Fisher, A.T., Racz, A., Wheat, C.G., Los Huertos, M., Lockwood, B.,
2012. Rapid nutrient load reduction during infiltration of managed aquifer
recharge in an agricultural groundwater basin: Pajaro Valley, California. Hydrol.
Process. 26, 2235–2247. https://doi.org/10.1002/hyp

Sebilo, M., Mayer, B., Nicolardot, B., Pinay, G., Mariotti, A., 2013. Long-term fate
of nitrate fertilizer in agricultural soils. Proc. Natl. Acad. Sci. U. S. A. 110,
18185–18189. https://doi.org/10.1073/pnas.1305372110

Shan, J., Zhao, X., Sheng, R., Xia, Y., Ti, C., Quan, X., Wang, S., Wei, W., Yan, X.,
2016. Dissimilatory Nitrate Reduction Processes in Typical Chinese Paddy
Soils: Rates, Relative Contributions, and Influencing Factors. Environ. Sci.
Technol. 50, 9972–9980. https://doi.org/10.1021/acs.est.6b01765

Smedley, P.L., Kinniburgh, D.G., 2002. A review of the source, behaviour and
distribution of arsenic in natural waters. Appl. Geochemistry 17, 517–568.
https://doi.org/10.1016/S0883-2927(02)00018-5

Valhondo, C., Carrera, J., Ayora, C., Barbieri, M., Nödler, K., Licha, T., Huerta, M.,
2014. Behavior of nine selected emerging trace organic contaminants in an
artificial recharge system supplemented with a reactive barrier. Environ. Sci.

Pollut. Res. 21, 11832–11843. https://doi.org/10.1007/s11356-014-2834-7

Valhondo, C., Carrera, J., Ayora, C., Tubau, I., Martinez-Landa, L., Nödler, K., Licha, T., 2015. Characterizing redox conditions and monitoring attenuation of selected pharmaceuticals during artificial recharge through a reactive layer. Sci. Total Environ. 512–513, 240–250. https://doi.org/10.1016/j.scitotenv.2015.01.030

Valhondo, C., Martínez-Landa, L., Carrera, J., Díaz-Cruz, S.M., Amalfitano, S., Levantesi, C., 2020. Six artificial recharge pilot replicates to gain insight into water quality enhancement processes. Chemosphere 240. https://doi.org/10.1016/j.chemosphere.2019.124826

Van Drecht, G., Bouwman, A.F., Knoop, J.F., Beusen, H.W., Meinardi, C.R., 2003. Global modeling of the fate of nitrogen from point and nonpoint sources in soils, groundwater, and surface water. Global Biogeochem. Cycles 17, 1115.

Van Meter, K.J., Basu, N.B., Veenstra, J.J., Burras, C.L., 2016. The nitrogen legacy: Emerging evidence of nitrogen accumulation in anthropogenic landscapes. Environ. Res. Lett. 11. https://doi.org/10.1088/1748-9326/11/3/035014

Vida, C., Bonilla, N., de Vicente, A., Cazorla, F.M., 2016. Microbial profiling of a suppressiveness-induced agricultural soil amended with composted almond shells. Front. Microbiol. 7, 1–14. https://doi.org/10.3389/fmicb.2016.00004

Wada, Y., Van Beek, L.P.H., Van Kempen, C.M., Reckman, J.W.T.M., Vasak, S., Bierkens, M.F.P., 2010. Global depletion of groundwater resources. Geophys. Res. Lett. 37, 1–5. https://doi.org/10.1029/2010GL044571

Weishaar, J.L., Aiken, G.R., Bergamaschi, B.A., Fram, M.S., Fujii, R., Mopper, K., 2003. Evaluation of specific ultraviolet absorbance as an indicator of the chemical composition and reactivity of dissolved organic carbon. Environ. Sci. Technol. 37, 4702–4708. https://doi.org/10.1021/es030360x

World Health Organization, 2017. Guidelines for drinking-water quality: fourth edition incorporating the first addendum.

Ying, S.C., Schaefer, M. V., Cock-Esteb, A., Li, J., Fendorf, S., 2017. Depth

Stratification Leads to Distinct Zones of Manganese and Arsenic Contaminated Groundwater. Environ. Sci. Technol. 51, 8926–8932. https://doi.org/10.1021/acs.est.7b01121

Zumft, W.G., 1997. Cell biology and molecular basis of denitrification. Microbiol. Mol. Biol. Rev. 61, 533–616.

Treatment	Infiltration Rate (m/day)	V_L[a] (m/day)	n_e[c] (-)	a_L[b] (cm)	PV_e[d] (L)
NS	0.36	1.8	0.20	30	1.6
WM	0.33	1.4	0.24	35	1.9
ALM	0.32	1.2	0.27	30	2.1

[a] linear velocity
[b] longitudinal dispersion
[c] effective porosity
[d] effective pore volume

Table S2-1. Hydraulic Properties determined by solute breakthrough curves

Analytes (units)	Concentration
Aluminum (mg/L)	0.02-0.06
Arsenic (ug/L)	ND
Fluoride (mg/L)	ND - 0.24
Nitrate as N (mg/L)	ND - 1.9
Iron (mg/L)	ND
Chloride (mg/L)	15-30
Manganese (ug/L)	ND - 2.3
Specific conductance (umhos/cm)	415 - 485
Sulfate (mg/L)	60 - 88
Total dissolved solids (mg/L)	270 - 280
Hardness (mg/L)	152 - 200
Sodium (mg/L)	22 - 28
Hexavalent chromium (ug/L)	0.054 - 0.18

Table S2. Tap water chemistry from the City of Santa Cruz, CA for 2021, the year that sampling was conducted (City of Santa Cruz Water Department, 2021).

Table S2-3. Summary of influent and effluent nutrient and DOC concentration data for each treatment at each infiltration rate.

Treatment	Infiltration days (IDs)	Infiltration rate	Influent [NO3-N]	Effluent [NO3-N]	Influent [NO2-N]	Effluent [NO2-N]	Influent [NH4-N]	Effluent [NH4-N]	Influent [DOC]	Effluent [DOC]
		m/day	mg/L	mg/L	mg/L	mg/L	mg/L	mg/L	mg/L	mg/L
NS	1-5	0.38	10.7	6.76	0.00	0.05	0.01	0.10	0.54	1.55
		(0.02)	(1.18)	(0.74)	(0.00)	(0.00)	(0.03)	(0.05)	(0.38)	(0.68)
NS	6-12	0.26	10.6	8.04	0.00	0.05	0.06	0.10	0.58	0.89
		(0.01)	(0.57)	(0.63)	(0.00)	(0.01)	(0.06)	(0.04)	(0.68)	(0.75)
NS	13-43	0.33	10.4	9.13	0.00	0.15	0.06	0.17	1.48	1.46
		(0.02)	(0.14)	(0.59)	(0.02)	(0.00)	(0.04)	(0.03)	(0.08)	(0.18)
NS	44-50	0.54	10.2	9.69	0.00	0.07	0.07	0.23	1.48	1.58
		(0.02)	(0.65)	(1.11)	(0.00)	(0.03)	(0.03)	(0.07)	(0.13)	(0.14)
NS	51-55	0.72	10.5	10.5	0.00	0.02	0.03	0.08	1.71	1.56
		(0.02)	(0.25)	(0.18)	(0.00)	(0.01)	(0.01)	(0.03)	(0.22)	(0.18)
NS	56-65	1.03	10.3	10.4	0.00	0.00	0.04	0.02	1.92	1.79
		(0.06)	(0.07)	(0.09)	(0.00)	(0.00)	(0.01)	(0.01)	(0.22)	(0.17)
NS	66-73	1.35	9.67	9.85	0.00	0.00	0.10	0.04	1.5	1.46
		(0.05)	(0.66)	(0.18)	(0.00)	(0.00)	(0.13)	(0.01)	(0.00)	(0.32)
NS	74-85	1.04	9.97	10.0	0.00	0.00	0.06	0.03	1.58	1.63
		(0.05)	(0.17)	(0.20)	(0.00)	(0.01)	(0.03)	(0.02)	(0.15)	(0.16)
NS	86-90	0.70	11.1	10.4	0.00	0.00	0.14	0.13	1.79	1.63
		(0.01)	(0.30)	(1.18)	(0.00)	(0.00)	(0.01)	(0.03)	(0.08)	(0.39)
NS	91-98	0.52	11.1	10.9	0.00	0.00	0.13	0.12	1.82	1.82
		(0.03)	(0.20)	(0.48)	(0.05)	(0.05)	(0.00)	(0.02)	(0.06)	(0.20)
NS	99-114	0.34	10.7	10.2	0.00	0.03	0.09	0.07	1.59	1.28

NS	115-141	0.53 (0.01)	21.6 (1.15)	21.9 (0.85)	0.00 (0.05)	0.00 (0.04)	0.09 (0.05)	0.04 (0.04)	1.21 (0.19)	1.29 (0.02)
NS	142-148	0.75 (0.02)	22.6 (0.73)	21.8 (0.47)	0.00 (0.01)	0.00 (0.01)	0.10 (0.08)	0.01 (0.02)	2.31 (0.16)	1.29 (0.05)
		(0.00)	(0.48)	(0.00)	(0.03)	(0.00)	(0.00)	(0.00)	(1.24)	(0.00)
WM	1-5	0.4 (0.01)	10.7 (1.18)	1.17 (1.28)	0.00 (0.00)	0.84 (0.88)	0.01 (0.03)	0.06 (0.02)	0.54 (0.38)	3.32 (0.78)
WM	6-12	0.25 (0.03)	10.7 (0.51)	0.00 (0.09)	0.00 (0.00)	0.00 (0.00)	0.06 (0.06)	0.09 (0.05)	0.58 (0.68)	2.91 (0.38)
WM	13-43	0.32 (0.02)	10.4 (0.43)	0.04 (0.03)	0.00 (0.02)	0.16 (0.00)	0.06 (0.31)	0.22 (0.03)	1.48 (0.08)	2.79 (0.55)
WM	44-50	0.53 (0.03)	10.2 (0.65)	2.80 (1.48)	0.00 (0.00)	1.28 (0.32)	0.07 (0.03)	0.31 (0.13)	1.48 (0.13)	2.37 (0.31)
WM	51-55	0.74 (0.02)	10.5 (0.25)	5.94 (0.23)	0.00 (0.00)	1.10 (0.02)	0.03 (0.01)	0.08 (0.03)	1.71 (0.22)	2.34 (0.09)
WM	56-65	1.03 (0.06)	10.3 (0.07)	7.41 (0.10)	0.00 (0.00)	0.61 (0.02)	0.04 (0.01)	0.05 (0.02)	1.92 (0.22)	2.37 (0.33)
WM	66-73	1.38 (0.04)	9.67 (0.66)	7.71 (0.15)	0.00 (0.00)	0.53 (0.05)	0.10 (0.13)	0.07 (0.05)	1.5 (0.00)	1.65 (0.18)
WM	74-85	1.06 (0.04)	9.97 (0.17)	6.47 (0.68)	0.00 (0.00)	0.77 (0.10)	0.06 (0.03)	0.09 (0.01)	1.58 (0.15)	1.82 (0.23)
WM	86-90	0.73 (0.04)	11.1 (0.26)	7.08 (0.34)	0.00 (0.00)	1.07 (0.02)	0.14 (0.01)	0.18 (0.03)	1.79 (0.08)	2.44 (0.59)
WM	91-98	0.55	11.2	5.62	0.02	1.12	0.13	0.17	1.82	2.8

WM	99-114	0.33 (0.04)	10.5 (0.27)	4.22 (1.66)	0.02 (0.05)	1.24 (0.12)	0.09 (0.00)	0.15 (0.02)	1.59 (0.06)	2.13 (0.44)
WM	115-141	0.5 (0.05)	21.8 (1.35)	16.7 (1.29)	0.08 (0.05)	0.96 (0.17)	0.09 (0.05)	0.13 (0.07)	1.21 (0.19)	1.89 (0.29)
WM	142-148	0.7 (0.04)	22.3 (0.73)	18.4 (0.09)	0.10 (0.01)	0.73 (0.10)	0.10 (0.08)	0.05 (0.05)	2.31 (0.16)	1.62 (0.09)
ALM	1-5	0.32 (0.00)	10.7 (0.48)	0.00 (0.43)	0.00 (0.03)	0.00 (0.22)	0.01 (0.00)	0.07 (0.00)	0.54 (1.24)	5.09 (0.14)
ALM	6-12	0.22 (0.02)	10.6 (1.18)	0.00 (0.00)	0.00 (0.00)	0.00 (0.00)	0.06 (0.03)	0.13 (0.07)	0.58 (0.38)	1.94 (3.47)
ALM	13-43	0.32 (0.01)	10.4 (0.57)	0.00 (0.00)	0.00 (0.00)	0.00 (0.00)	0.06 (0.06)	0.17 (0.03)	1.48 (0.68)	2.62 (0.73)
ALM	44-50	0.51 (0.01)	10.2 (0.14)	0.00 (0.00)	0.00 (0.01)	0.00 (0.00)	0.07 (0.00)	0.48 (0.03)	1.48 (0.08)	1.9 (0.38)
ALM	51-55	0.70 (0.04)	10.5 (0.65)	0.00 (0.00)	0.00 (0.00)	0.24 (0.00)	0.03 (0.03)	0.38 (0.20)	1.71 (0.13)	2.27 (1.18)
ALM	56-65	1.00 (0.02)	10.3 (0.25)	0.15 (0.00)	0.00 (0.00)	2.37 (0.19)	0.04 (0.01)	0.34 (0.12)	1.92 (0.22)	2.14 (0.10)
ALM	66-73	1.32 (0.01)	9.67 (0.07)	1.05 (0.24)	0.00 (0.00)	3.53 (0.33)	0.10 (0.01)	0.11 (0.14)	1.50 (0.22)	1.94 (0.17)
ALM	74-85	1.04 (0.03)	9.97 (0.66)	0.25 (0.21)	0.00 (0.00)	3.14 (0.33)	0.06 (0.13)	0.13 (0.03)	1.58 (0.00)	1.87 (0.00)
ALM	86-90	0.69 (0.05)	11.1 (0.17)	0.00 (0.26)	0.00 (0.00)	0.34 (0.24)	0.14 (0.03)	0.21 (0.04)	1.79 (0.15)	2.22 (0.29)

ALM									
91-98	0.51 (0.02)	11.1 (0.30)	0.02 (0.00)	0.00 (0.00)	0.00 (0.15)	0.13 (0.01)	0.24 (0.08)	1.82 (0.08)	2.22 (0.10)
99-114	0.33 (0.05)	10.7 (0.2)	0.00 (0.03)	0.00 (0.05)	0.03 (0.09)	0.09 (0.00)	0.24 (0.02)	1.56 (0.06)	2.15 (0.13)
115-141	0.5 (0.03)	21.6 (1.15)	2.73 (0.00)	0.00 (0.05)	1.54 (0.04)	0.09 (0.05)	0.35 (0.07)	1.76 (0.16)	1.53 (0.18)
142-148	0.67 (0.03)	22.6 (0.73)	11.4 (2.86)	0.00 (0.01)	1.16 (0.82)	0.10 (0.08)	0.24 (0.14)	2.31 (0.95)	1.26 (0.17)
	(0.02)	(0.48)	(2.91)	(0.03)	(0.35)	(0.00)	(0.00)	(1.24)	(0.19)

Table S2-4. Summary of influent and effluent Mn, Fe, and As concentration data for each treatment at each infiltration rate.

Treat ment	Infiltration days (IDs)	Infiltration rate	Influent [Mn]	Effluent [Mn]	Influent [Fe]	Effluent [Fe]	Influent [As]	Effluent [As]
		m/day	mg/L	mg/L	mg/L	mg/L	ug/L	ug/L
NS	1-5	0.38	3.0E-3	0.10	0.05	0.07	0.35	0.32
		(0.02)	(8.6E-4)	(0.05)	(0.07)	(0.03)	(0.02)	(0.02)
NS	6-12	0.26	4.5E-3	0.59	5.2E-3	0.02	0.33	0.20
		(0.01)	(5.0E-3)	(0.52)	(3.0E-3)	(0.02)	(0.07)	(0.04)
NS	13-43	0.33	9.6E-4	1.26	2.9E-3	0.00	0.32	0.20
		(0.02)	(2.4E-4)	(0.28)	(1.4E-3)	(0.00)	(0.07)	(0.04)
NS	44-50	0.54	1.2E-3	1.22	2.3E-3	0.00	0.31	0.18
		(0.02)	(9.6E-4)	(0.18)	(1.5E-3)	(0.00)	(0.03)	(0.02)
NS	51-55	0.72	8.5E-4	0.68	5.6E-3	0.00	0.31	0.17
		(0.02)	(3.2E-4)	(0.33)	(4.0E-3)	(0.01)	(0.02)	(0.02)
NS	56-65	1.03	1.5E-3	0.00	1.6E-2	0.01	0.36	0.23
		(0.06)	(8.7E-4)	(0.00)	(2.3E-2)	(0.02)	(0.10)	(0.09)
NS	66-73	1.35	9.0E-4	0.00	8.9E-3	0.02	0.34	0.24
		(0.05)	(1.4E-4)	(0.00)	(8.6E-3)	(0.01)	(0.04)	(0.03)
NS	74-85	1.04	1.5E-3	0.00	2.1E-2	0.01	0.37	0.29
		(0.05)	(9.0E-4)	(0.00)	(2.4E-2)	(0.02)	(0.06)	(0.11)
NS	86-90	0.70	1.3E-3	0.00	1.1E-2	0.02	0.31	0.25
		(0.01)	(9.0E-4)	(0.00)	(1.1E-2)	(0.01)	(0.01)	(0.05)
NS	91-98	0.52	1.7E-3	0.00	1.9E-2	0.01	0.32	0.28
		(0.03)	(8.4E-4)	(0.00)	(1.6E-2)	(0.02)	(0.02)	(0.04)
NS	99-114	0.34	8.4E-4	0.00	1.7E-2	0.01	0.37	0.33
		(0.01)	(2.0E-3)	(0.00)	(1.9E-2)	(0.00)	(0.07)	(0.11)
NS	115-141	0.53	4.0E-4	0.00	1.9E-2	0.02	0.43	0.37
		(0.02)	(2.0E-3)	(0.00)	(1.4E-2)	(0.01)	(0.17)	(0.15)
NS	142-148	0.75	1.9E-3	0.00	2.8E-2	0.07	0.37	0.64
		(0.00)	(1.2E-3)	(0.00)	(1.8E-2)	(0.02)	(0.07)	(0.00)
WM	1-5	0.40	3.0E-3	2.23	0.05	0.02	0.35	0.53
		(0.01)	(8.6E-4)	(0.49)	(0.07)	(0.01)	(0.02)	(0.08)
WM	6-12	0.25	4.5E-3	3.44	5.2E-3	0.03	0.33	0.66
		(0.03)	(5.0E-3)	(0.99)	(3.0E-3)	(0.01)	(0.07)	(0.16)
WM	13-43	0.32	9.6E-4	4.28	2.9E-3	0.02	0.32	0.56
		(0.02)	(2.4E-4)	(0.47)	(1.4E-3)	(0.01)	(0.07)	(0.21)
WM	44-50	0.53	1.2E-3	3.81	2.3E-3	0.01	0.31	0.38

		(0.03)	(9.6E-4)	(0.17)	(1.5E-3)	(0.01)	(0.03)	(0.02)
WM	51-55	0.74	8.5E-4	3.10	5.6E-3	0.19	0.31	0.94
		(0.02)	(3.2E-4)	(0.10)	(4.0E-3)	(0.29)	(0.02)	(0.89)
WM	56-65	1.03	1.5E-3	2.04	1.6E-2	0.01	0.36	0.52
		(0.06)	(8.7E-4)	(0.45)	(2.3E-2)	(0.01)	(0.10)	(0.05)
WM	66-73	1.38	9.0E-4	1.28	8.9E-3	0.03	0.34	0.69
		(0.04)	(1.4E-4)	(0.58)	(8.6E-3)	(0.03)	(0.18)	(0.11)
WM	74-85	1.06	1.5E-3	0.94	2.1E-2	0.04	0.37	0.72
		(0.04)	(9.0E-4)	(0.48)	(2.4E-2)	(0.07)	(0.23)	(0.18)
WM	86-90	0.73	1.3E-3	0.84	1.1E-2	0.04	0.31	0.62
		(0.04)	(9.4E-4)	(0.34)	(1.1E-2)	(0.07)	(0.59)	(0.11)
WM	91-98	0.55	1.7E-3	0.94	1.9E-2	0.02	0.32	0.61
		(0.04)	(8.4E-4)	(0.23)	(1.6E-2)	(0.02)	(0.44)	(0.10)
WM	99-114	0.33	8.4E-4	0.69	1.7E-2	0.02	0.37	0.56
		(0.05)	(2.0E-4)	(0.32)	(1.9E-2)	(0.02)	(0.29)	(0.13)
WM	115-141	0.50	4.0E-3	0.15	1.9E-2	0.01	0.43	0.60
		(0.04)	(7.3E-3)	(0.13)	(1.4E-2)	(0.02)	(0.17)	(0.03)
WM	142-148	0.70	1.9E-3	0.30	2.8E-2	0.01	0.37	0.69
		(0.00)	(1.2E-3)	(0.05)	(1.8E-2)	(0.02)	(0.07)	(0.03)
ALM	1-5	0.32	3.0E-3	1.71	0.05	1.06	0.35	14.5
		(0.02)	(8.6E-4)	(0.09)	(0.07)	(0.10)	(0.02)	(0.67)
ALM	6-12	0.22	4.5E-3	4.25	5.2E-3	2.18	0.33	13.6
		(0.01)	(5.0E-3)	(1.36)	(3.0E-3)	(0.26)	(0.07)	(1.52)
ALM	13-43	0.32	9.6E-4	6.16	2.9E-3	2.48	0.32	13.7
		(0.01)	(2.4E-4)	(0.30)	(1.4E-3)	(0.28)	(0.07)	(1.03)
ALM	44-50	0.51	1.2E-3	7.24	2.3E-3	3.14	0.31	15.0
		(0.04)	(9.6E-4)	(0.39)	(1.5E-3)	(0.52)	(0.03)	(0.58)
ALM	51-55	0.70	8.5E-4	7.18	5.6E-3	3.14	0.31	17.0
		(0.02)	(3.2E-4)	(0.21)	(4.0E-3)	(0.55)	(0.02)	(1.61)
ALM	56-65	1.00	1.5E-3	5.24	1.6E-2	2.34	0.36	17.3
		(0.01)	(8.7E-4)	(1.60)	(2.3E-2)	(0.45)	(0.10)	(3.41)
ALM	66-73	1.32	9.0E-4	3.16	8.9E-3	1.78	0.34	17.5
		(0.03)	(1.4E-4)	(0.93)	(8.6E-3)	(0.12)	(0.04)	(1.22)
ALM	74-85	1.04	1.5E-3	1.82	2.1E-2	1.41	0.37	14.3
		(0.05)	(9.0E-4)	(0.57)	(2.4E-2)	(0.34)	(0.06)	(2.18)
ALM	86-90	0.69	1.3E-3	1.43	1.1E-2	0.55	0.31	4.51
		(0.02)	(9.0E-4)	(0.54)	(1.1E-2)	(0.29)	(0.01)	(1.93)
ALM	91-98	0.51	1.7E-3	1.57	1.9E-2	0.54	0.32	2.99
		(0.05)	(8.4E-4)	(0.42)	(1.6E-2)	(0.24)	(0.02)	(0.47)

ALM	99-114	0.33	8.4E-4	1.70	1.7E-2	0.40	0.37	7.02
		(0.03)	(2.0E-3)	(0.70)	(1.9E-2)	(0.29)	(0.07)	(2.62)
ALM	115-141	0.50	4.0E-4	0.69	1.9E-2	0.02	0.43	2.02
		(0.03)	(2.0E-3)	(0.21)	(1.4E-2)	(0.01)	(0.17)	(0.49)
ALM	142-148	0.67	1.9E-3	0.51	2.8E-2	0.03	0.37	2.22
		(0.02)	(1.2E-3)	(0.05)	(1.8E-2)	(0.03)	(0.07)	(0.45)

Treatment	Average analyte differences/day (mg/L)				Average DOC needed/day (mg/L)				
	ΔDO*	ΔNO3-N	ΔMn	ΔFe	DO consumption*	NO3-N reduction	Mn-oxide reduction	Fe-oxide reduction	Total
NS	-9.00	1.0E-03	-3.0E-03	1.0E-03	3.03	-7.6E-04	-3.2E-04	5.0E-05	3.03
	-	(0.51)	(7.0E-03)	(1.6E-02)		(0.55)	(7.9E-04)	(8.3E-04)	(0.55)
WM	-9.00	-4.72	0.19	-4.0E-03	3.03	5.10	0.02	-2.2E-04	8.15
	-	(1.08)	(0.12)	(7.0E-03)		(1.17)	(0.02)	(3.8E-04)	(1.19)
ALM	-9.00	-16.70	0.64	1.0E-02	3.03	18.07	0.08	5.5E-04	21.18
	-	(4.80)	(0.19)	(8.0E-03)		(5.20)	(0.02)	(4.4E-04)	(5.22)

* DO was estimated by assuming influent water was fully saturated with oxygen (DO = 9 mg/L) and subsequently fully depleted (DO = 0 mg/L) following infiltration.

Table S2-5. Average differences in analyte concentrations (effluent minus influent) and [DOC] needed for the associated redox reactions during infiltration (aerobic respiration, nitrate reduction, Mn-oxide reduction, and Fe-oxide) during IP 7, when influent [NO3-N] was highest.

Treatment	Average DOC influent/day (mg/L)	Average DOC PRB effluent/day (mg/L)	Average DOC column effluent/day (mg/L)
NS	1.57	1.06	1.32
	(0.81)	(0.21)	(0.10)
WM	1.57	1.98	1.81
	(0.81)	(0.25)	(0.16)
ALM	1.57	1.49	1.46
	(0.81)	(0.11)	(0.21)

Table S2-6. Average [DOC] in the influent, PRB effluent, and column effluent during IP 7.

Comparison	ΔNO3-N (gNO$_3$/m^2/d)		ΔNO2$_L$ (gNO$_2$/m^2/d)		ΔNH4$_L$ (gNH$_4$/m^2/d)	
	p.value	sig @ 0.05	p.value	sig @ 0.05	p.value	sig @ 0.05
NS > WM	< 2.2E-16	1	NA	NA	NA	NA
NS > ALM	< 2.2E-16	1	NA	NA	NA	NA
WM > ALM	2.8E-12	1	NA	NA	NA	NA
NS < WM	NA	NA	< 2.2E-16	1	0.01	1
NS < ALM	NA	NA	< 4.4E-6	1	2.8E-7	1
WM < ALM	NA	NA	0.01	1	4.8E-5	1

Table S2-7. Single-tailed t-test results comparing N species load change between treatments over the duration of the experiments, where ΔX_L is equal to the effluent load minus the influent load.

Comparison	ΔDOC$_L$ (gDOC/m^2/d)		ΔMn$_L$ (gMn/m^2/d)		ΔFe$_L$ (gFe/m^2/d)		ΔAs$_L$ (gAs/m^2/d)	
	p.value	sig @ 0.05	p.value	sig @ 0.05	p.value	sig @ 0.05	p.value	sig @ 0.05
NS < WM	2.5E-9	1	4.6E-12	1	0.06	0	2.0E-11	1
NS < ALM	4.9E-5	1	2.0E-11	1	6.1E-12	1	2.1E-12	1
WM < ALM	0.79	0	5.6E-5	1	9.8E-12	1	5.6E-12	1

Table S2-8. Single-tailed t-test results comparing DOC load and metals load change between treatments over the duration of the experiments, where ΔX_L is equal to the effluent load minus the influent load.

Comp.	TOC (%)		TN (%)		Mn (ug/g)		Fe (%)		As (ug/g)	
	p.val	sig @ 0.05	p.val	sig @ 0.05	p.val	sig @ 0.05	p.val	sig @ 0.05	p.val	sig @ 0.05
Before > NS	NA	NA	NA	NA	0.55	0	0.49	0	0.17	0
Before > WM	NA	NA	NA	NA	0.06	0	0.07	0	0.14	0
Before > ALM	NA	NA	NA	NA	0.004	1	0.56	0	0.09	0
Before < NS	0.01	1	0.004	1	NA	NA	NA	NA	NA	NA
Before < WM	0.07	0	0.04	1	NA	NA	NA	NA	NA	NA
Before < ALM	0.08	0	0.06	0	NA	NA	NA	NA	NA	NA

Table S2-9. Single-tailed t-test results comparing TOC, TN, Mn, Fe, and As in soils before and after infiltration for each treatment.

Variable 1	Variable 2	Treatment	Correlation coefficient (tau)	p.value	sig @ 0.05
Inflowing nitrate load	Fraction of nitrate removed	All	-0.27	1.3E-7	1
Inflowing nitrate load	Effluent [Mn]	All	-0.19	3.1E-4	1
Inflowing nitrate load	Effluent [Fe]	All	-0.1	0.07	0
Inflowing nitrate load	Effluent [As]	All	0.03	0.62	0
Inflowing nitrate load	Fraction of nitrate removed	NS	-0.39	1.1E-5	1
Inflowing nitrate load	Effluent [Mn]	NS	-0.34	2.8E-4	1
Inflowing nitrate load	Effluent [Fe]	NS	-0.03	0.71	0
Inflowing nitrate load	Effluent [As]	NS	0.04	0.69	0
Inflowing nitrate load	Fraction of nitrate removed	WM	-0.71	5.4E-16	1
Inflowing nitrate load	Effluent [Mn]	WM	-0.32	4.5E-4	1
Inflowing nitrate load	Effluent [Fe]	WM	-0.20	0.03	1
Inflowing nitrate load	Effluent [As]	WM	0.18	0.04	1
Inflowing nitrate load	Fraction of nitrate removed	ALM	-0.50	3.9E-8	1
Inflowing nitrate load	Effluent [Mn]	ALM	-0.15	0.09	0
Inflowing nitrate load	Effluent [Fe]	ALM	-0.12	0.19	0
Inflowing nitrate load	Effluent [As]	ALM	0.04	0.68	0

Table S2-10. Kendall's tau test results assessing correlations between the inflowing nitrate load and nutrient and trace metal cycling for each treatment over the duration of the experiments.

Variable 1	Variable 2	Treatment	Correlation coefficient (tau)	p.value	sig @ 0.05
Infiltration day	Fraction of nitrate removed	All	-0.19	1.5E-4	1
Infiltration day	Effluent [Mn]	All	-0.34	2.7E-11	1
Infiltration day	Effluent [Fe]	All	-0.15	2.5E-3	1
Infiltration day	Effluent [As]	All	0.04	0.49	0
Infiltration day	Fraction of nitrate removed	NS	-0.42	2.7E-6	1
Infiltration day	Effluent [Mn]	NS	-0.52	1.6E-8	1
Infiltration day	Effluent [Fe]	NS	-0.03	0.74	0
Infiltration day	Effluent [As]	NS	0.32	5.3E-4	1
Infiltration day	Fraction of nitrate removed	WM	-0.44	4.3E-7	1
Infiltration day	Effluent [Mn]	WM	-0.66	3.1E-13	1
Infiltration day	Effluent [Fe]	WM	-0.27	3.0E-3	1
Infiltration day	Effluent [As]	WM	0.02	0.02	1
Infiltration day	Fraction of nitrate removed	ALM	-0.31	6.1E-4	1
Infiltration day	Effluent [Mn]	ALM	-0.47	6.6E-8	1
Infiltration day	Effluent [Fe]	ALM	-0.57	7.0E-11	1
Infiltration day	Effluent [As]	ALM	-0.38	1.8E-5	1

Table S2-11. Kendall's tau test results assessing correlations between time (infiltration day) and nutrient and trace metal cycling for each treatment over the duration of the experiments.
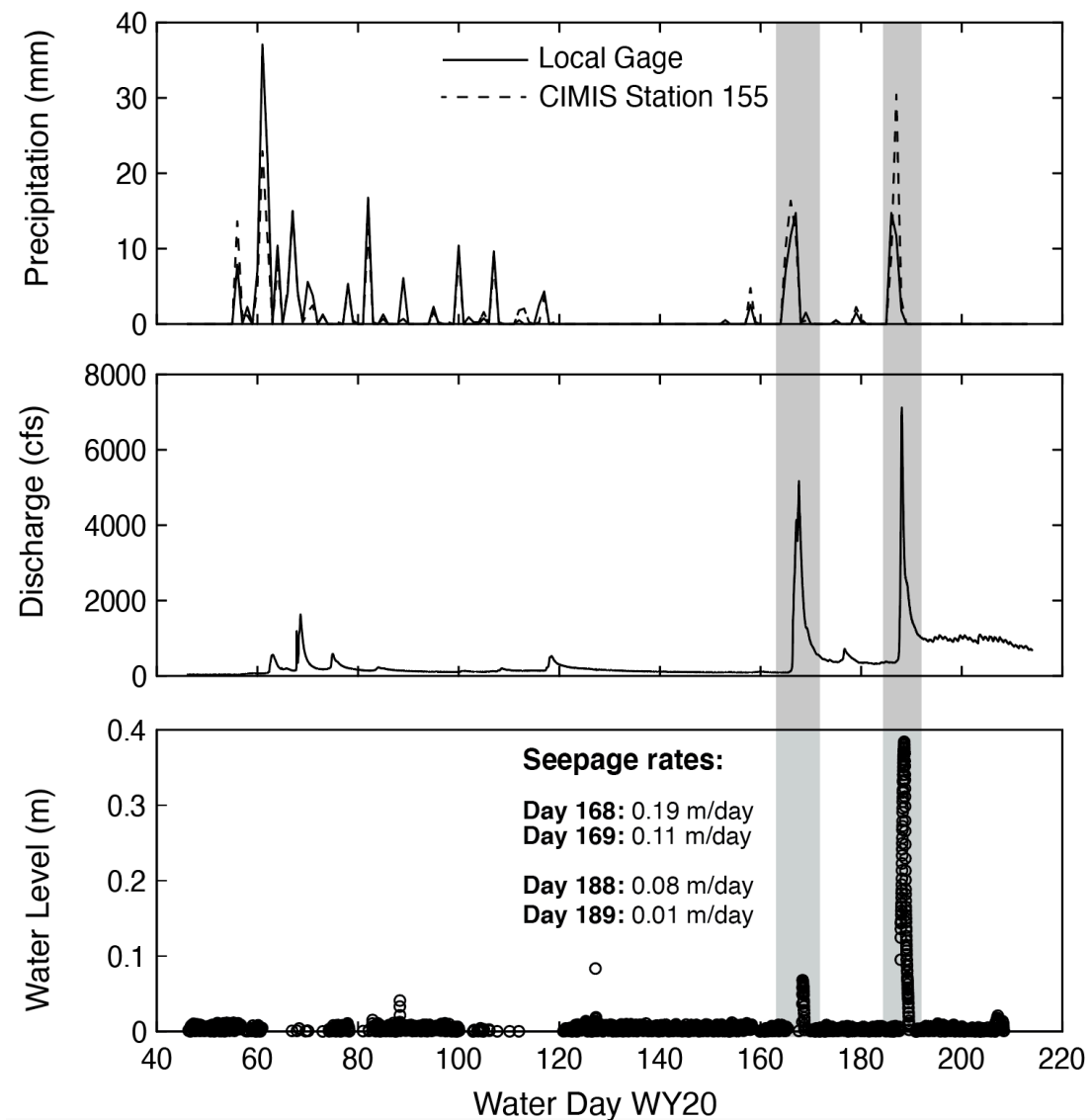
Figure S2-1. **Precipitation, discharge, and surface water level data, WY2020. A.** Records of daily precipitation from a tipping bucket rain gauge on site, and another gauge at CIMIS #155, in West Sacramento. **B.** Discharge measurements from USGS stream gage #11335000 at Michigan Bar, located approximately 11 mi upstream from Teichert Ranch. **C.** Water level on the site measured from stilling well SW-04, located on the southwestern portion of the site approximately 300 m southeast of Deer Creek. Seepage rates are reported from temperature probes co-located with SW-04.
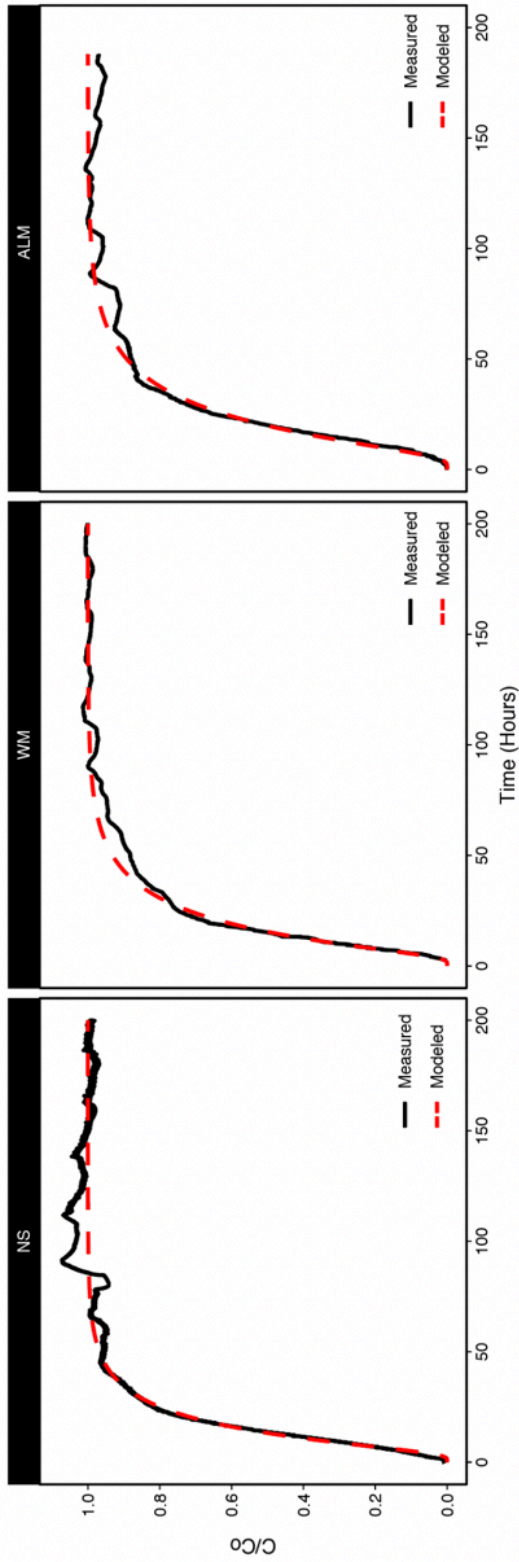
Figure S2-2. NaCl tracer breakthrough curves for experiments in the NS, WM, and ALM columns. The ratio C/Co is a measure of the effluent electrical conductivity and the tracer solution normalized to the maximum electrical conductivity measured. The measured C/Co (black) was modeled (red) using a simplified solution of the advection-dispersion equation (eq. S1) to determine the hydraulic properties of the columns (i.e. average linear velocity, longitudinal dispersion coefficient, and effective porosity).
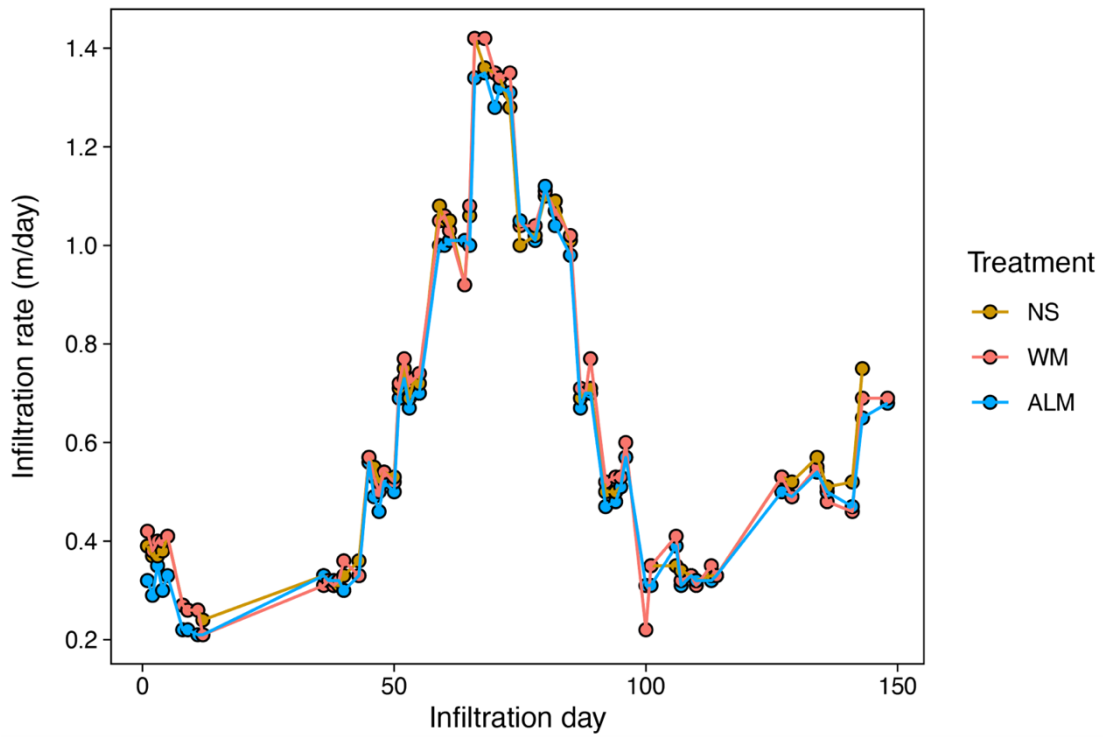
134

Figure S2-3. Infiltration rates for all three columns for the duration of the experiment.
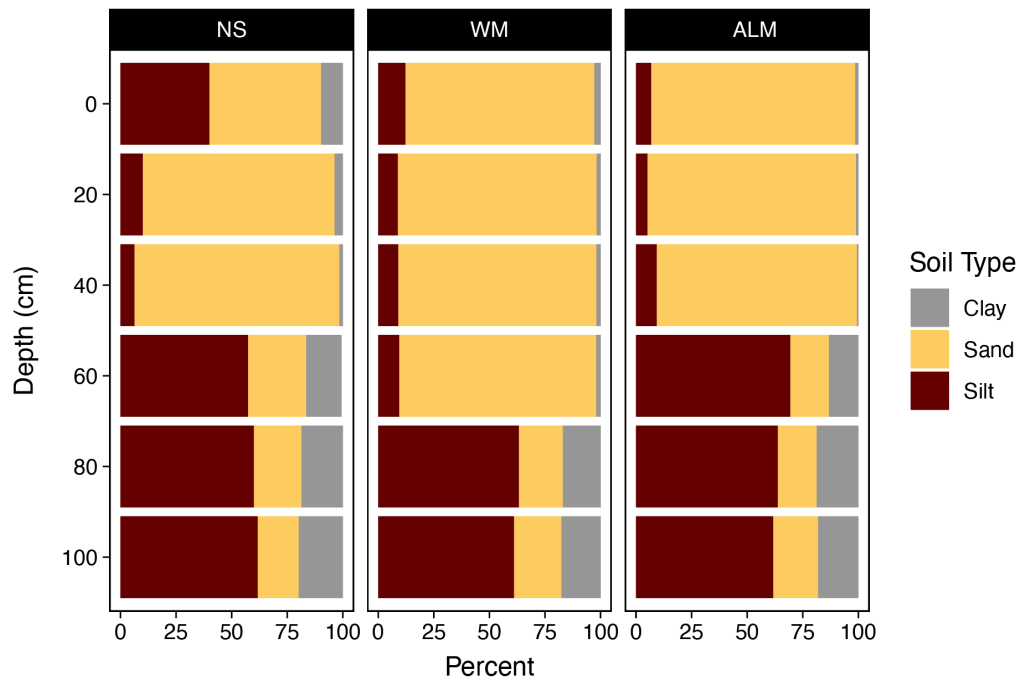
Figure S2-4. **Soil grain size** for each column.
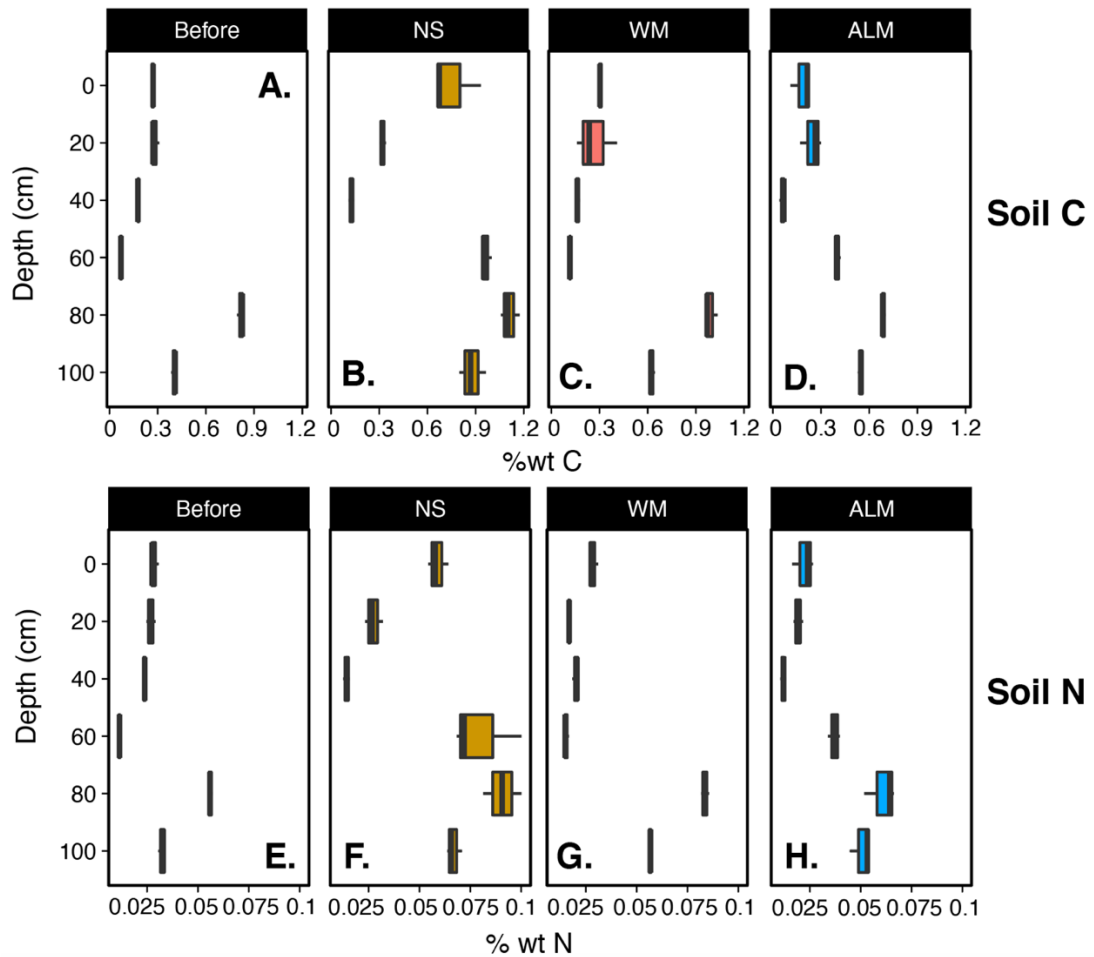
Figure S2-5. Soil TOC and TN Soil TOC % wt (A-D) and TN % wt (E-F) for each column before infiltration (A and E) and following infiltration (B-D, F-H) for each treatment.
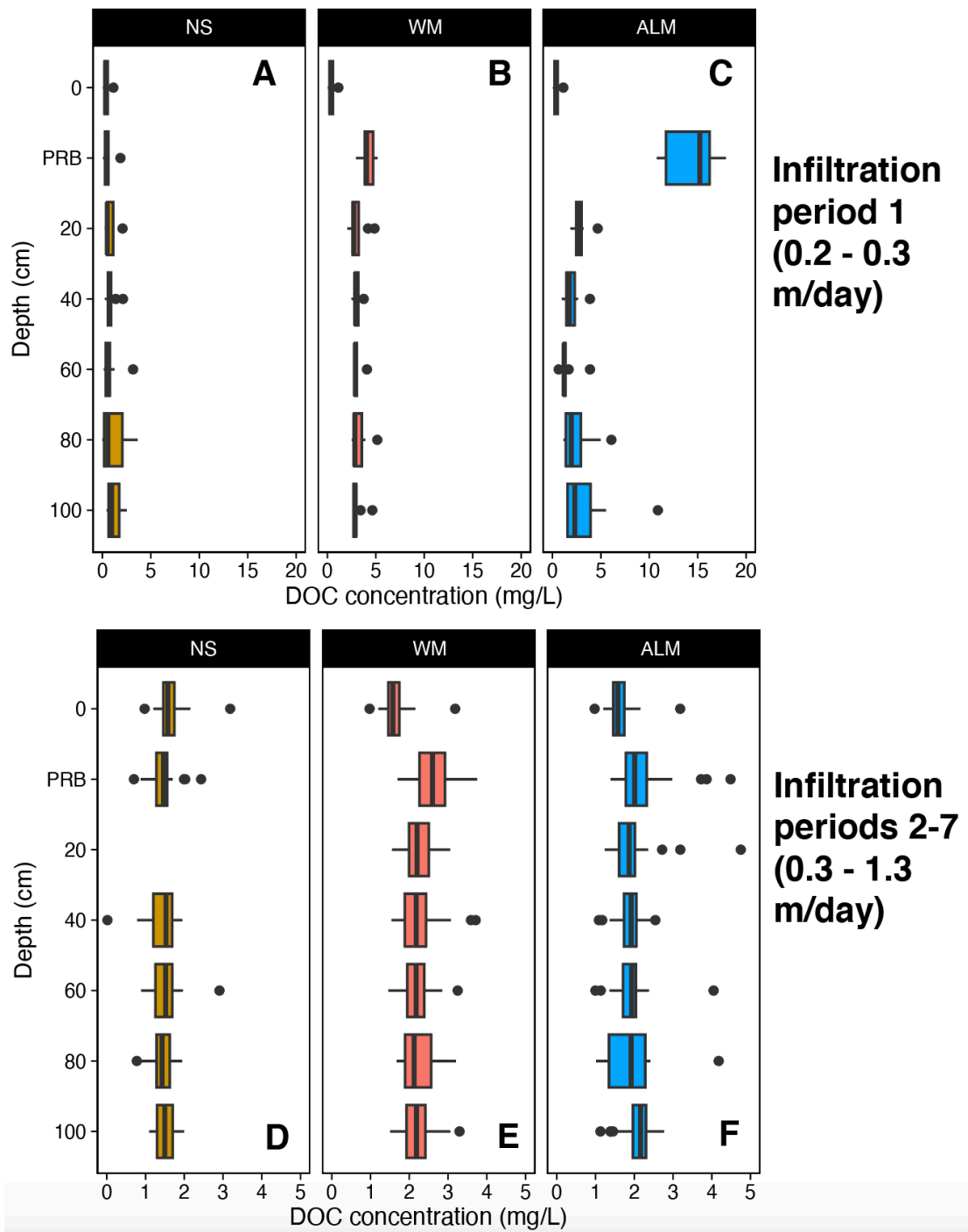
Figure S2-6. DOC with depth Box-and-whisker plots of DOC with depth during the infiltration period (IP) 1 (A-C) and IPs 2-7 (D_F) for each column.
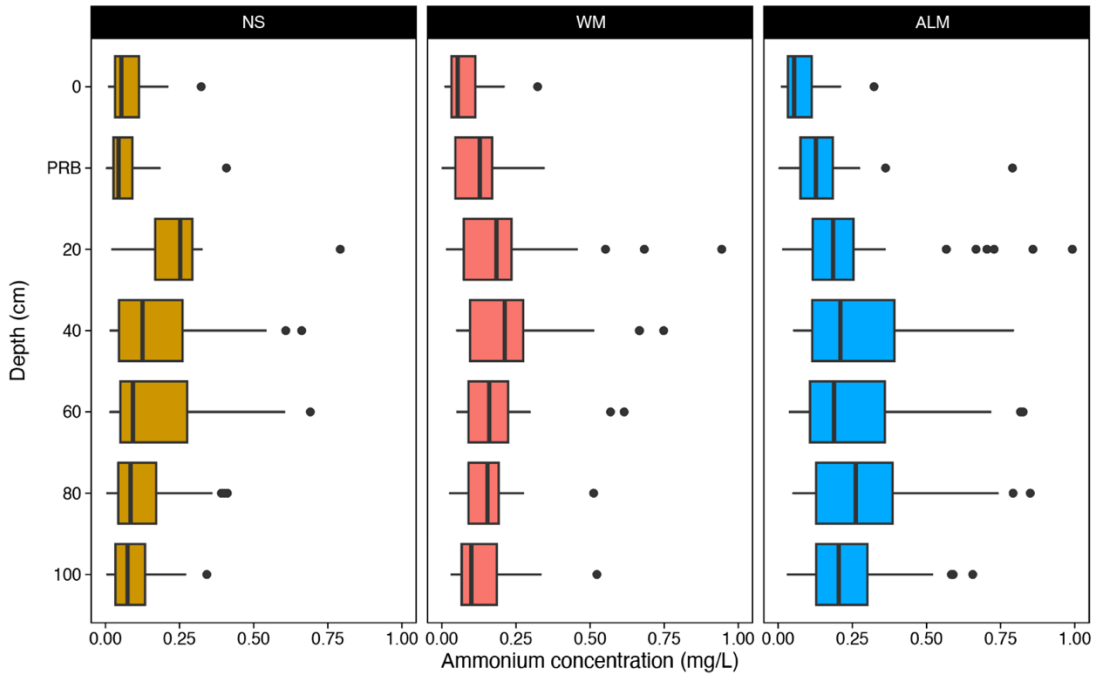
Figure S2-7. Ammonium concentrations Box plots depicting ammonium concentrations from each depth of each column (NS, WM, and ALM) over the duration of the test.
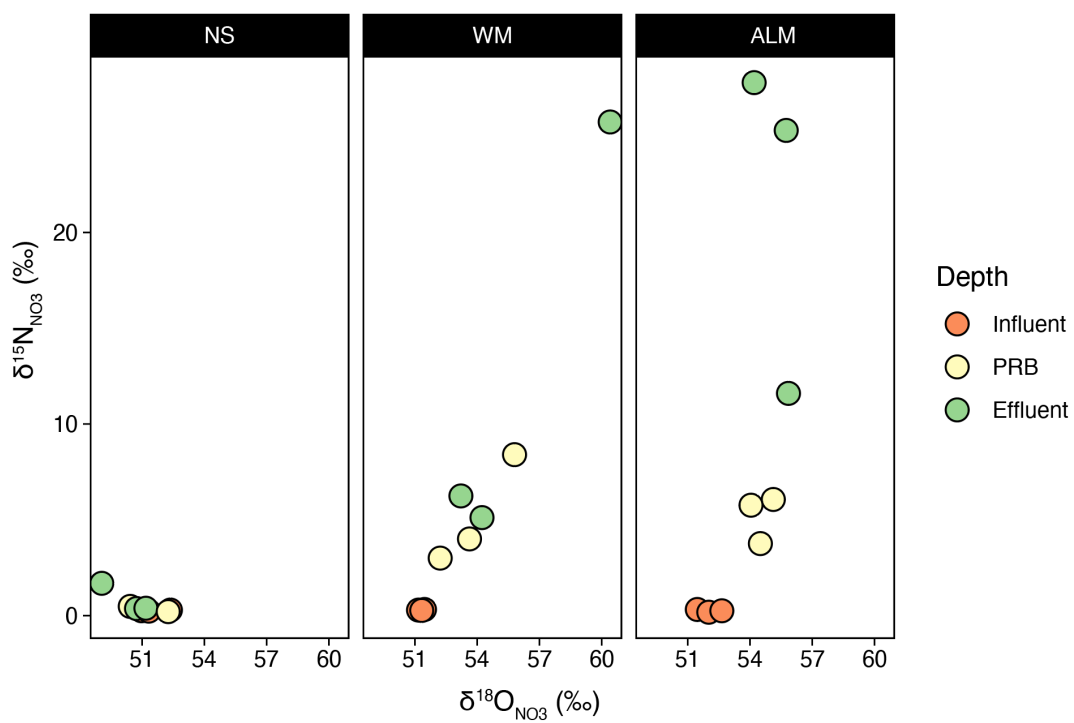
Figure S2-8. Nitrate isotopes d15N values of nitrate plotted against d18O values of nitrate in the influent, PRB, and effluent samples for each treatment on a selection of days in which NO_3^- removal was detected.
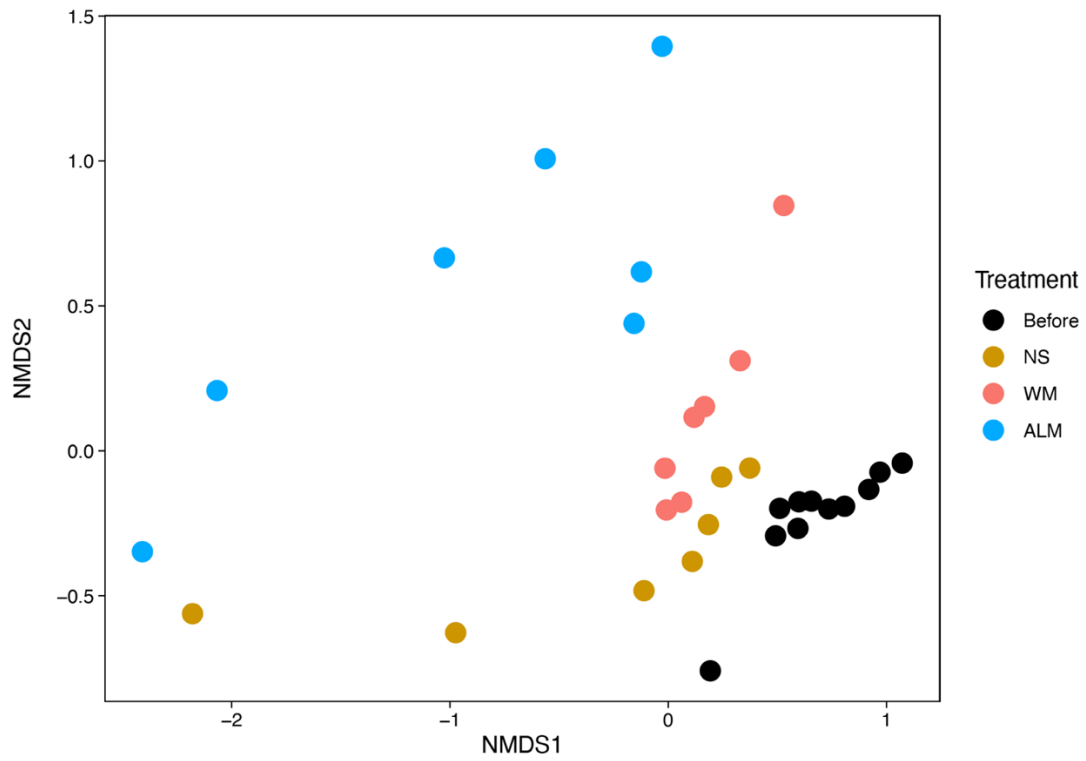
Figure S2-9. NMDS of 16S RNA of soil samples collected before infiltration and soil samples collected after infiltration for each treatment. Each group (before, NS, WC, and ALM) cluster separately, with the most between sample diversity found in the ALM samples.
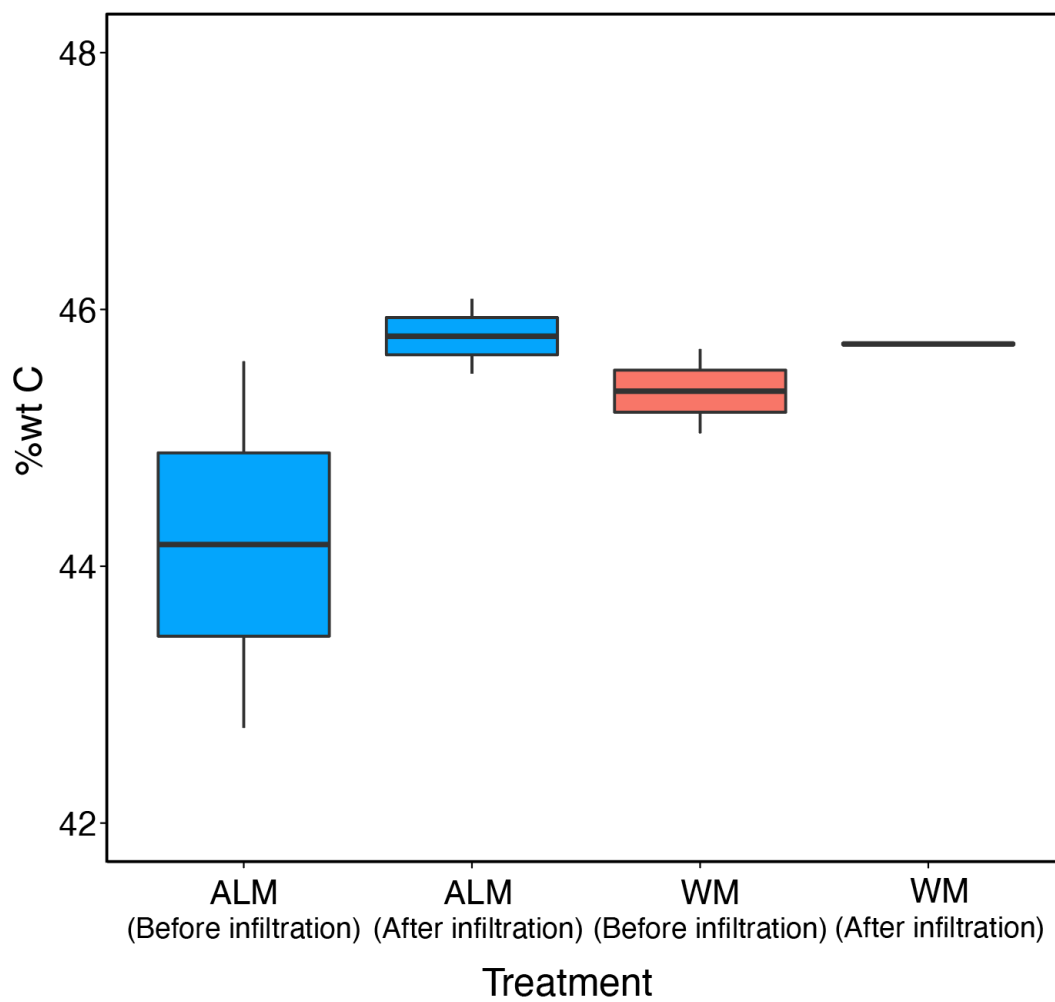
Figure S2-10. **TOC % wt for each carbon amendment** (almond shells and wood mulch) before infiltration and following infiltration.
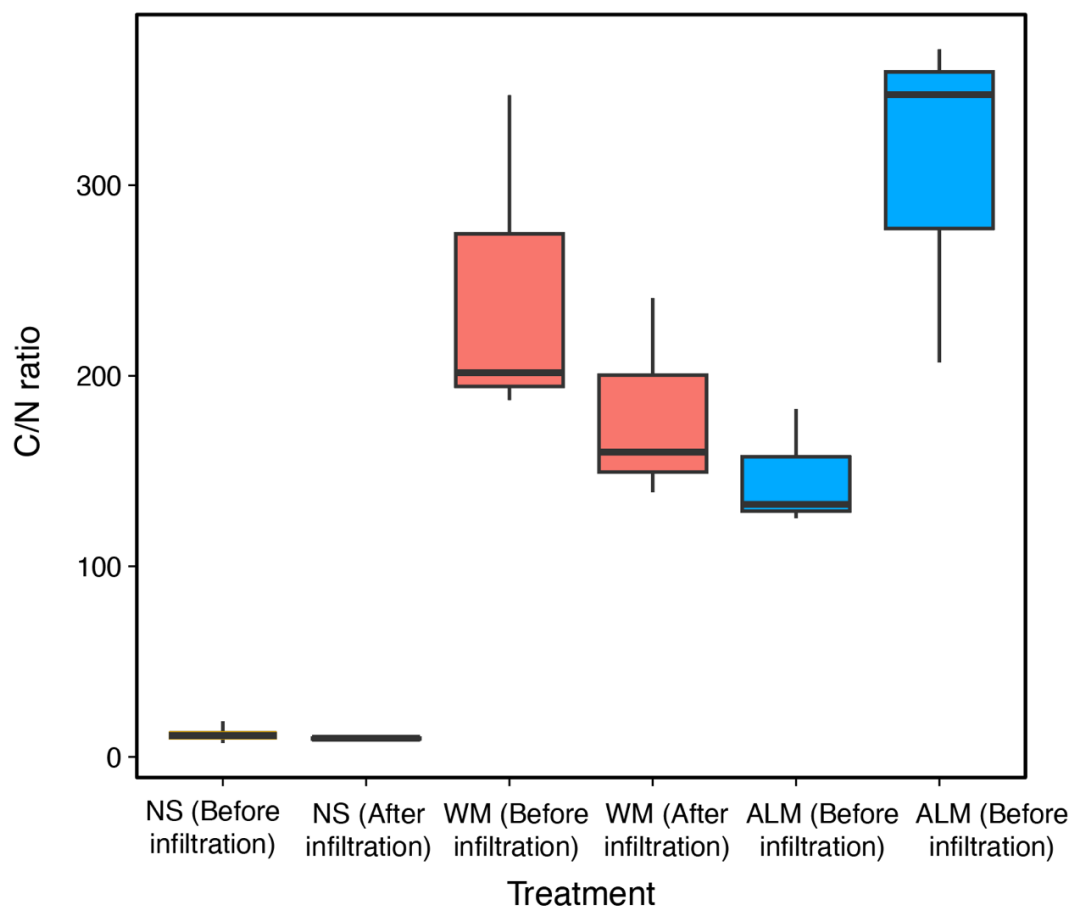
Figure S2-11. C/N ratios for the materials in each PRB capsule (NS, WM, and ALM) before and after infiltration.
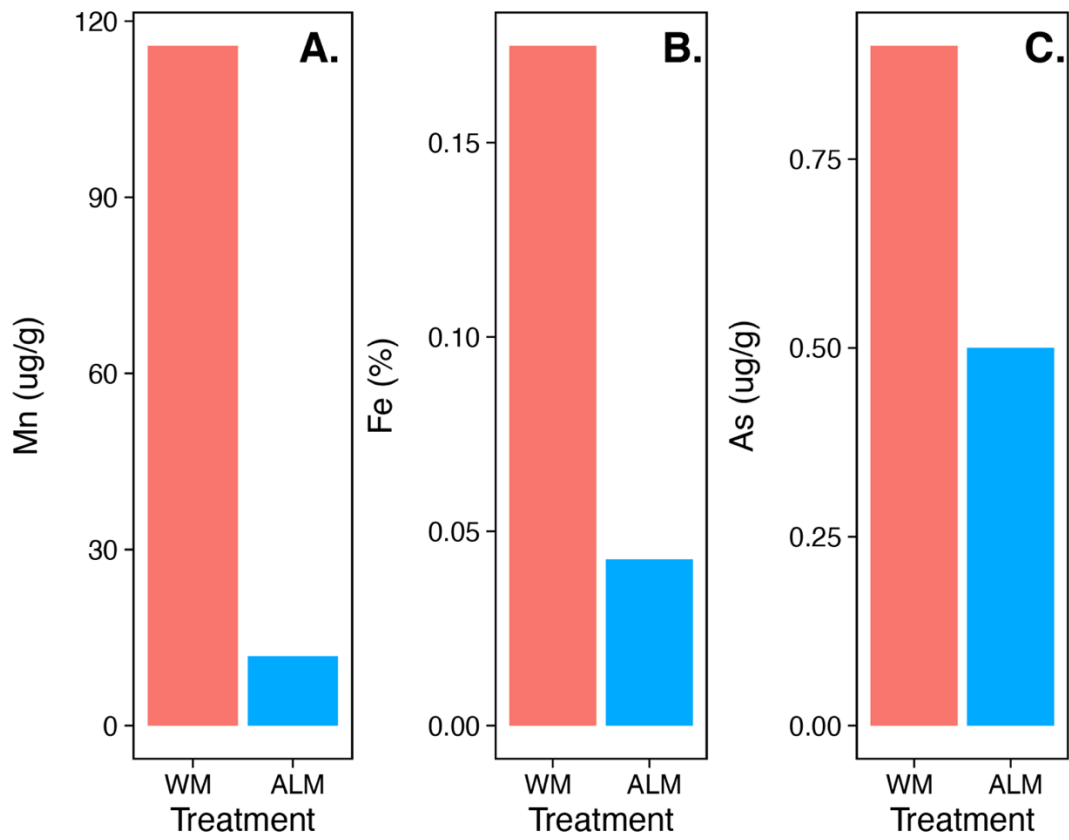
Figure S2-12. Metals concentrations for each carbon amendment Comparison of Mn (A), Fe (B), and As (C) in each carbon amendment (wood mulch and almond shells) before infiltration experiments.

Chapter Three

ASSESSMENT OF SURFACE AND SUBSURFACE SUITABILITY FOR

MANAGED AQUIFER RECHARGE USING MULTI-CRITERIA DECISION

ANALYSIS (MCDA) AND GIS

Abstract

Managed aquifer recharge (MAR) is a water management strategy that can help to improve both water supply and quality, but it can be difficult to determine where on a landscape MAR projects are likely to be successful. In order to address this issue, we developed a tool to assess the potential for the implementation of MAR projects in Santa Clara County, CA. The tool uses multi-criteria decision analysis (MCDA) with spatial data in a geographic information system (GIS), to identify locations having multiple conditions that are favorable for MAR. Within the three primary groundwater management areas of Santa Clara Valley, between the Santa Cruz and Diablo Mountain Ranges, conditions favorable for MAR are found on >30% of the land area, covering over 30,000 hectares. Sites with the highest MAR suitability tend to be located where multiple criteria are well satisfied: on old stream channels, on or near active (although often ephemeral) stream channels, and on other coarse Quaternary fluvial and alluvial deposits; where land is undeveloped, has low-intensity development, or is used for agricultural activities; where there is a vadose zone 6-30 m thick; and where there have been large differences in groundwater levels during dry climate periods compared to wet periods. Results from this work have important implications for designing MAR projects in this region, and this methodology could serve as a template for other regions interested in developing MAR projects to address water supply and quality concerns.

3.1 Introduction

Groundwater resources around the world are increasingly stressed by rising demand, a changing climate, and shifting land use (Bierkens and Wada, 2019; Wada et al., 2010). Managed aquifer recharge (MAR) is a suite of techniques that can improve the supply of groundwater by routing excess surface water into aquifers (Bouwer, 2002; O'Leary et al., 2012). Techniques for MAR can include dedicated infiltration basins, injection wells, aquifer storage and recovery (ASR), and stream bank infiltration (Doussan et al., 1998; Maliva et al., 2006; Pavelic et al., 2006). In addition to benefiting groundwater supplies, MAR projects can also improve water quality, enhance baseflow to streams, and help reduce flooding (Bekele et al., 2011; Dillon, 2005; Hartog and Stuyfzand, 2017; Schmidt et al., 2011).

One MAR strategy that can be particularly useful in delivering these additional benefits is flood managed aquifer recharge (flood-MAR), which uses excess water from high magnitude winter flows from major rivers or hillslope runoff for recharge on open lands to simultaneously enhance groundwater recharge and manage flood waters (Kocis and Dahlke, 2017; Marr et al., 2018). This technique has been of particular interest in California, where precipitation is highly seasonal, periodic flooding occurs, and there is abundant land (often agricultural) on which infiltration can occur (Dahlke et al., 2018; O'Geen et al., 2015; Waterhouse et al., 2020). However, questions remain about the hydrogeologic constraints of MAR, and there is a particular need to identify locations that would be suitable for inundation and/or stormwater collection.

147

Identifying areas suitable for managed recharge can be challenging, as there are many hydrogeologic, socioeconomic, and institutional challenges involved in finding ideal locations for projects (Fuentes and Vervoort, 2020; Ringleb et al., 2016). There are complex surface and subsurface conditions that impact both infiltration and subsequent groundwater recharge, which can make it difficult to assess where projects can be most beneficial. There are also important socioeconomic factors to consider, including proximity to disadvantaged communities, reported drinking water supply shortages, and poverty status (Marwaha et al., 2021). Additionally, there are many institutional challenges, such as securing water rights, attaining available land for projects, and constructing infrastructure to convey and infiltrate water (Dillon et al., 2019). These challenges also often vary considerably by region, so assessments often have to be conducted at a local scale.

While field testing at scale is the most direct method for determining if a location could be suitable for a MAR project, field studies can be costly and are difficult to implement over large areas (e.g., Bouwer, 2002; Beganskas and Fisher, 2017; ASCE, 2020). For this reason, computational approaches, including use of geographic information systems (GIS), are particularly well-suited for assessing MAR suitability criteria (Jha et al., 2007). Several recent studies have used multi-criteria decision analysis (MCDA) paired with a GIS in order to identify locations for potential MAR projects (Malczewski and Rinner, 2015; Russo et al., 2015; Sallwey et al., 2019; Zhang et al., 2019). GIS-based MCDA approaches integration of spatial factors pertinent to MAR projects, which are classified, weighted, and combined (Chenini et al., 2010; Yeh

et al., 2009). However, methods for the selection of and weighting of factors vary greatly from study to study, and there is no standardized or widely accepted methodology for this type of analysis (Giove et al., 2009; Sallwey, 2019).

The most commonly cited factors in designing MAR suitability analysis include physical criteria such as slope, land use, geology, soil type, and aquifer properties (Chowdhury et al., 2010; Sallwey et al., 2019). Some studies also include an assessment of land availability, regional groundwater quality, and the predictions of hillslope runoff (e.g., Casanova et al., 2016; Yuan et al., 2016; Owour et al., 2016; Beganskas et al., 2019). While these factors do not necessarily influence the physical suitability of the landscape for groundwater recharge, they can be paired with suitability analyses to identify locations that could deliver significant benefits to both water supply and quality.

The primary goal of this study is to assess sites where there may be good opportunities to improve groundwater resources using MAR in Santa Clara County, CA, particularly distributed locations that could host recharge systems supplied by local stormwater collection. The focus of this work is on method development and implementation of a documented MCDA approach, with a regional application. Results of this work have direct implications for this region, and may serve as a template for other regions where planning and implementation of new groundwater projects are expected to be increasingly common and important in coming years.

3.2 Methods

3.2.1 Study region

This study focuses on Santa Clara County, California, USA, located at the southern edge of San Francisco Bay, in an area of mixed urban, suburban, rural, and agricultural land use that is home to ~2 million residents (cite). Water supplies in Santa Clara County include groundwater (40% of water use), local surface water (40% of water use), imported water (15% of water use), and recycled water (5% of water use), and are managed by the Santa Clara Valley Water District (VW) (Valley Water, 2021). The region includes two primary groundwater subbasins: the Santa Clara Subbasin, which consists of two groundwater management areas, Santa Clara Plain and Coyote Valley, and the Llagas Subbasin (Figure 3-1). The Santa Clara Plain is more urbanized, although there are population centers in Coyote Valley and the Llagas Subbasin as well. In general, Coyote Valley and the Llagas Subbasin have a larger fraction of land area in agricultural production or designated as undeveloped. Groundwater flow directions are generally from the NNW to SSE in the Llagas Subbasin, and from SSE to NNW in Coyote Valley and the Santa Clara Plain; of course there are local gradients and flow patterns in association with variations in stratigraphy, recharge, and pumping.

3.2.2 Multi-criteria decision analysis for mapping managed recharge

Spatial datasets (Table 3-1) were acquired and imported into the GIS in digital format, with adjustments made as needed to the geographic projection, resolution, data gaps or errors, and/or units of measurement and display (further described in Sections

150
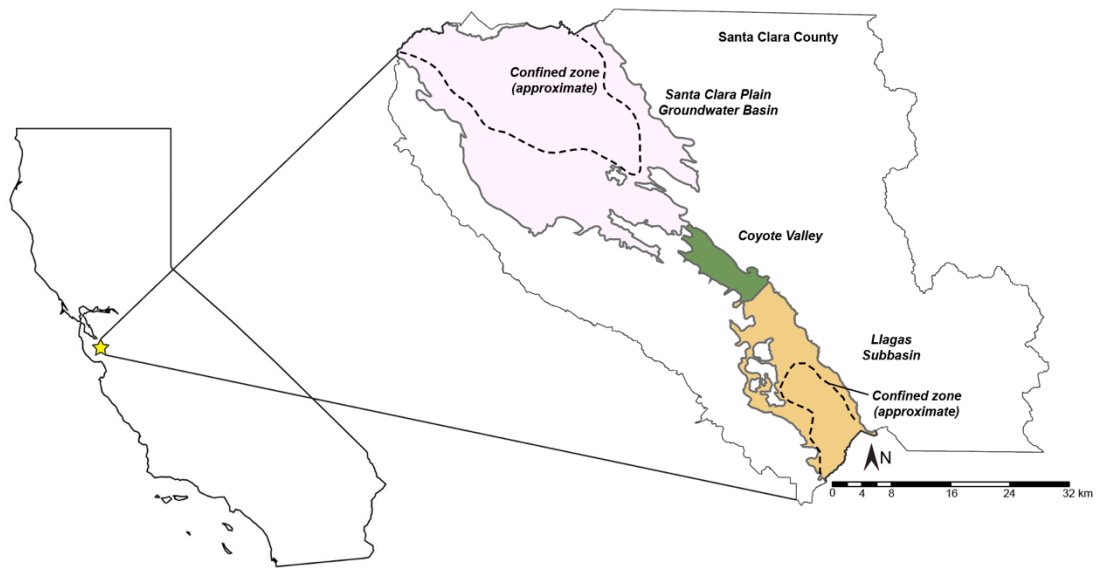
Figure 3-1 Regional map and project area. Map of the project area, including groundwater basins and the approximate extent of confined zones.

Table 3-1. Main data types and sources used for multi-criteria decision analysis (MCDA).

Surface	Data Source [a]
Soil infiltration capacity	SSURGO
Land use/Land cover	NLCD
Geology	USGS
Subsurface	
Vadose zone thickness	VW
Aquifer transmissivity	VW
Aquifer storage	VW
Sensitivity of water levels to climate	VW
Filter	
Slope	USGS
Applications	
Selected open space areas	SCV OSA, VW
Groundwater benefit zones	VW
Water quality (TDS and nutrients)	VW

[a] SSURGO = Soil Survey Geographic Database, USDA/NRCS
NLCD = National Land Cover Database
USGS = United States Geological Survey
VW = Santa Clara Valley Water Agency
SCV-OSA = Santa Clara Valley, Open Space Authority

3.2.3 – 3.2.9). Each dataset used as part of the formal analysis is referred to as a "factor." We divided the assessment into two general classes of factors: surface and subsurface.

Surface factors included the soil infiltration capacity, land use/land cover, and the nature of shallow geologic units. Shallow geologic units were considered as a surface factor because they were interpreted as linking surface water to subsurface aquifer units. Subsurface factors included hydrogeologic parameters such as the geometry (lateral extent, thickness) of aquifers and confining layers, vadose zone thickness (distance from the ground surface to top of groundwater), the sensitivity and inter-annual variability of groundwater levels to climate, and the transmissive and storage properties within uppermost aquifer units.

Factors used quantitatively as part of MCDA for MAR suitability were rated on an integer scale having eight levels: 0 to 7, where 0 indicates poor suitability and 7 indicates excellent suitability. In general, we sought to have intermediate values on each rating scale (3 to 4) apply for conditions that were "acceptable" or "satisfactory" for MAR, with higher values (5 to 7) being good to excellent and lower values (0 to 2) being poor to fair.

Different classification methods were used for numerical and nonnumerical datasets (e.g., soil infiltration capacity and land use, respectively). Two approaches were used for classifying numerical datasets: (1) classifying values based on knowledge of properties that are beneficial for MAR operations, and (2) classifying values using a "natural breaks" method based on the distribution of property values. The first approach was used for soil infiltration capacity and vadose zone thickness because there are

established standards for these factors in MAR operations (American Society of Civil Engineers, 2020). The second approach was used for the transmissivity, storage, and the sensitivity and inter-annual variability of groundwater levels to climate because there are not standard values for these factors in MAR operations. Nonnumerical datasets (land use and surficial geology) were classified based on interpretation of associated properties that could influence MAR, as further explained in Sections 3.2.5 and 3.2.6.

Once all the factors of interest were classified, multiple factors were combined according to their importance ("weight") to generate a spatial suitability "index," helping to identify locations where there is alignment of properties that are the most favorable for the processes or activities of interest (Figure 3-2A).

In an initial analysis, each of the three surface factors were weighted equally ($W_{\text{f-surf}} = 0.33$ for each). Each of the four subsurface factors were also weighted equally ($W_{\text{f-subsurf}} = 0.25$ for each). Surface and subsurface MAR suitability indices were weighted equally and combined to create a map of composite MAR suitability (Figure 3-2B). There is no standard basis for assigning relative weights to different factors, so as an initial analysis, we chose equal weighting, reasoning that the initial set of seven factors were all fundamentally important for siting MAR projects.

3.2.3 Terrain slope

A United States Geological Survey (USGS) digital elevation model (DEM) was used as the basis for the full project, with pixel dimensions and locations forming a template for incorporation of all additional raster data (Figure 3-3A). The selected
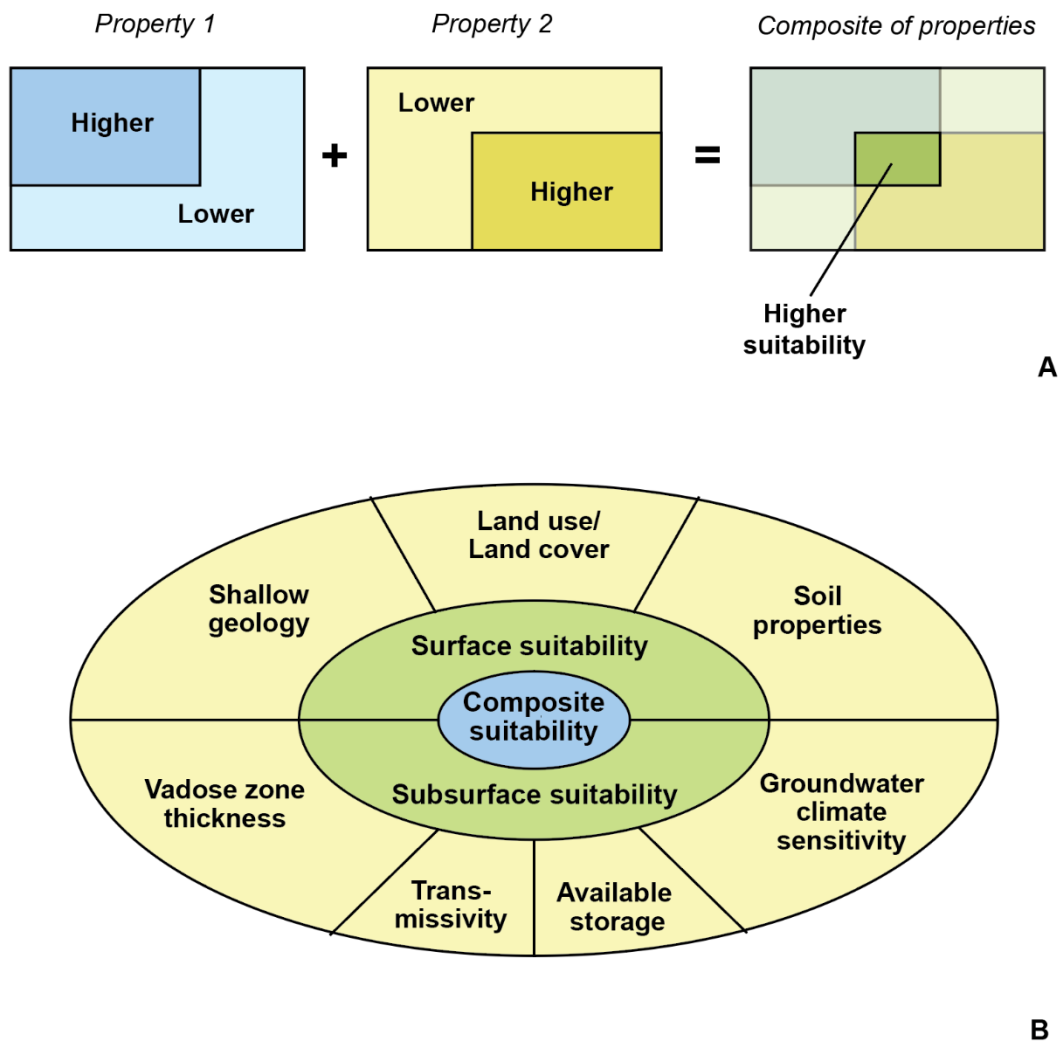
Figure 3-2 MCDA approach. Overview of general approach taken using a geographic information system (GIS), with independent factors rated on the basis of perceived suitability for MAR, then combined to identify areas with a higher or lower suitability index (A). Conceptual approach illustrated with two hypothetical factors. (B). Individual factors were weighted equally within two primary data classes, surface and subsurface, then these classes were weighted equally for calculating a compositve suitability map. Rating scales and weights can be adjusted as desired to explore the influence and sensitivity of individual or multiple factors.
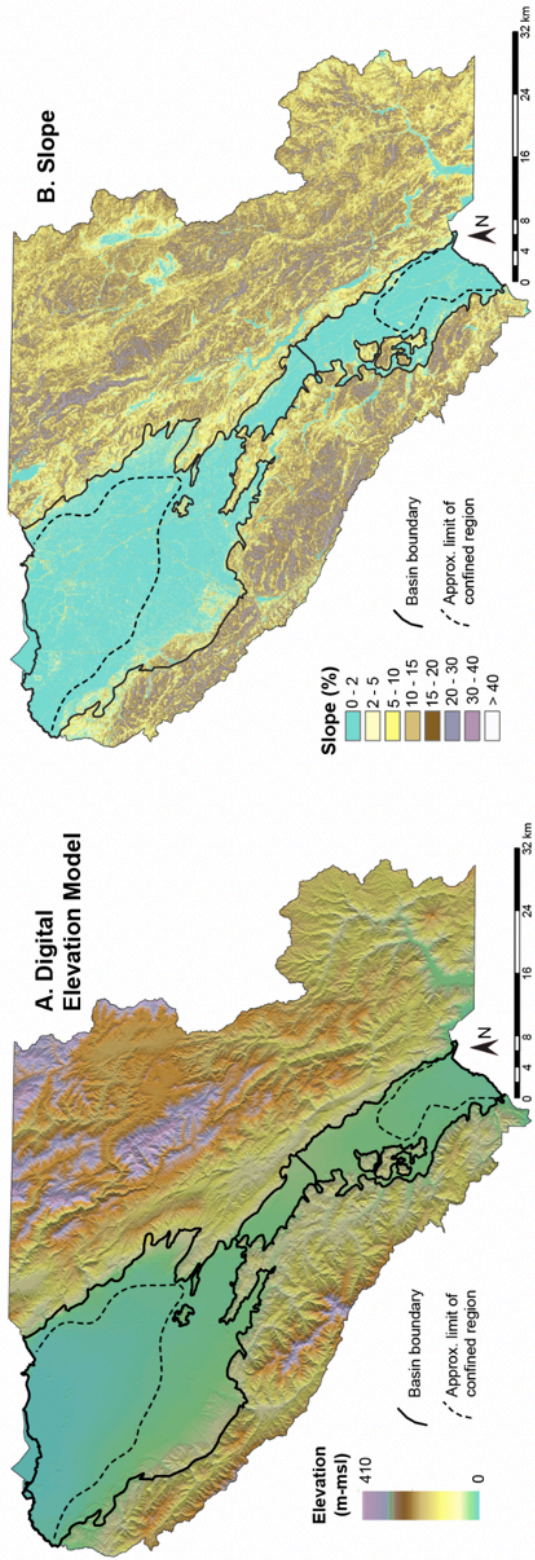
Figure 3-3 Digital Elevation Model (DEM). DEM for the project area (A) and percent slope derived from the DEM (B). In general, areas with high slopes are less suitable for a MAR project, although these areas may be good for generating runoff that could supply a project.

DEM used in this study has a resolution of 1/9-arc-second, equivalent in the project area to ~3.4 m x 3.4 m (using the North American Datum of 1983, NAD83) and has complete coverage across Santa Clara County. This resolution is fine enough to allow relatively detailed assessment, without creating excessive computational or visualization burdens. The DEM also allowed for the derivation of terrain slope (Figure 3-3B).

DEM slope was applied as a filter to suitability index calculations, removing areas having a ground surface slope $\geq$ 10%, reasoning that these areas are less desirable based on challenges in collection of hillslope runoff under steep conditions (Figure 3-3B). Some areas with slopes >10% might still be viable for projects, but the most feasible sites are likely to be in or close to the main groundwater basins that occupy valleys, where slopes are typically $\leq$2%.

3.2.4 Soil infiltration capacity

Soil information was extracted from the Natural Resources Conservation Service (NRCS) Soil Survey Geographic Database (SSURGO) and processed for analysis and display (Soil Survey Staff, 2014). Data was extracted for each soil type represented in Santa Clara County and linked to soil polygons (Figure S3-1). For each soil type, we took the arithmetic mean of saturated conductivity listed for each soil horizon, then calculated the harmonic mean of layer values (Hiscock and Bense, 2014), accounting for both differences in properties and the thickness reported for each soil layer:

$$IC_E = \frac{\sum_{i=1}^{n} d_i}{\sum_{i=1}^{n}\left(\dfrac{d_i}{\overline{K}_i}\right)} \tag{1}$$

where IC_E = soil infiltration capacity (m/day), d_i = layer thickness (ft), and $\overline{K}_i$ = arithmetic mean of the range of conductivity values reported for individual layers (m/day). This approach allowed for a wide range of soil properties to be represented, while giving more importance during vertical infiltration to layers having the lowest (limiting) infiltration capacity.

The rating scale was set so that IC values that are moderately favorable for a MAR project would be rated IC_r = 3 to 4 on a scale of 0 to 7, representing values of IC = 0.3 to 0.6 m/day (Table 3-2).

3.2.5 Land use/land cover

Land use/land cover (LULC) can have a significant influence on MAR site selection. Land use data was obtained from the 2019 National Land Cover Dataset, a well-established data product generated for the full continental United States by the U.S. Geological Survey in collaboration with regional partners (Dewitz and U.S. Geological Survey, 2021). The NLCD includes the full project region at a spatial resolution of 30 m, and uses a self-consistent set of LULC designations with sufficient granularity for the present application (Figure S3-2). For example, the NLCD includes four designations for "developed" land, ranging from high intensity to open space,

158

Table 3-2. Summary of ratings for surface factors.

Suitability Rating	Infiltration Capacity		Land/Land Cover		Geology	
	Values (cm/day)	% Land Area[a]	Values	% Land Area[a]	Lithology	% Land Area[a]
0	< 8	39.3	Open Water, Woody Wetlands, Emergent Herbaceous Wetlands	2.7	Ultramafic rocks, chiefly Mesozoic, unit 3 (Coast Ranges and Western Klamath Mountains), H2O, nm	3.1
1	8 - 15	20.8	Developed-High Intensity	3.5	Franciscan mélange/Franciscan Complex, unit 1 (Coast Ranges)/Tertiary intrusive rocks (hypabyssal), unit 2 (Quien Sabe Volcanic Field)/Qhbm/adf/Qhb/Qhf	44.6
2	> 15 - 30	25.2	NA	NA	Mesozoic volcanic rocks, unit 1 (Coast Ranges)/Cretaceous marine rocks (in part nonmarine), unit 1 (Coast Ranges)/Eocene marine rocks/Miocene marine rocks	20
3	> 30 - 45	4	Developed-Medium Intensity	5.8	Plio-Pleistocene and Pliocene loosely consolidated deposits/Pliocene marine rocks/Qhff/Qt/Qhfe/Qhf/Qhty/Qhc-br/Qot/Qpt/Qht1/Qht2/Qt1/Qt2	8.3
4	> 45 - 60	5.1	NA	NA	Older Quaternary alluvium and marine deposits/Quaternary alluvium and marine deposits/Qha/Qa/Qpa/Qf/Qhfy/Qoa/Qhly-Qhty/Qhf-Qhff	6.4
5	> 60 - 76	1.6	Developed-Low Intensity, Shrub/Scrub	35.1	Qhl1/Qpf/Qhly/Qhf1/Qhl/Qhf2/Qhf/Qof/Qhf-Qpf/Qhf-Qhl/Qhl-Qpf/Qof2/Qof1	17
6	> 76 - 91	0.2	Herbaceous	14.3	Qhc-Qhly	0.01
7	> 91	3.6	Developed-Open Space, Barren Land, Deciduous Forest, Evergreen Forest, Mixed Forest, Hay/Pasture, Cultivated Crops	38.5	Qhc/gq	0.5

[a] Percent land area calculated based on the total area represented in Santa Clara County (335,000 hectares).

[b] Lithologic units as identified on USGS geological maps.

distinguishes between deciduous, evergreen, and mixed forests, and has separate classifications for cultivated crops and hay/pasture. The rating system used for LULC extends across the full range of 0 to 7, but we elected to use a somewhat lower resolution categorization scheme, with six rating values (0, 1, 3, 5, 6, 7). $LULC_r = 0$ was assigned mainly for open water and wetlands (which often have hydrophobic soils), whereas $LULC_r = 1$ was assigned only for high-intensity development (urban areas) (Table 3-2). Medium- and low-intensity development was rated 3 and 5, respectively, reasoning that the latter could prove suitable for MAR if there were contiguous open spaces capable of hosting a project, e.g., if a parcel were zoned as a park or for environmental benefit.

Areas with LULC categories indicating extensive vegetation, other than wetland, were rated $LULC_r = 5$, 6, or 7 (Table 3-2). Scrub/shrub and herbaceous landscapes were rated $LULC_r = 5$ and 6, respectively, and all forests, cultivated crops, and hay/pasture were rated $LULC_r = 7$. The latter rating requires justification. Unlike other studies that favored particular crop types based on resilience to inundation and/or crop practices such as nitrogen or pesticide application (Marwaha et al., 2021; O'Geen et al., 2015), we take a different approach with this factor for several reasons. In this region, agricultural areas are considered to be highly suitable for MAR because they often contain well-drained soils, are mostly open and working landscapes, have basic infrastructure in place for routing water, and may use a lot of groundwater for irrigation, thus creating space for supplemental inflows. To the extent that groundwater quality has been impaired by past agricultural practices, increasing recharge of surplus surface

water can help to dilute salts and nutrients. The presence of specific crops is likely to be a weak indicator of MAR suitability in this area because: (a) cropping changes frequently over time, (b) for specific crops there can be large differences in management, (c) and it is possible that a grower may wish to set aside some land for MAR, even if that land is productive, particularly if there is an incentive to do so. Alternatively, there could be incentives for land fallowing, or limitations in access to water for that makes land less valuable for agriculture.

The current framework allows for more specificity that could include different LULC ratings for particular cropping or other agricultural land uses, but we have not attempted this in the initial set of calculations. Future work may explore this option.

3.2.6 Geology

Regional geology puts hydrogeologic conditions in context, and local geology can limit or facilitate recharge depending formation characteristics. In general, Quaternary deposits comprise the primary aquifer units in the three groundwater management areas, but particularly at basin edges, older units may be in contact with younger deposits and therefore could be important for MAR suitability assessment. Basin edges, where alluvial and fluvial units may pinch out against bedrock deposits, are often locations of "mountain front" recharge because primary aquifer units are sometimes exposed in these areas. In contrast, areas closer to valley centers may contain wetland or estuarine deposits that are fine grained, can perch shallow groundwater, and can result in development of confined conditions in underlying

aquifers. Thus, the nature of geologic formations throughout groundwater basins important for assessing MAR suitability.

Regional geology maps for the study region were combined to develop a composite coverage (Figure S3-3), using a USGS geodatabase (Horton et al., 2017). For Quaternary deposits that are found near the surface in most of the designated groundwater basin areas, we used a compilation that defines 55 Quaternary deposit types (Witter et al., 2006; Wentworth et al., 2006). For areas with older geological units, data was obtained from the USGS State Geologic Map Compilation (SGMC) geodatabase, including 13 formations ranging in age from Eocene to Mesozoic, and four Quaternary units. Where the latter were also represented by Quaternary deposits in the more detailed Quaternary compilation, the latter designations superseded those from the regional map. All lithology codes and associated lithology names are included in Table S3-1.

Quaternary units that include former stream channels were assigned the highest ratings ($Geol_r$ = 6 or 7), based on experience elsewhere indicating that these materials can penetrate shallow fine-graned layers and provide a more direct connection to underlying aquifers (e.g., Weissman et al., 2004; Beganskas and Fisher, 2017) (Table 3-2). Other Quaternary valley fill and fluvial units were assigned moderately high ratings ($Geol_r$ = 4 or 5), with the higher rating used for units that seems likely to be connected to or part of aquifers. Some units were largely undifferentiated (gravel to sand to silt to clay) or were identified as generally being older and more lithified, resulting in classification of $Geol_r$ = 3. Ratings of $Geol_r \leq 3$ were generally assigned to

units that were Plio-Pleistocene or older, including crystalline rocks in the Santa Cruz Mountains.

3.2.7 Vadose zone thickness

Vadose zone thickness is critical to consider when evaluating recharge suitability, since the vadose zone must be thick enough to receive infiltrated water, but thin enough to allow confidence that water will reach the underlying aquifer. Vadose zone thickness can also influence processing of nutrients or other contaminants. Several groundwater level datasets were made available by VW, expressed as depth below ground surface (depth to water, *DTW*), and used for multiple calculations and data coverages: (a) median water levels in groundwater wells during 2010-19, (b) maximum depth to water during a recent drought, 2014-15, and (c) minimum depth to water during a long time interval that includes multiple periods with relatively wet conditions, 1978-2019 (majority being post-1994, and ~25% of data collected in 2005-06. All of these subsurface datasets extend spatially near to the limits of groundwater basin extent, a subset of the total project area (Santa Clara County, Fig. 3-1). In application to the MAR suitability index, median water level was interpreted to be equivalent to vadose zone thickness, the depth from the ground surface to groundwater level in an unconfined aquifer (Figure S3-4A).

Ratings for vadose zone thickness have the most complex categorization system using in this study (Table 3-3). At the lower limit, a high water table with *DTW* < 3.5 m was considered too shallow for MAR, as this is likely to result in undesired mounding and saturation of shallow soils ($VZ_r = 0$ in this analysis). At the other

extreme, a vadose zone >60 m thick suggests that groundwater is so deep that surface infiltration is likely to result in perched water, rather than recharge penetrating to a depth from which groundwater pumping commonly occurs ($VZ_r = 1$). VZ values between 3.5 and 60 m were assigned intermediate VZ_r values, with highest rating assigned when DTW = 6-18 m ($VZ_r = 7$). We used a limited rating scale, omitting values of 4 and 6, mainly because there was not enough confidence in finer granularity in the classification (e.g., it was not clear if $DTW = 35$ m is really much better than $DTW = 55$ m).

3.2.8 Groundwater climate sensitivity

The coverages for maximum depth to water (under dry conditions, DTW_{dry}) and minimum depth to water (wet conditions, DTW_{wet}) were used to calculate a climate sensitivity factor, $C_s = DTW_{dry} - DTW_{wet}$, resulting in higher ratings at locations where there were the greatest differences in water levels between dry and wet conditions (Figure S3-4A). We note that higher groundwater levels under wet conditions and lower water levels under dry conditions could result from differences in pumping. Thus, the phrase "climate sensitivity" represents a hybrid of hydrologic and human influences. We interpret larger values of C_s to be a positive indicator of MAR suitability, identifying locations where infiltrated surface water may have a good opportunity to reach an aquifer where there is available storage space. C_s values less than 12 m were assigned poor to fair values ($C_s = 0 - 2$), values greater than 12 m and less than 24 m were considered moderately suitable ($C_s = 3 - 4$), and values greater than 24 m were considered good to excellent ($C_s = 5 - 7$) (Table 3-3).

Table 3-3. Summary of ratings for subsurface factors.

Suitability Ranking	Vadose Zone Thickness		Climate Sensitivity		Transmissivity		Storage	
	Values (m)	% Land Area[a]	Values (m)	% Land Area[a]	Values (m²/day)	% Land Area[a]	Values (m)	% Land Area[a]
0	< 3	15.7	< 0	13.9	0 - 46	0	0	1.4
1	3 - 6	12.2	0 - 6	12.7	> 46 – 116	8.4	0 – 0.3	51.1
2	> 60	18.4	> 6 - 12	18.7	> 116 – 232	5.4	> 0.3 – 0.6	13.4
3	30 - 60	9.8	> 12 - 18	20.2	> 232 – 465	12.7	> 0.6 – 0.9	8.7
4	NA	NA	> 18 - 24	13.4	> 465 – 929	20.7	> 0.9 – 1.2	6.4
5	> 18 - 30	11.2	> 24 - 37	12.7	> 929 – 1,858	22.2	> 1.2 – 1.5	4.9
6	NA	NA	> 37 - 49	5.8	> 1,858 – 3,716	28.8	> 1.5 - 3	9.8
7	> 6 - 18	32.6	> 49	2.7	> 3,716	1.8	> 3	4.4

[a] Percent land area was calculated based on the total extent of the subsurface rating coverage (80,000 hectares)

3.2.9 Hydrogeologic properties: transmission and storage

Multiple data coverages were used to assemble maps of aquifer properties, as applied for groundwater models currently in use by VW, including updated versions of simulations developed for the Santa Clara Plain, Coyote Valley, and the Llagas Subbasin (Calpine Corporation and Bechtel Enterprises Holdings Inc., 2000; CH2M Hill, 2005, 1992). Acquisition and development of these data coverages for use in the current project varied by management area and model, as summarized in this section. Transmissivity is defined as the product of horizontal hydraulic conductivity multiplied by aquifer thickness for a tabular, horizontal aquifer layer or layers. Thus, for unconfined conditions, transmissivity varies with water level. The storage factor calculated for the present application is the product of specific yield (S_y) and aquifer layer thickness, indicating space available for storage of infiltrated surface water.

For the model of groundwater flow in the Santa Clara Plain (CH2M Hill, 1992), data were evaluated for the top three model layers (1, 2, 3), for which lateral grid resolution was typically ~300 to 1,800 m. Layers 1 and 2 exist for this model only where the principal aquifer is confined, representing the upper unconfined and confining layers, respectively. Where Layer 1 exists, in the confined region, its thickness is ~24 to 30 m. Where Layers 1 and 2 are absent, Layer 3 is the uppermost active model layer and is ~30 to 150 m thick. For transmissivity calculations for this model, we multiplied horizontal conductivity (K_h) by layer thickness for Layer 1 in confined areas, or by the layer thickness for Layer 3 where the main aquifer is unconfined. This approach accounts for there being limited (but often non-zero)

transmissivity above confined parts of the Santa Clara Plain, but generally results in greater transmissivity when Layers 1 and 2 are absent. Layer 1 values of horizontal conductivity were constant in the model, $K_h = 21$ m/day, whereas Layer 3 values varied, $K_h = 1.5$ to 100 m/day.

A similar approach was applied for storage from the Santa Clara Plain model, using Layer 1 where it was active above a confining layer, and Layer 3 where this was the shallowest model layer. In each case, we multiplied the value of S_y by layer thickness in the same cell location. Specific yield in the Layers 1 and 3 of this model varied with location, $S_y = 0.02$ to 0.21.

For input data used with groundwater models for Coyote Valley and the Llagas Subbasin, we worked only with the uppermost layer, Layer 1. For the Coyote Valley model, Layer 1 has spatial resolution of 76 m by 76 m. Although K_x and K_y are specified separately (with a range of ~10 to 200 m/day), they are assigned the same values ($K_x = K_y$) in individual cells. In addition, $S_y = 0.08$ in this model throughout the domain, so differences in storage calculations as applied in this study depend entirely on cell thickness. Cells in Layer 1 of the Coyote Valley model are assigned thicknesses of 4 to 115 m.

For the Llagas Subbasin model, calculations were made for Layer 1, which has a spatial resolution of ~150 m x 150 m. As with the Coyote Valley model, K_x and K_y are specified separately (with a range of 4 to 40 m/day), but assigned the same values ($K_x = K_y$) within individual cells. Specific yield is much lower in the Llagas Subbasin

model than in the other two models, with values of $S_y = 0.005$ to 0.06, and cell thicknesses are 45 to 90 m.

Resulting values of transmissivity vary from <50 m²/day to $>3,700$ m²/day, with the highest values calculated from model input data in the unconfined part of the Santa Clara Plain (Figure S3-5). There are some elevated values apparent along the center of Coyote Valley, and transmissivity is lower along valley edges, especially on the southwest side. Transmissivity values tend to be lower overall in Llagas Subbasin, with the lowest values in the confined area along the southeastern side of the basin. The overall coarse granularity of model cells is apparent in the calculated transmissivity values, as the model resolution is several orders of magnitude coarser than the ~3.4 x 3.4 m pixel size applied in this study, but there is "structure" in the variability that seems to be broadly consistent with the nature of basin fill deposits.

The distribution of storage factor values suffers in comparison, with large areas in which there is little variability. In the Santa Clara Plain, there appears to be considerable storage associated with the unconfined area along the southwestern side of the basin (Figure S3-5B). There are much smaller parts of Coyote Valley and Llagas Subbasin with elevated storage values, and large sections of Llagas Subbasin, in particular, with little available storage based on values used in the groundwater models.

3.2.10 Constraints for application of MAR

Remaining factors applied in this pre-feasibility assessment of MAR suitability for the VW service area were not applied directly as part of suitability index

calculations, but were used instead as overlays that help to focus investigation of specific subregions.

Overlays included parcels designated as open space, existing recharge areas (both natural and managed), groundwater nitrate concentrations, and groundwater total dissolved solids (TDS) concentrations. Considerations for placement of a MAR project could include identification of parcels designated as open space, for which restoration goals might be consistent with enhanced infiltration for MAR. Additionally, water quality indicators (groundwater nitrate and TDS) were included as overlays in order to assess if projects could improve water quality. Whether these or other factors were considered to be positive or negative with respect to placement of a MAR project depends on numerous additional considerations, and it will often be useful to simply render maps of a MAR suitability index with an overlay of data representing additional information.

3.3 Results

3.3.1 Infiltration capacity

Areas with the highest infiltration capacity (IC) rating are located mainly in association with active streams, paleochannels, and sandstone units in the Santa Cruz Mountains (Figure 3-4A). Active stream channels (either perennial or ephemeral) are not likely to be used for creation of new MAR projects, but near-stream areas could prove useful for this purpose if there is a suitable water supply available.

Overall, soils in Santa Clara County tend to be unfavorable for infiltration for recharge, with $IC \leq 0.3$ m/day (ir ≤ 2) mainly because many of the valley fill and

wetland units are a complex mixture of textures and depositional facies, including common fine units. About 10% of the study region has moderately to highly favorable soils based on *IC*, comprising ~36,000 hectares (Table 3-2). Within the groundwater management areas, favorable soils tend to occur in clusters, particularly at the southern end of Coyote Valley, the northern and southwestern side of the Llagas Subbasin, and around the edges of the limit of confined aquifer conditions in the Santa Clara Plain (Figure 3-4A). In many cases, these are active, ephemeral, or paleo-stream channels or associated deposits, as identified in earlier studies (Helley et al., 1979).

3.3.2 Land use/land cover

Much of the project area appears to be favorable for MAR on the basis of land use/land cover (LULC) (Figure 3-4B), more a preponderance of high ratings especially in Coyote Valley, the Llagas Subbasin, and the western edge of the Santa Clara Plain. However, the regions with the most continuous favorable LULC ratings are outside to groundwater management areas, particularly in the Santa Cruz Mountains and Diablow Range to the east.

3.3.3 Geology

In general, the groundwater basins (Santa Clara Plain, Llagas Subbasin, and Coyote Valley) have more favorable geology for MAR compared to the rest of Santa Clara County, and there is considerable variability within the subbasins (Figure 3-4C). More than 7% of the land area in Santa Clara County has geology characterized as $Geol_r \geq 5$, comprising nearly 25,000 hectares, most of which is located in the groundwater management areas.
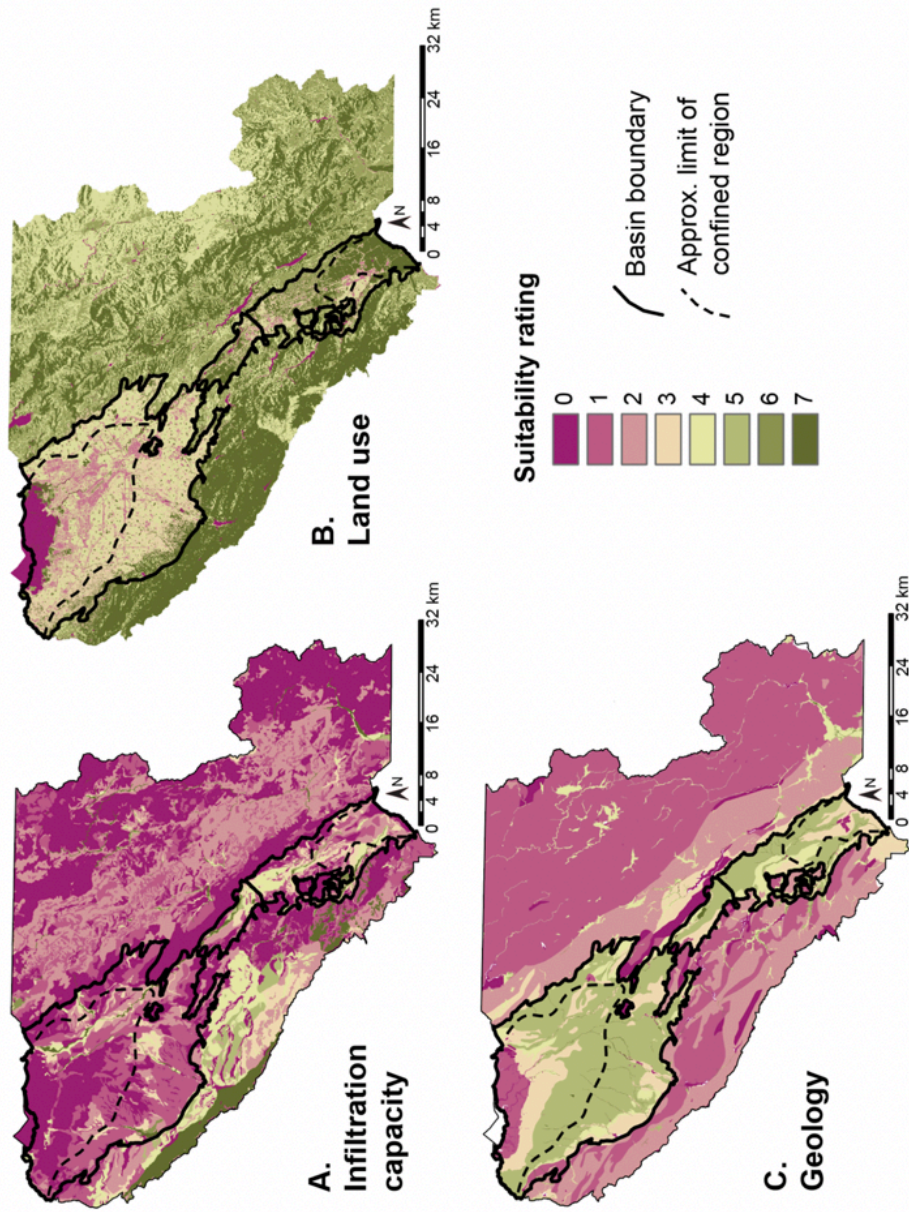
Figure 3-4 Surface rating factors. Suitability ratings for factors used in the surface suitability analysis, including infiltration capacity (A), land use (B), and geology (C).

3.3.4 Surface suitability index

The three surface factors were weighted equally to derive a MAR Suitability Index (SI_{surf}) (Figure 3-5A). Because the three surface factors applied are mostly independent (perhaps with limited correlation between IC_r and $Geol_r$), the resulting map is highly granular and shows considerable variability and complexity across the project region. We also filtered out all pixels having slopes ≥10%, which removed mountainous areas to the west and east of the groundwater basins. More than 7% of the land area was characterized as SI_{surf} = 4 to 7, comprising ~24,000 hectares, most of which is located in the groundwater management areas, and particularly Coyote Valley and the Llagas Subbasin. If we consider areas with SI_{surf} = 3-4, the center of the range calculated, this comprises another ~19% of land area, an additional ~60,000 hectares that is also mostly in the groundwater management areas.

3.3.5 Vadose zone thickness

Much of the project area (groundwater basins for this and other subsurface datasets) has relatively high vadose zone ratings (VZ_r = 5 to 7, 44% of the basin areas), particularly unconfined areas in the Santa Clara Plain and Llagas Basins, and the southern and eastern sides of Coyote Valley (Figure 3-6A). The vadose zone tends to be thinnest near the basin centers, particular at the north end of the Santa Clara Plain and the southern end of the Llagas Subbasin, where confined conditions are dominant, and on the northern side of Coyote Valley. The vadose zone tends to be thickest where there are local topographic highs, including locations where bedrock formations are
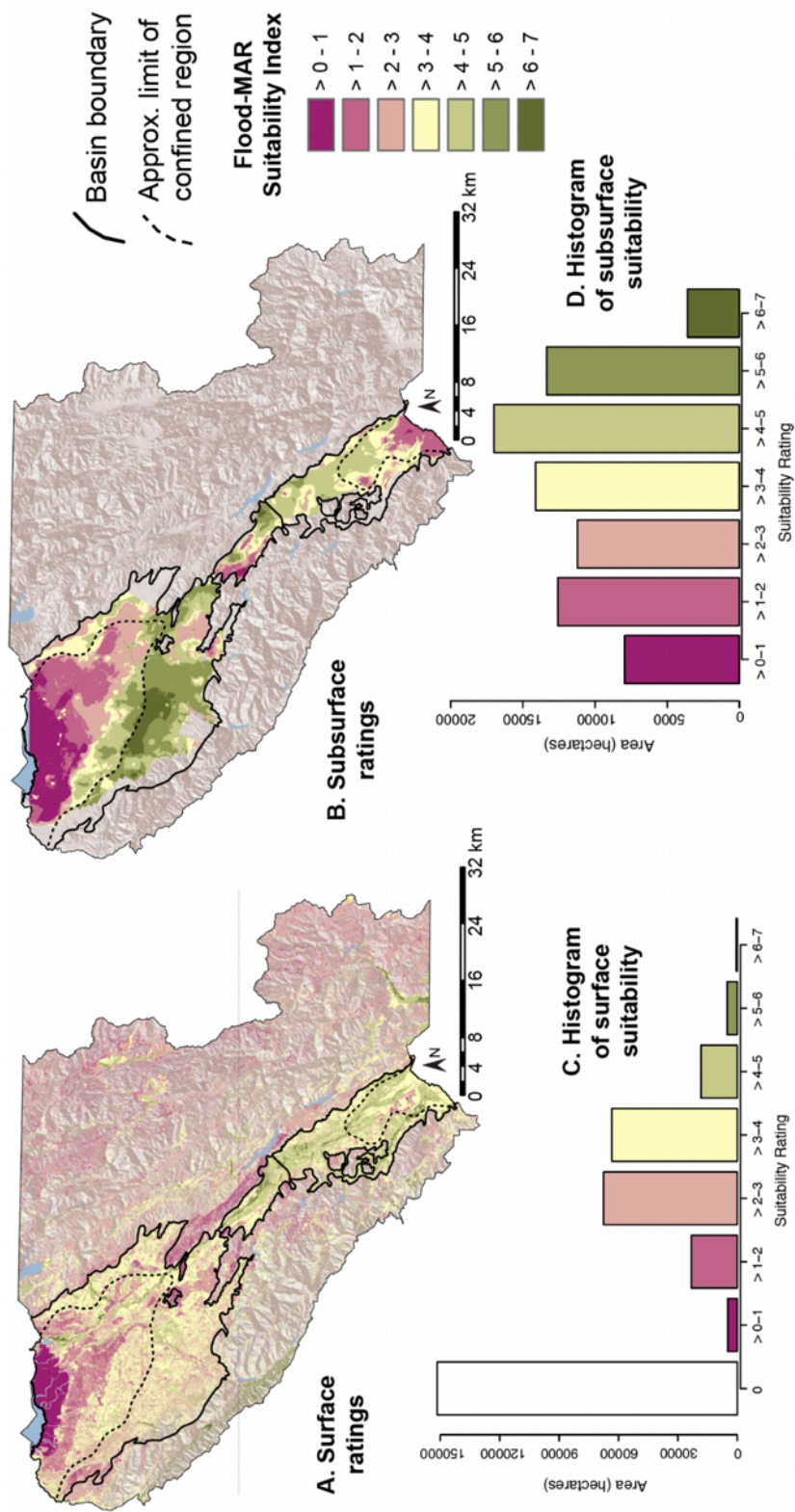
Figure 3-5. Surface and subsurface suitability maps. Suitability ratings for surface (A) and subsurface (B) coverages, including histograms of the surface suitability (C) and subsurface suitability (D) rating values.
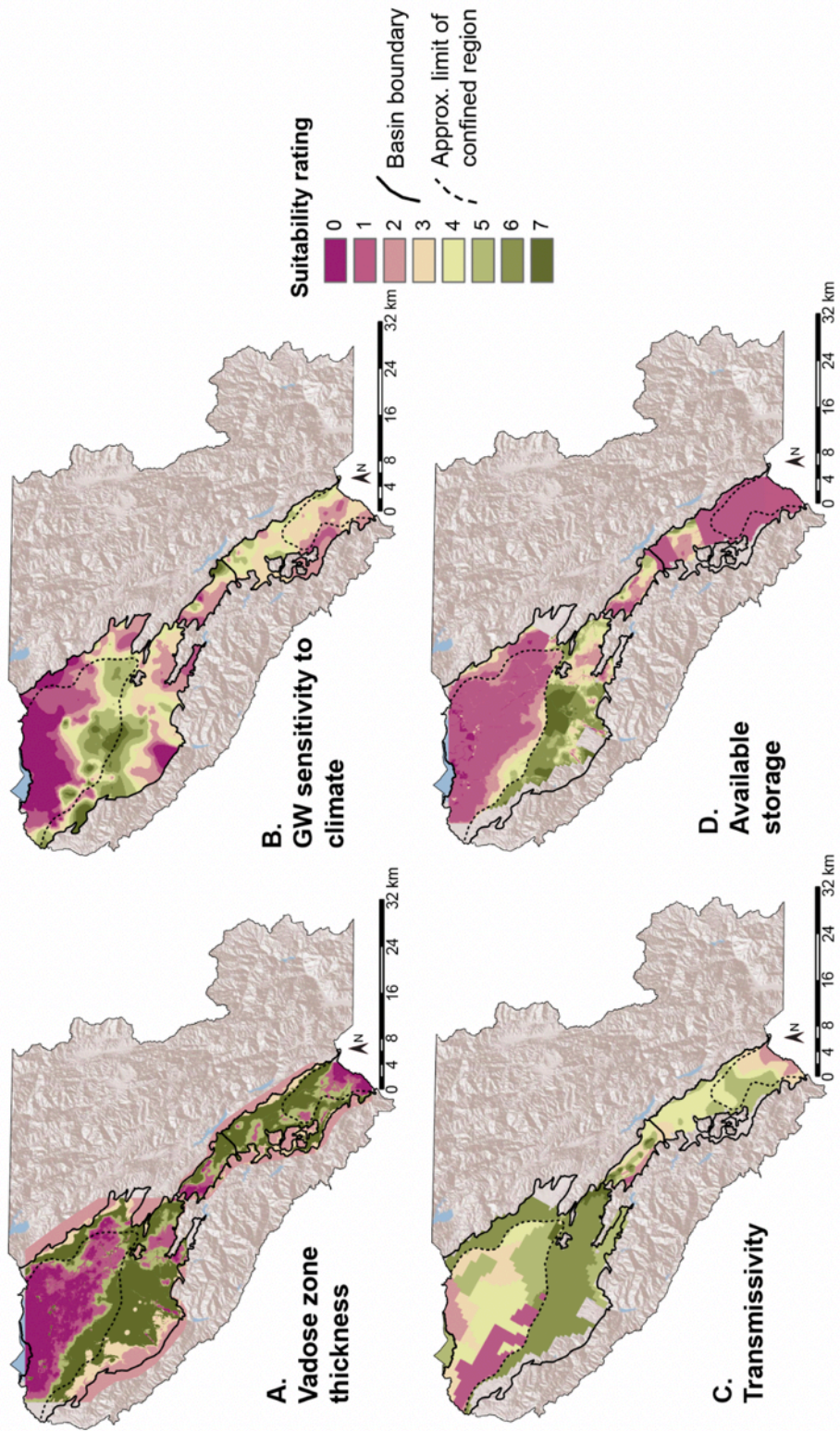
Figure 3-6. Subsurface rating factors. Suitability ratings for factors used in the subsurface suitability analysis, including vadose zone thickness (A), groundwater sensitivity to climate (B), transmissivity (C), and available aquifer storage (D).

surrounded by valley fill deposits, and on the edges of the groundwater basins as they slope upward into surrounding mountain ranges.

3.3.6 Climate sensitivity of groundwater levels

Climate sensitivity of groundwater levels is more variable across the project region, with scattered patches having elevating ratings (Figure 3-6B). Large areas of elevated CS_r (5 to 7) are found in the Santa Clara Plain, but there are also patches in Coyote Valley and the Llagas Subbasin, particularly along the eastern basin edges. These areas comprise >20% of the groundwater management areas, covering >20,000 hectares (Table 3-3).

3.3.7 Transmissivity

Transmissivity ratings are highest ($T_r = 6$ to 7) in unconfined areas where there are thick and conductive surface layers, with the highest values in southern Santa Clara Plain and central Coyote Valley. Moderate ratings ($T_r = 4$ to 5) are common in clusters throughout the project region, including much of Llagas Subbasin (Figure 3-6C). Because the Santa Clara Plain groundwater model incorporates no variation in horizontal conductivity in the confined area, variations in T_r result entirely from variations in modeled aquifer layer thickness. Somewhat greater granularity is apparent in Coyote Valley and the Llagas Subbasin (Figure 3-6C). The majority of the management areas have transmissivity in shallow model layers that fall on the upper 50% of the rating scale (Table 3-3).

3.3.8 Available storage

The distribution of rated storage factors (S_r) is similar in some ways to that for shallow transmissivity, with the lowest values in confined areas (Figure 3-6D). The overall range is low, with 85% of the study areas apparently having <1.5 m of available storage ($S_r \leq 5$, product of vadose zone thickness and specific yield). There is reason to suspect that values of aquifer thickness and/or specific yield might be underrepresented in computer models. The majority of the study region is rated as having little or no available storage, particularly in the Llagas Subbasin. Given the distribution of values derived from the regional computer models, there would be little benefit to expanding the storage rating scale to boost intermediate values ($S_r = 3$ to 5), but this analysis suggests that it may be worth considering a more holistic assessment of basin stratigraphy that incorporates detailed information available from groundwater well logs and other data (Carle et al., 2006). Still, >25% of the study region has moderate to high S_r values based on available data (Table 3-3).

3.3.9 Subsurface suitability index

Subsurface datasets were combined to generate a MAR suitability index based on these data coverages alone ($SI_{subsurf}$) (Figure 3-5B). The areas with the highest suitability index for MAR based on subsurface data are in unconfined regions of the three groundwater management areas where water levels are moderately deep, resulting is good opportunities for infiltration to reach the water table and demonstrating considerable variability between wet and dry climate periods. There is a relatively uniform distribution of $SI_{subsurf}$ ratings, and ~50% of the study region has moderate to high suitability based on subsurface data, $SI_{subsurf} = 4$ to 7 (Table 3-4).

Table 3-4. Summary of ratings for surface, subsurface, and composite suitability coverages.

Suitability Ranking	Surface Suitability[a,b]		Subsurface Suitability[c]		Composite Suitability[d]	
	Area (hectares)	% Land Area	Area (hectares)	% Land Area	Area (hectares)	% Land Area
0	1.52E+05	45.3	1.09E+04	11.9	3.56E+03	3.9
> 0 - 1	4.82E+03	1.4	1.02E+04	11	4.49E+03	5.1
> 1 - 2	2.33E+04	6.9	1.10E+04	12	7.37E+03	8
> 2 - 3	6.76E+04	20.2	9.06E+03	9.9	1.63E+04	17.8
> 3 - 4	6.35E+04	18.9	1.42E+04	15.5	2.76E+04	30.1
> 4 - 5	1.84E+04	5.5	1.90E+04	20.7	2.74E+04	29.9
> 5 - 6	5.14E+03	1.5	1.36E+04	14.8	4.65E+03	5.1
> 6 - 7	6.56E+02	0.2	3.88E+03	4.2	1.62E+02	0.2

[a] Percent land area was calculated based on the total area of Santa Clara County (335,000 hectares).
[b] Includes land filtered by slope >10%.
[c] Percent land area was calculated based on the total extent of the subsurface rating coverage (80,000 hectares).
[d] Percent land area was calculated based on the total extent of the composite rating coverage (80,000 hectares).

3.3.10 Composite suitability index

A composite MAR suitability index map, based on all surface and subsurface factors that were rated and weighted, shows considerable spatial variability (SI_{comp}) (Figure 3-7). This is largely a consequence of the granularity and resolution of surface datasets. More than 35% of the study region for which all datasets exist (i.e., within the groundwater subbasins) has SI_{comp} values of 4 to 7, comprising ~32,000 hectares (Table 3-4). Importantly, patches with elevated SI_{comp} values are found throughout the basins.

3.4 Discussion

3.4.1 Implications for managed recharge in Santa Clara County

Suitability maps indicate that there could be many good opportunities to accomplish MAR objectives in Santa Clara County. In general, MAR opportunities appear to be most common (as a percentage of groundwater management areas) in the Coyote Valley and Llagas Subbasin. Areas with the highest suitability include old stream channels and other features that have relatively coarse surface and near-surface lithologies, in addition to room in the subsurface to receive and transmit excess surface water.

Three additional displays illustrate ways in which preliminary MAR SI maps can be helpful in planning and screening project activities. Parks and open spaces were overlaid with SI_{comp} in order to identify potential project sites on existing public open lands (Figure 3-8A). This could also help to generate multiple ancillary benefits, including improved habitat, where there are fewer concerns about food safety compared to areas that are developed for agriculture.
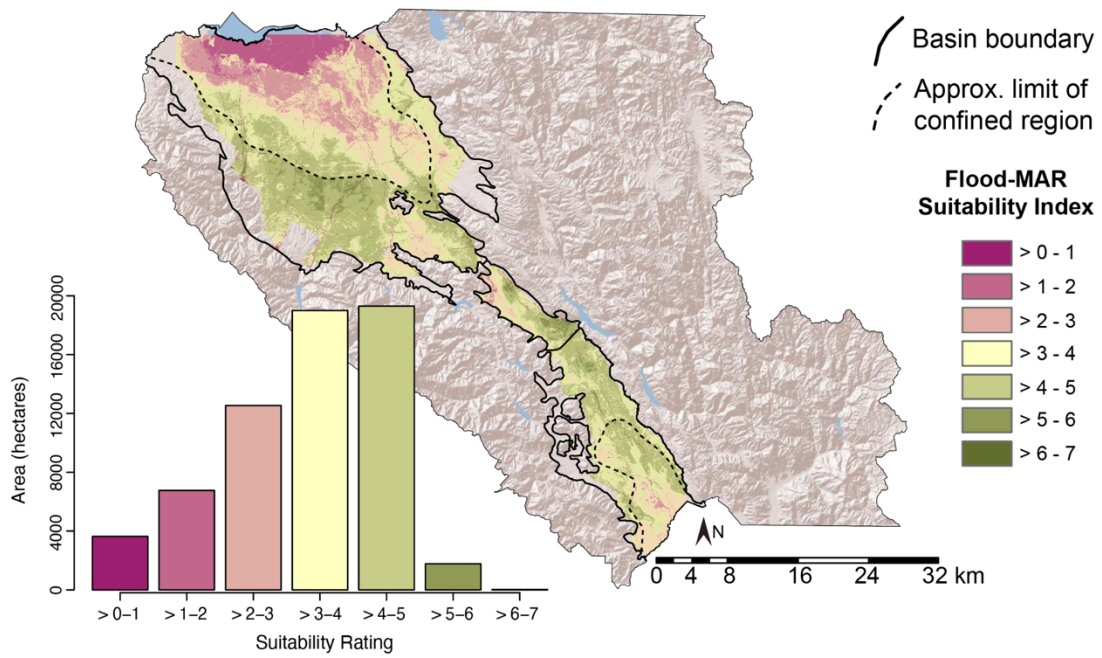
Figure 3-7 Composite suitability map. Flood-MAR suitability ratings for Santa Clara County combining both surface and subsurface ratings, as well as a histogram of the composite suitability rating values.
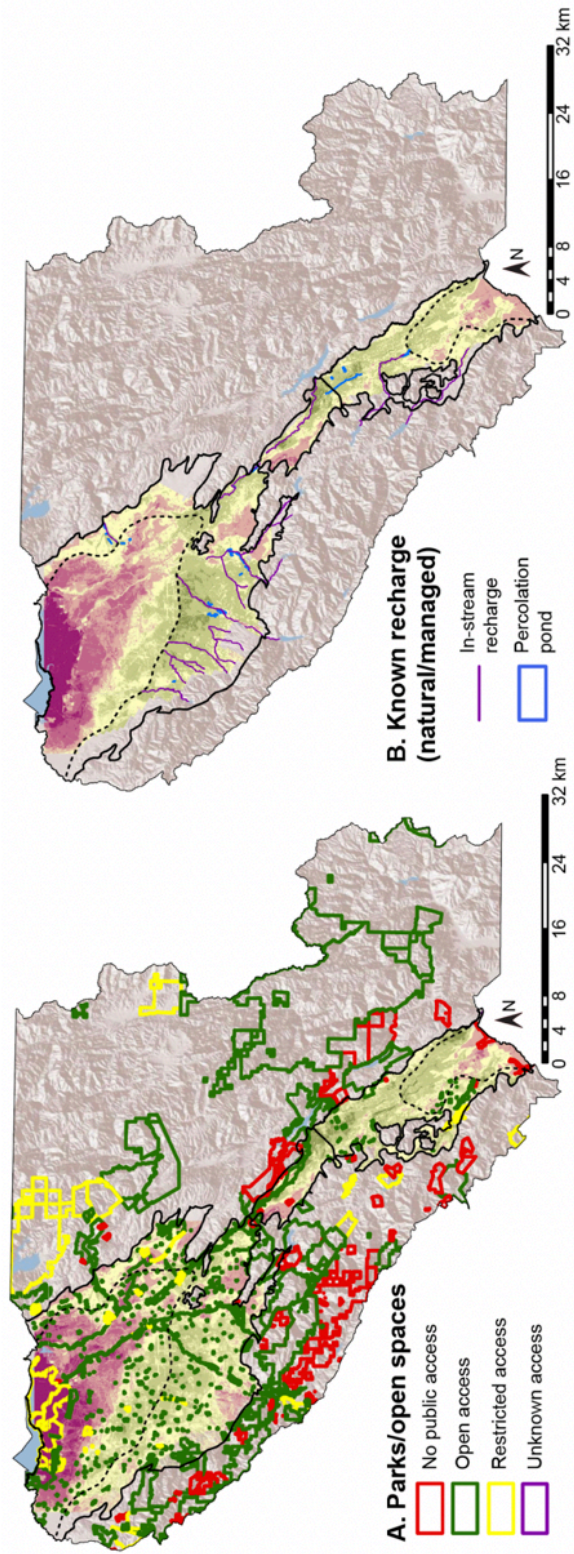
Figure 3-8 Open space, known recharge, and flood-MAR suitability. Selected categories of open space (A) and known recharge (natural and managed) (B) overlaid with flood-MAR suitability, which could be used to focus application of flood-MAR projects.

We also overlaid a map showing SI_{comp} values with Valley Water's existing recharge locations (both natural and managed), including in-stream recharge and groundwater recharge ponds (Figure 3-8B). This helps to visualize where new projects could complement or supplement existing operations and/or known natural recharge areas.

The SI_{comp} map was also overlaid with two water quality indicators, nitrate-nitrite and total dissolved solids, which helps to show where areas with elevated suitability have more or less water quality issues in ambient groundwater (Figure 3-9A-B). Depending on project goals, MAR projects could be prioritized where was quality is better or worse, implying consequent application of recovered water having higher quality or likely dilution where groundwater is impaired, respectively.

All MAR suitability maps also contain the approximate location of known confined areas in the groundwater basins. The location of the mapped boundary between the confined and unconfined aquifer conditions is based on long-standing geologic interpretations, going back decades. While this boundary is considered approximate due to geologic uncertainty and aquifer heterogeneity, it continues to be supported by substantial geologic and hydrogeologic data. MAR projects would likely be prioritized outside the confined areas in the recharge zones and in locations that complement the spatial coverage of existing managed recharge operations.

3.4.2 Application to other regions

While the results of our approach are directly applicable in Santa Clara County, this methodology is rooted in past studies and should be adaptable for use in other
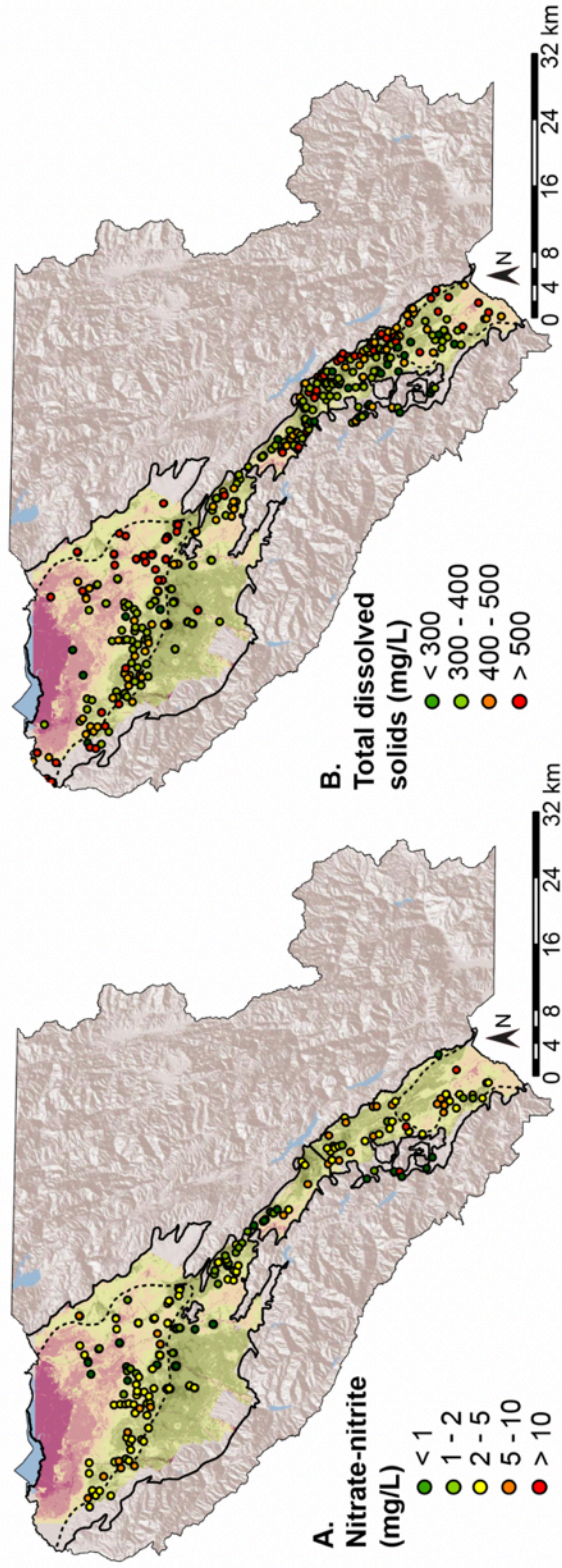
Figure 3-9 Water quality and flood-MAR suitability. Water quality indicator examples, including nitrate-nitrite (A) and total dissolved solids (B), overlaid with flood-MAR suitability, which could be used to focus application of flood-MAR projects.

regions. These analysis used physical criteria that are measured in most groundwater basins and are often publicly available. The data used in surface suitability index, including infiltration capacity, land use, and geology, was all obtained from publicly available datasets for the continental United States. Additionally, subsurface data, such as groundwater levels, aquifer transmissivity, and available aquifer storage, are available in most regions and can be substituted with local data. Globally, there is a growing availability of high-resolution remote sensing data for assessing land use, slope, and subsurface characteristics, such as groundwater levels (Jha et al., 2007). This data can easily be incorporated into a model framework as applied for Santa Clara County, modifying classification and/or ranking systems as appropriate based on regional and local conditons.

3.4.3 Study limitations and next steps

Even within this context and use case, the site suitability maps are fundamentally limited by the accuracy and resolution of available data. For surface coverages like land use/land cover, these can change over short time scales, and factor coverages derived over multiple years (or even decades) could result in inconsistent merging of data periods. For subsurface coverages like transmissivity or available storage, there are limitations based on groundwater model resolution and the direct measurements that provided the basis for calibrating these models. Groundwater models have been calibrated multiple times over a period of years in the Santa Clara Valley, beginning when there was much less available data and the development of a

three-dimensional stratigraphic model was more difficult than it would be today, and the resolution of existing models is relatively coarse.

Some MAR site suitability studies have conducted a sensitivity analysis or field validation from existing recharge sites to assess model performance (Chowdhury et al., 2008; Ghayoumian et al., 2007; Owusu et al., 2017). While a formal sensitivity analysis was not conducted, we compared this new analysis with another suitability analysis that includes the project area, the Soil Agricultural Groundwater Banking Index, SAGBI (O'Geen et al., 2015). SAGBI uses five soil characteristics derived from the NRCS SSURGO database, and includes groundwater basins throughout California. SAGBI assigned suitability ratings on a 100-point scale with six categories of rankings, where 0-15 was rated as "very poor," >15-30 was rated as "poor," >30-50 was rated as "moderately poor," >50-70 was rated as "moderately good," >70-85 was rated as "good," and >85 was rated as "excellent." We normalized SI_{comp} from the present study using a six-point scale, where a rating of 0-1 was considered to be "very poor," >1-2 was rated as "poor," >2-3 was rated as "moderately poor," >3-4 was rated as "moderately good," >4-5 was rated as "good," and >5-7 was rated as "excellent." For both SAGBI and SI_{comp}, ratings were reclassified on a numerical scale, with "very poor" rated as 1 and "excellent" rated as 6.

Once SAGBI and SI_{comp} results were put on the same scale, SAGBI ratings were subtracted from SI_{comp} values to see how the two suitability rating systems compared, demonstrating considerable (Figure 3-10). The two models were in agreement (within one ranking category) for ~79% of the land area, while SAGBI was
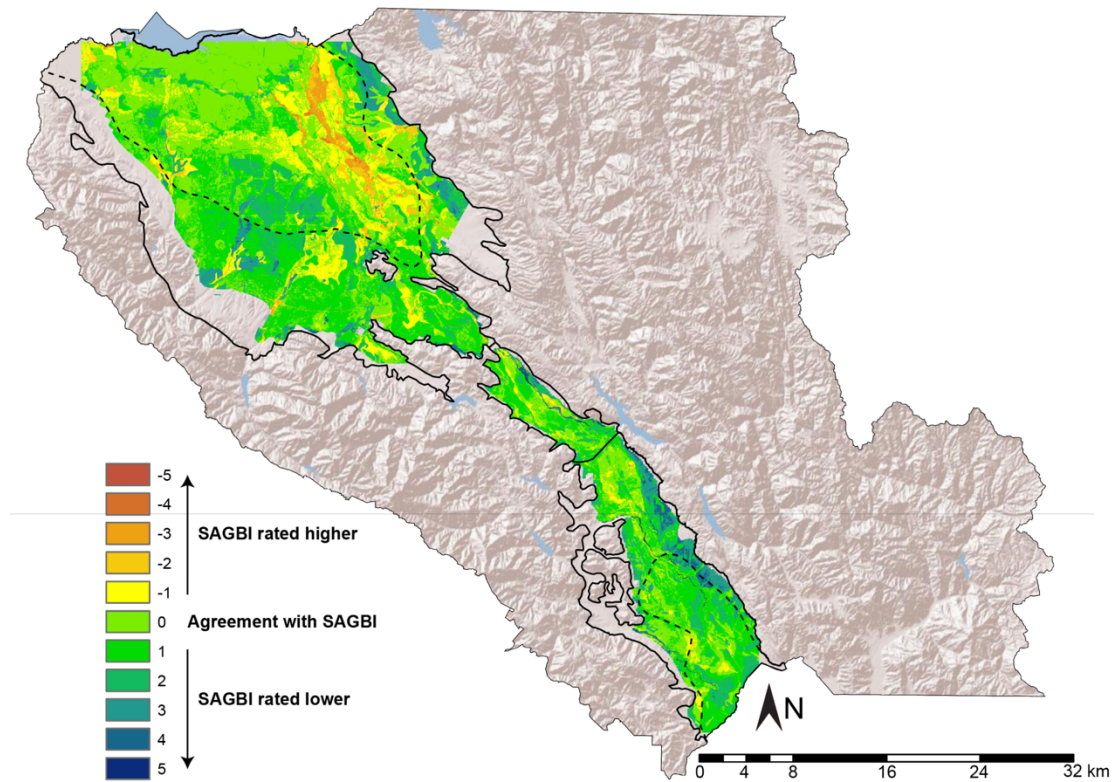
Figure 3-10 Comparison of our flood-MAR suitability ratings with SAGBI. SAGBI ratings from O'Geen et. al (2015) subtracted from flood-MAR suitability ratings from this study, which were normalized to the same 6 point scale for comparison. A rating of "0" indicates agreement with SAGBI ratings. Positive values indicate that SAGBI rated the area with lower suitability than this study, while negative values indicate that SAGBI rated the area with higher suitability than this study.

rated higher for ~17% of the land area (primarily in eastern Santa Clara Plain) and SAGBI was rated lower for ~4% of the land area (primarily in eastern Llagas Subbasin). Some of the differences between the two models are likely to have resulted from incorporation of subsurface data in the present study. However, the strong agreement between the two analyses helps to give confidence that there developed with consistent approaches.

Future work could involve more extensive sensitivity analyses or field validation from existing recharge sites to test the accuracy and robustness of the MCDA approach. While VW maintains 27 active managed recharge sites, data was not available to quantify and compare the performance of these sites. Looking at recharge basins overlaid on the composite suitability map (Figure 3-8b), some existing recharge basins are located where the suitability was rated fairly low, because our analysis identified existing recharge basins as "open water" land use (Figure 8B). Infiltration data from existing managed recharge basins would be needed to accurately field validate MCDA predictions.

Next steps in this work include an analysis of water availability for MAR projects, specifically assessing hillslope runoff in Santa Clara County under different climate scenarios. Previous work pairing MAR suitability with hillslope runoff analyses in the nerarby Pajaro Valley, CA helped to further identify locations where projects could deliver the significant benefits (Beganskas et al., 2019). Another area of future work could include field testing soil infiltration properties in areas that have been identified as suitable for MAR by the GIS-MCDA analyses. Field testing and validation

efforts could be focused in areas with the highest suitability ratings. With the addition of hillslope runoff modeling and field testing, our GIS-MCDA method will become more robust for assessing MAR site suitability.

3.5 Summary and Conclusions

In this study, we used multi-criteria decision analysis with spatial data, combined in a geographic information system, to identify locations with multiple favorable conditions that could motivate MAR project development. Within the three primary groundwater management areas, physical conditions favorable for MAR are found on >30% of the land area, covering over 30,000 hectares. Sites with the highest MAR suitability tend to be located where multiples of these criteria are satisfied: on old stream channels, on or near active (although often ephemeral) stream channels, and on other coarse Quaternary fluvial and alluvial deposits; where land is undeveloped, has low-intensity development, or is used for agricultural activities; where there is a vadose zone 6-30 m thick; and where there have been large differences in groundwater levels during dry climate periods compared to wet periods.

REFERENCES

American Society of Civil Engineers, 2020. Standard Guidelines for Managed Aquifer Recharge, Standard Guidelines for Managed Aquifer Recharge. https://doi.org/10.1061/9780784415283.

Beganskas, S., Fisher, A.T., 2017. Coupling distributed stormwater collection and managed aquifer recharge: Field application and implications. J. Environ. Manage. 200, 366–379. https://doi.org/10.1016/j.jenvman.2017.05.058

Beganskas, S., Young, K.S., Fisher, A.T., Harmon, R., Lozano, S., 2019. Runoff Modeling of a Coastal Basin to Assess Variations in Response to Shifting Climate and Land Use: Implications for Managed Recharge. Water Resour. Manag. 33, 1683–1698. https://doi.org/10.1007/s11269-019-2197-4

Bekele, E., Toze, S., Patterson, B., Higginson, S., 2011. Managed aquifer recharge of treated wastewater: Water quality changes resulting from infiltration through the vadose zone. Water Res. 45, 5764–5772. https://doi.org/10.1016/j.watres.2011.08.058

Bierkens, M.F.P., Wada, Y., 2019. Non-renewable groundwater use and groundwater depletion: A review. Environ. Res. Lett. 14. https://doi.org/10.1088/1748-9326/ab1a5f

Bouwer, H., 2002. Artificial recharge of groundwater: Hydrogeology and engineering. Hydrogeol. J. 10, 121–142. https://doi.org/10.1007/s10040-001-0182-4

Calpine Corporation, Bechtel Enterprises Holdings Inc., 2000. Coyote Valley Groundwater Report.

Carle, S.F., Esser, B.K., Moran, J.E., 2006. High-resolution simulation of basin-scale nitrate transport considering aquifer system heterogeneity. Geosphere 2, 195–209. https://doi.org/10.1130/GES00032.1

Casanova, J., Devau, N., Pettenati, M. (2016). Managed Aquifer Recharge: An Overview of Issues and Options. In: Jakeman, A.J., Barreteau, O., Hunt, R.J., Rinaudo, JD., Ross, A. (eds) Integrated Groundwater Management. Springer,

Cham. https://doi.org/10.1007/978-3-319-23576-9_16

CH2M Hill, 2005. Llagas Basin Numerical Groundwater Model.

CH2M Hill, 1992. Santa Clara Valley Groundwater Model Project - Basin Groundwater Flow Model.

Chenini, I., Mammou, A. Ben, May, M. El, 2010. Groundwater recharge zone mapping using GIS-based multi-criteria analysis: A case study in Central Tunisia (Maknassy Basin). Water Resour. Manag. 24, 921–939. https://doi.org/10.1007/s11269-009-9479-1

Chowdhury, A., Jha, M.K., Chowdary, V.M., 2010. Delineation of groundwater recharge zones and identification of artificial recharge sites in West Medinipur district, West Bengal, using RS, GIS and MCDM techniques. Environ. Earth Sci. 59, 1209–1222. https://doi.org/10.1007/s12665-009-0110-9

Chowdhury, A., Jha, M.K., Chowdary, V.M., Mal, B.C., 2008. Integrated remote sensing and GIS-based approach for assessing groundwater potential in West Medinipur district, West Bengal, India. Int. J. Remote Sens. 30, 231–250. https://doi.org/10.1080/01431160802270131

Dahlke, H.E., LaHue, G.T., Mautner, M.R.L., Murphy, N.P., Patterson, N.K., Waterhouse, H., Yang, F., Foglia, L., 2018. Chapter 8 - Managed Aquifer Recharge as a Tool to Enhance Sustainable Groundwater Management in California: Examples from Field and Modeling Studies. Adv. Chem. Pollution, Environ. Manag. Prot. 3, 215–275.

Dewitz, J., U.S. Geological Survey, 2021. National Land Cover Database (NLCD) 2019 Products (ver. 2.0, June 2021). https://doi.org/10.5066/P9KZCM54.

Dillon, P., 2005. Future management of aquifer recharge. Hydrogeol. J. 13, 313–316. https://doi.org/10.1007/s10040-004-0413-6

Dillon, P., Stuyfzand, P., Grischek, T., Lluria, M., Pyne, R.D.G., Jain, R.C., Bear, J., Schwarz, J., Wang, W., Fernandez, E., Stefan, C., Pettenati, M., van der Gun, J., Sprenger, C., Massmann, G., Scanlon, B.R., Xanke, J., Jokela, P., Zheng, Y., Rossetto, R., Shamrukh, M., Pavelic, P., Murray, E., Ross, A., Bonilla Valverde,

J.P., Palma Nava, A., Ansems, N., Posavec, K., Ha, K., Martin, R., Sapiano, M., 2019. Sixty years of global progress in managed aquifer recharge. Hydrogeol. J. 27, 1–30.

Doussan, C., Ledoux, E., Detay, M., 1998. River-Groundwater Exchanges, Bank Filtration, and Groundwater Quality: Ammonium Behavior. J. Environ. Qual. 27, 1418–1427. https://doi.org/10.2134/jeq1998.00472425002700060019x

Fuentes, I., Vervoort, R.W., 2020. Site suitability and water availability for a managed aquifer recharge project in the Namoi basin, Australia. J. Hydrol. Reg. Stud. 27, 100657. https://doi.org/10.1016/j.ejrh.2019.100657

Ghayoumian, J., Mohseni Saravi, M., Feiznia, S., Nouri, B., Malekian, A., 2007. Application of GIS techniques to determine areas most suitable for artificial groundwater recharge in a coastal aquifer in southern Iran. J. Asian Earth Sci. 30, 364–374. https://doi.org/10.1016/j.jseaes.2006.11.002

Giove, S., Brancia, A., Satterstrom, F.K., Linkov, I., 2009. Decision Support Systems and Environment: Role of MCDA, in: Marcomini, A., Suter II, G.W., Critto, A. (Eds.), Decision Support Systems for Risk-Based Management of Contaminated Sites. Springer US, Boston, MA, pp. 1–21. https://doi.org/10.1007/978-0-387-09722-0_3

Hartog, N., Stuyfzand, P.J., 2017. Water quality considerations on the rise as the use of managed aquifer recharge systems widens. Water (Switzerland) 9. https://doi.org/10.3390/w9100808

Helley, E.J., Lajoie, K.R., Spangle, W.E., Blair, M.L., 1979. Flatland deposits of the San Francisco Bay region, California — Their geology and engineering properties, and their importance to comprehensive planning, Professional Paper. https://doi.org/10.3133/pp943

Horton, J.D., San Juan, C.A., Stoesser, D.B., 2017. State Geologic Map Compilation (SGMC) Geodatabase of the Conterminous United States. USGS Sci. Cat.

Jha, M.K., Chowdhury, A., Chowdary, V.M., Peiffer, S., 2007. Groundwater management and development by integrated remote sensing and geographic

information systems: Prospects and constraints. Water Resour. Manag. 21, 427–467. https://doi.org/10.1007/s11269-006-9024-4

Kocis, T.N., Dahlke, H.E., 2017. Availability of high-magnitude streamflow for groundwater banking in the Central Valley, California. Environ. Res. Lett. 12. https://doi.org/10.1088/1748-9326/aa7b1b

Malczewski, J., Rinner, C., 2015. Multicriteria decision analysis in geographic information science. Springer.

Maliva, R.G., Guo, W., Missimer, T.M., 2006. Aquifer Storage and Recovery: Recent Hydrogeological Advances and System Performance. Water Environ. Res. 78, 2428–2435. https://doi.org/10.2175/106143006x123102

Marr, J., Arrate, D., Maendly, R., Dhillon, D., Stygar, S., 2018. FLOOD-MAR: Using Flood Water for Managed Aquifer Recharge to Support Sustainable Water Resources.

Marwaha, N., Kourakos, G., Levintal, E., Dahlke, H.E., 2021. Identifying Agricultural Managed Aquifer Recharge Locations to Benefit Drinking Water Supply in Rural Communities. Water Resour. Res. 57. https://doi.org/10.1029/2020WR028811

O'Geen, A.T., Saal, M.B.B., Dahlke, H., Doll, D., Elkins, R., Fulton, A., Fogg, G., Harter, T., Hopmans, J.W., Ingels, C., Niederholzer, F., Solis, S.S., Verdegaal, P., Walkinshaw, M., 2015. Soil suitability index identifies potential areas for groundwater banking on agricultural lands. Calif. Agric. 69, 75–84. https://doi.org/10.3733/ca.v069n02p75

O'Leary, D.R., Izbicki, J.A., Moran, J.E., Meeth, T., Nakagawa, B., Metzger, L., Bonds, C., Singleton, M.J., 2012. Movement of Water Infiltrated from a Recharge Basin to Wells. Ground Water 50, 242–255. https://doi.org/10.1111/j.1745-6584.2011.00838.x

Owuor, S.O., Butterbach-Bahl, K., Guzha, A.C. *et al.* Groundwater recharge rates and surface runoff response to land use and land cover changes in semi-arid environments. *Ecol Process* **5**, 16 (2016). https://doi.org/10.1186/s13717-016-

0060-6

Owusu, S., Mul, M.L., Ghansah, B., Osei-Owusu, P.K., Awotwe-Pratt, V., Kadyampakeni, D., 2017. Assessing land suitability for aquifer storage and recharge in northern Ghana using remote sensing and GIS multi-criteria decision analysis technique. Model. Earth Syst. Environ. 3, 1383–1393. https://doi.org/10.1007/s40808-017-0360-6

Pavelic, P., Dillon, P.J., Barry, K.E., Gerges, N.Z., 2006. Hydraulic evaluation of aquifer storage and recovery (ASR) with urban stormwater in a brackish limestone aquifer. Hydrogeol. J. 14, 1544–1555. https://doi.org/10.1007/s10040-006-0078-4

Ringleb, J., Sallwey, J., Stefan, C., 2016. Assessment of managed aquifer recharge through modeling-A review. Water (Switzerland) 8, 1–31. https://doi.org/10.3390/w8120579

Russo, T.A., Fisher, A.T., Lockwood, B.S., 2015. Assessment of managed aquifer recharge site suitability using a GIS and modeling. Groundwater 53, 389–400. https://doi.org/10.1111/gwat.12213

Sallwey, J., Bonilla Valverde, J.P., Vásquez López, F., Junghanns, R., Stefan, C., 2019. Suitability maps for managed aquifer recharge: A review of multi-criteria decision analysis studies. Environ. Rev. 27, 138–150. https://doi.org/10.1139/er-2018-0069

Schmidt, C.M., Fisher, A.T., Racz, A.J., Lockwood, B.S., Los Huertos, M., 2011. Linking Denitrification and Infiltration Rates during Managed Groundwater Recharge. Environ. Sci. Technol. 45, 9634–9640.

Soil Survey Staff, 2014. Soil Survey Geographic (SSURGO) Database.

Wada, Y., Van Beek, L.P.H., Van Kempen, C.M., Reckman, J.W.T.M., Vasak, S., Bierkens, M.F.P., 2010. Global depletion of groundwater resources. Geophys. Res. Lett. 37, 1–5. https://doi.org/10.1029/2010GL044571

Waterhouse, H., Bachand, S., Mountjoy, D., Choperena, J., Bachand, P.A.M., Dahlke, H.E., Horwath, W.R., 2020. Agricultural managed aquifer recharge - water

quality factors to consider. Calif. Agric. 74, 144–154.
https://doi.org/10.3733/CA.2020A0020

Weissmann, G. S., Y. Zhang, G. E. Fogg, J. F. Mount, J. S. Bridge, and D. W.
Hyndman (2004), Influence of Incised-Valley-Fill Deposits on Hydrogeology of
a Stream-Dominated Alluvial Fan, in *Aquifer Characterization*, edited, SEPM
Society for Sedimentary Geology, 10.2110/pec.04.80.0015

Witter, R.C., Knudsen, K.L., Sowers, J.M., Wentworth, C.M., Koehler, R.D.,
Randolph, C.E., 2006. Maps of Quaternary Deposits and Liquefaction
Susceptibility in the Central San Francisco Bay Region, California. Reston, VA.

Yeh, H.F., Lee, C.H., Hsu, K.C., Chang, P.H., 2009. GIS for the assessment of the
groundwater recharge potential zone. Environ. Geol. 58, 185–195.
https://doi.org/10.1007/s00254-008-1504-9

Yuan, J., Van Dyke, M.I., Huck, P.M., 2016. Water reuse through managed aquifer
recharge (MAR): Assessment of regulations/guidelines and case studies. Water
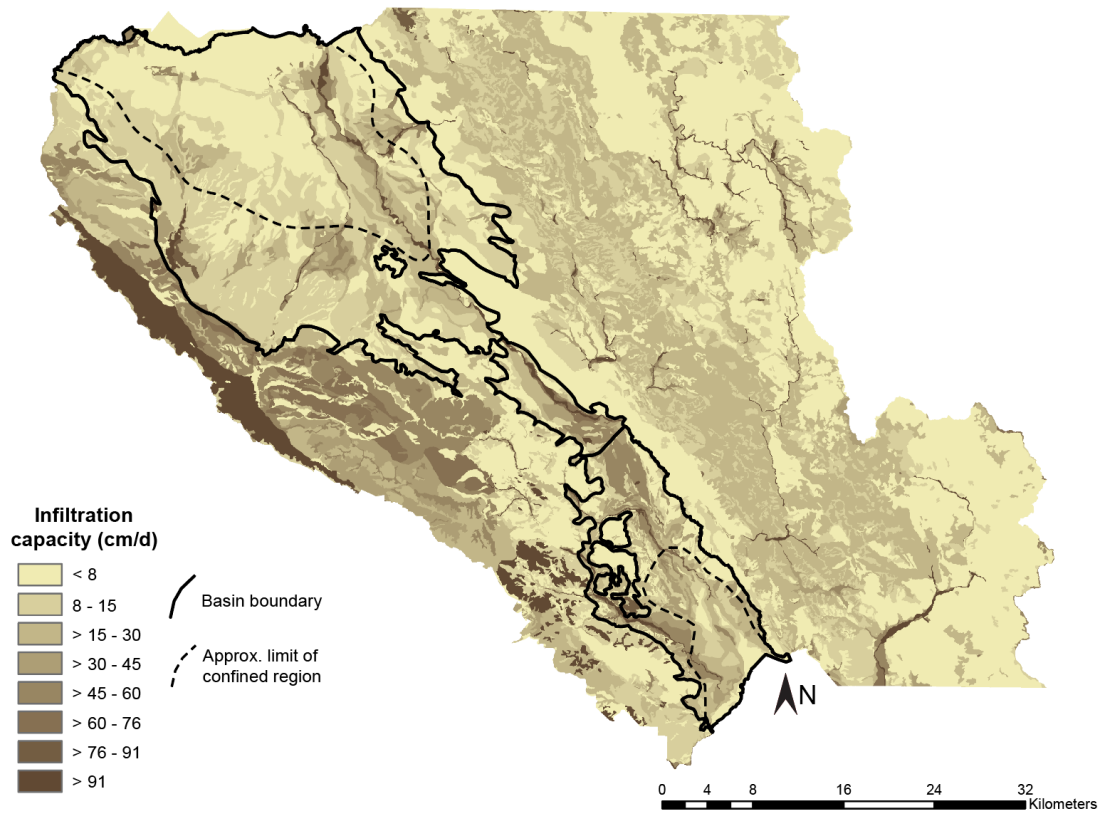Qual. Res. J. Canada 51, 357–376. https://doi.org/10.2166/wqrjc.2016.022

Figure S3-1. Infiltration capacity of soils in study area, binned to highlight areas with most favorable properties for MAR. In general, MAR project sites should be identified in areas where infiltration rates are ≥30 cm/d.
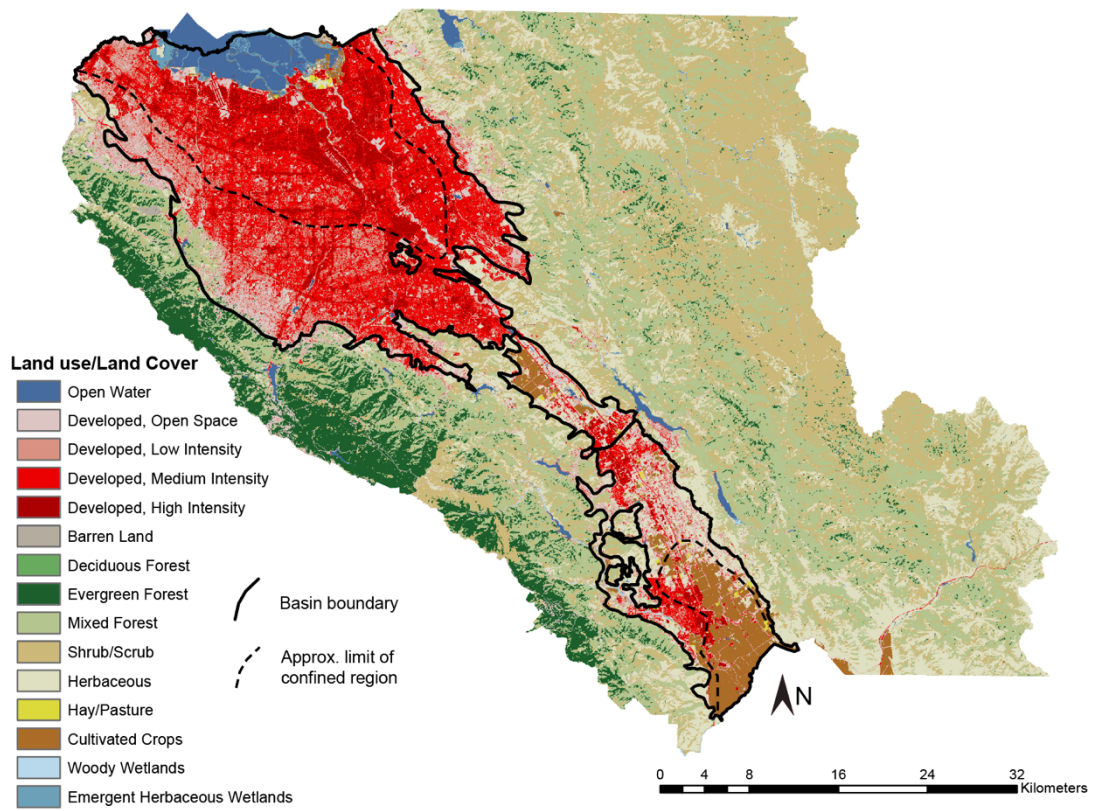
Figure S3-2. Land use/land cover in the study area, based on categories in the National Land Cover Database 2019.
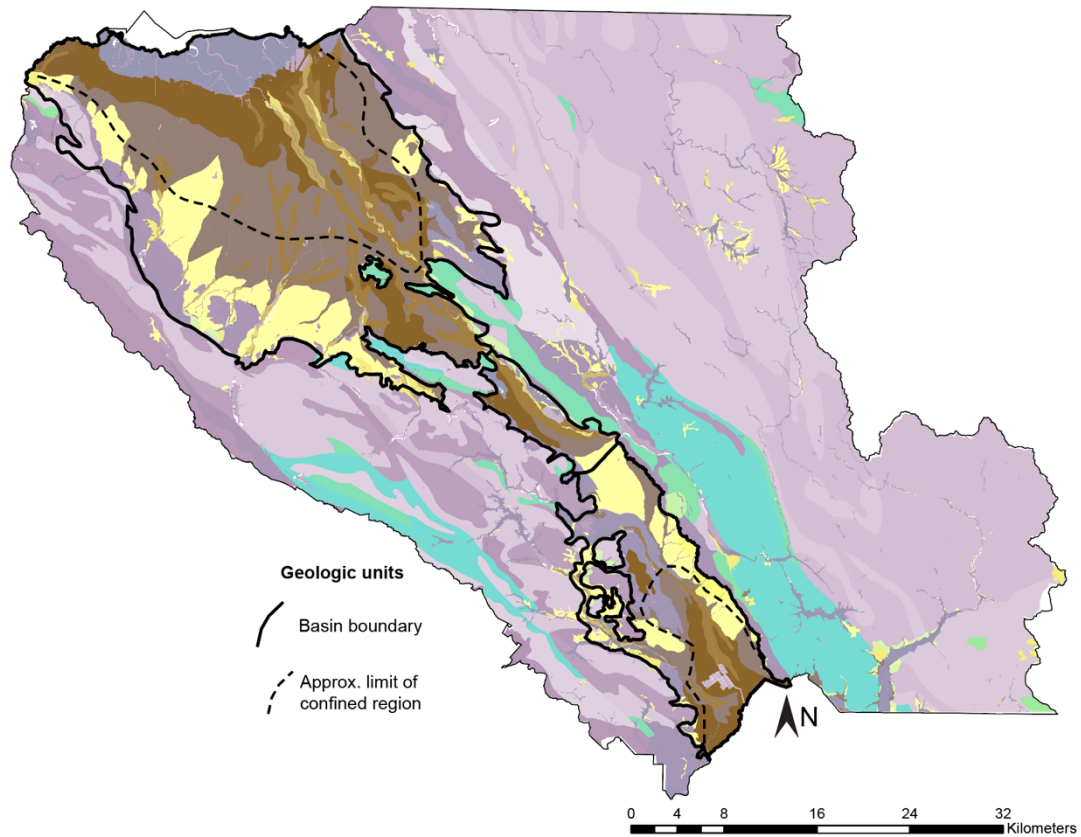
Figure S3-3. Geologic units mapped across the study area, including 72 distinct lithologies. A full listing is included in Table S3-1, but in general, yellow/brown colors represent Quaternary alluvial deposits, while turquoise/lavender colors represent Upper Cretaceous and Pliocene marine rocks, Mesozoic volcanic rocks, and Franciscan Melange.
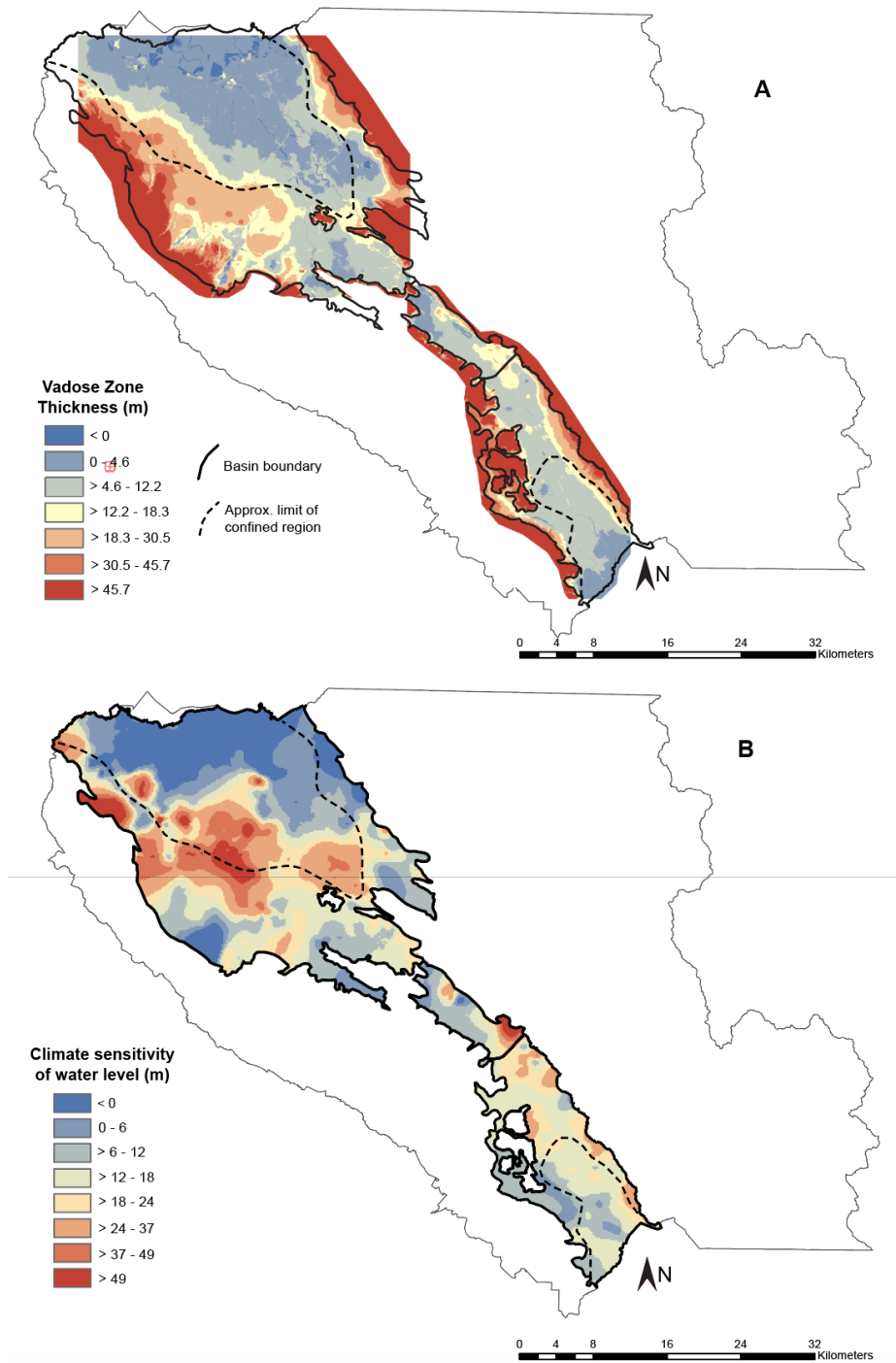
Figure S3-4. A. Vadose zone thickness based on median depth to water (DTW) during 2010 – 2019. B. Climate sensitivity of DTW defined as DTW_{dry} (2014 – 2015) – DTW_{wet} (1978 – 2019, minimum water level).
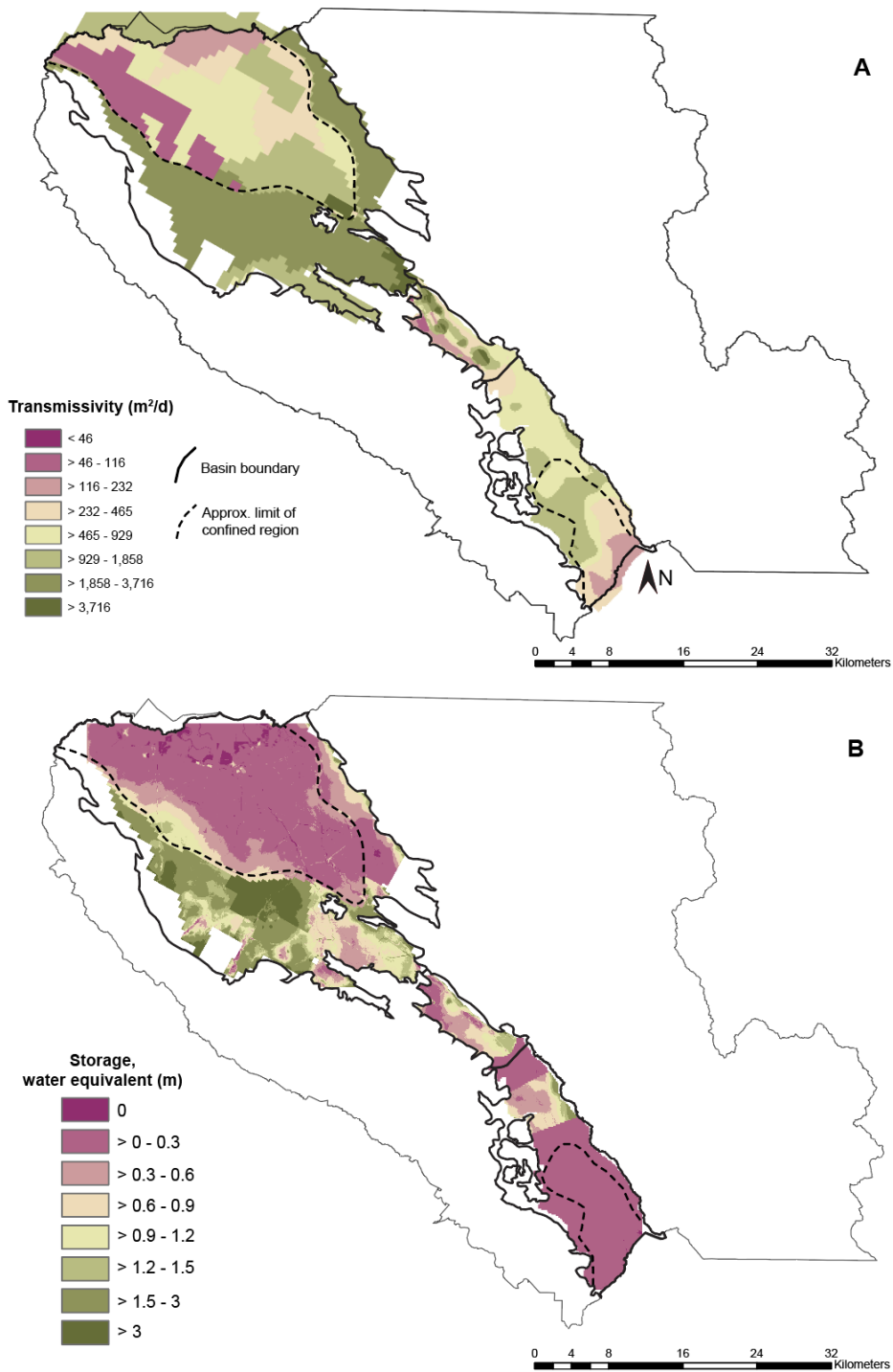
Figure S3-5. Aquifer properties from MODFLOW property files. A. Transmissivity from upper layers. B. Storage from upper layers, defined as specific yield x thickness of vadose zone.

Table S3-1. Lithology codes and associated lithology names used in the surficial geology coverage.

Lithology Code	Lithology Name
adf	Artificial dam fill (historical)
af	Artificial fill (historical)
alf	Artificial levee fill (historical)
br	Early Quaternary and older (>1.4 Ma) deposits and bedrock, undifferentiated
gq	Gravel quarries and percolation ponds (historical)
H2O	Water
nm	Not mapped
Qa	Latest Pleistocene to Holocene alluvial deposits, undifferentiated
Qf	Latest Pleistocene to Holocene alluvial fan deposits
Qha	Holocene alluvial deposits, undifferentiated
Qhay	Latest Holocene alluvial deposits, undifferentiated
Qhb	Holocene Basin Deposits
Qhbm	Holocene San Francisco Bay mud
Qhc	Historical stream channel deposits
Qhc-br	Combination of Qhc, br
Qhc-Qhly	Combination of Qhc, Qhly
Qhf	Holocene alluvial fan deposits
Qhf-Qhff	Combination of Qhf, Qhff
Qhf-Qhl	Combination of Qhf, Qhl
Qhf-Qpf	Combination of Qhf, Qpf
Qhf1	*Related to Qhf*
Qhf2	*Related to Qhf*
Qhfe	Holocene alluvial fan-estuarine complex deposits
Qhff	Holocene alluvial fan deposits, fine facies
Qhff-br	Combination of Qhff, br
Qhfy	Latest Holocene alluvial fan deposits
Qhl	Holocene alluvial fan levee deposits

Qhl-Qhty	Combination of Qhl, Qhty
Qhl-Qpf	Combination of Qhl, Qpf
Qhl1	*Related to Qhl*
Qhly	Latest Holocene alluvial fan levee deposits
Qhly-Qhty	Combination of Qhly, Qhty
Qht	Holocene stream terrace deposits
Qht-Qhty	Combination of Qht, Qhty
Qht-Qpf	Combination of Qht, Qpf
Qht1	*Related to Qht*
Qht2	*Related to Qht*
Qhty	Latest Holocene stream terrace deposits
Qhty-Qpf	Combination of Qhty, Qpf
Qoa	Early to late Pleistocene alluvial deposits, undifferentiated
Qof	Early to late Pleistocene alluvial fan deposits
Qof1	*Related to Qof*
Qof2	*Related to Qof*
Qot	Early to late Pleistocene stream terrace deposits
Qot1	*Related to Qot*
Qot2	*Related to Qot*
Qpa	Latest Pleistocene alluvial deposits, undifferentiated
Qpf	Latest Pleistocene alluvial fan deposits
Qpf-Qpt	Combination of Qpf, Qpt
Qpf?	See Qpf
Qpt	Latest Pleistocene stream terrace deposits
Qpt?	See Qpt
Qt	Latest Pleistocene to Holocene stream terrace deposits
Qt1	*Realted to Qt*
Qt2	*Related to Qt*
E	Eocene marine rocks
K	Cretaceous marine rocks (in part nonmarine), unit 1 (Coast Ranges)

KJf	Franciscan Complex, unit 1 (Coast Ranges)
KJfm	Franciscan melange
Ku-Ep	Upper Cretaceous and Paleocene marine rocks, undivided
Ku	Upper Cretaceous marine rocks, unit 1 (Upper Great Valley Sequence)
M	Miocene marine rocks
Mzv	Mesozoic volcanic rocks, unit 1 (Coast Ranges)
O	Oligocene marine rocks
P	Pliocene marine rocks
Q	Quaternary alluvium and marine deposits
Qls	Quaternary large landslide deposits
Qoa	Older Quaternary alluvium and marine deposits
Qpc	Plio-Pleistocene and Pliocene loosely consolidated deposits
Ti	Tertiary intrusive rocks (hypabyssal), unit 2 (Quien Sabe Volcanic Field)
Tv	Tertiary volcanic flow rocks, unit 1 (Quien Sabe-Burdell Mountain)
um	Ultramafic rocks, chiefly Mesozoic, unit 3 (Coast Ranges and Western Klamath Mountains)